Breakup and Mesozoic seafloor spreading between the Australian and Indian plates

Dona Mihut

Submitted in fulfilment of the requirement for the degree of Doctor of Philosophy, Department of Geology and Geophysics, University of Sydney

July, 1997

Certification

I certify that this thesis has not been submitted for a higher degree at any other university or institution, and that the help in preparing this thesis and all sources used have been duly acknowledged.

Dona Mihut

Acknowledgements

I would like to express my profound gratitude to my supervisor Dr. R.Dietmar Müller for his invaluable contribution to the accomplishment of this thesis. I have benefited from his constant instructive guidance and support during my postgraduate study. His earnest efforts to pass on his extensive knowledge about geodynamics have been greatly appreciated.

I am also grateful to Dr. Jean-Yves Royer for his interest in my work and his helpful suggestions during the time he spent in this Department. Some programs written by him were indispensable for the plate reconstruction carried out in Chapter 3. Many thanks go to Dr. Sverre Planke whose expertise in volcanic margin evolution expanded my knowledge about this subject. Fruitful discussions with Dr. Steven Cande guided me to a clearer understanding of my own thoughts.

I would like to thank Mr. Ian Russel chief geologist with Mobil Exploration and Producing Australia for supplying the seismic and well data from the Carnarvon Terrace and also for other support provided. Thanks are also due for discussions, advice and suggestions regarding the seismic interpretation carried out in Chapter 4 of this thesis.

I would also like to express my thanks to the staff of the Department, in particular Dr. Jock Keene, (Head of Department) Mr. Joop Stienstra, Dr. Richard Facer, Mr. David Mitchell and Mr. Phil Manning. I should take the opportunity to thank to my fellow

students David Haddad, Alison Cole, Carmen Gaina and Alexa Troedsen for valuable discussions and with whom I shared all the excitement (?) of being a PhD student in this Department.

Special thanks go to Professor Iain Mason for being a friend in deed. I would also like to thank him for giving me the opportunity to refresh some rusty geophysical memories.

A big thank you to my family from here and overseas for their continuous support and love: my daughter, my mother, my father and my brother. And last, but most important to my lovely husband who made me stick to the job!

Abstract

The early opening between India and Australia in terms of plate motion, spreading directions and rates represents one of the last frontier in better understanding the evolution of the eastern Indian Ocean. In this study a set of reinterpreted and new magnetic anomaly data in the abyssal plains adjacent to the western Australian margin and in the southern Wharton Basin were combined to compute Indian-Australian stage rotations poles, finite rotations, and to estimate the relative positions of the two continents through a series of tectonic stages between about 156 Ma and 96 Ma. The plate kinematic model for Indian-Australian motions correlates well with a number of tectonic events recorded in the eastern Indian Ocean and suggests that the separation between Greater India and Australia was mostly accomplished by the fast southeastward motion of Australia relative to the mantle.

A northeast structural trend of magnetic isochrons was determined in the Argo Abyssal Plain. Seafloor spreading started in the northern Gascoyne Abyssal Plain and the southern Cuvier Abyssal Plain before chron M14 at about 136.2 Ma, 3.7 Ma earlier than previously interpreted (e.g *Veevers and Li*, 1991). Three different trends are suggested by the new satellite-derived gravity anomaly data in the Wharton Basin (1) north-south oriented fracture zones, (2) east-west striking shorth-wavelength lineations perpendicular to the fracture zones and (3) northeast-southwest striking crenulations assumed to be the result of ridge propagator events triggered by a major change in spreading direction between the Indian and Australian plates at about 96 Ma.

A tectonic model for the breakup of Greater India, Australia and Antarctica was developed which suggests that Greater India was separated from Australia and Antarctica by three phases of a propagating rift. It first separated North Greater India (former Argo Land) and then Middle Greater India from South Greater India by dextral strike-slip. South Greater India was in turn separated from Antarctica latest at chron M0. The northern tectonic block of Greater India became fixed to Middle Greater India at about 136 Ma, when spreading in the Cuvier, Gascoyne and Perth abyssal plains started. At 96 Ma, Middle Greater India became fixed to South Greater India. The revised fit of Greater India, Australia, Antarctica and Madagascar shows that the original size of Greater India might have been underestimated by about 25% and the present size of India may only represent about half of its original size. Pre- and post-breakup magmatism affected almost the entire western Australian margin. Uplift and subsequent erosion of the Bernier Platform and Exmouth Sub-basin shortly before the onset of seafloor spreading are the results of a mantle plume centered on the rift in the tectonic model presented here. The direction of Late Tertiary compression observed on the Bernier Platform matches the northwest-southeast direction of convergence between the Capricorn and Australian plates described by the model of *Gordon and Roger* (in prep.).

TABLE OF CONTENTS

List of tables

List of figures

Chapter 1

Chapter 2

Chapter 3

Chapter 4

Chapter 5

CHAPTER 1

Introduction

1.1 Preamble

This study originated as an integrated geophysical and geological analysis of the Carnarvon Terrace. The initial seismic interpretation raised many questions as to the cause of the syn-rift and post rift magmatism and uplift observed in the southern part of the Exmouth Sub-basin and on the Bernier Platform. Answering these questions required an understanding of the evolution of the adjacent abyssal plains, plateaus and oceanic basins.

The availability of a new satellite gravity grid by *Sandwell and Smith* (1997) initiated a change in the focus of this study to the tectonic evolution of the Argo, Gascoyne, Cuvier and Perth abyssal plains, and part of the Wharton Basin in the eastern Indian Ocean. The first step was a re-examination of the joint magnetic and gravity anomaly data set along the western Australian margin. A complex and exciting adventure came out of reconstructing the early tectonic evolution of the eastern Indian Ocean (defined in this study as the area north of the Diamantina Zone and east of Ninetyeast Ridge). The results present a complete history of the opening of this part of the ocean as well as a new scenario, which explains the widespread Cretaceous volcanism along the Cuvier Margin.

1.2 Previous work

The Indian Ocean, although the smallest of the three major ocean basins, appears to be geologically and tectonically one of the most complex. The numerous published

studies of the eastern Indian Ocean (Figure 1.1) fall into three categories: (1) studies of the geology and tectonic evolution of the western Australian margin; (2) studies of the seafloor magnetic anomalies and plate reconstructions of the abyssal plains and adjacent basin and (3) studies of the volcanic activity along the margin during rifting and after breakup.

1.2.1 The geology and tectonic evolution of the western Australian margin

The western Australian margin was first referred to as a single entity by *Teichert* (1939), who proposed the name '*Westralia(n) Geosyncline*' for a largely submerged sequence of sedimentary rocks, mainly of Jurassic to Cretaceous age. Although Triassic sediments were unknown in Western Australia and a Permian sequence was only suspected offshore the use of the new term allowed for inferred, possible pre-Permian sediments to be included in its northern portion. Further studies indicated that the region may have been submerged in the Early to Middle Paleozoic. The term '*geosyncline*' became obsolete in the early 1970s and studies carried out in this area concentrated on its sub-elements rather than the whole entity. Teichert's concept was later revived under a different name ('*the Westralian Superbasin*') by *Yeates et al.*, (1986), *Bradshaw et al.*, (1988) and *Hocking et al.*, (1994). The term '*superbasin*' is analogous in rank to '*geosyncline*', and defines a complex of basins filled with Permian to Cretaceous sediments, approximately 10 km thick, preserved along the western margin of Australia. Many regional geological analyses of the western Australian margin have been published over the last twenty years including *Veevers and Johnstone* (1974), *Veevers* (1988), *Exon* (1994), *Hocking et al.* (1994),

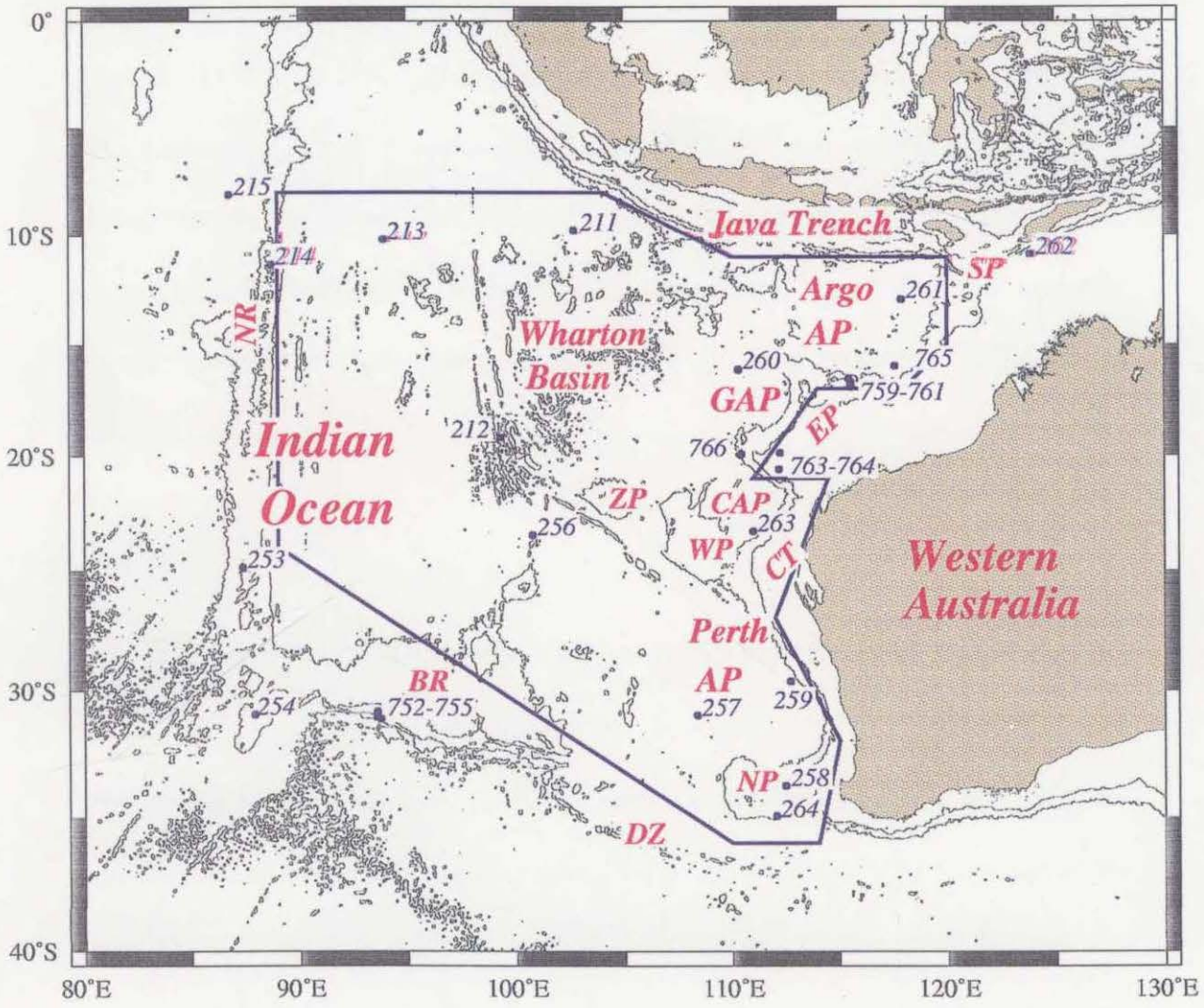

Fig.1.1 Principal physiographic features of the eastern Indian Ocean as defined by isobaths at 2000 m intervals and location of Deep Sea Drilling (DSDP) and Ocean Drilling Program (ODP) sites. The polygon represents the study area. Abbreviations are: SP - Scott Plateau, Argo AP - Argo Abyssal Plain, GAP - Gascoyne Abyssal Plain, EP - Exmouth Plateau, CAP - Cuvier Abyssal Plain, WP - Wallaby Plateau, ZP - Zenith Plateau, Perth AP - Perth Abyssal Plain, NP - Naturaliste Plateau, CR - Carnarvon Terrace, BR - Broken Ridge, NR - Ninetyeast Ridge, DZ-Diamantina Zone.

and *Baillie et al.* (1994), as well as numerous detailed analyses of individual basins. Part of the studies used in this research are listed below: *Barber* (1988), *Lorenzo et al.* (1991), *von Stackelberg et al.* (1980), *Ramsey and Exon* (1994), and *Colwell et al.* (1994) for the Exmouth Plateau; *Thomas and Smith* (1976), *Wiseman* (1979), *Hocking* (1988 and 1990), *Malcolm et al.* (1991), and *Stagg and Colwell* (1994) for the Carnarvon Basin; *Symonds and Cameron* (1977) and *Baillie and Jacobson* (1995) for the Carnarvon Terrace and *Playford et al.* (1976), *Marshall et al.* (1989), and *Quaife et al.* (1994) for the Perth Basin. Many areas are covered by a relatively dense network of bathymetric and seismic profiles recorded by petroleum exploration companies.

1.2.2 Plate reconstruction and seafloor magnetic interpretation

Before the onset of seafloor dating by magnetic anomaly modeling and deep sea drilling, reconstructions of Gondwanaland were constrained only by the shape of the continental margins and by the postulated continuities of geological features and later by paleomagnetic studies from the continents. Until the interpretation of seafloor magnetic anomalies in the Indian Ocean (*McKenzie and Sclater*, 1971; *Sclater and Fisher*, 1974), the previous reconstructions (e.g. *Du Toit*, 1937; *Smith and Hallam*, 1970) did not model the complete breakup of eastern Gondwanaland (between Greater India and Australia) due to the then unknown subduction of a significant part of Greater India under the Eurasian plate (Figures 1.2a, b and c). *McKenzie and Sclater* (1971) calculated the position of India with respect to Australia-Antarctica between 75 Ma and present. *Larson* (1975) and *Heirtzler et al.*

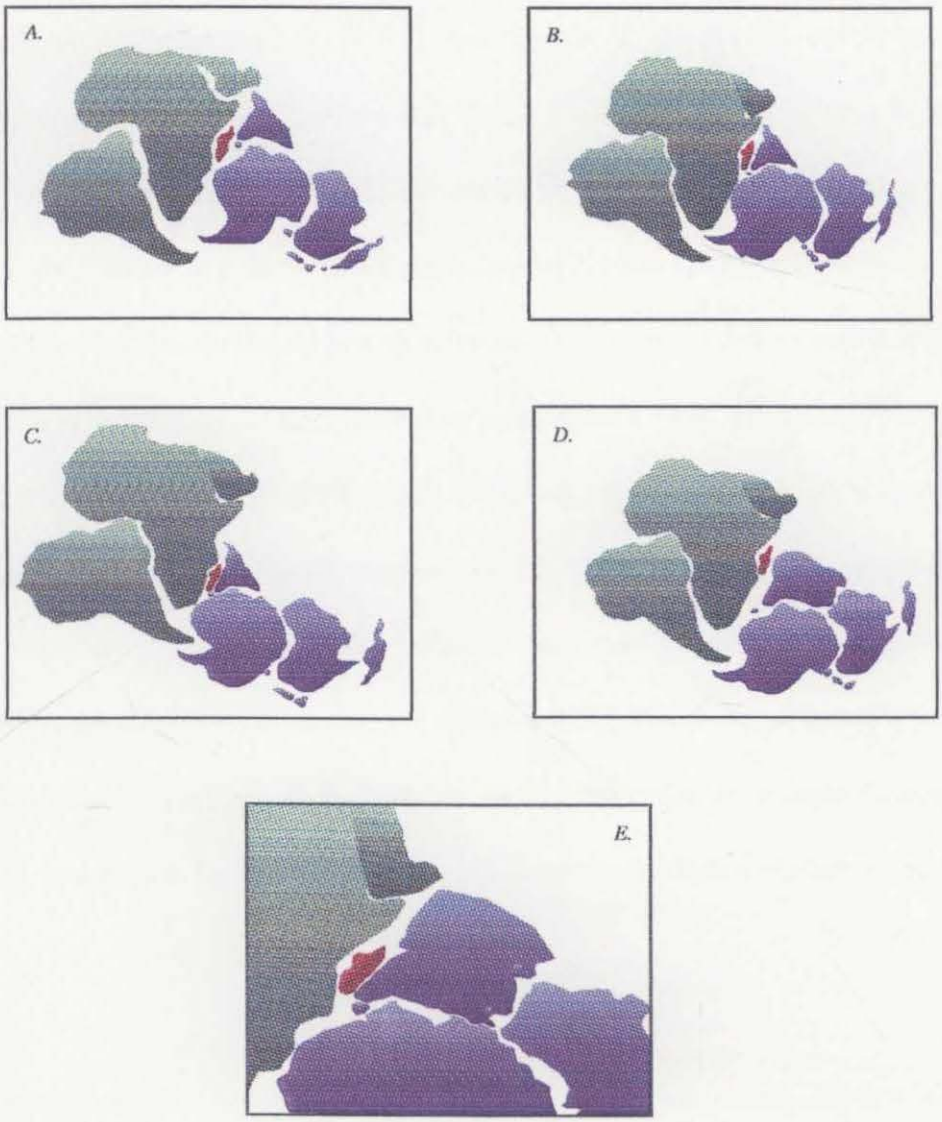

Fig. 1.2 Various reconstructions of East (blue) and West (green) Gondwanaland with Madagascar shown in red (sketches only). A.- Du Toit (1937); B.-Smith and Hallam (1970); C.-Tarling (1972); D-Powell et al. (1980); E.-Lawer and Scotese (1987) - fit at ~160 Ma.

(1978) postulated the presence of an unknown plate northeast of Greater India which would have separated from Australia in the Mid-Jurassic (ca. 155 Ma) creating the Argo Abyssal Plain. The magnetic lineations in the Argo Abyssal Plain were reviewed by *Fullerton et al.* (1989) and *Sager et al.* (1992) based on new aeromagnetic data and results from the Ocean Drilling Program (ODP) Leg 123. They concluded that seafloor spreading started immediately prior to anomaly M26 (ca. 163 Ma) earlier than the Mid-Jurasssic date of *Larson* (1975) and *Heirtzler et al.* (1978). The seafloor spreading history between Greater India and Australia has been studied by a number of authors including *Larson* (1977 and 1979), *Johnson et al.* (1980), *Falvey and Mutter* (1981) and *Fullerton et al.* (1989). In these models breakup started in the Early Cretaceous *ca.* 125 Ma (anomaly M10), creating the Gascoyne, Cuvier and Perth abyssal plains with small pieces of the Indian Plate accreted to the Australian Plate for the first two plains. A comprehensive review of Early Cretaceous seafloor spreading led to the isolation of a distinct magnetic anomaly interpreted by *Veevers et al.* (1985) to be the continent-ocean boundary (COB).

Scotese et al. (1988) noted the global synchroneity of the major changes in plate motion: (1) the breakup of Pangea, starting in the Middle Jurassic (~175 Ma) with a (2) climax in the Early Cretaceous (~132.5 Ma) and three plate reorganizations in (3) the mid-Cretaceous (Quiet Zone, ca. 96 Ma), (4) the early Paleocene (~64 Ma), and (5) the Early Eocene (~49 Ma). *Veevers et al.* (1991) recognized three of these changes off the western and southeastern margins of Australia: the slightly later divergence of the so called Argo Land from Australia (~160 Ma), the southward penetration of the Indian ocean ridge separating India from Australia/Antarctica (ca.

132.5 Ma), and the mid-Cretaceous eastward penetration of the southeast Indian ocean ridge separating Australia from Antarctica.

Sclater and Fisher (1974) identified magnetic anomalies with an east-west oriented pattern in the Wharton Basin decreasing in age from the Late Cretaceous in the south to the Late Eocene in the north. *Liu et al.* (1983) and *Geller et al.* (1983) interpreted major "ridge jumps" in the Middle Eocene (anomaly C20 or C19), east of Ninetyeast Ridge coincident with the termination of seafloor spreading and a major plate reorganization throughout the Indian Ocean (*Curray et al.*, 1982). *Royer and Sandwell* (1989) completed the chron sequence of *Liu et al.* (1983) out to anomalies 26 to 32B. *Krisna et al.* (1995) reinterpreted the chain of abandoned spreading centers considered to be the western extension of the Wharton Ridge based on new magnetic data, which merged the Indian and Australian plates into a single Indo-Australian Plate. *Besse and Courtillot* (1991) revised paleomagnetic data from the African Plate to restore the paleogeographic position of the continents bordering the Indian Ocean, relative to a fixed African continent.

The seismic refraction survey of *Larson et al.* (1979) revealed a typical oceanic crust structure beneath the Cuvier Abyssal Plain and the adjacent Wharton Basin, with two crustal layers (velocity ranges between 5.3 and 6.9 km/s) of about 6.1 to 8.1 km thickness overlaying the mantle, with velocities in the range from7.9 to 8.1 km/s to a total depth range of 12.1 - 14.2 km. Velocity variations found in the western Cuvier Abyssal Plain were associated with the interpreted flank of an abandoned spreading ridge.

1.2.3 Volcanic activity along the western Australian margin and adjacent abyssal plains

Vast areas of the western Australian margin have been affected by magmatic activity before and after breakup and have been included in discussions of the Large Igneous Provinces (LIPs) of the eastern Indian Ocean (*White and McKenzie*, 1989; *Coffin and Eldholm*, 1992). The magmatism is most clearly expressed in large oceanic plateaus such as the Naturaliste and Wallaby plateaus (Figure 1.3), but is also evident in intrusives, extrusives and underplated magmatic material that have been described on the basis of seismic data, core samples, and dredges (*von Rad and Exon*, 1983; *von Rad et al.* 1992; *Veevers*, 1984; *Mutter et al.* 1988; *Colwell et al.* 1994; *Crawford and von Rad*, 1994). *Colwell et al.* (1994) distinguished four styles of magmatism at this margin associated with different processes and episodes: (1) rift related volcanics of possible Late Triassic age (e.g. *ODP Site 766, Exon and Buffer*, 1992); (2) volcanics of Late Jurassic to Early Cretaceous age, probably emplaced prior to breakup (e.g. southern margin of the Exmouth Plateau); (3) seaward-dipping reflectors (SDR) identified from seismic data on the lower slope of the Carnarvon Terrace - the Cuvier Margin - and interpreted as subaerial volcanism, formed after the onset of seafloor spreading (*Hopper et al.*, 1992); (4) underplated crust beneath the western and southern Exmouth Plateau related to melt generation during the Early Cretaceous seafloor spreading in the Cuvier Abyssal Plain and consequent transform motion along the Cape Range Fracture Zone (CRFZ) (*Lorenzo et al.*, 1991).

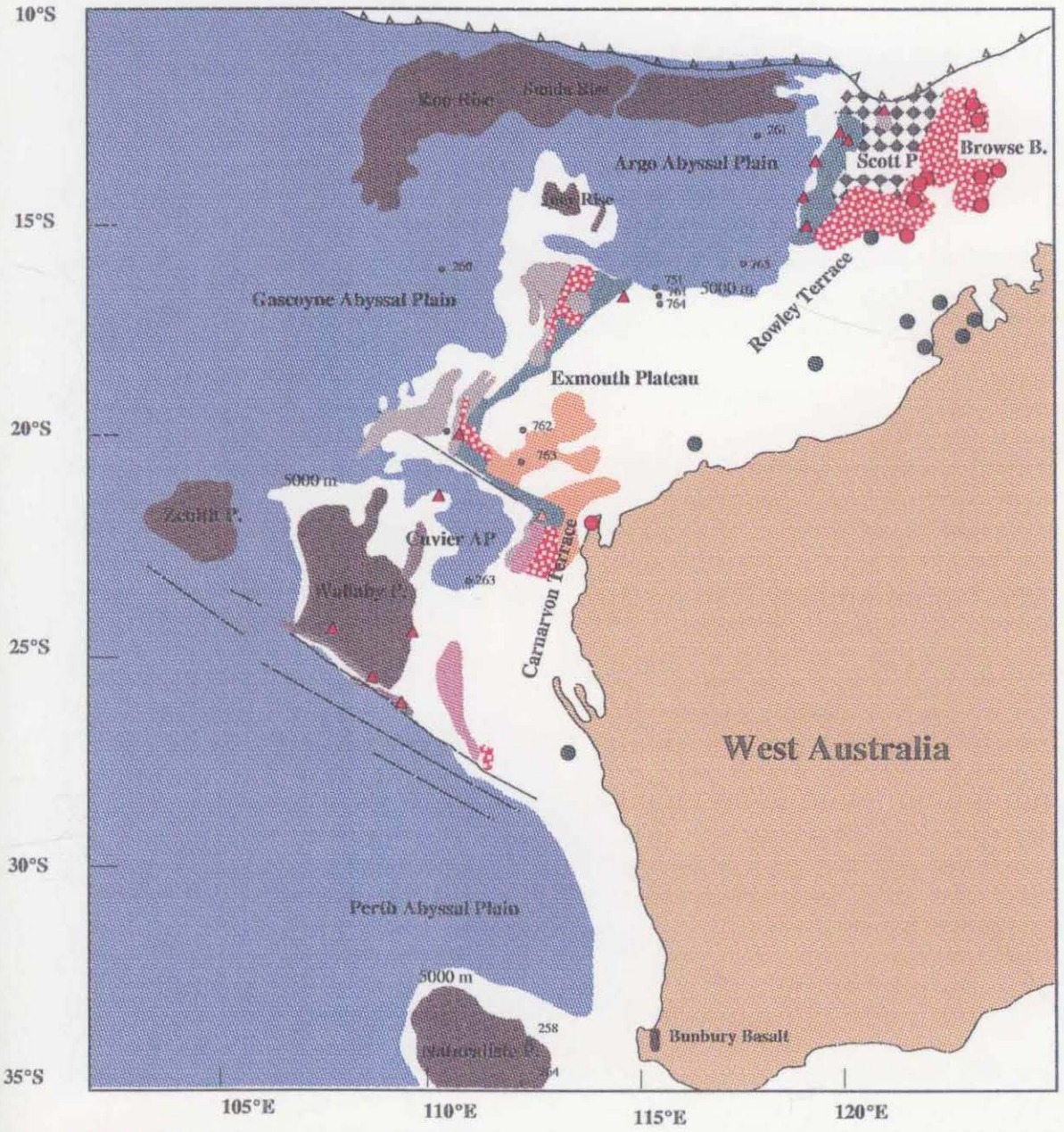

Fig. 1.3 Map of breakup and related volcanic provinces, major oceanic ridges and plateaus on the western Australian margin (modified after Planke and Symonds, in prep.).

Several different arguments have been presented in attempting to account for the volcanism along the western Australian margin. The Bunbury Basalt (Figure 1.3) which erupted at ~130 and 123 Ma has a strong geochemical signature of continental crust reflecting interaction of mantle-derived basaltic magma with continental lithosphere (*Frey et al.*, 1996). If there is a genetic relationship between the plume and the Bunbury lavas, the Kerguelen plume affected a very large region, incubated for a long time below the western Australian lithosphere prior to formation of LIPs (*Kent*, 1991). The Naturaliste Plateau (Figure 1.3) has been related to the early evolution of the Kerguelen mantle plume source (e.g., *Davies et al.*, 1989, *Coffin and Eldholm*, 1992, *Storey et al.*, 1992). Geochemical studies of lavas from the Naturaliste Plateau suggest a significantly greater proportion of continent-derived material compared to other products of the Kerguelen hotspot (*Mahoney et al.*, 1995). Accepting a Kerguelen plume origin for the Naturaliste Plateau the incorporation of continental lithospheric material was possible via (1) the entrainment into the plume of isotopically distinct, non-plume material, or (2) the interaction of plume derived magmas with extraneous material at relatively shallow depths. *Hopper et al.* (1992) were not able to relate the formation of the Wallaby Plateau to known sources/hotspots. *White and McKenzie* (1989) suggested that the volcanism along the margin was associated with the breakup and was caused by a broad thermal anomaly generated by a single mantle plume. *Colwell et al.* (1994) argued that the emplacement of the Triassic to Early Cretaceous volcanics which includes areas of seaward-dipping reflectors, flows, sills, and possibly underplated material, can be explained by models involving convective partial melting (e.g. *Mutter et al.*, 1988) or dynamic mantle upwelling (e.g. *Holbrook and Kelemen*, 1993) without the necessity of a mantle plume. The authors invoked a combination

of a non-plume dynamic rift-related volcanism, including breakup and plume related, post-breakup volcanism.

1.3 Regional setting

The west and northwest margin of Australia is an old, sediment starved volcanic continental margin which formed as a result of multistage rifting and seafloor spreading during the Late Paleozoic and Early Mesozoic (*Bradshaw et al.* 1988; *Veevers*, 1988; *Baillie et al.*, 1995). It can be divided into four main segments: the Argo, Gascoyne, Cuvier and Perth margins (Figure 1.1). To the north, the Argo margin includes the Argo Abyssal Plain, the Browse and Roebuck (former offshore Canning Basin) basins. The Gascoyne margin extends from the southern margin of the Argo Abyssal Plain to the Cape Range Fracture Zone (CRFZ), incorporating the Northern Carnarvon Basin and Gascoyne Abyssal Plain. The Cuvier margin is delimited by the CRFZ and Wallaby-Zenith Fracture Zones (WZFZ) and includes the Southern Carnarvon Basin, the Exmouth Sub-basin, the Cuvier Abyssal Plain and the Wallaby and Zenith plateaus. Finally, the Perth margin extends from the (WZFZ) to the Naturaliste Plateau in the south and includes the Perth Basin, the Perth Abyssal Plain and the Naturaliste Plateau.

1.3.1 Phanerozoic basins

In the following, a brief description of basins offshore western Australia (Figure 1.4) from north to south is given primarily based on *Hocking et al.* (1994). The Browse Basin extends from the Roebruck to the Bonaparte basins, and contains Permian, Mesozoic and Cainozoic rocks in a succession that reaches up to 17 km in thickness. It is considered to have formed either as a passive-margin rift-basin associated with the breakup of Gondwana (e.g. *Willis*, 1988), or as a lower plate rifted margin province during a major Late Carboniferous-Early Permian extension (*O'Brien et al.*, 1993).

The Roebuck Basin represents the offshore Canning Basin (*Horstmann and Purcell*, 1988). The basin is formed from several 'stacked' basins (*Stagg and Collwell*, 1994). A northeast-trending passive margin basin of Late Palaeozoic and Mesozoic age overlies a major northwest-trending intracratonic basin of mainly early Palaeozoic age with the boundary between these two systems being of Late Carboniferous age.

The Northern Carnarvon Basin consists of the main Mesozoic depocentres of the southern North West Shelf (e.g. Exmouth, Barrow and Dampier sub-basins, as well as the Exmouth Plateau) and contains a succession of ?Upper Permian, Mesozoic and Cainozoic sediments; Palaeozoic sediments have only been found along the southern margin of the basin. The basins previously discussed, following *Bradshaw et al.* (1988) and *Cockbain* (1989), are grouped into the Westralian Superbasin together with the offshore part of the Bonaparte Basin (not discussed in this study).

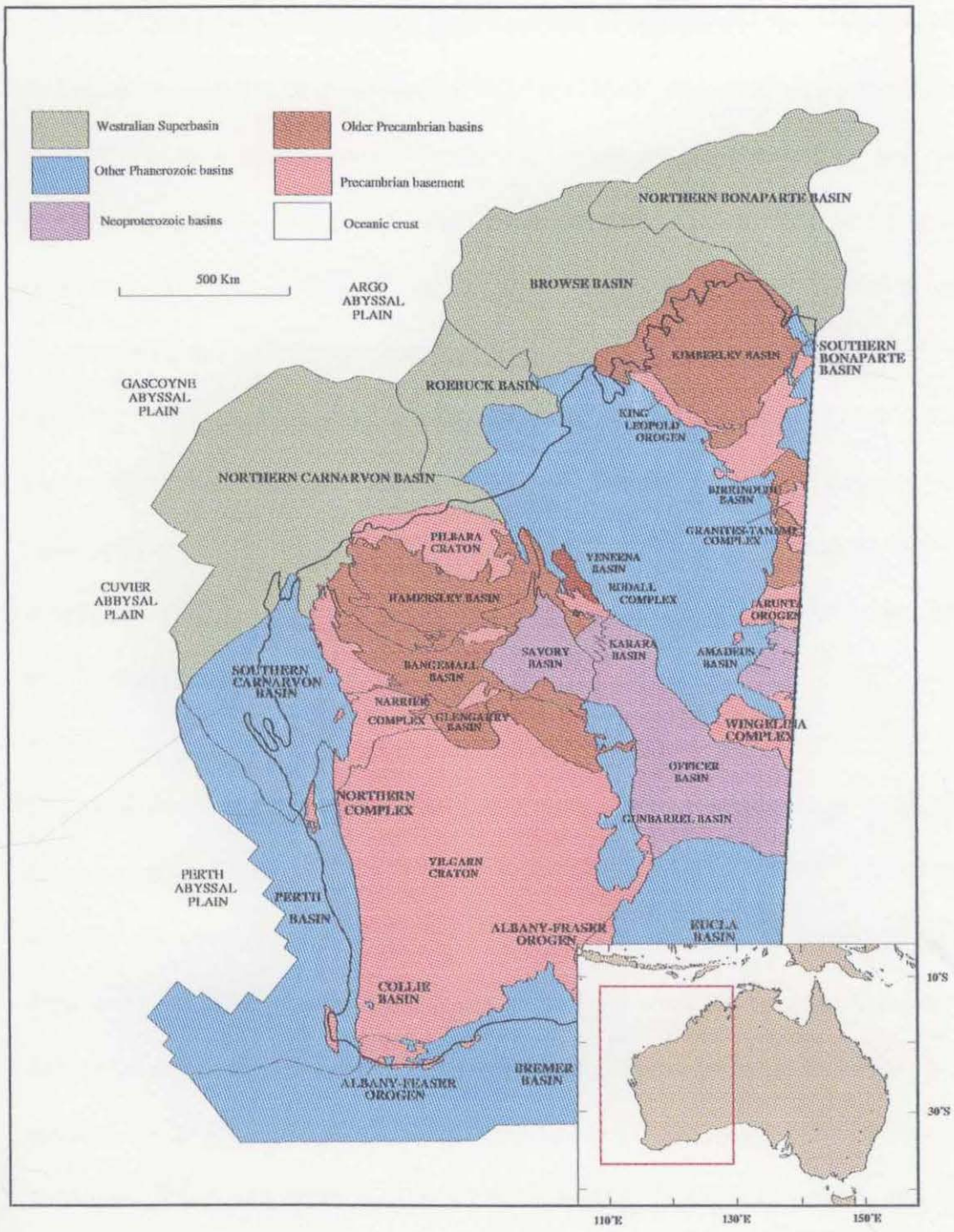

Fig. 1.4 Major structural elements in the Western Australian margin and adjacent abyssal plains (modified after Hocking et al., 1994).

The Southern Carnarvon Basin, originally referred to as the North West Basin (*Maitland and Montgomery*, 1924), was renamed the Carnarvon Basin by *Gentilli and Fairbridge* (1951), and adopted by *Condon* (1954). This term was extended in the 1960's to the southern North West Shelf as well as the adjacent onshore area and described by *Condon* (1954, 1965, 1967, 1968) and later re-defined by *Hocking et al.* (1987) and *Hocking* (1990). It is equivalent to the 'Palaeozoic sub-basins' of *Thomas and Smith* (1976) and describes the southern, primarily onshore, portion of the Carnarvon Basin. The basin contains Silurian, Devonian and Early Carboniferous-Permian sequences. A westward-thickening veneer of Cretaceous and Cainozoic rocks is present over the western half of the basin. The basin developed initially as northward trending rift-basin in the Upper Ordovician-Silurian and has been essentially inactive since the latest Permian.

The offshore Perth Basin was contiguous with the Carnarvon Basin until the development of the modern continental margin (*Playford et al.*, 1976). The oldest sediments known within the basin are Ordovician or Silurian fluvial clastics, deposited prior to the segmentation of the Perth Basin from the Southern Carnarvon Basin (*Hocking*, 1990), with no evidence of a Devonian sequence. The section also contains Silurian, Upper Carboniferous-Permian, Mesozoic and Cainozoic sequences. There was continuing deposition over the northern boundary, into the Southern Carnarvon Basin. The Perth Basin has a history of rifting that extends from the Early Permian up until the final separation of Greater India and Australia during the Early Cretaceous (Neocomian). In the northern Perth Basin the initial phase of rifting in the Early and Late Permian was followed by a prolonged period of subsidence and deposition. A later phase of rifting during the Early Cretaceous

produced oblique-slip extension and reactivation of previous structures (*Marshall and Lee*, 1988).

1.3.2 Results from the Ocean Drilling Program (ODP) and Deep Sea Drilling Project (DSDP)

The major physiographic features of the Indian Ocean are shown in Figure 1.1, and were first described by *Laughton et al.*, (1970). The occurrence of many aseismic ridges and plateaus is an interesting feature of the eastern Indian Ocean. Some of these features have been shown to have shallow water, volcanic origin (Ninetyeast Ridge and the southerly escarpment of Broken Ridge). Despite several drilling attempts, the origin of the Naturaliste and Wallaby plateaus still remains obscure.

Deep Sea Drilling Project (DSDP) sites drilled by the Drilling Vessel (D/V) *Glomar Challenger* during cruise Legs 22 (sites 211 - 217), 26 (sites 252 - 258), and 27 (sites 259 - 263), and Ocean Drilling Program (ODP) sites by the D/V *Joides Resolution* during cruise Legs 121 (sites 752, 754, 755 and 758), 122 (sites 759 - 764) and 123 (sites 765 and 766) provide direct geological age control throughout the eastern Indian Ocean. The description of the sites are given in *von der Borch et al.* (1974) for DSDP Leg 22, *Davies et al.* (1974) for DSDP Leg 26 and 27, *Pierce et al.* (1989) for ODP Leg 121, *von Rad et al.* (1990) for ODP Leg 122, and *Gradstein et al.* (1992) for ODP Leg 123. Below is a brief synthesis of the DSDP and ODP cores as they relate to the features of the eastern Indian Ocean (i.e. palaeobathymetry, regional unconformities, etc.):

- Ninetyeast Ridge (sites 214, 216, 217, 253, 254 and 758) is an elevated linear crustal feature of a shallow-water volcanic origin, Late Cretaceous to Eocene age and is considered to belong tectonically to the Indian Plate.
- Broken Ridge (sites 255, 752, 754 and 755) is a Late Cretaceous shallow marine carbonate platform that was uplifted above sea level and subsequently eroded during the initiation of the Southern Indian Ridge in the middle Eocene. Since then Broken Ridge has subsided and accumulated pelagic carbonates.
- The Naturaliste Plateau (sites 258 and 264), considered to be a submerged western extension of the southwest Australian continental margin, has been an area of quiet pelagic sedimentation with gradual shoaling during the later part of the Cretaceous and uplift and erosion in the early Eocene.
- The Wharton Basin (sites 211, 212, 213, 256), including the Perth (site 257 and 259), Cuvier (site 263), Gascoyne (sites 260 and 766), and Argo (sites 260, 759, 760, 761, 764) abyssal plains was formed by the opening of the Indian Ocean during the Early Cretaceous and has progressively deepened since the Late Palaeogene.

Regional hiatuses in sedimentation based on drilling results and recognized in the Indian Ocean are centered on the Late Cretaceous, early Tertiary and Oligocene (*Luyendyk et al.*, 1972). The upper limit of the Oligocene and younger hiatus is in the late Miocene or Pliocene, the upper limit of the early Tertiary hiatus in the early Eocene and that of the Late Cretaceous in the Campanian. These hiatuses are either expressed as true disconformities or are implied by the existence of dissolution facies and deposited as condensed series. Pelagic sediments have been deposited

since the Late Cretaceous with volcanic activity affecting the deposition in limited areas.

1.4 Purpose and scope of this study

The syn-rift and post-rift magmatism on the western margin of Australia is still not well understood. This is despite the existence of models which attempt to relate the magmatism to a mantle plume (e.g. *Davies et al.*, 1989; *White and McKenzie*, 1989) and alternative origins (e.g. *Mutter et al*, 1988; *Holbroock and Kelemen*, 1993). For example none of these models have taken into account the time and origin of the later major uplift undergone by the southern part of the Exmouth Sub-basin and the Bernier Platform.

Interpretation of magnetic lineations in the western Australian margin continuously improved as new magnetic data were acquired. Although the most recent interpretation of magnetic anomalies in the Argo Abyssal Plain (*Sager et al.*, 1992) appeared to confirm the general opening history as inferred by earlier models, the west to west-northwest trends of the basement structure revealed by seismic data (*Gopala et al.*, 1994) is inconsistent with the N70°E direction of seafloor spreading.

Several reconstruction models have been developed for the eastern Indian Ocean since the first trial (*Du Toit*, 1937), based on compilations of magnetic anomaly data and fracture zone traces from bathymetric and satellite altimeter data (e.g. *Smith and Hallam*, 1970; *Powell et al.*, 1980; *Royer and Sandwell*, 1989). Unlike the Tertiary

and Late Cretaceous evolution of the Indian Ocean (0-84 Ma), reconstructions for the early opening are still poorly constrained (*e.g. Lawver et al.*, 1991, 1992; *Royer and Coffin*, 1992). The kinematics established by *Royer et al.* (1992) in the most recent plate reconstruction model in the Indian Ocean offer no detail regarding the half-spreading rates used between anomaly C34 and M0 for the Wharton Basin. A simple computation of the half spreading rate in the Cretaceous Quiet Zone (anomalies M0 - C34) would lead to incompatible results on different segments along the western Australian margin like an extremely high value of the half-spreading rate in the Perth Basin. An interpreted mid-Cretaceous extinct spreading axis (*Markl*, 1974; *Powell et al.*, 1988) west of the Perth Abyssal Plain was included in the reconstruction but cannot solve the problem for the entire area.

The present study attempts to resolve some of these problems by defining a better constrained reconstruction of the eastern Indian Ocean in Chapters 2 and 3. A new tectonic model for this area is established by using the new satellite gravity grid (*Sandwell and Smith*, 1997), corroborated with existing magnetic and bathymetric data. Also the development of a mantle plume related model accounts for the magmatic and ridge propagator aspects.

Chapter 2 includes an analysis of the synthetic anomalies used in this study based on the *Gradstein et al.* (1994) time scale and identification of magnetic anomalies and fracture zones on the four segments of the western Australian margin (the Argo, Gascoyne, Cuvier and Perth segments) and southern Wharton Basin. It also incorporates a description of the propagating ridge model used in the interpretation of conjugate magnetic anomalies identified on accreted Indian Plate accreted to the

Australian Plate. Based on these results, Chapter 3 outlines the inferred spreading histories of the abyssal plains and the adjacent Wharton Basin and their parameterization: spreading rates are calculated, new stage and finite poles are determined and synthetic flowlines are computed. Using the new poles of rotation the position of the Indian, Antarctic and Australian plate are calculated in an absolute plate motion frame at eight different times after breakup. Chapter 4 includes a seismic interpretation of the major sequences (Triassic to Tertiary) encountered on the Carnarvon Terrace, as well as breakup related volcanic intrusions. With these results in Chapter 5 a mantle plume scenario is tested as a possible explanation for the uplift of the Bernier Platform and the southern part of the Exmouth Sub-basin as well as the origin of the excessive pre- and post-breakup volcanism (continental intrusions and oceanic plateaus respectively). A plume-trail origin is one of the hypotheses taken into account for the formation of the Wallaby and Zenith plateaus. The model of the complex volcanic evolution of the margin and adjacent abyssal plains and basin are summarized in Chapter 6 along with an outlook for future research in this area.

CHAPTER 2

Seafloor spreading history in the eastern Indian Ocean

In this chapter magnetic, satellite-derived gravity anomaly and topography data are combined to determine the structural trends in the abyssal plains adjacent to the western Australian margin, and in the Wharton Basin. Information from DSDP/ODP sites was also utilised for crustal age constraint.

2.1 Data processing and presentation

Magnetic data used in this study were obtained from several sources (see Appendix 1a and 1b). Aeromagnetic data from Operation Seascan (OS) were provided by Dr. W.W. Sager (Texas A&M University). Other marine geophysical data were procured from the National Geophysical Data Center in Denver, Colorado, USA (NGDC) archives, and the Australian Geological Survey Organisation (AGSO). In addition, five magnetic profiles from HMAS Cook were digitized from publications (*Veevers et al.*, 1985). Appendix 1 lists the source, identification number, navigation method, and types of available data for each survey used in this study.

Most of the magnetic data were previously interpreted in *Veevers et al.* (1985), *Fullerton et al.* (1989) and *Sager et al.* (1992). Five magnetic anomaly profiles collected by AGSO in 1994 across the Wallaby Plateau were added to the existing database. Figure 2.1 displays all marine geophysical and aeromagnetic data tracks used in the interpretation superimposed on the satellite derived gravity anomaly grid.

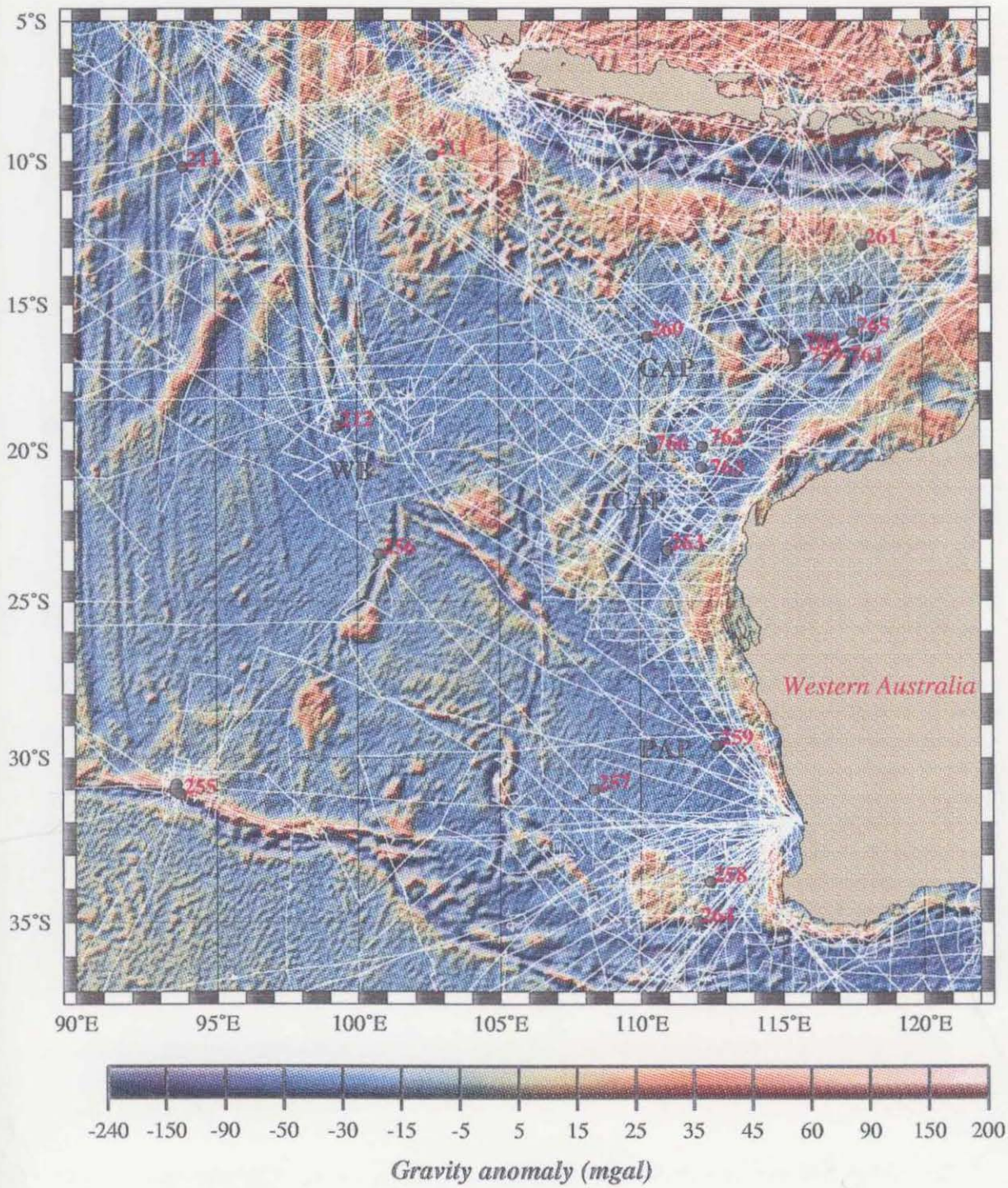

Fig. 2.1 Satellite-derived gravity anomaly grid (mgal). White lines identify marine geophysical and aeromagnetic data tracks obtained from NGDC, BMR/AGSO, and other sources listed in Appendix 1. Black dots represent DSDP and ODP sites. Abbreviations are: AAP, GAP, CAP and PAP - Argo, Gascoyne, Cuvier and Perth abyssal plains, WB -Wharton Basin.

All of the magnetic data are total field intensity values measured with proton-precession magnetometers and reduced to magnetic anomaly values using various versions of the International Geomagnetic Reference Field (IGRF90). The aeromagnetic data were measured at an altitude of 305 m. Four different types of navigation were used in the course of data acquisition. The flights were positioned by inertial navigation. Ship tracks were located by both celestial (40%) and Doppler or GPS satellite (60%) methods. For a broad-scale study of magnetic lineations such as this, navigational errors of less than a few kilometers are insignificant. This level of accuracy is provided by the Doppler satellite, GPS and inertial navigation systems. Although celestial and inertial navigation methods are not as accurate as satellite navigation, the errors of all of these techniques in this area are less than a few kilometers (there are no major misties between lines acquired with different types of navigation).

For the identification and correlation of the magnetic anomalies, the following processing stream was adopted:

- ship tracks were plotted onto a Mercator projected basemap;
- residual magnetic anomalies were plotted at 45° azimuth (measured clockwise from north) to the ship track;
- stacked magnetic profiles were used to compare anomalies and seafloor spreading rates with synthetic profiles;
- all existing data were interpreted jointly; trends of magnetic anomaly lineations and discordant features were constrained by gravity anomaly data (e.g. fracture zones, abyssal hills and ridges), seismic reflection data (basement structures), bathymetry data (possible extinct ridges), DSDP and ODP results (age control).

2.2 Time scale

In previous studies of the oceanic crust adjacent to the Australian margin, geomagnetic time scales were based on that of *Harland et al.* (1982). For the present study, two geomagnetic reversal time scales were used: the *Cande and Kent*'s (1995) time scale for the Cenozoic sequence and *Gradstein et al.*'s (1994) time scale for the Mesozoic sequence. One of the reason for the construction of a new time scale for the Mesozoic was that new radiometric ages have become available since 1989 (65 new Triassic, Jurassic and Cretaceous age dates). Improvements were also made in the calibration of stages, standard zones and magnetic polarity reversals and in interpolation techniques for sparse age control. The geomagnetic reversal time scale was used to determine spreading rates and to assign absolute ages to the magnetic isochrons. Appendix 2 shows the combined polarity time scale of *Cande and Kent* (1995) for the Present – Early Cretaceous "C-sequence" (0 - 83.5 Ma) and the timescale of *Gradstein et al.* (1994) for the Early Cretaceous – Late Jurassic "M-sequence" (115.3 – 159.0 Ma) used in this study.

2.3 Synthetic magnetic anomalies

Total intensity magnetic data recorded over oceanic crust reflect the present day magnetic field of remanently magnetized blocks due to the reversal chronology, the magnetic response due to variations in ocean floor topography and properties of magnetization. However, the effects of topography and magnetization properties are

minor compared with magnetic anomaly data due to reversals in the magnetic field. Theoretical foundations and principles established for modeling marine magnetic anomalies by *Bott* (1967), *Schouten* (1971) and *Schouten and McCamy* (1972) as well as the "theta method" of *Shouten and Cande* (1976) are still used today.

Synthetic anomaly analysis assumes that magnetized bodies in the ocean floor can be approximated as two dimensional structures confined by horizontal planes, because the anomaly patterns are fairly continuous parallel to the spreading axis. The magnetic sources are near the surface, with the oceanic depth defining the top horizontal plane, and the shallow Curie point isotherm within the crust defining the lower plane. Both depths are of the same order of magnitude (see Table 2.1). Another assumption used for modeling is that the direction of the magnetization is parallel with the central axial dipole field of the Earth, and that the magnetic and geographic poles coincide if averaged over geological time. With this simple model the skewnes (or degree of asymmetry) of the anomalies is measured by a phase parameter, θ (the "theta method" of *Schouten and Cande*, 1976). The skewness of anomalies is only dependent on the ambient field and remanent magnetization directions and the strike of the body (*Shouten and Cande*, 1976).

For identifying magnetic anomalies, synthetic sequences were computed for the geomagnetic reversal time scale of *Cande and Kent* (1995) and *Gradstein et al.* (1994). A two-dimensional magnetic modeling routine was used (see Table 2.1 and Figure 2.2).

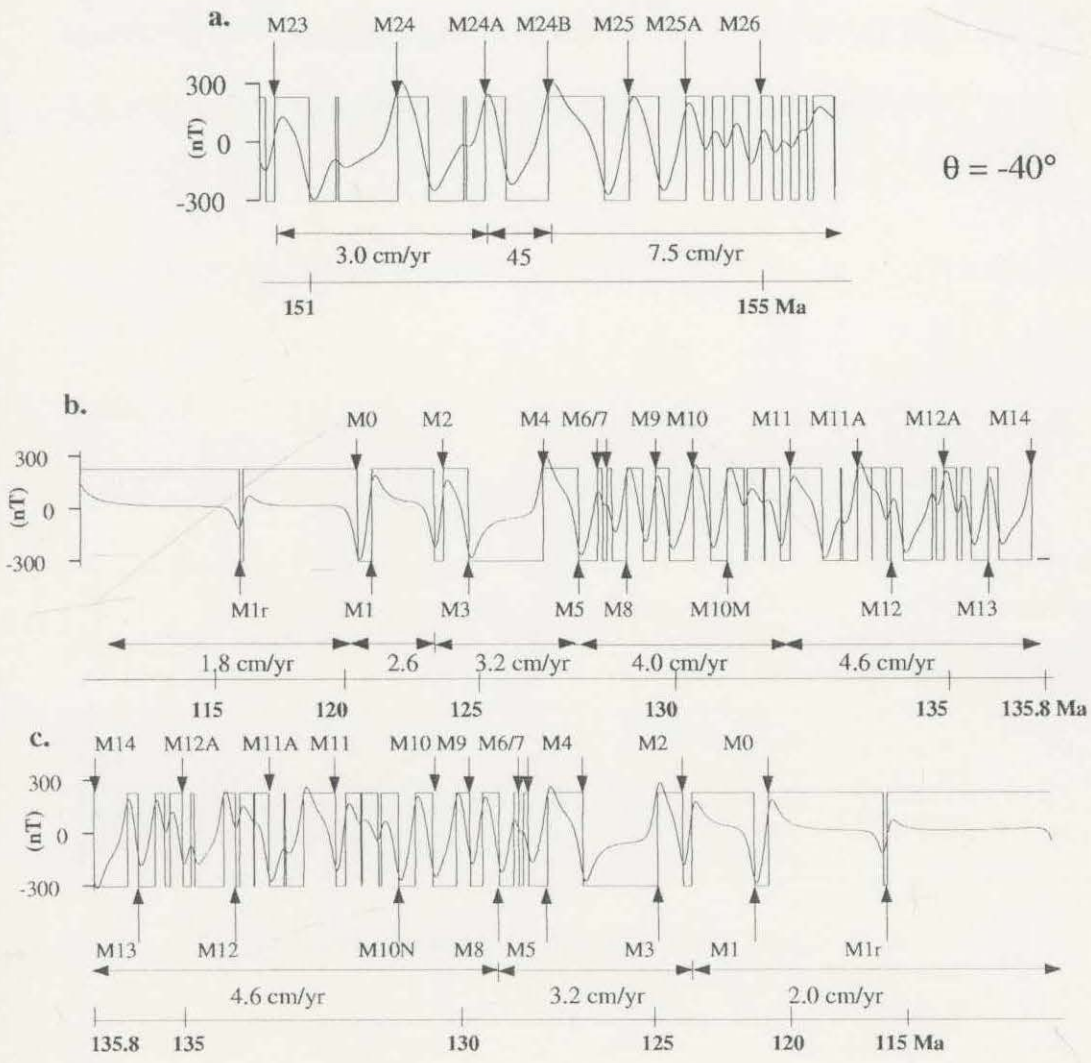

Fig. 2.2 Synthetic anomaly profiles used in interpreting magnetic anomalies in the Argo Abyssal Plain (profile a) and in the Cuvier Abyssal Plain (profiles b and c) by employing the combined Cande and Kent (1995) and Gradstein et al. (1994) time scale. Parameters used to generate synthetic magnetic anomalies are presented in Table 2.1.

As indicated in Table 2.1, the set of magnetic anomalies is projected along a profile direction perpendicular to the strike of the magnetized body. The present magnetic inclination (down is positive) of the surveyed area was read from an isoclinic chart and the present declination (clockwise is positive) from an isogonic chart. The remanent inclinations and declinations were calculated based on the position of two known paleopoles (paleolatitude and paleolongitude) for Australia taken from *Irving and Irving* (1982): one from the Cygnet Complex, Tasmania at 104 Ma (50.0°S and 158.0°E) and the other from Tasmanian Dolerite (west group) at 168 Ma (50.7°S and 174.5°E).

Table 2.1

Parameters used to generate synthetic magnetic anomalies

Abyssal Plain	Present field (°) Inc.	Decl.	Strike	Rem. field (°) Inc.	Dec.	Intens.(A/m)	Block depth (km) top	bottom	Half spreading rate * (cm/yr)
Argo	-46	1	45	-62	0	14	6	6.5	3.0 - 7.5
Gascoyne	-47	0	45	-65	0	12	6	6.5	2.2 – 4.0
Cuvier	-57	5	45	-67	0.5	12	6	6.5	1.8 – 4.6
Perth	-65	355	45	-68	0.5	10	6	6.5	2.0 – 3.6

* - *spreading rates are discussed in more detail in Chapter 3.*

Average seafloor spreading rates were determined by measuring the distance between magnetic isochrons in representative spreading compartments and by plotting distance versus age. The results were compared with calculated half spreading rates, and will be discussed in detail in Chapter 3.

2.4 Rift propagator model

Ridge jumps have been recognized in earlier interpretations in the Cuvier Abyssal Plain (*Larson*, 1977; *Larson et al.*, 1979; *Veevers et al.*, 1985) and in the Gascoyne Abyssal Plain (*Fullerton et al.*, 1989). The additional magnetic data have improved the interpretation by the recognition of curved "fracture zones" and lineations in the Gascoyne and Cuvier abyssal plains (*Fullerton et al.*, 1989) leading to the idea that they are the result of rift propagating events rather than simple ridge jumps. However, the model of *Fullerton et al.* (1989) is not consistent with the general understanding of the rift propagating process. For example, the distance between a particular anomaly and the ridge should increase in the same direction that the ridge propagates. This process is not shown by the schematic evolution of the ridge-system in their interpretation.

In order to illustrate the interpretation used in the case of conjugate magnetic anomalies, I present a schematic representation of the evolution of a propagating rift event (Figure 2.3). A propagating rift model was first developed by *Hey* (1977) and has been tested in various regions (e.g. *Wilson et al.*, 1984; *Hey and Wilson*, 1982, *Kleinrock and Hey*, 1989; *Brozena and White*, 1990).

A simplified description of a rift propagator includes a sequence of spreading center jumps propagating along a spreading center. Prior to each discrete jump, the new (growing) spreading center is connected to the old (dying) spreading center by a transform fault. With each discrete jump the previously active transform fault becomes inactive and together with the segment of the now extinct, old spreading

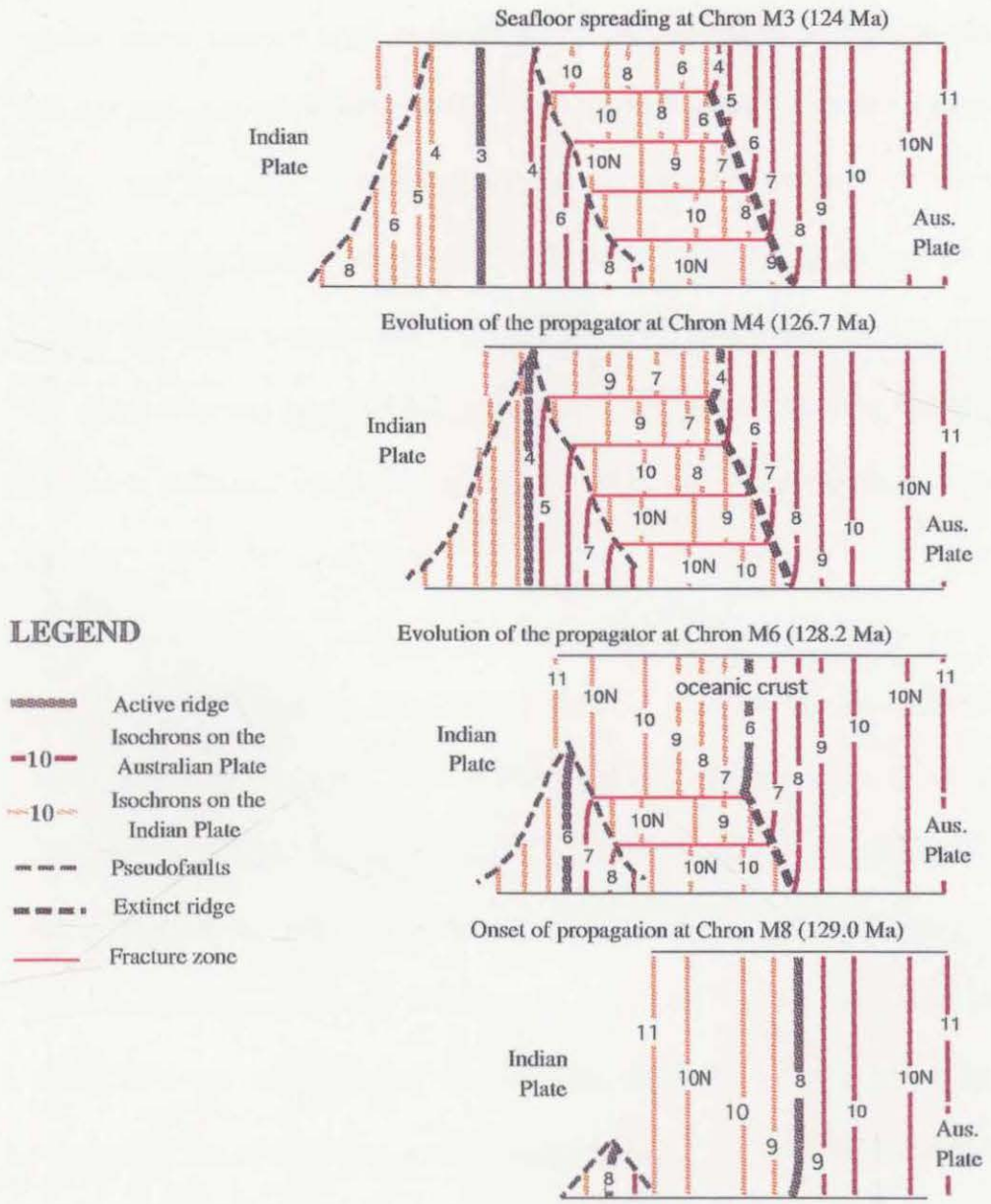

Fig. 2.3 Schematic representation of the evolution of a rift propagation event similar to the second propagation event in the Cuvier Abyssal Plain. In the begining the tip of the active ridge propagates to the north, accreting a small fraction of the Indian Plate to the Australian Plate. The pattern of the magnetic anomalies at that time consists of a continuous sequence of anomalies on the Australian and Indian plates, with the exception of the southern segment. The propagating and the retreating ridge are contemporaneous. The process continues step by step, successively accreting Indian oceanic crust onto the Australian Plate.

center is transferred to the conjugate plate. The position of the active transform fault moves with a distance equal to the length of the segment of the old spreading center that has just become extinct. In this model the relative direction of opening does not change and spreading is perpendicular to the transform fault. The fracture zone pattern (pseudofaults) that separates old oceanic crust from young oceanic crust creates a V-shape arrangement that can be easily recognised on the gravity map, if the entire sequence is preserved. The en-echelon fossil spreading centers resulting from this sequence of discrete jumps and the closest pseudofault are generally parallel.

The model in Figure 2.3 describes a possible scenario for the evolution of the northern part of the Cuvier Abyssal Plain. Initially, the tip of the active ridge north of a transform fault propagates to the northwest accreting a small fraction of the Indian Plate to the Australian Plate. The pattern of the magnetic anomalies at that time contains a continuous sequence of anomalies on the Australian and Indian plates with the exception of the southern segment. The propagating and the retreating ("extinct") ridges are contemporaneous. The process continues step by step as illustrated in Figure 2.3. The captured Indian Plate is separated from the Australian Plate by a sequence of fossil ridges to the east and a pseudofault to the west. The old Indian Plate that was not captured in this process is separated from the young Australian Plate by a second pseudofault that forms together with the previously described pseudofault in the V-shape arrangement. At the time of anomaly 4 the rift propagator ceases to be active. The three major elements left by the propagator are an extinct/failed ridge and two pseudofaults. Half of the V-shape structure generated by the two pseudofaults which would have originally been found

on the Indian Plate is lost due to the collision between the Indian and Eurasian plates.

2.5 Magnetic and gravity interpretation in the Eastern Indian Ocean

Within the study area, there are four abyssal plains (Argo, Gascoyne, Cuvier and Perth) and several submarine plateaus (Wallaby, Zenith and Naturaliste). The new satellite-derived gravity grid plays an important role in supporting the magnetic anomaly interpretation by displaying in more detail features whose structure and origin were only vaguely understood. In order to better describe their tectonic evolution, the interpretation was carried out on each abyssal plain separately, by combining results from magnetic, satellite-derived gravity, topographic and seismic (where available) surveys. These results were subsequently included and analysed in a regional tectonic plate reconstruction in Chapter 3.

2.5.1 The Argo Abyssal Plain

2.5.1.1 Previous work

The Argo Abyssal Plain is bounded to the north by the Java Trench and to the east and south by the submerged continental crust of the Scott and Exmouth plateaus and Rowley Terrace (Figure 2.4). A series of horsts, grabens and half-grabens (Wombat Plateau, Echidna and Emu spurs, Swan Canyon) are cut by major northeast and east-

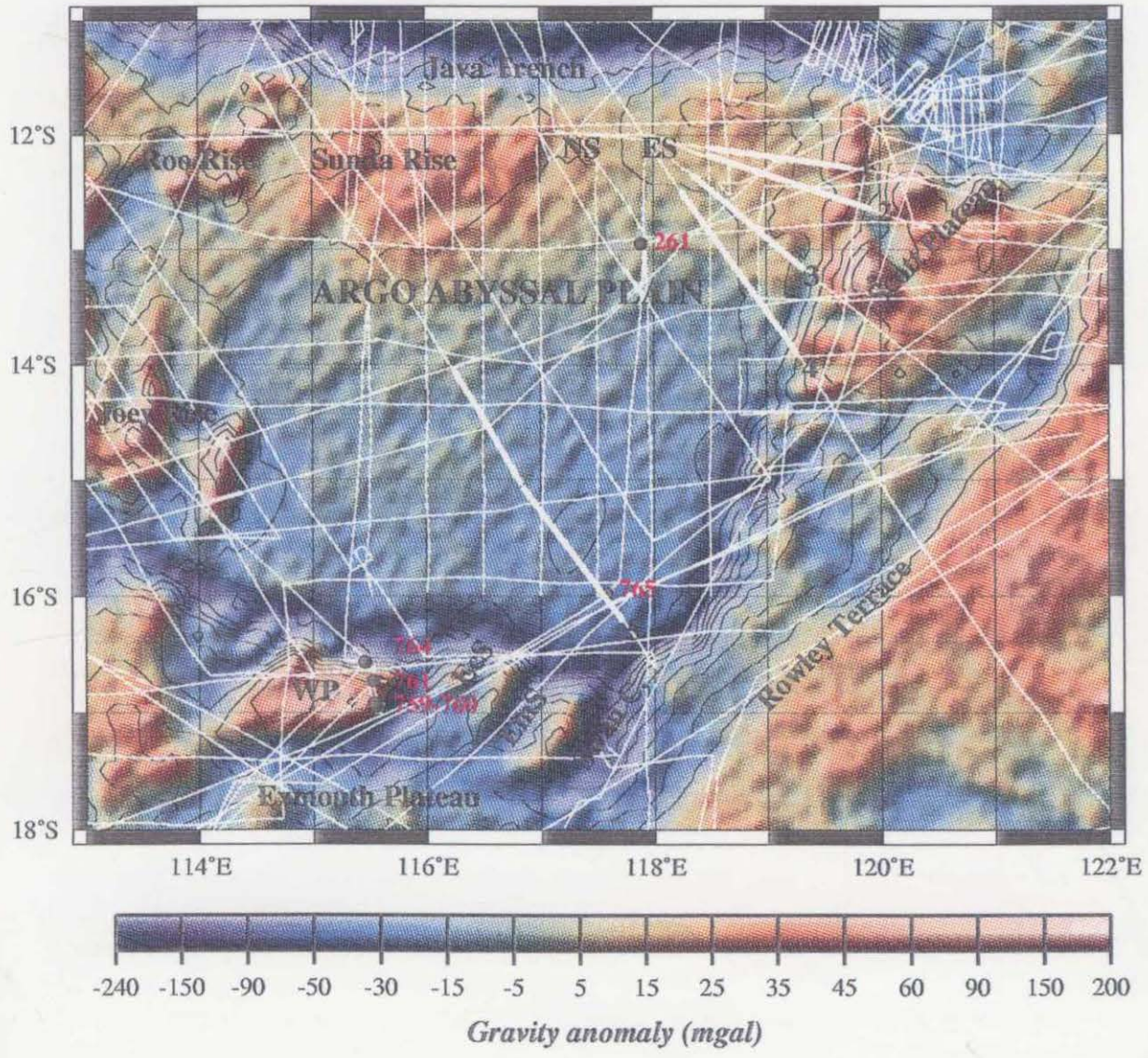

Fig. 2.4 Satellite-derived gravity anomaly grid (mgal) and bathymetry contours (500 m) of the Argo Abyssal Plain. White lines identify marine geophysical and aeromagnetic data tracks. Black dots represent DSDP and ODP sites. Abbreviations are: WP-Wombat Plateau, EcS-Echidna Spur, EmS-Emu Spur, Swan C.-Swan Canyon, NS-Northern Step, ES-Eastern Step. Highlighted profiles are displayed in Fig. 2.5.

trending, steeply dipping faults (*von Rad et al*, 1992; *Exon and Buffler*, 1992). To the west the basin is bounded by the Joey and Roo rises considered to be of volcanic origin *(Cook et al.*, 1978).

Magnetic lineation trendings approximately N60°E were first identified by *Falvey* (1972) as anomalies C22 - C32. The interpretation was tested by drilling at DSDP site 261. The sediments found ranged in age from Jurassic to Early Cretaceous and implied that *Falvey* (1972) misidentified the lineations. *Larson* (1975) reinterpreted the anomalies as sequence M22-M25, with the oldest chron nearest Australia. This interpretation was consistent with the late Oxfordian age estimated for basement at DSDP site 261 situated between anomalies M23 and M24. Further interpretations of the iochron patterns were later made by *Heirtzler et al.* (1978), *Powell* (1978), *Powell and Luyendyk* (1982), *Veevers et al.* (1985), *Fullerton et al.* (1989) and *Sager et al.* (1992). As a result, correlatable magnetic anomalies were found over nearly the whole basin. Most of these studies revealed similar anomaly patterns in the eastern, southern and central parts of the basin. The lineations were traced over most of the basin from the Scott Plateau westward to the Joey and Roo rises and northward from the Scott and Exmouth plateaus to the Java Trench. Problematic areas included the western and northern parts of the Argo Abyssal Plain. Although the most recent studies agreed that the anomalies from the southern side of the Joey Rise represent the M22 - M25 sequence, its northern part was interpreted in various ways. *Powell*'s (1978) and *Powell and Luyendyk*'s (1982) interpretation postulated a M5 - M14 sequence in this area. Because these anomalies have similar ages to those interpreted in the Gascoyne Abyssal Plain, but different trends, they postulated that a southward ridge jump occurred during the Early Cretaceous, forming a triple

junction off the northern Exmouth Plateau. *Fullerton et al.* (1989) preferred a simpler model, in which these anomalies were identified as the M16 - M25 sequence, separated from younger anomalies of the Gascoyne Abyssal Plain by a northwest-southeast trending system of transform faults. *Sager et al.* (1992) reviewed this last interpretation by examining two models for the area in discussion: the first model compared the magnetic lineations in the basin with a M0 - M11 sequence model while the second model used a M26 - M16 sequence model. The first model partially solved the initial age discrepancy between the oldest sediment recovered at site 765 (ODP Leg 123) and the crustal age inferred from the magnetic anomalies, but did not explain for example, the existence of M0 east of the Roo Rise. The correct model at the time appeared to be that developed by *Fullerton et al.* (1989) although it still does not explain the discrepancy between the ages of the oldest sediments at site 765 and that of the underlying lithosphere. This discrepancy was considered to be the result of extremely low Jurassic sedimentation rates in the Argo Abyssal Plain.

2.5.1.2 Interpretation

A reinterpretation of all available magnetic anomaly data jointly with satellite gravity anomalies, bathymetry and DSDP/ODP data was necessary in order to explain the linear, northwest-southeast trending, short-wavelength gravity anomalies visible in the satellite derived gravity anomaly grid (*Sandwell and Smith*, 1997). This direction agrees with a published basement structure map based on seismic data

(*Gopala et al.*, 1994) and disagrees with all published plate models for its formation, suggesting a west-northwest oriented direction of opening.

The correlation in the Argo Abyssal Plain was based on positive anomalies. Residual magnetic anomalies (profile locations in Figure 2.4) with amplitudes ranging between -300 and +300 nT were identified by visual comparison with the synthetic anomalies (Figure 2.5). The synthetic profiles in the Argo Abyssal Plain were calculated for three different average seafloor half-spreading rates: 7.5 cm/yr for the M25B - M32 sequence; 4.5 cm/yr for anomaly M24A; and 3.0 cm/yr for the M22A – M24A.

The relatively high-amplitude magnetic anomalies in the northwestern part of the basin were considered unreliable for magnetic anomaly interpretation, biased by the widespread volcanics in this area. The Roo Rise and the Joey Rise were previously interpreted as having a volcanic origin (*Cook et al.*, 1978). Recently acquired data strenghtened the theory (e.g. *Crawford and von Rad*, 1994) that the Scott Plateau represents a volcanic plateau of continental origin. This interpretation was based on ocean bottom seismometer data (OBS) and land refraction stations (4 stations) and combined with previously acquired magnetic, gravity, reflection and refraction seismic data (*J. Sayers*, 1997, AGSO/personal communication). The satellite-derived gravity anomaly grid shows a zone of continuous positive anomalies between the Roo Rise and the Scott Plateau trending mostly northwest – southeast, suggesting that the volcanic province probably extends along the entire northern part of the plain. Therefore, no interpretation was carried out in this part of the basin. Anomaly M22, as interpreted by *Sager et al.* (1992) may represent either the magnetic

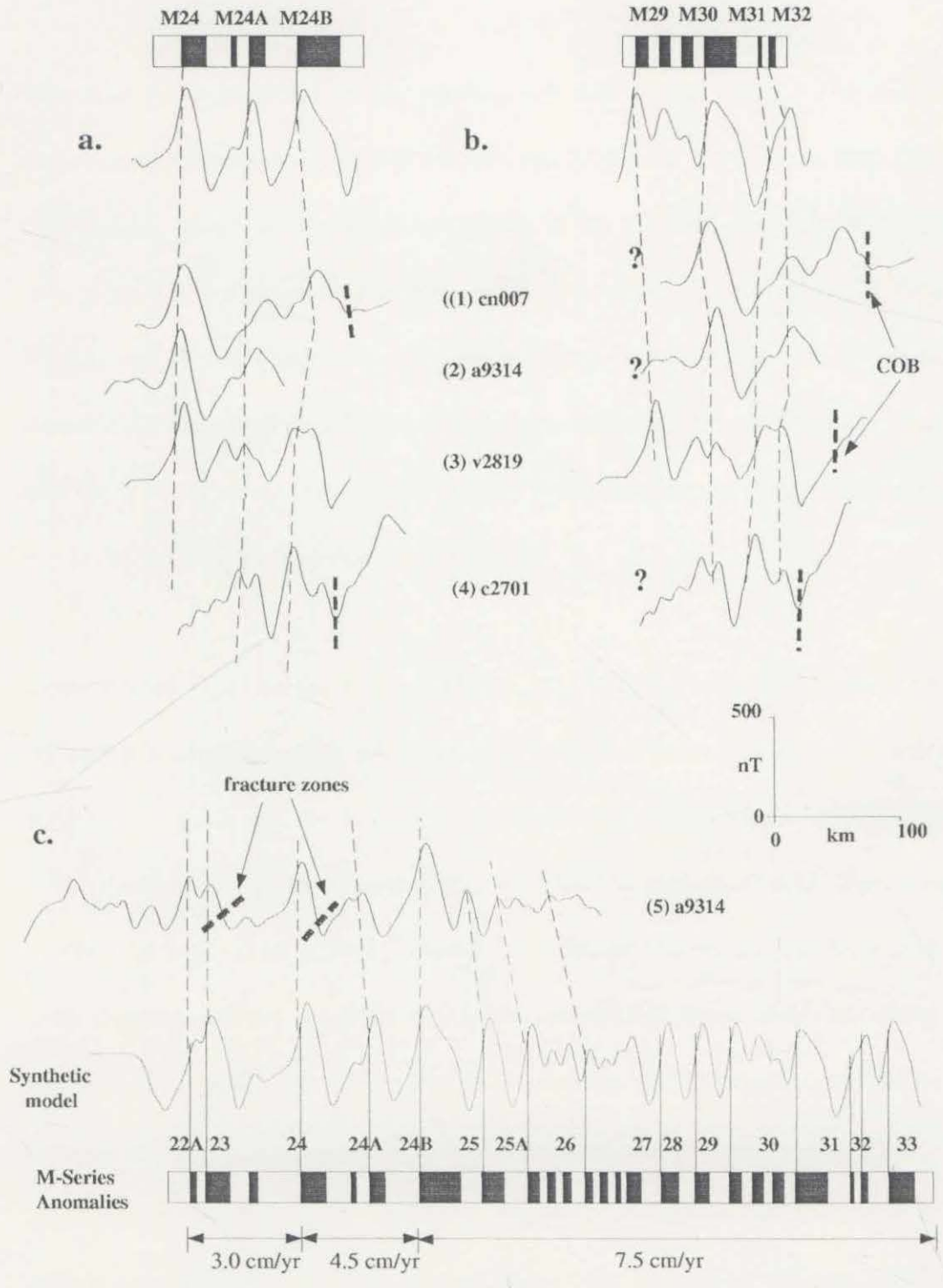

Fig. 2.5 Selected magnetic profiles and synthetic model for the magnetic lineations in a. and b. - the northeatern Argo Abyssal Plain and c.- central Argo Abyssal Plain (profile location in Fig. 2.4). The synthetic model and the ages of chrons is based on the Gradstein et al. (1994) time scale.

expression of an extinct ridge or a pseudofault. Another possibility is that this magnetic negative anomaly marks the outer limit of the volcanic province.

Two models were tested in the northeastern part of the basin. The magnetic sequences were compared with M24-M24B and M29-M32 synthetic models (Figures 2.5a and b). Both models have weaknesses: in the first case anomaly M24 can be interpreted along three of the tracks but none of the other two anomalies (M24A and M24B) can be interpreted with confidence, while in the second case the distance between anomaly M30 and M31 would decrease from north to south. It is possible that the second model is more likely but due to its uncertainty and lack of age control it was not included in the interpretation.

In the central Argo Abyssal Plain anomalies M22A-M26 were re-interpreted (Figures 2.6 and 2.7). In this region, relatively high-amplitude anomalies on the central side of the basin grade into low amplitude anomalies near the Australian margin (Figure 2.6). Some of the picks presented here are identical with those of *Fullerton et al.* (1989) and *Sager et al.* (1994) (Figure 2.5c). The anomalies that can be interpreted with most confidence are M24 and M24B, anomalies easily identified along the entire central basin. The interpretation follows the N45°E direction visible on the satellite-derived gravity anomaly grid in the entire basin. The fracture zones were identified by combining the offsets of magnetic anomalies and disruption in the gravity trend (Figure 2.7). Four fracture zones were labelled in this area, fracture D marking the southern limit of the plain. The southern and south - western part of the basin remain uninterpreted as a result of poor coverage and inappropriate direction of magnetic profiles, as well as the presence of volcanics.

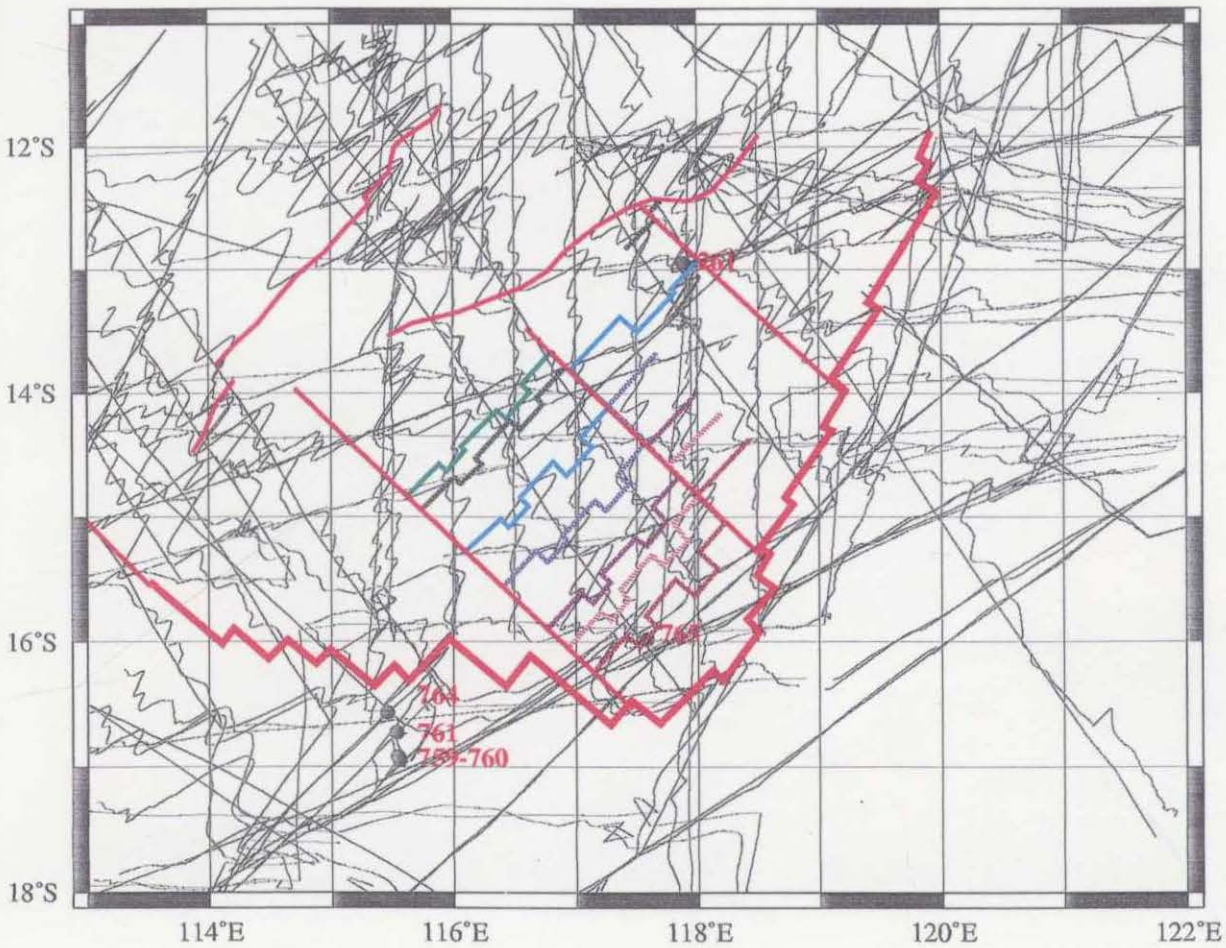

Fig. 2.6 Magnetic anomaly correlation in the Argo Abyssal Plain. Magnetic anomalies are ploted at 45 degrees to the ship track, which are shown as thin, solid black lines. Red lines represent COB and fracture zones (see Fig. 2.7 for anomaly legend).

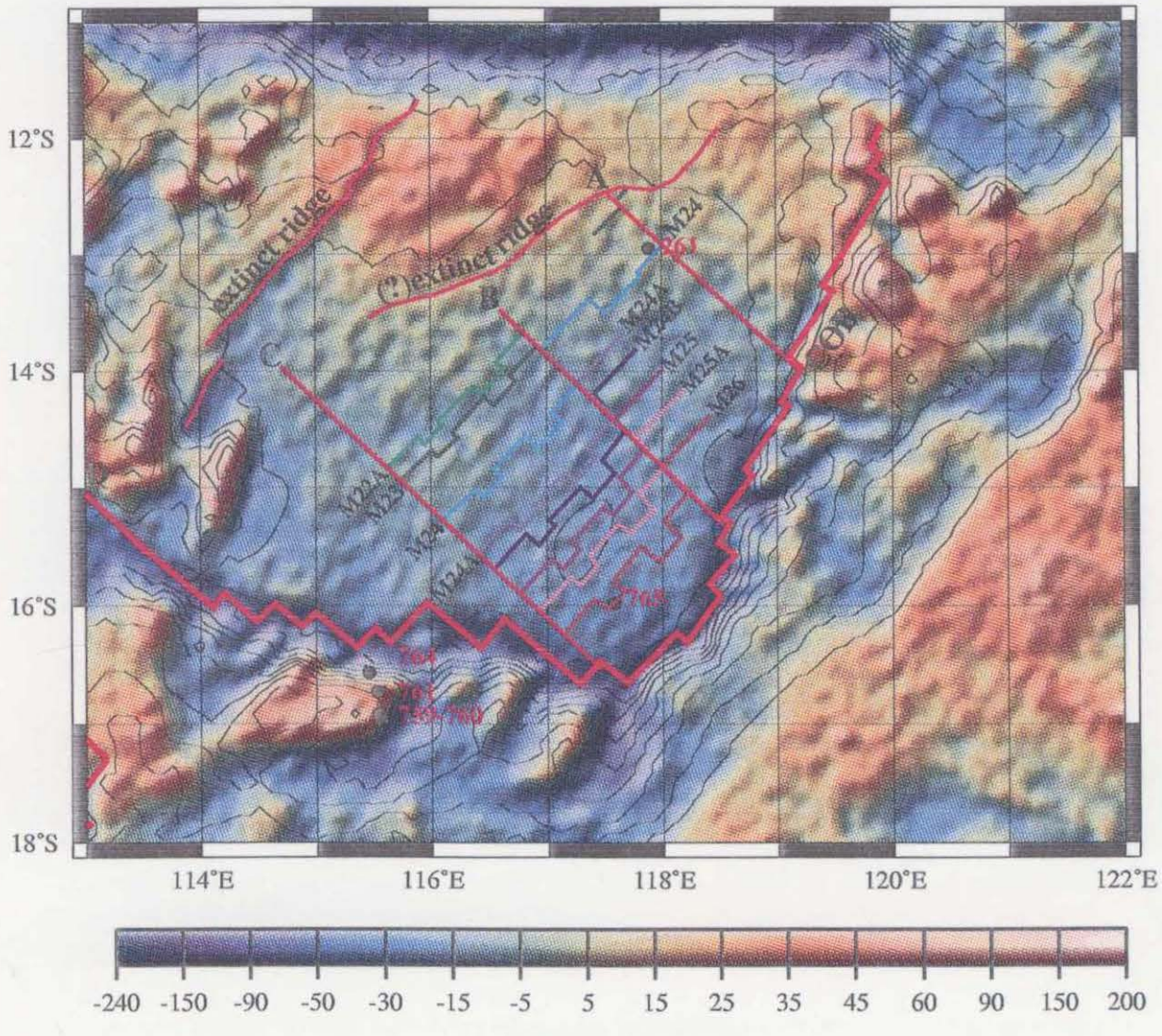

Fig. 2.7 Isochrons, COB and fracture zones (red) and extinct ridges (magenta) superimposed on the satellite-derived gravity anomaly grid (mgal) in the Argo Abyssal Plain.

During the interpretation one question was raised: Is it possible that the trends displayed by the satellite-derived gravity anomaly grid do not represent real geological features? In order to eliminate these uncertainties Figure 2.8 shows the satellite-derived gravity grid that displays areas where no satellite data were acquired. As clearly seen on this map the short-wavelength gravity lineations visible in the Argo Abyssal Plain are still present even if only those grid cells are shown that reflect satellite data.

To assess the resolution of the satellite-derived gravity and improvement gained by adding ERS-1 altimeter data, *Marks* (1996) has compared 7 well-navigated shipboard profiles with the satellite derived gravity anomaly grid used in this study. She found agreement (0.5 coherence) to wavelengths of 23-30 km for this Geosat/ERS-1 grid and 26-30 km for the Geosat-only grid. A comparison between the satellite-derived gravity anomaly grid and ship gravity anomaly in the study area (Figure 2.8a) shows that there is a good agreement between the two profiles including the short-wavelengths that the present interpretation relies upon.

An extinct ridge was identified east of the Roo Rise based on combined analysis of gravity, magnetic and topography data along two profiles (Fig. 2.9). It is not possible to deduce the age of this feature as no interpretation was carried out west of anomaly M22A. It is likely to be younger than anomaly M22A since the ocean floor became younger to the northwest. As oceanic crust becomes deeper it becomes older.

Therefore one would expect the topography to show an increase in depth on both sides of the ridge if it has not been affected by intruded material. Topography data

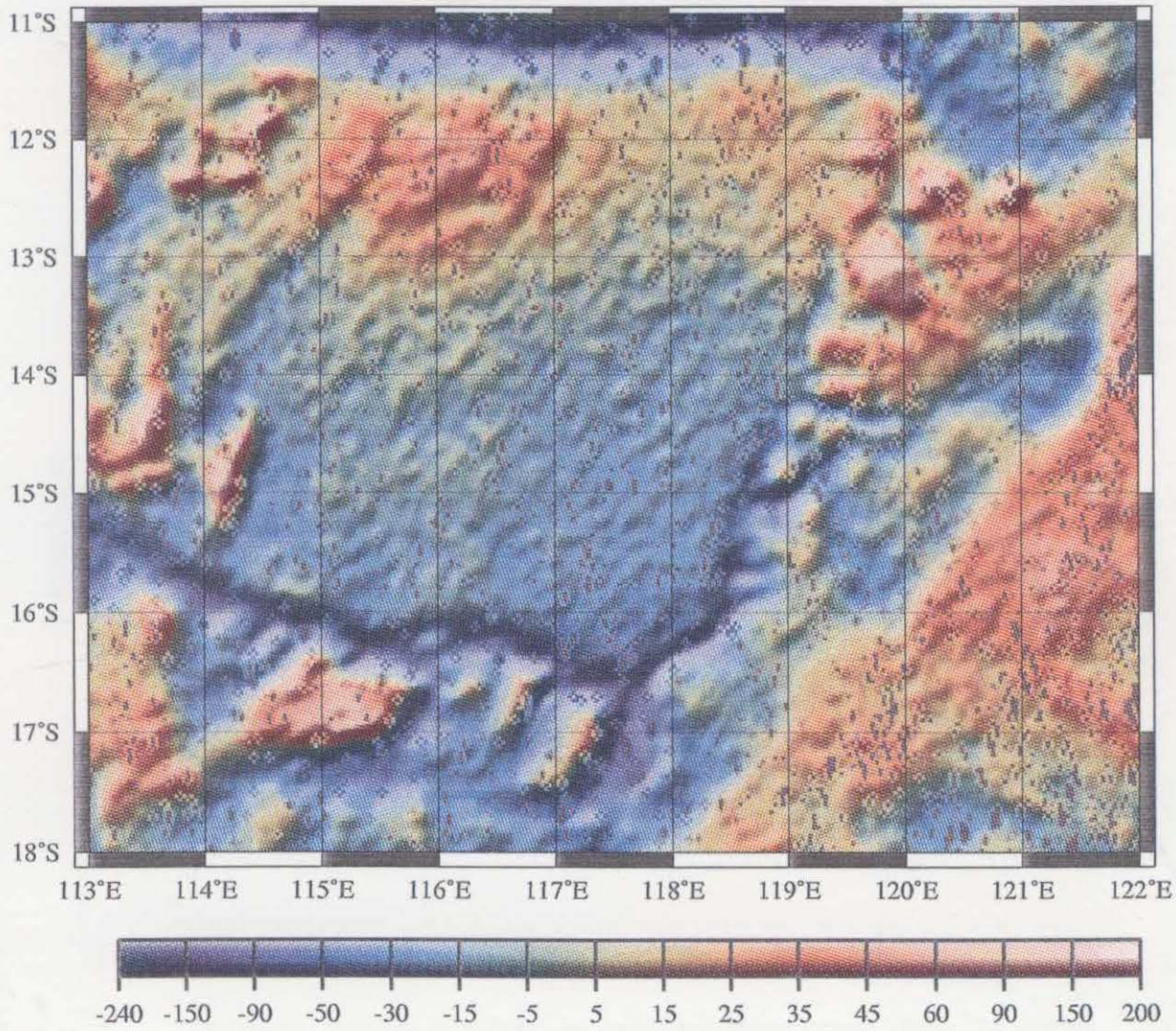

Fig. 2.8 Satellite-derived gravity anomaly grid (mgal) showing areas where no data exist (grey spots).

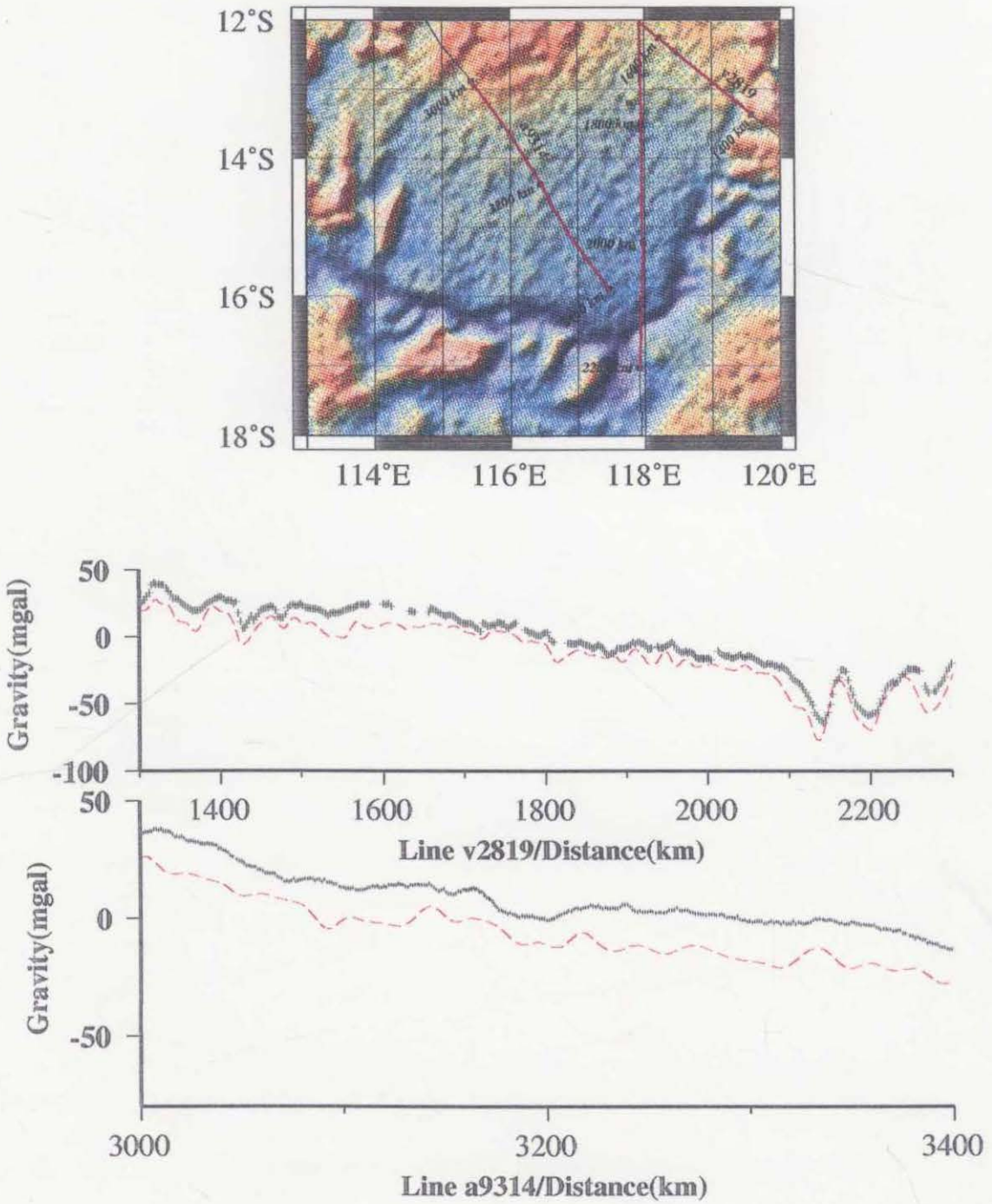

Fig.2.8a Comparison between the satellite gravity (red line) and ship track gravity (black stars). The small map shows the location of selected ship tracks.

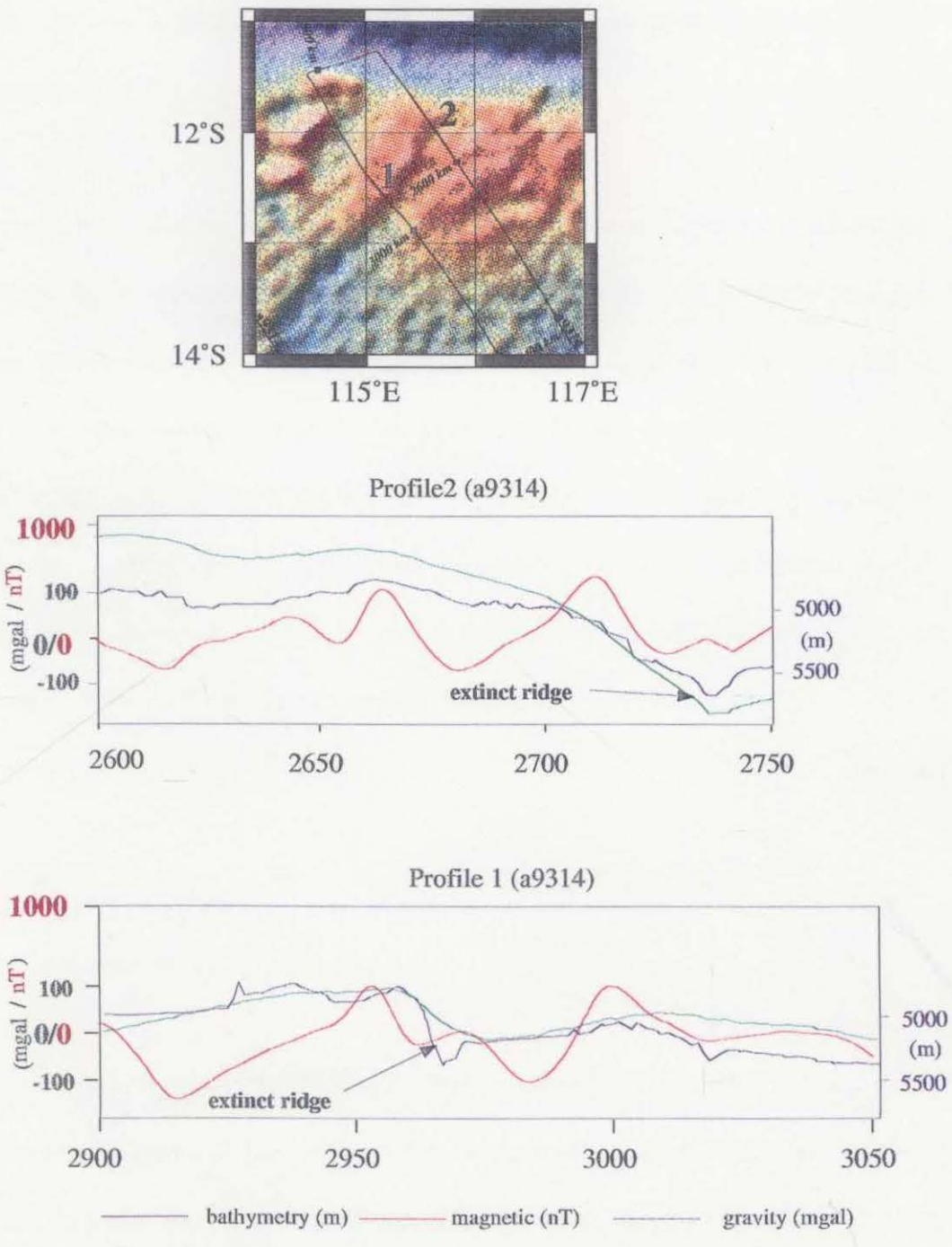

Fig. 2.9 Magnetic, gravity and topography profiles correlation along an interpreted possible extinct ridge. A good correlation is observed between the topography and gravity troughs on both profiles.

on both profiles (Figure 2.9) show increasing depth on both sides of the trough, in agreement with the assumption of an extinct ridge at this location. The magnetic profile, as one would expect, shows a symmetric anomaly centered on the topography trough.

The continental-oceanic boundary (COB) in the Argo Abyssal Plain was interpreted based mainly on satellite derived gravity anomaly grid. The COB follows a staircase shaped gravity anomaly trough, which according to the present interpretation in general becomes younger towards the south. It appears that the margin is not a simple rifted margin, but a combination of rifted segments linked by transform segments. This interpretation explains the absence of Jurassic sediments in the north-western Exmouth Plateau as well as the development of the horsts, grabens and half-grabens on the northern Exmouth Plateau (see Figures 2.4 and 2.7).

2.5.2 The Gascoyne Abyssal Plain

2.5.2.1 Previous work

The Gascoyne Abyssal Plain (Figure 2.10) is separated from the Argo Abyssal Plain to the north by Roo and Joey rises, to the east is bounded by the Platibus Spur and the Exmouth Plateau. To the south there is no clear boundary between Gascoyne and Cuvier abyssal plains. Based on only two magnetic profiles, *Falvey* (1972) correlated magnetic lineations trending N60°E in the Gascoyne Basin, identified as Cenozoic anomalies C24 - C31. The identity of anomalies was disputed by *Powell* (1978), who agreed with the trend, but made no attempt to interpret the anomalies.

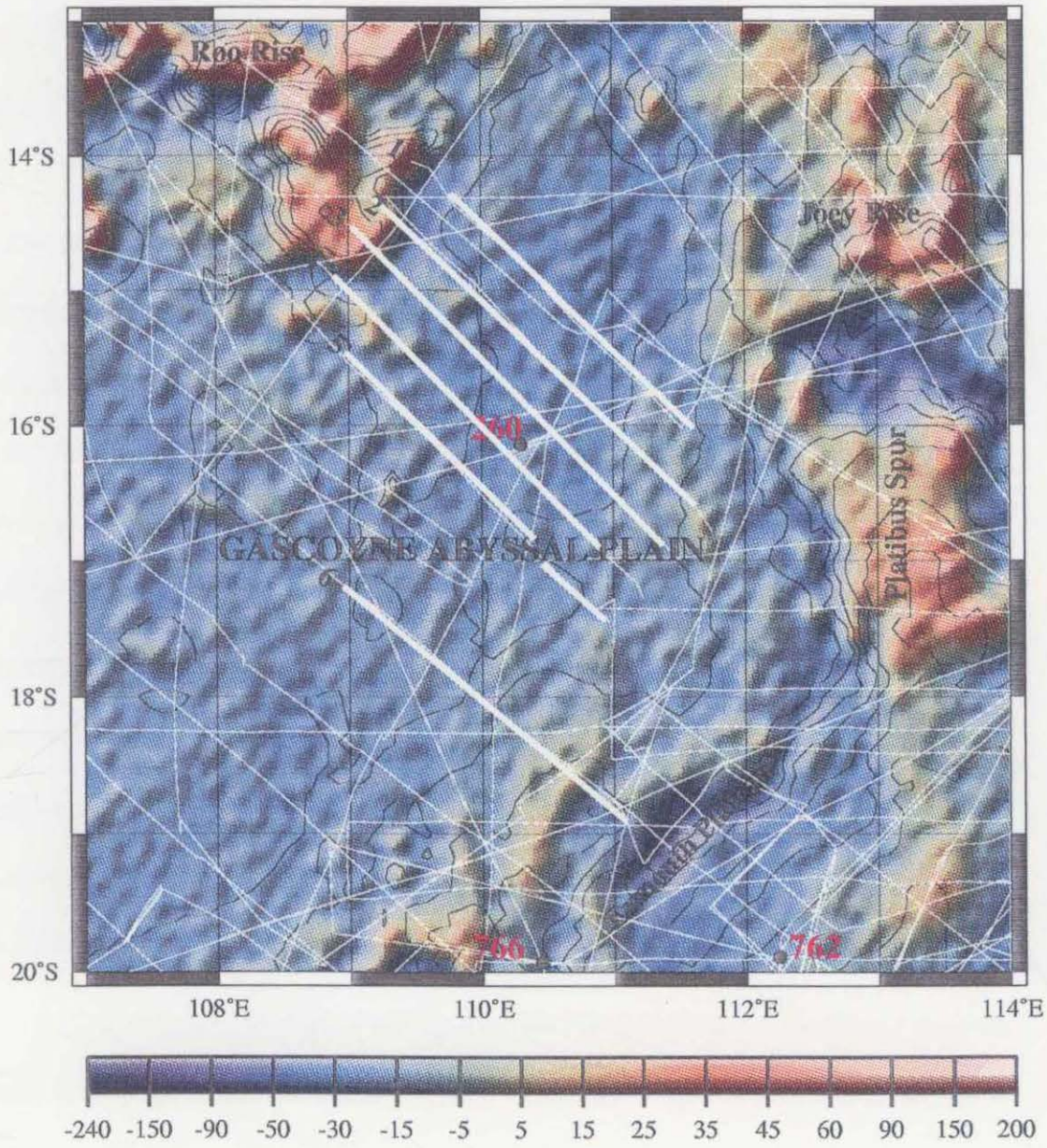

Fig. 2.10 Satellite-derived gravity anomaly grid (mgal) and bathymetry contours (500 m) in the Gascoyne Abyssal Plain. White lines identify marine geophysical and aeromagnetic data tracks. Black dots represent DSDP and ODP sites. Highlighted profiles are displayed in Fig. 2.11.

He did, however, identify the M0 - M6 anomaly sequence, farther south in the basin, trending N30°E. This interpretation agreed with the middle Albian age of sediments overlying a basalt sill at DSDP site 260 (*Davies et al.* 1974). *Veevers et al.* (1985) considered these lineations as evidence of a northward continuation of the same ridge jump interpreted in the Cuvier Abyssal Plain.

New aeromagnetic data acquired in 1981 allowed *Fullerton et al.* (1989) to recognise M10 as the oldest anomaly found in all spreading compartments interpreted in the Gascoyne and Cuvier basins. Their interpretation suggested a nearly simultaneous breakup time along the western Australian margin. The N30°E trend of the identified anomalies (M0 - M10) was different from that in the Argo Abyssal Plain (N60°E). The oblique intersection of the trends of the Argo and Gascoyne magnetic lineations was interpreted as indicating that the younger spreading system in the Gascoyne Abyssal Plain probably propagated northward into older seafloor along the western boundary of the Joey Rise. A major "ridge jump" was interpreted to have occurred by a northward propagating rift, triggered by a 10° clockwise change in spreading direction at M4 - M5 time (about 127 Ma). Evidence for the rift propagation was given by overlapping spreading on the newly forming and extinct ridges, curved lineations and fracture zones; however the locations of pseudofaults and failed ridge were not mapped.

2.5.2.2 Interpretation

Anomalies M0 – M11 for the central and the southern sectors were interpreted based on relatively good magnetic coverage especially in the area of accreted Indian Plate (Figures 2.11a and 2.11b). Based on magnetic data and on short-wavelength satellite-derived gravity anomaly lineations a revised interpretation of the magnetic anomalies was carried out in the Gascoyne Abyssal Plain. The satellite-derived altimetry grid shows the same trend (N45°E) as interpreted in the Argo (Figure 2.7) and further south in the Cuvier and Perth abyssal plains (Figures 2.17 and 2.21).

Three new interpreted major fracture zones (E, F and G) with N45°W orientation that changes to a N55°W (at M5 time) divide the plain in three sectors (Figure 2.13). The central sector, between fracture zones E and F, includes the area where conjugate anomalies M11 - M7 were identified (Figure 2.11a), and the southern sector with interpreted conjugate anomalies M2 - M3 (Figure 2.11b). In the northern part of the basin magnetic anomalies M10N-M12A were interpreted (Figures 2.12 and 2.13).

The magnetic coverage is relatively good in the central part of the plain and poor in the eastern part. Based on the satellite-derived gravity anomaly trends, two different seafloor spreading directions were interpreted: a N45°E (from the formerly N22°-26°E, *Fullerton et al.*, 1989) for anomalies older than M5, and a N35°E trend, slightly different from the previous N33°E, for anomalies younger than M5.

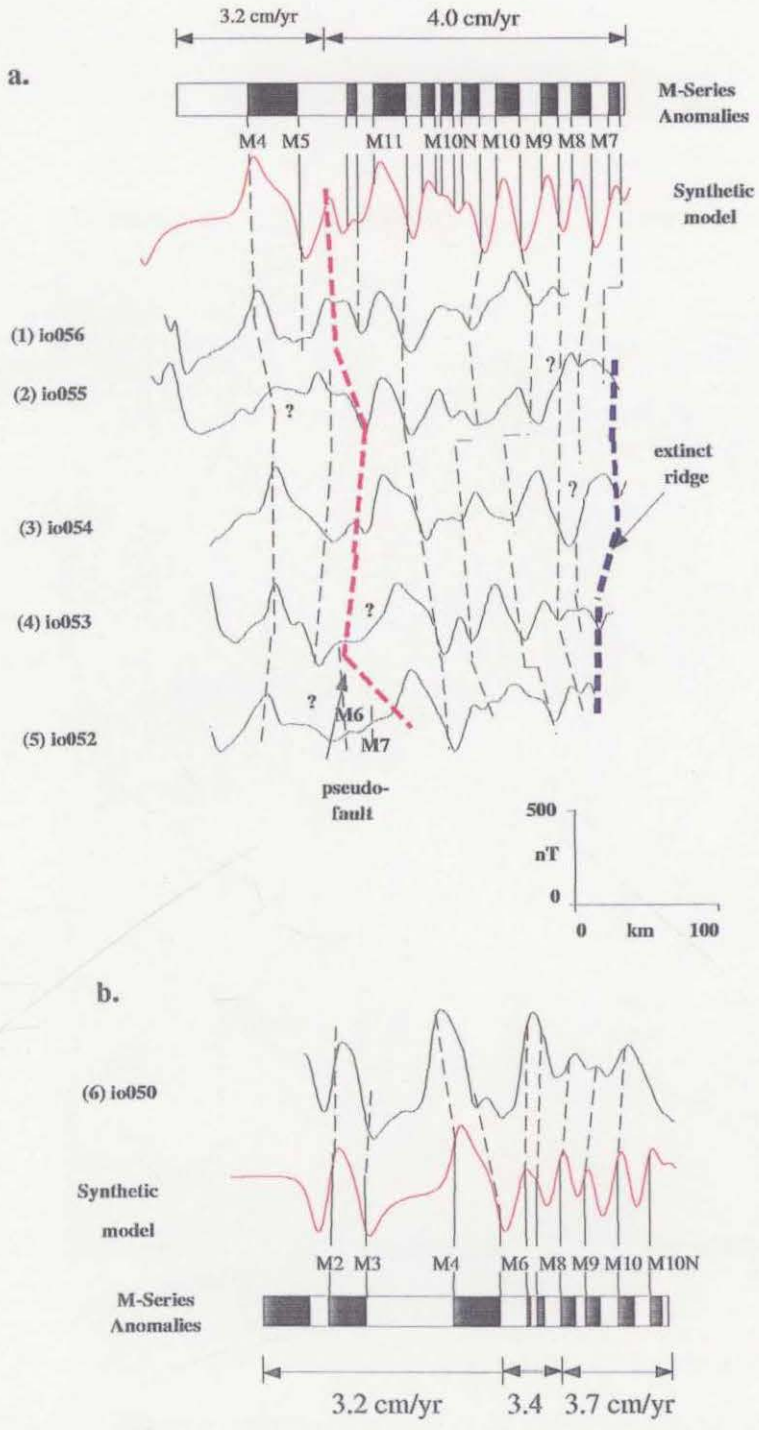

Fig. 2.11 Selected magnetic profiles and synthetic model for the magnetic lineations in a.- the central Gascoyne Abyssal Plain and b.- the southern Gascoyne Abyssal Plain (profiles location in Fig.2.10). The synthetic model and the ages of chrons are based on the time scale of Gradstein et al. (1994).

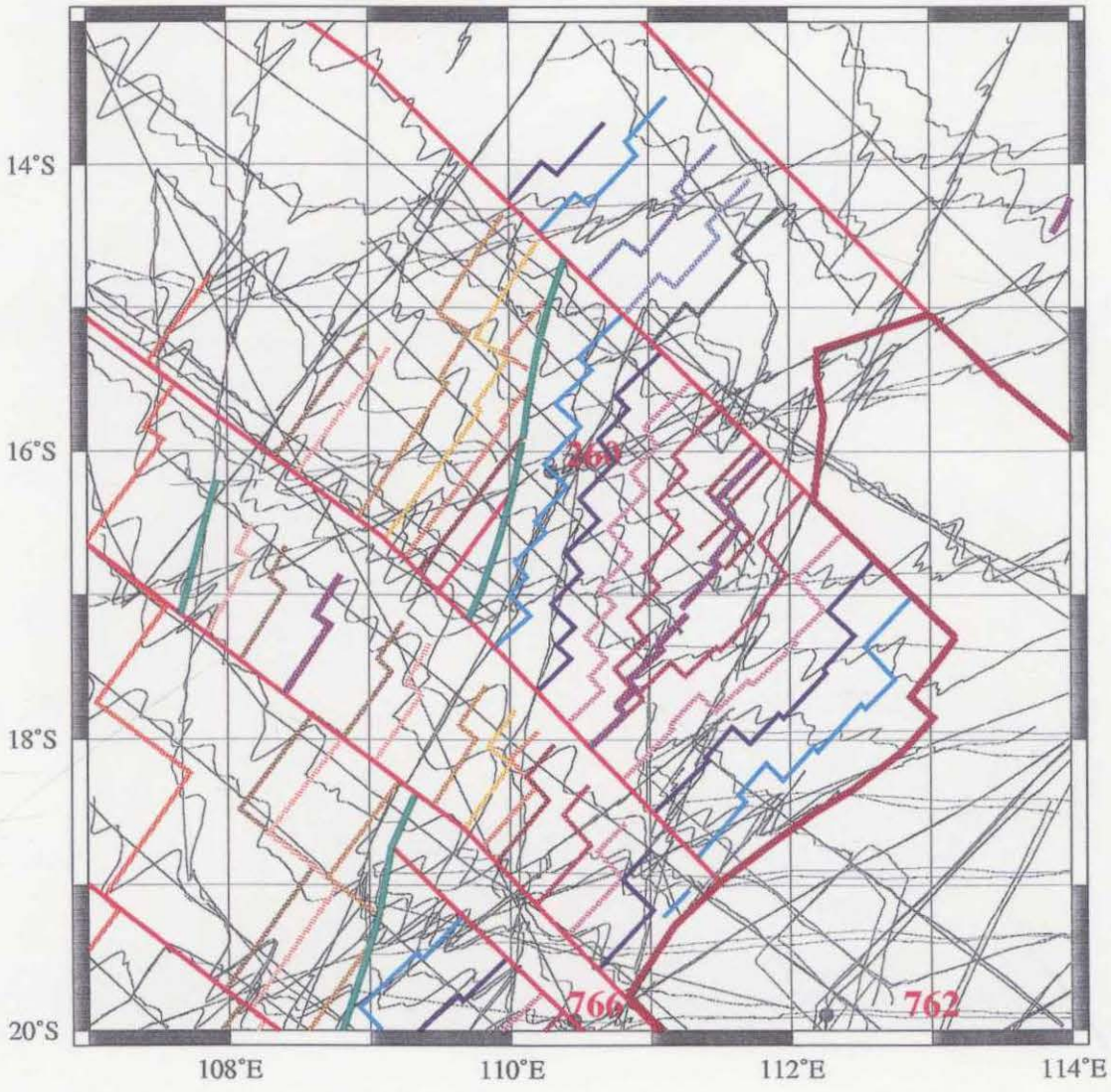

Fig. 2.12 Magnetic anomaly correlation in the Gascoyne Abyssal Plain. Magnetic anomalies are ploted at 45 degrees to the ship thack, which are shown as thin solid black lines. Red lines represent COB and fracture zones, green and magenta lines represent pseudofaults and extinct ridges respectively (see Fig.2.13 for anomaly and fracture zone legend).

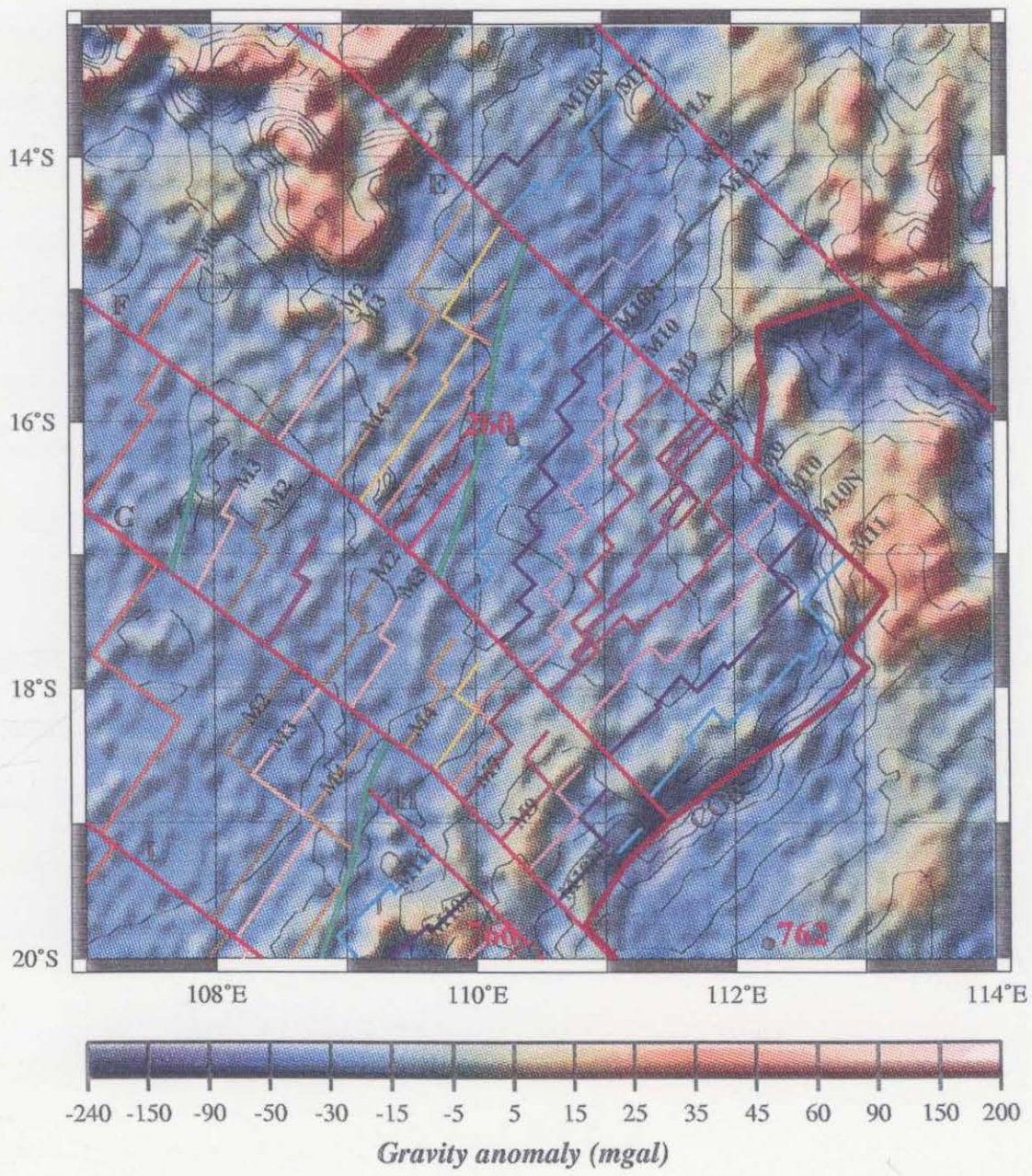

Fig. 2.13 Isochrons, COB and fracture zones (red), extinct ridges (magenta) and pseudofaults (green) superimposed on the satellite-derived gravity anomaly grid (mgal) in the Gascoyne Abyssal Plain.

In the central part of the basin anomalies M0 (120.4 Ma) - M11 (132.5 Ma) were interpreted (Figure 2.12). Several local fracture zones were identified by offsets in the magnetic lineations and segmentation in the satellite-derived gravity anomaly grain (Figure 2.13). An extinct spreading ridge, which formed by retreating to the north, was interpreted in this area with conjugate anomalies becoming progressively younger towards the extinct ridge. Anomaly M11 is clearly recognized in compartments that formerly belonged to the Indian Plate (Figure 2.11a). The extinct ridge and pseudofault are not as clear on the gravity map as in the Cuvier Abyssal Plain. The rift propagator had a short life (about 1.2 Ma, from M9 to M7). Anomalies M8 - M0 were interpreted west of the pseudofault; the anomalies become younger towards the pseudofault.

For the southern part of the Gascoyne Abyssal Plain a more simplified evolution than that of *Fullerton et al.* (1989) was favoured. Conjugate anomalies M2 - M3 were recognized, as a result of a very short rift propagating event that retreated to the north. Anomalies M2 through M11 were also interpreted west of this extinct ridge and anomaly M0 east of the pseudofault (Figures 2.12 and 2.13).

2.5.3 The Cuvier Abyssal Plain

2.5.3.1 Previous work

The Cuvier Abyssal Plain (Figure 2.14) is separated from the Exmouth Plateau by the CRFZ and from the Perth Abyssal Plain by the Wallaby-Zenith Fracture Zone (WZFZ) and the Lost Dutchman Ridge (LDR). There are no clear limits to the north

between the Cuvier and the Gascoyne abyssal plains. To the east it is bounded by the Exmouth Sub-basin and the Bernier Platform.

Larson (1977) identified the anomaly sequence M0-M4 northwest of the central Cuvier Basin. He also mapped other lineations with the same strike 220 km southeast of anomaly M4 without identifying them. These anomalies were considered as representing either the M7-M10 sequence or the M13-M15 sequence. *Larson* (1977) proposed a "ridge jump" to explain the 220 km gap based on the roughness of the seafloor between these sequences.

Subsequent studies using additional data confirmed the "ridge jump" hypothesis. The unindentified anomalies were confirmed to be the M5-M10 sequence (*Larson et al.*, 1979). The conjugate anomaly sequence was identified by *Johnson et al.* (1980), M8 and M9 anomalies completing the sequence which was recognized by *Veevers et al.* (1985). The positive anomaly considered previously as resulting from the COB (*Veevers*, 1985), was interpreted by *Fullerton et al.* (1989) as M10 and the small positive amplitude anomalies farther landward were interpreted as having been generated by small dikes. This implied that all spreading started simultaneously in the Gascoyne and Cuvier abyssal plains. *Fullerton et al.* (1989) pointed out that the early seafloor spreading that occurred in the Cuvier Abyssal Plain was punctuated by a 10° clockwise reorientation of spreading; a major "ridge jump" occurred at M4-M5 time as a rift propagated south from a salient of Australian Plate intruding the Indian Plate. Evidence for rift propagation was given by interpreted curved lineations and fracture zones by *Fullerton et al.* (1989) but no attempt at identifying pseudofaults and extinct ridges was made.

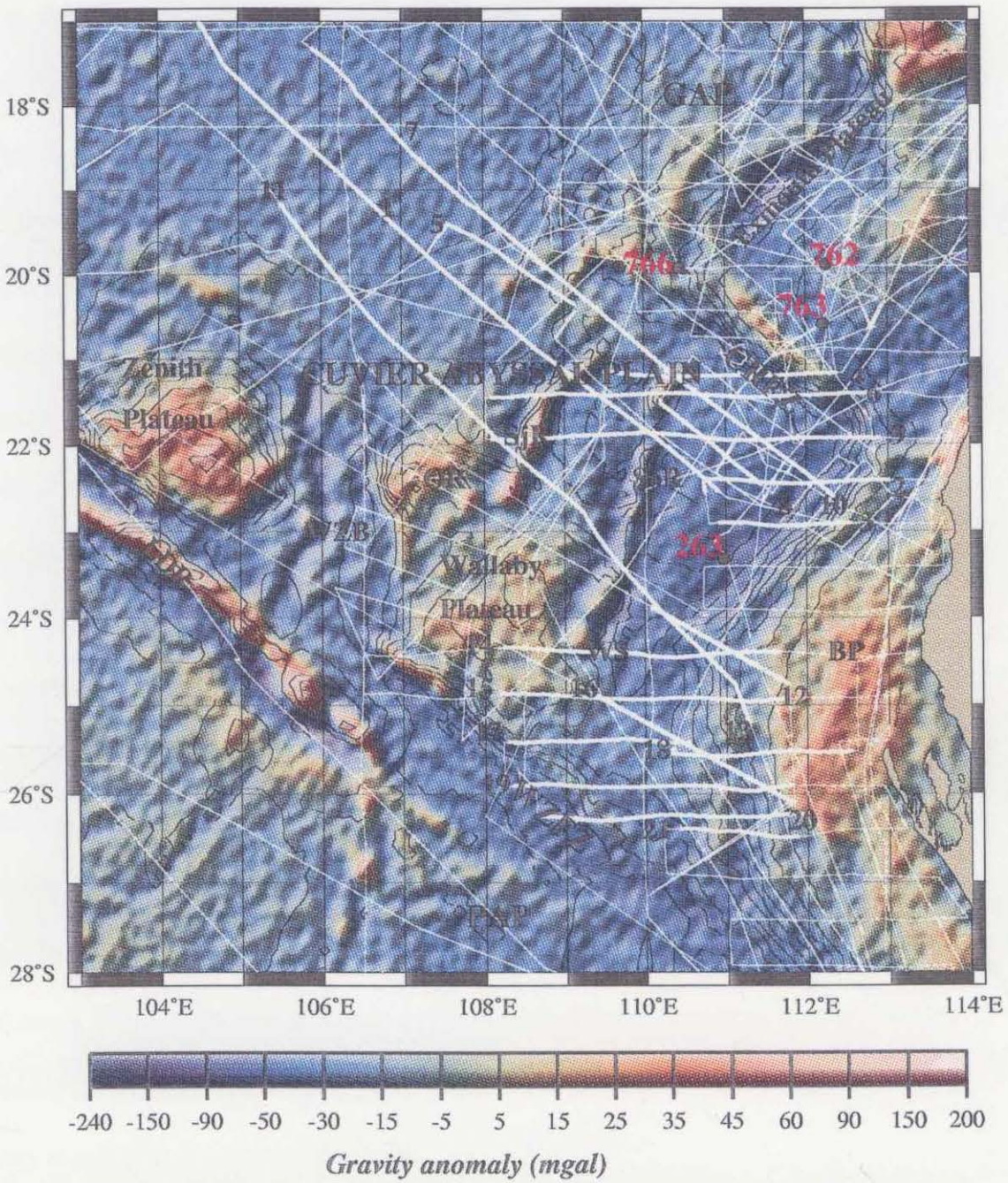

Fig. 2.14 Satellite-derived gravity anomaly grid (mgal) and bathymetry contours (500 m) of the Cuvier Abyssal Plain. White lines identify marine geophysical and aeromagnetic data tracks. Abbreviations are: GAP-Gascoyne Abyssal Plain, PAP-Perth Abyssal Plain, CRFZ-Cape Range Fracture Zone, WZFZ-Wallaby-Zenith Fracture Zone, QR-Quokka Rise, SoR-Sonne Ridge, SjR-Sonja Ridge, LDR- Lost Dutchman Ridge, WS-Wallaby Saddle, WZB-Wallaby-Zenith Basin. Black dots represent DSDP and ODP sites. Highlighted profiles are displayed in Fig. 2.15.

2.5.3.2 Interpretation

The satellite-derived gravity anomaly grid from *Sandwell and Smith* (1997) reveals two undulating, narrow gravity highs representing the Sonne and Sonja ridges (Figure 2.14). A negative gravity anomaly separates the Wallaby Plateau from its northwestern segment, the Quokka Rise. The Zenith and Wallaby plateaus are separated by a basin, which in this study is referred to as the Wallaby-Zenith Basin, expressed by a gravity anomaly low, with a central linear staircase shaped negative gravity anomaly. These linear tectonic features appear to be time-progressive, i.e. they are oblique to seafloor spreading isochrons, and their geometry suggests a relationship to propagating rift processes.

The magnetic record in the northern part of the Cuvier Abyssal Plain (Figure 2.15a) resembles those identifications made previously by *Fullerton et al.* (1989). However, some additional anomalies have been tentatively identified: anomaly M10N - M11A on line bmr17c and M11 - M12 on line bmr17d. A complete revision has been made on the magnetic record of the magnetic anomaly pattern lying between 23°S - 26°S east and west of the Wallaby Plateau and described by *Veevers et al.* (1985). Elsewhere many former identifications have been changed in accord with the new fracture zone distribution.

Anomalies M1r (115.3 Ma - M12 (134.0 Ma) and M14 (135.8) for the northern and southern sectors, respectively, were interpreted based on good magnetic data coverage (Figures 2.15a and 2.15b). Most of the fracture zones in this region were identified by offsets in the magnetic lineations and segmentation in the grain of

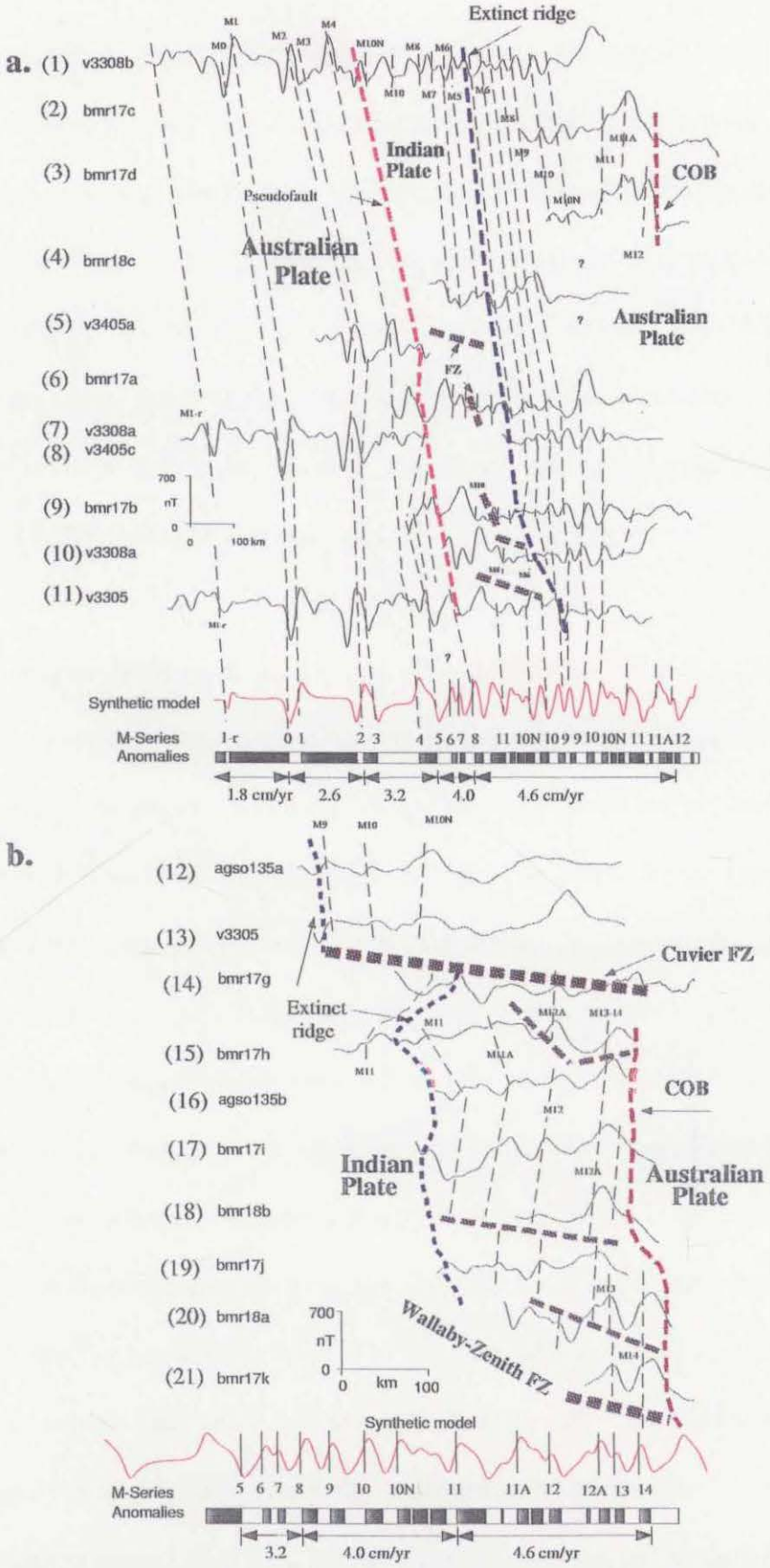

Fig. 2.15 Selected magnetic profiles and synthetic model for the magnetic lineations in a.- the northern Cuvier Abyssal Plain and b.- in the southern Cuvier Abyssal Plain (location in Fig.2.14). The synthetic model and the ages of chrons are based on the timescale of Gradstein et al. (1994).

gridded satellite-derived gravity anomalies. Three major fracture zones with large offsets were recognized. They divide the Cuvier Abyssal Plain into three sectors: (1) the northern sector separated from the Exmouth Plateau and the Gascoyne Abyssal Plain by the CRFZ (G, H), (2) the southern sector separated from the Perth Abyssal Plain by the WZFZ (M, N, O), and (3) the Cuvier Fracture Zone CFZ (L) which divides the Cuvier Abyssal Plain into north and south compartments (Figures 2.16 and 2.17). Their trends are identical with those described for the fracture zones identified in the Gascoyne Abyssal Plain.

In the northern sector, east and west of the Sonne Ridge (Figures 2.15A, 2.16 and 2.17), conjugate anomaly sequences offset by local fracture zones were interpreted, which become progressively younger towards the interpreted extinct spreading ridge (M10N-M9/M9-M12? to M5-M10N/M5-M12). The Sonne Ridge appears on the satellite-derived gravity grid as a staircase-shaped feature displaying segments oriented approximately 45°E linked by segments oriented 45°W (Figure 2.17). West of the Sonja Ridge anomalies from M8 to M1r were interpreted. The anomalies become younger towards the Sonja Ridge. In the spreading corridor defined by the Sonne and Sonja ridges, complete anomaly sequences can be interpreted only to the north where the magnetic data coverage is good. From the satellite-derived gravity anomaly data the Sonja Ridge appears to consist of two segments: the main, southern segment, striking ~10° and a northern part striking ~40°. By combining magnetic and gravity anomaly data, only the southern part of the feature represents a pseudofault (Figure 2.17). The northern extension of the pseudofault conjugate to the Sonne Ridge (the failed rifts/ridge) seems to be represented by a linear gravity high striking ~20°north of the Sonja Ridge (Figure 2.17).

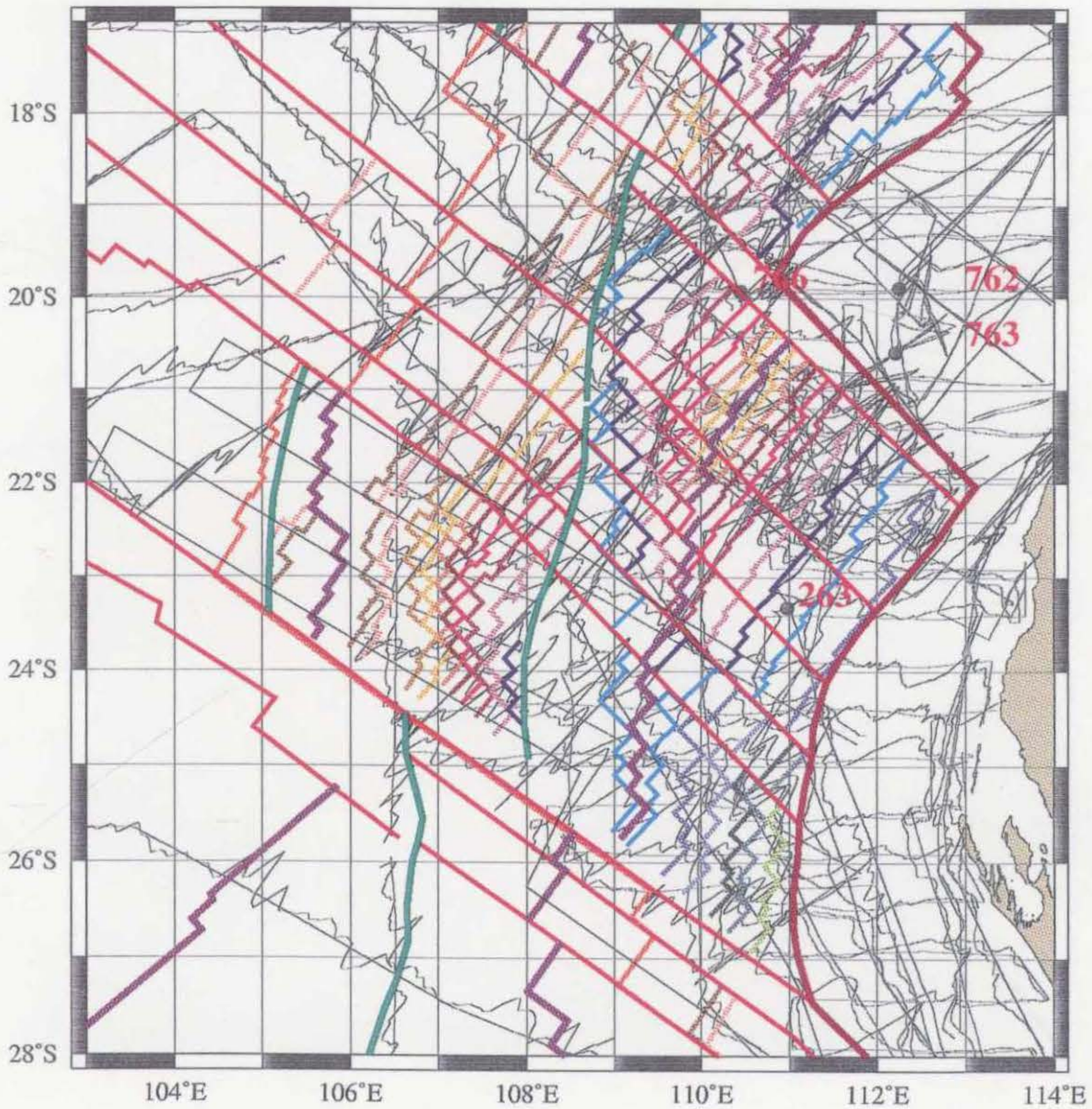

Fig. 2.16 Magnetic anomaly correlation in the Cuvier Abyssal Plains. Magnetic anomalies are plotted at 45 degrees to the ship track, which are shown as thin, solid black lines. Red lines represent COB and fracture zones, green and magenta lines represent pseudofaults and extinct ridges respectively (see Fig. 2.17 for anomaly and fracture zones legend).

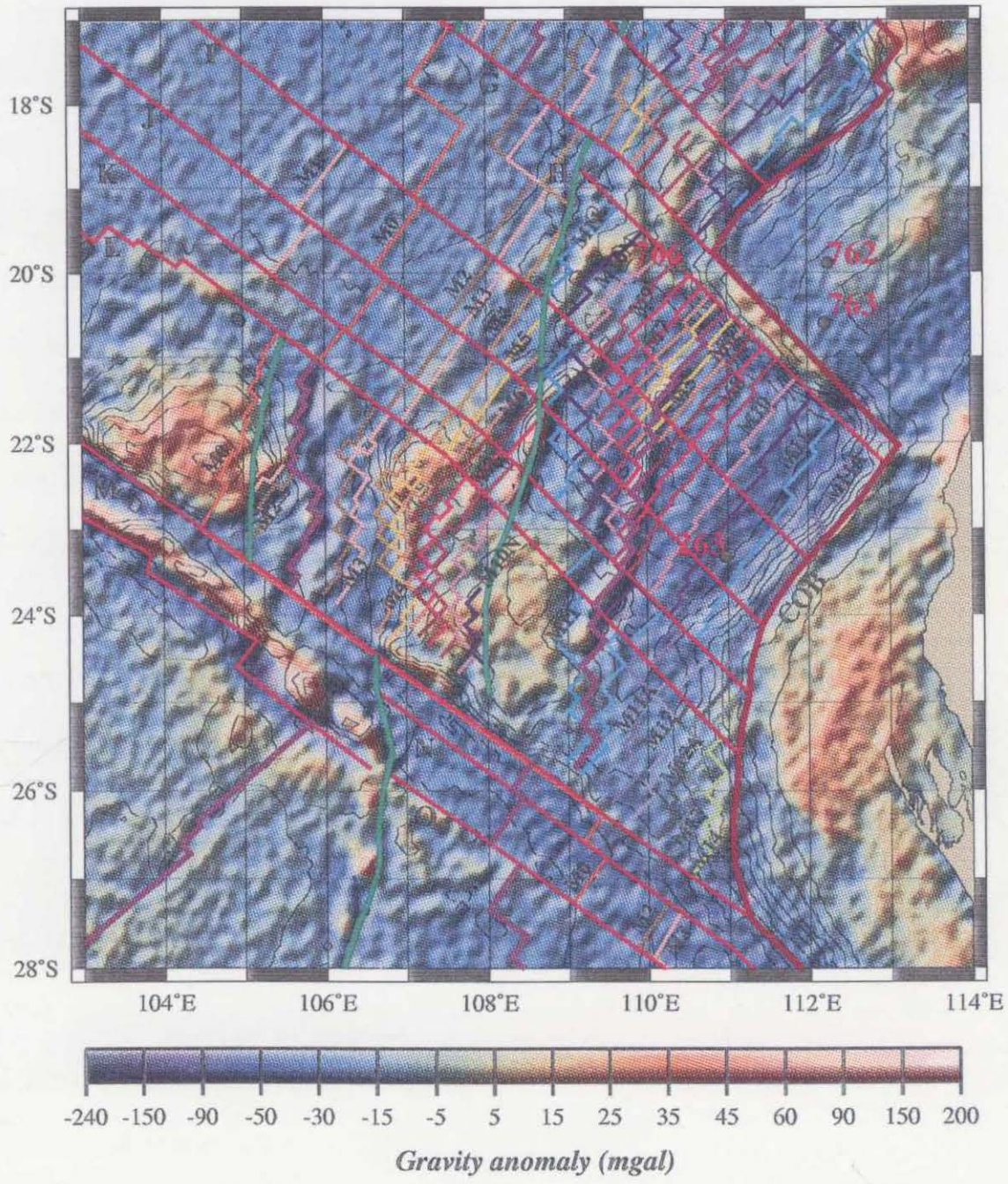

Fig. 2.17 Isochrons, COB and fracture zones (red), extinct ridges (magenta) and pseudofaults (green) superimposed on the satellite-derived gravity anomaly grid (mgal) in the Cuvier Abyssal Plain.

In the southern sector of the Cuvier Abyssal Plain (Figure 2.15b) magnetic anomalies were interpreted east and west of the Wallaby Plateau and east of the Zenith Plateau. Magnetic anomalies over the plateaus are too noisy to be interpreted. The sequence identified on the eastern part of the Wallaby Plateau is represented by anomalies M11 to M14, offset by four local fracture zones. The distance between anomaly M11 and the extinct ridge east of the Wallaby Plateau increases toward the north. Conjugate anomalies (M2 - M3) symmetric about a staircase shaped failed rift, followed to its eastern part by anomalies M4 to M10N are present in the Wallaby-Zenith Basin area (Figure 2.17). The distance between anomalies bounding the failed ridge(s) increases from south to north. West of the pseudofault interpreted in the eastern sector of the Zenith Plateau anomaly M0 was interpreted.

In the northern compartments M11A is the oldest anomaly interpreted. The distance between anomaly M11A and the interpreted COB is variable, therefore the breakup age is slightly asynchronous along this margin. This variability may be the result of a differential stretching which occurred prior to continental breakup, or the breakup may not have occurred in the center of the initial rift valley (*Veevers and Cotterill*, 1978). In the southern compartment the oldest anomaly is M14, older than the oldest anomaly in any other western compartment. A possible scenario of this earlier breakup is discussed in detail in Chapter 3.

2.5.4 The Perth Abyssal Plain

2.5.4.1 Previous work

The Perth Abyssal Plain is bounded to the north and south by two fracture zones (the WZFZ and the Naturaliste Fracture Zone - NFZ), to the east by the Perth Basin and to the west by the Wharton Basin (Figure 2.18). Magnetic anomalies in the Perth Abyssal Plain were firstly identified by *Markl* (1974), confirmed by deep sea drilling (*Veevers et al.*, 1974) and by further magnetic studies of *Markl* (1978) and *Veevers et al.* (1985). The anomalies interpreted were divided into two sets: (1) a set from the COB (anomaly M10) to anomaly M4 with a faster spreading rate and lower intensity; and (2) a set from M4 to the Cretaceous Quiet Zone (anomaly M0) with a slower spreading rate and higher intensity. No "ridge jump" was recognized in this area. The magnetic anomalies were interpreted as near parallel along an azimuth of 32° with M0 through M4 and M9 as well defined isochrons.

2.5.4.2 Interpretation

The coverage with magnetic data is fairly good in the eastern part of the Perth Abyssal Plain (Figure 2.18). The magnetic interpretation (Figure 2.19) in the Perth Abyssal Plain resembles that of *Veevers et al.* (1985). With the aid of the satellite-derived gravity grid, several local fracture zones were interpreted in this sector (Figures 2.20 and 2.21). They have similar trends to those interpreted in the Argo, Gascoyne and Cuvier abyssal plains and are delimited by the WZFZ and a fracture north of the Naturaliste Plateau (herein referred to as the North Naturaliste Fracture

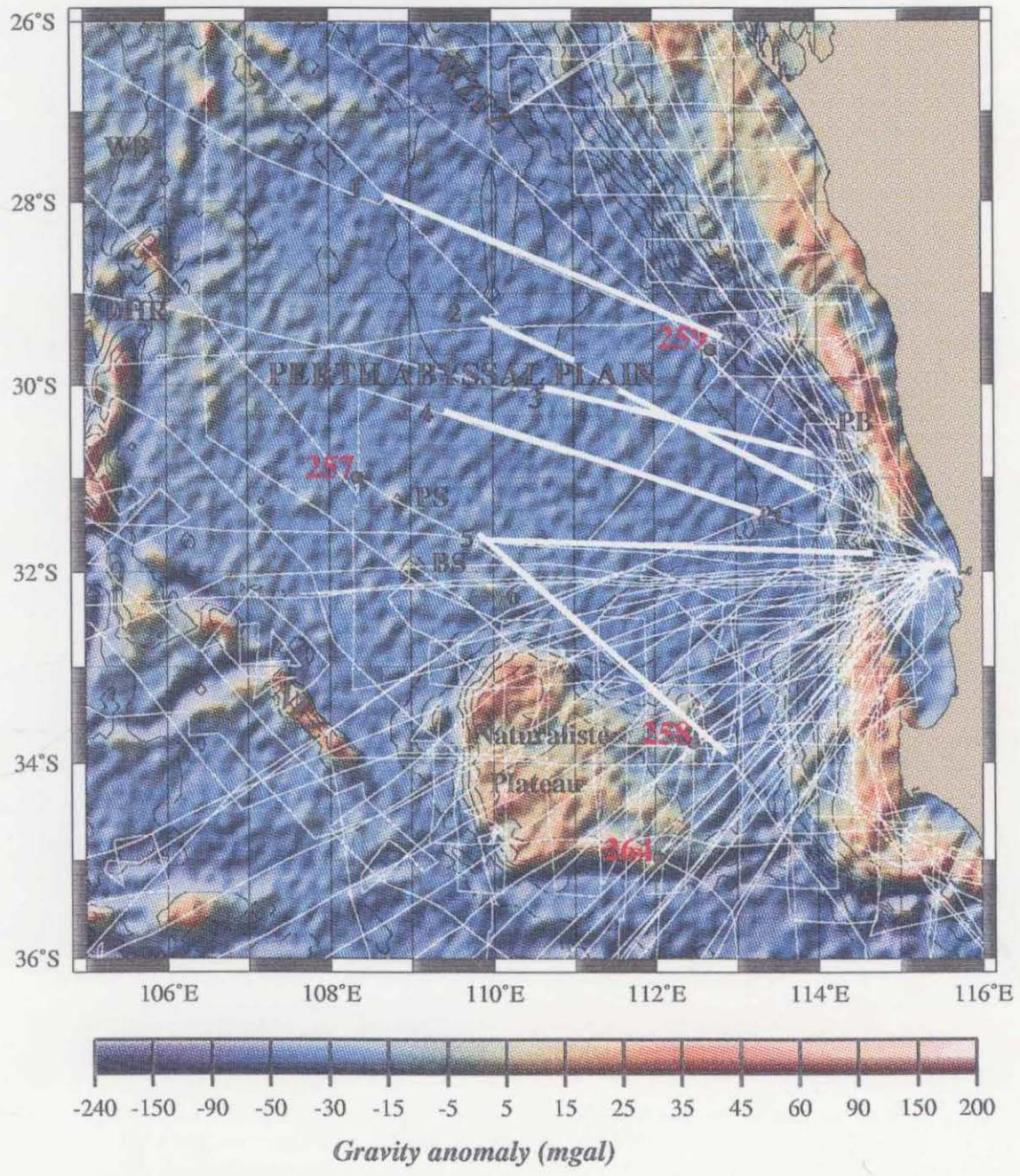

Fig. 2.18 Satellite-derived gravity anomaly grid (mgal) and bathymetry contours (500 m) of the Cuvier Abyssal Plain. White lines identify marine geophysical and aeromagnetic data tracks. Abbreviations are: WZFZ-Wallaby-Zenith Fracture Zone, NFZ-Naturaliste Fracture Zone, DHR-Dirck Hartog Ridge, PS-Pelsaert Seamount, BS-Brouwer Seamount, PC-Perth Canyon, PB-Perth Basin, WB-Wharton Basin. Black dots represent DSDP and ODP sites.

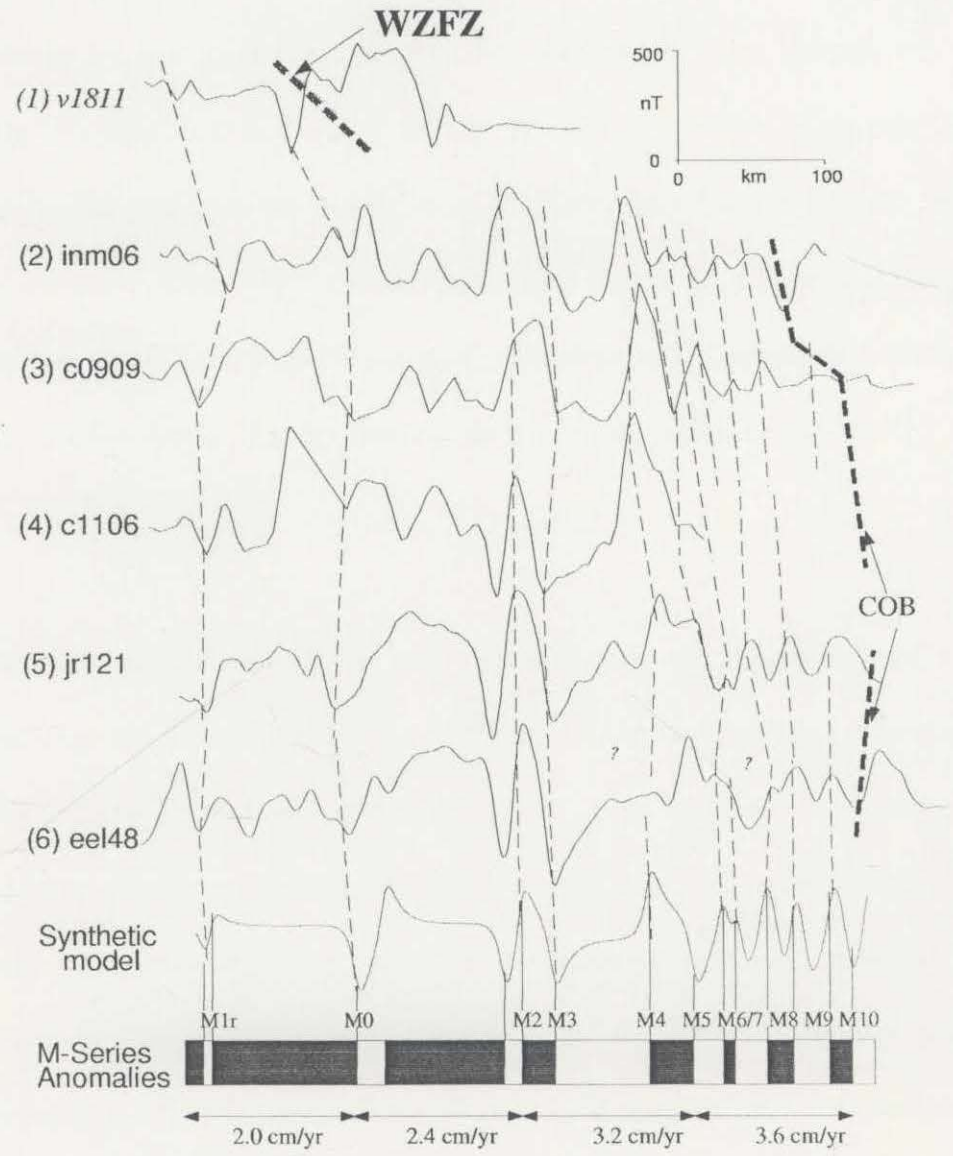

Fig. 2.19 Selected magnetic profiles and synthetic model for the magnetic lineations in the Perth Abyssal Plain (profile location in Fig.2.18). The synthetic model and the ages of chrons are based on the time scale of Gradstein et al. (1994). WZFZ - Wallaby-Zenith Fracture Zone.

Zone -NNFZ). The centre of the basin is defined by a set of parallel anomalies that ranges from M1r to M10? (Figures 2.20 and 2.21).

Several narrow spreading segments, trending N45°E, were identified in the Perth Abyssal Plain: two in the area defined by the WZFZ where no attempt to interpret anomalies older than M3 was made, eight south of this fracture with the complete set of anomalies M1r - M10? and one west of the Naturaliste Plateau with sequence M0 -M5 recognized (Figure 2.20 and 2.21). These spreading segments, correlatable with the satellite-derived gravity anomaly grain, were considered to account for the offsets in the COB.

Magnetic anomalies over and west of the plateau are too noisy to be interpreted. Although the Naturaliste Plateau was considered by many authors to have an oceanic origin there are still controversies about its origin. Recent reconstructions of pre-breakup Gondwana indicate that the Naturaliste and Kerguelen plateaus must be largely oceanic in origin; however the presence of small, stranded blocks of continental crust left from the early stages of drifting cannot be ignored from existing geophysical information (*Coffin and Endholm*, 1992). Continental-derived material introduced long ago into the plume's source region via deep subduction of marine sediments was invoked in the case of oceanic island sources in the Pacific (e.g., *Woodhead and McCulloch*, 1979) but in the case of the Naturaliste Plateau samples are chemically as well as isotopocally distinct from those of other oceanic hotspots (*Mahoney et al.*, 1995). The significantly greater proportion of continental-derived material in some of the Naturaliste Plateau eruption - accepting a mantle plume scenario - might be explained by either: (1) the entrainment into the plume of

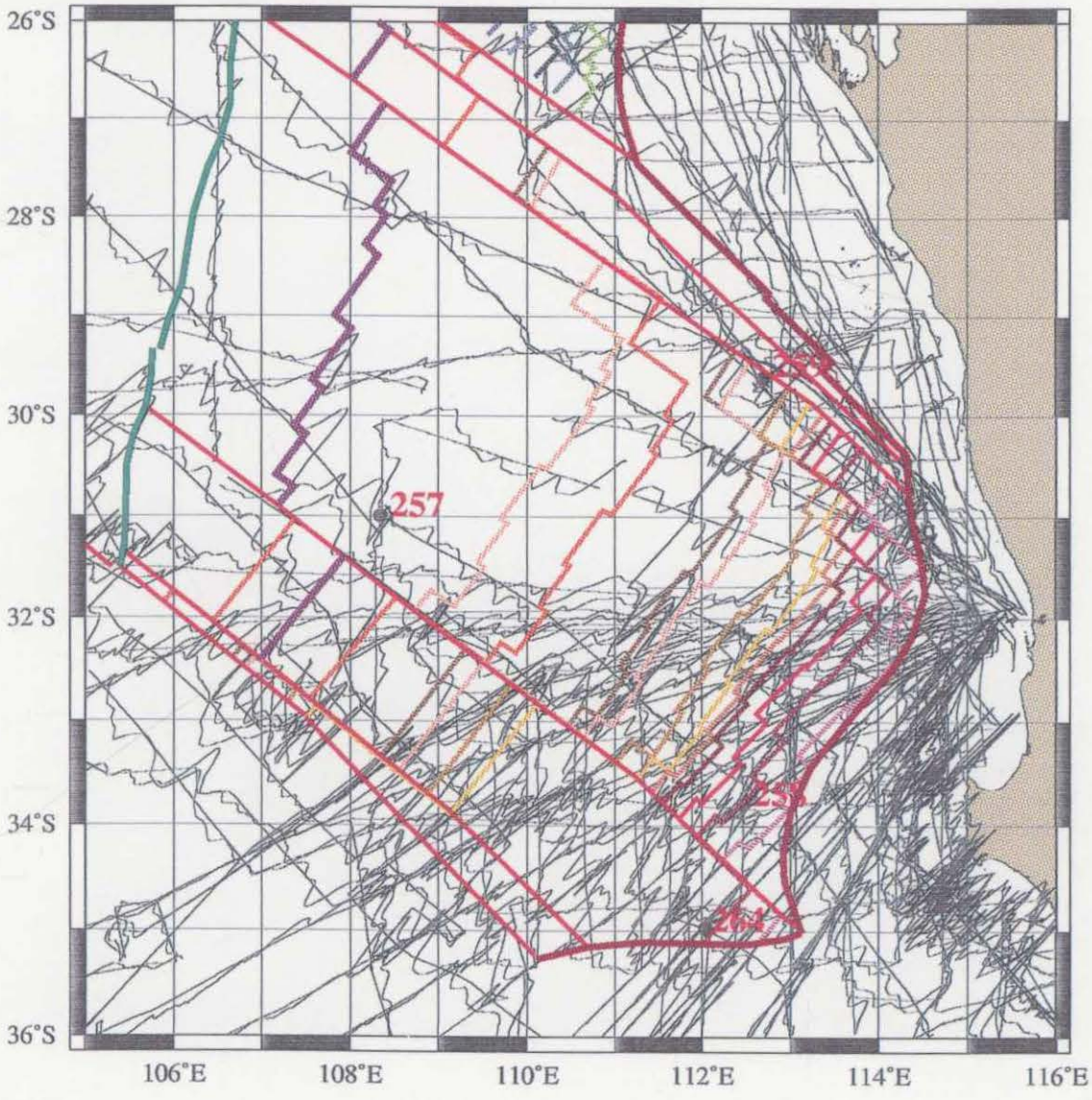

Fig. 2.20 Magnetic anomaly correlation in the Perth Abyssal Plain. Magnetic anomalies are plotted at 45 degrees to the ship track, which are shown as thin, solid black lines. Red lines represent COB and fracture zones, green and magenta lines represent pseudofaults and extinct ridges respectively (see Fig.2.21 for anomaly and fracture zone legend).

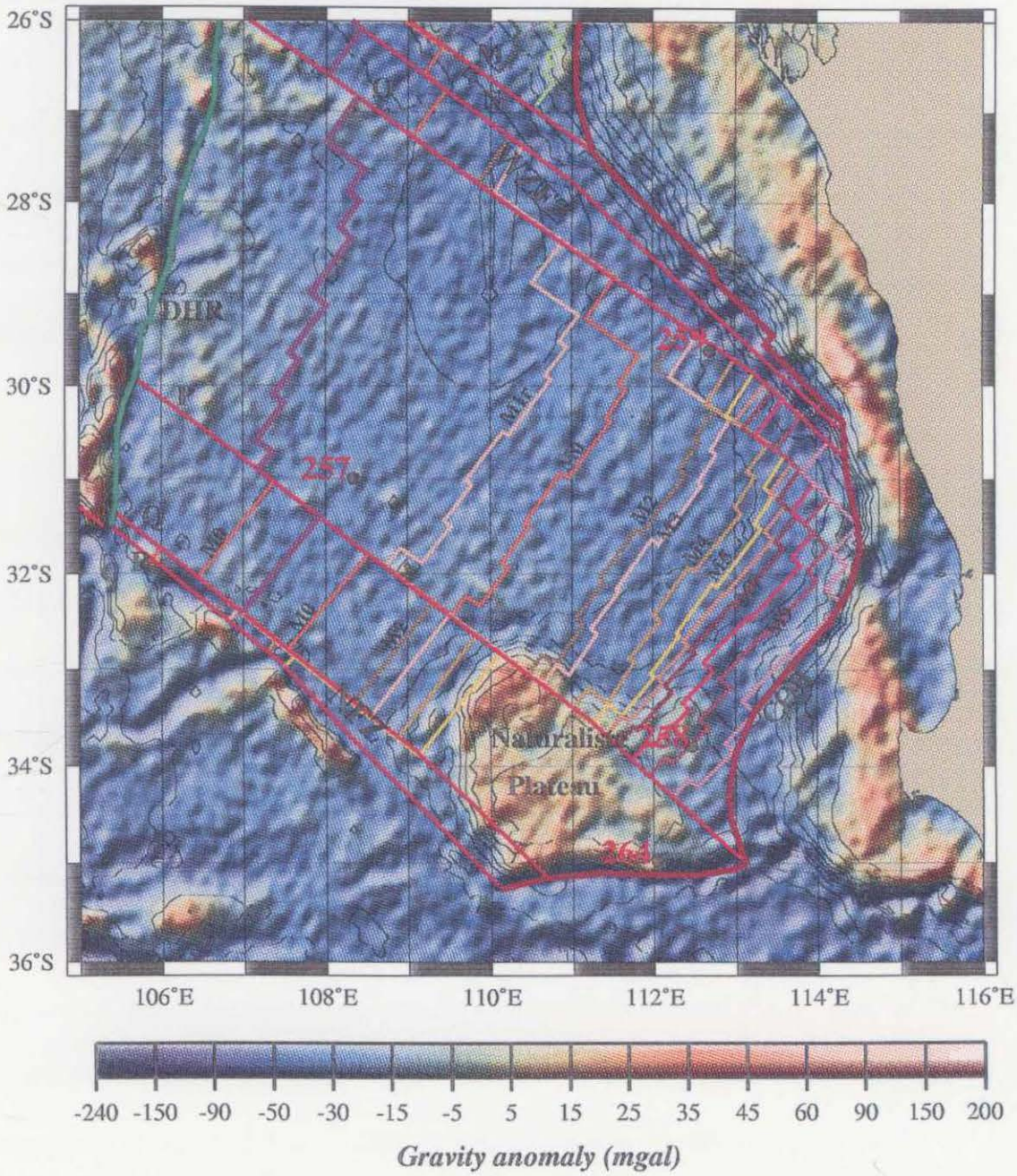

Fig. 2.21 Isochrons, COB and fracture zones (red), extinct ridges (magenta) and pseudofaults (green) superimposed on the satellite-derived gravity anomaly grid (mgal) in the Perth Abyssal Plain.

isotopocally distinct, non-plume material, or (2) the interaction of plume-derived magmas with external material at relatively shallow depths (*Mahoney et al.*, 1995). The main point in favour of an oceanic origin for this plateau as well as for the Wallaby Plateau was the apparent continuity of the breakup unconformity from plateau to ocean basin (*Willcox*, 1981). In their fit reconstruction (~160 Ma) *Royer and Sandwell*, (1989) also consider the Naturaliste Plateau being underlain by oceanic crust. However, the oceanic versus continental origin question for the Naturaliste Plateau is beyond the purpose of this study.

An extinct ridge was identified west of the interpreted anomaly M1r based on a combined analysis of gravity, magnetic and topographic data along three profiles (Figure 2.22). It is well known that the oceanic crust becomes deeper as it becomes older. Therefore the topography across an extinct spreading ridge would show an increase in depth on both sides of the ridge. This is the case for profile 3 (Figure 2.22c) where the extinct ridge can be recognized in the topography (deepening of seafloor on both sides of the ridge, which is represented by a sharp trough), magnetic (symmetric anomaly centered on the ridge), and gravity (small trough on the gravity). The extinct ridges are recognized along the entire Perth Abyssal Plain. West of the Naturaliste Plateau was the only location where a conjugate anomaly (M0) was interpreted; in the WZFZ compartment interpretation is impeded by the absence of magnetic data. In the central part of the basin the position of the extinct ridges in the Cretaceous Quiet Zone restrained any interpretation of conjugate anomalies.

The variable distance between the closest anomaly (M0 in the WZFZ sector and M1r in the central Perth Abyssal Plain) and the interpreted extinct ridge lead to the

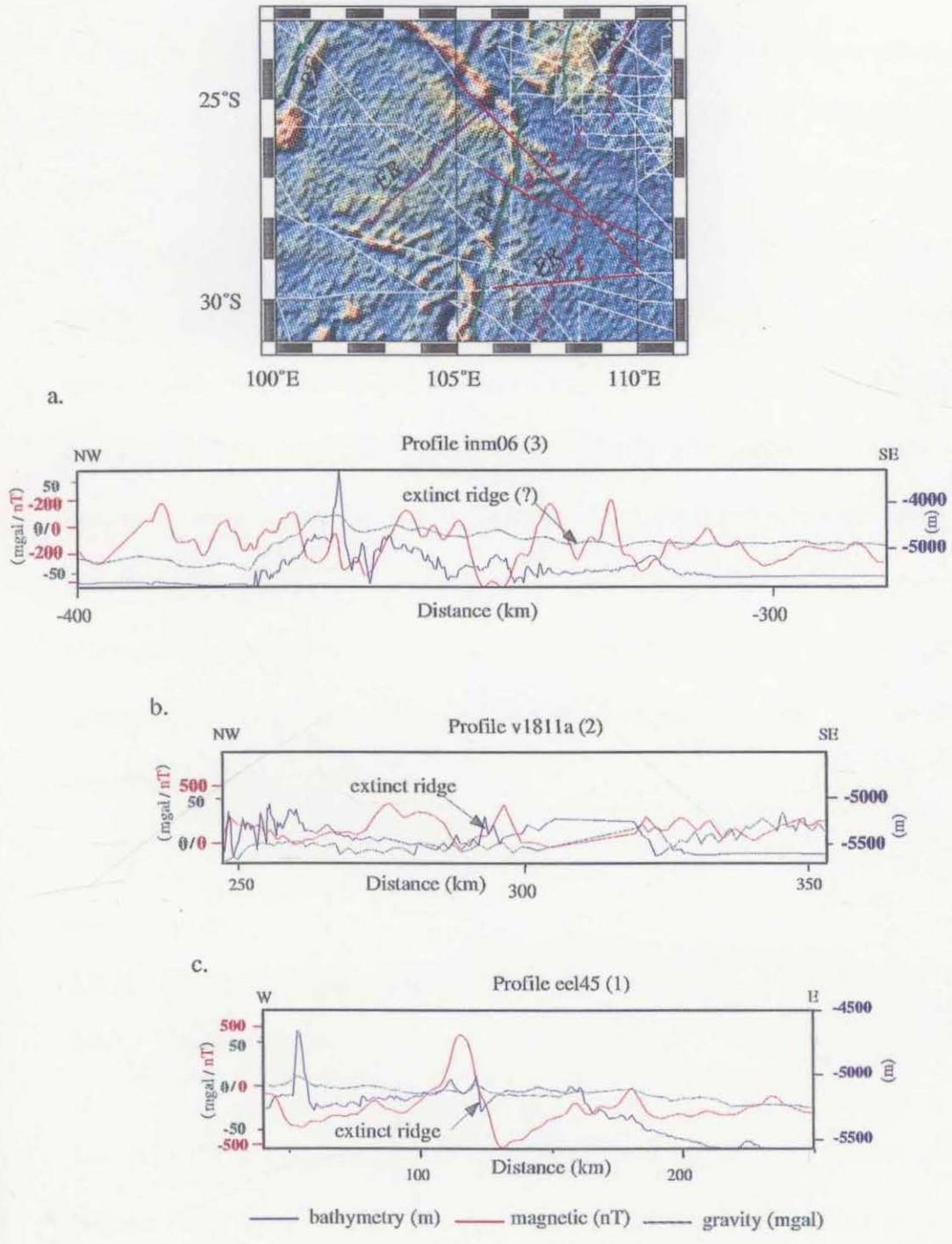

Fig. 2.22 Projected magnetic, gravity and topography profiles along an interpreted extinct ridge (ER) shown in magenta. Pseudofaults are shown in green, ship tracks and selected profiles are shown in white and red respectively.

conclusion that these features represent propagating rifts such as those described in the Cuvier and Gascoyne abyssal plains. The pseudofaults are expressed in the gravity anomaly grid by undulating, continuous linear highs (the Dirk Hartog Ridge) paralleling the failed ridge represented by a gravity low. Considering that the spreading rate remained unchanged after anomaly M1r, the time during which the propagating rift in the central Perth Basin was active is about 2 m.y. (between 110 and 108 Ma). West of anomaly M0 on the Naturaliste Plateau the pseudofault is well expressed in the satellite-derived gravity anomaly grid by an undulating feature continuing from the central part of the basin, while the failed ridges cannot be traced clearly to the north due to absence of data. Therefore this element was interpreted as a straight line instead of the stair-step shape normally expected. All these processes caused accretion of pieces of the Indian Plate onto the Australian Plate until the rift propagation ceased to be active.

2.5.5. The Wharton Basin

2.5.5.1 Previous work

The Wharton Basin is delimited to the northeast by the Java Trench and Argo Abyssal Plain, to the east by the Gascoyne, Cuvier and Perth abyssal plains, to the south by Broken Ridge and to the west by Ninetyeast Ridge (Figure 1.1 and 2.23). The great water depths in the Wharton Basin led *McKenzie and Sclater* (1971) to suggest that this basin was Cretaceous or older.

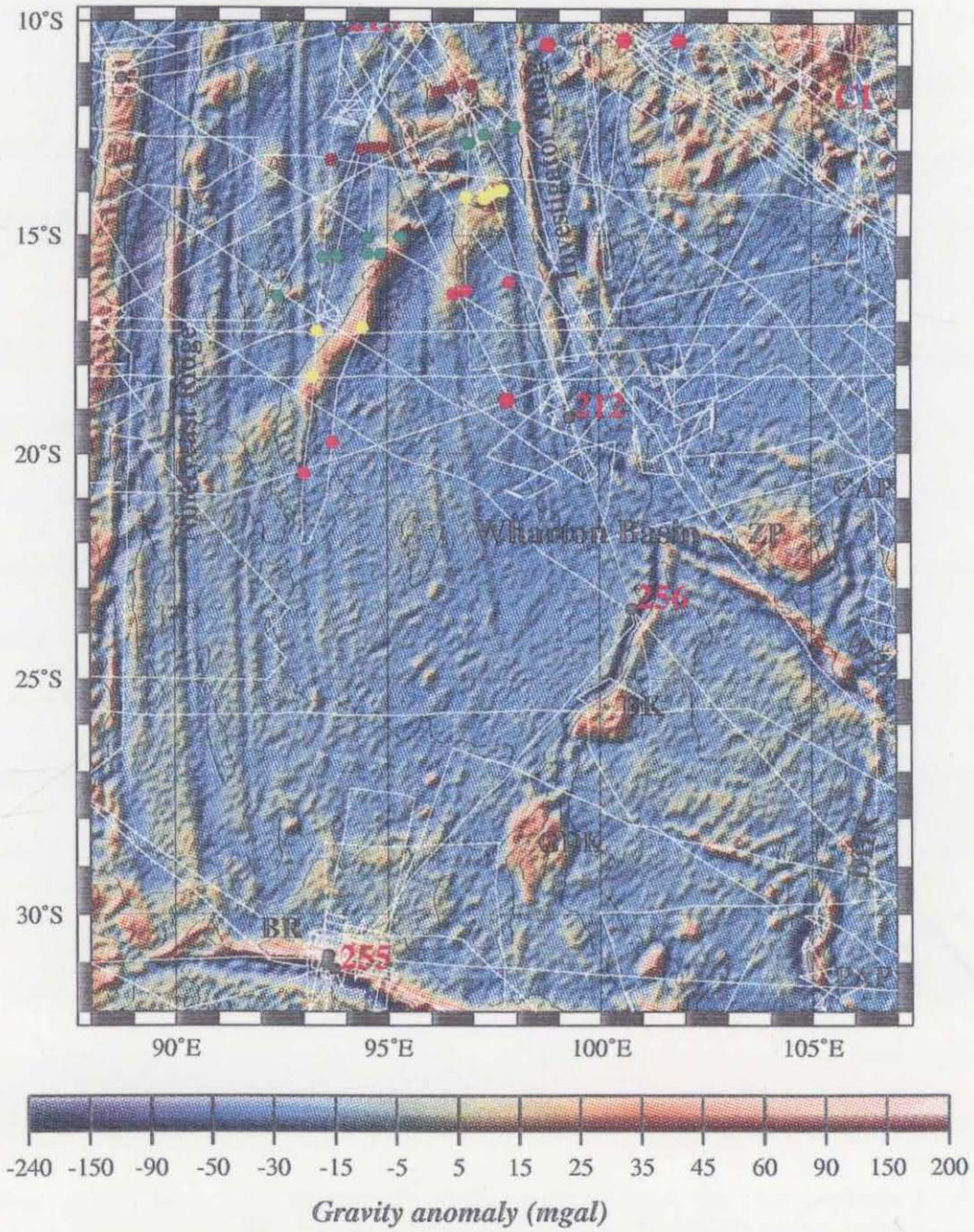

Fig. 2.23 Satellite-derived gravity anomaly grid (mgal) and bathymetry contour (500 m) of the Wharton Abyssal Plain. White lines identify marine geophysical and aeromagnetic data track. Abbreviations are: WZFZ-Wallaby-Zenith Fracture Zone, DHR-Dirk Hartog Ridge, GDK-Gulden Draak Knoll, BK-Batavia Knoll, ZP-Zenith Plateau, BR- Broken Ridge, CAP and PAP-Cuvier and Perth abyssal plains, CI-Christmas Island. Black dots represent DSDP and ODP sites. Previously interpreted picks are: red - C33, magenta - C32, yellow - C31, green - C29, brown - C28.

Sclater and Fisher (1974) were first to find Cenozoic marine magnetic anomalies trending east-west in the northern part of the basin, which became older southward. These anomalies were confirmed by *Liu et al.* (1983), whose model include a ridge jump at anomaly 20 and several transform faults trending north-south that offset the anomalies. Their model was improved with new identified anomalies and fracture zones showing a complete series of anomalies C33 to C20 (*Krishna et al.*, 1995). Spreading stopped in the eastern Wharton Basin shortly after anomaly C20 - ~46.2 Ma - (*Liu et al.*, 1983) possibly as a direct result of the collision between Greater India and Eurasia. Four major fracture zones were defined east from Ninetyeast Ridge (labeled X, Z, U, and M in Figure 2.24), using trends from Geosat Exact Repeat Mission Data *(Royer and Sandwell*, 1989), the easternmost, the Investigator Fracture Zone (M) continuing the WZFZ.

Early Cretaceous magnetic anomalies identified in the Gascoyne and Cuvier (e.g. *Fullerton et al.*, 1989) display northeast-southwest orientations normal to the fracture zones recognized in the eastern Christmas Island area (*Borissova*, 1995). It has been accepted (e.g. *Powell et al.*, 1988) that the pattern of spreading in the Early Cretaceous persisted until the beginning of the Late Cretaceous (~95-96 Ma). *Powell et al.* (1988) predicted a position of the spreading ridge, which became extinct at ~96 Ma. The abandoned mid-oceanic ridge in his interpretation based mainly on topography data runs parallel to the magnetic lineations on the Cuvier Abyssal Plain at about 104° E, offset by the WZFZ at the Lost Dutchman Ridge, and down to the Dirk Hartog Ridge west of the Naturaliste Plateau.

A study carried out on the Christmas Island area seafloor morphology by *Borissova* (1995), shows that Late Cretaceous magnetic lineations C34 – C22 (84 –50 Ma) were identified only in the westernmost part of the island. The fracture zones trending north - south, with left-lateral displacement, observed in the northeastern part of the island were interpreted as faults developed during the same period, therefore the age of the crust was also interpreted to be Late Cretaceous. According to these observation, it was considered that the Christmas Island Rise was initially formed as a mid-ocean ridge, abandoned at about 95 - 96 Ma (*Borissova*, 1995).

2.5.5.2 Interpretation

Before the release of the new satellite-derived gravity grid (*Sandwell and Smith*, 1997) the interpretation in the Wharton Basin was carried out in principal using magnetic data and age control from DSDP sites. Old gravity data showed little of the structural grain, although major north - south trends were recognized. The interpretation carried out in this study combines all the available data in an attempt to better understand the early tectonic evolution of the Wharton basin.

Several major linear elements were identified on the satellite-derived gravity anomaly grid west of the Perth Abyssal Plain (Figure 2.24). They are represented by three undulating linear lows (shown in green and magenta in Figure 2.24) between 97°E and 106°E and south of WZFZ. The two lateral features are bordered by irregular linear gravity highs (Gulden Draak Knoll, Batavia Knoll and Dirk Hartog Ridge – labeled in Figure 2.24 as GDK, BK and DHK respectively), and have a

~N20°E orientation; the gravity low in between is oriented ~N35°E. The easternmost feature (the Dirk Hartog Ridge), was discussed previously as representing a pseudofault in a north growing rift propagating system, formed in the Perth Basin at about 110 - 108 Ma (Fig. 2.24). The only information related to the age of the other features is the DSDP site 256 drilled closed to the westernmost feature (~102 Ma). Magnetic data are extremely sparse in this area, with just two ship tracks crossing these corridors (Figure 2.23). This area falls in the Cretaceous Quiet Zone (CQZ) according to age range shown on DSDP sites 256 (>106 Ma) and 257 (~102 Ma) (*Luyendyk and Davies* 1974). No attempt to interpret magnetic anomalies was made, although the magnetic record shows a few positive anomalies, which one would not expect in the CQZ (Figures 2.25b and c). One of them, a positive magnetic anomaly (Figure 2.25c) coincides with the gravity low mentioned before in the middle of this area. Combined magnetic, gravity and topography data (Figures 2.25b and c) suggest the presence of an extinct ridge (as in the case discussed in the Perth Abyssal Plain). It is possible that between the interpreted failed rift (the middle gravity anomaly low) and the pseudofault (the easternmost gravity anomaly low), several such events have occurred as the pseudofault does not parallel the failed rift except for the southern part (Figure 2.25a). However with the actual data coverage it is impossible to say how many and when such events took place. It is also difficult to explain with the available data the localized patches of positive gravity anomalies, some of them quite wide (e.g Batavia Knoll and Gulden Draak Knoll with areas of about 200 km^2, and 300 km^2 respectively) following the two interpreted pseudofaults (Figure 2.24).

One major element in interpreting the tectonic evolution in the Wharton Basin is finding the time when the major change in spreading direction took place.

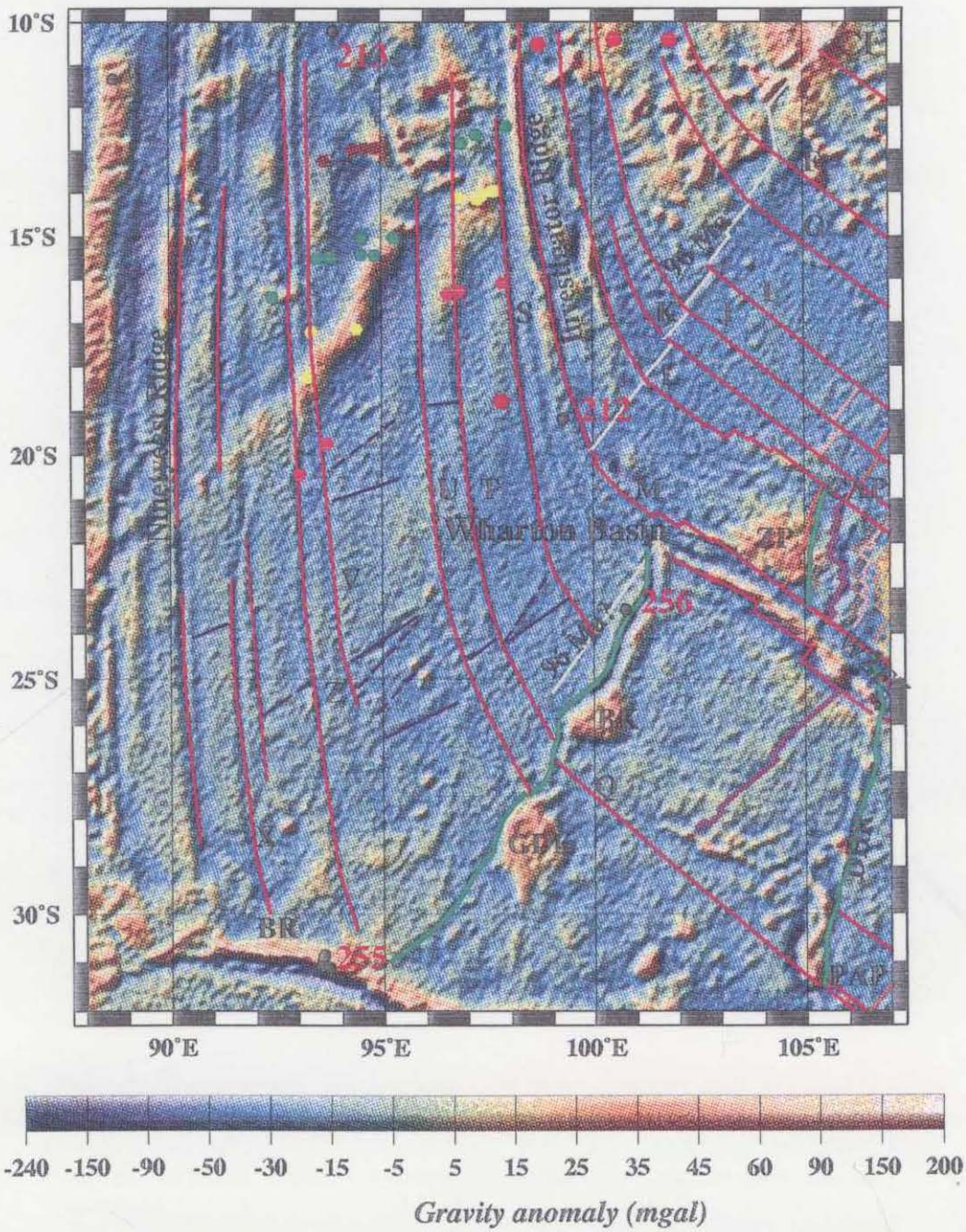

Fig.2.24 96 Ma isochron, fracture zones (red), extinct ridges (magenta) and pseudofaults (green) superimposed on the satellite-derived gravity anomaly grid (mgal) in the Wharton Basin. In blue are shown the two major gravity trends: continuous lines reflect the spreading direction whereas the dashed lines show features resulted from ridge propagators. Abbreviations and previously interpreted picks as in Figure 2.23.

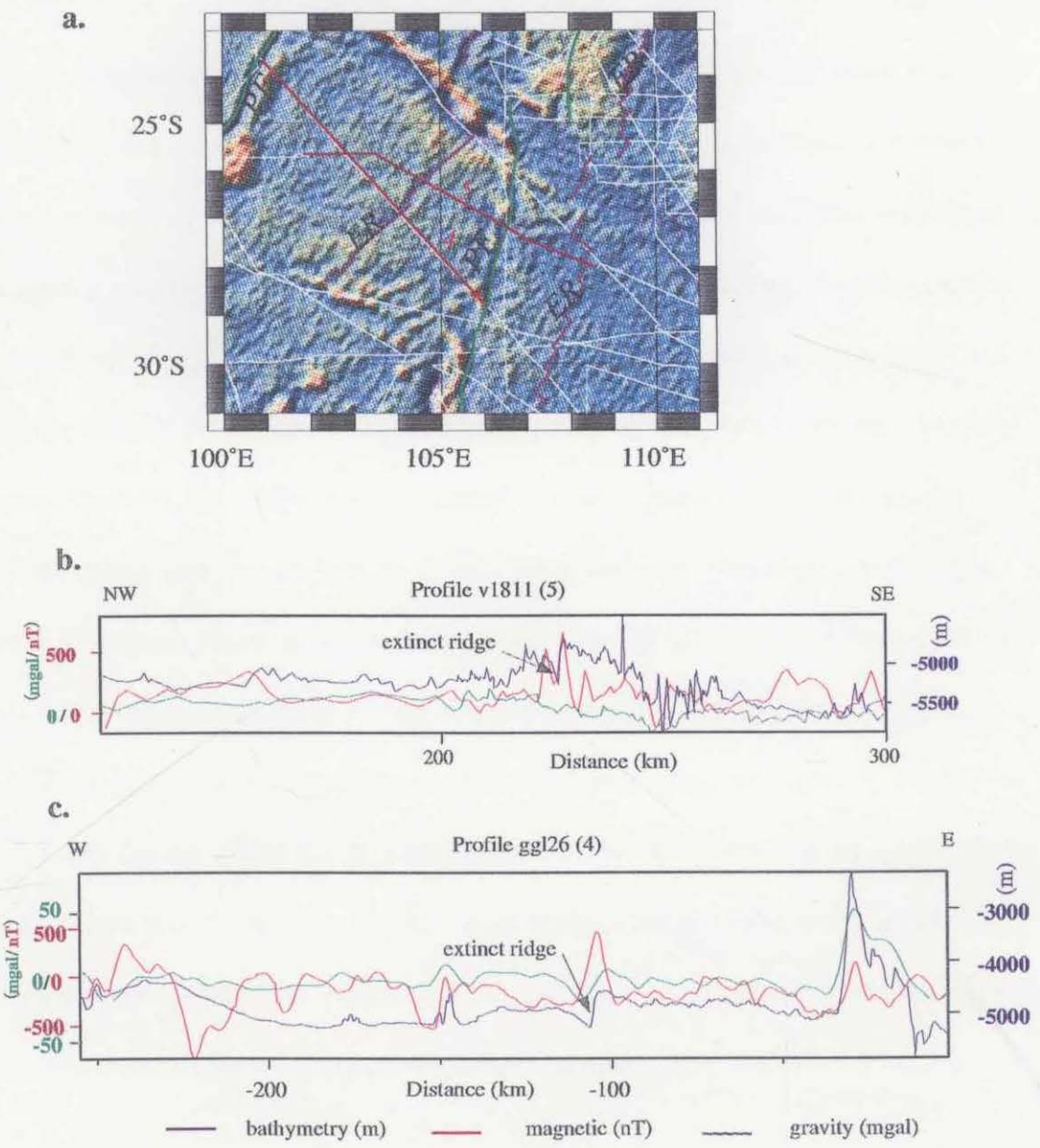

Fig.2.25 Projected magnetic, gravity and topography profile correlation (b and c) along an interpreted extinct ridge (ER) shown on the map (a) in magenta. Pseudofaults (PF) are shown in green, shiptrack and selected profiles are shown in white and red respectively.

According to the interpretation carried out in the area of Christmas Island (Figure 2.23) (*Borissova*, 1995), it appears that to the east of the island fracture zone directions follow a northwest-southeast trend, whereas to the west the fracture zones are oriented north – south. The fracture zones revealed by the satellite-derived gravity anomaly grid successively change their direction from northwest - southeast to north - south over about 120 - 130 km. The initial change in direction can be followed on the gravity grid which shows a continuous linear gravity anomaly low starting west of the Gascoyne Abyssal Plain and continuing south into the Wharton Basin (Figure 2.24). This trend is represented by a gravity high (possibly due to constructional volcanism which took place along the ridge soon after it was formed) in the Christmas Island area. With constraints from DSDP results on both sides of this feature (sides 212 about 91 Ma, and 256 about 102 Ma) and assuming that the spreading rate did not change between M0 and C34, the age estimated by *Powell et al.* (1988) for the initial major reorganisation (95/96 Ma) seems to be reasonable. However, in their interpretation there is an abrupt change in direction, which took place at about 95/96 Ma. Therefore, the age for the linear gravity anomaly low considered in the present study agrees with an estimated age of 96 Ma.

At least ten major fracture zones have been interpreted in the Wharton Basin based on the satellite-derived altimetry grid, six more than previously interpreted (Figure 2.24). Their offset possibly continues to be left-lateral as interpreted in the abyssal plains.

Surprisingly the satellite-derived gravity grain shows two trends, a northeast-southwest trend and an east-west trend (Figure 2.24). The northeast-southwest trend

is not perpendicular to the fracture zones. Several major positive gravity trends also follow the same orientation. The east-west trend, perpendicular to the fracture zones would show the spreading direction. The northeast-southwest trend might be the result of ridge propagator events. Such a major change in spreading direction as occurred in the eastern Indian Ocean might have triggered several ridge propagator events whose elements (extinct ridge and pseudofaults) would show an oblique trend to the fracture zones. If this assumption is correct, and the fact that most of the magnetic picks interpreted previously in the Wharton Basin seem to be located along new interpreted major fracture zones (Figure 2.24) lead to the conclusion that the interpreted magnetic anomalies in the Wharton Basin might not be correct. Due to the sparsity of magnetic data as well as the tectonic complexity revealed by the satellite-derived gravity anomaly grid a proper magnetic interpretation would be possible only after acquiring more data.

A comparison between satellite-derived gravity data and ship gravity data was carried out to investigate whether the oblique direction of the satellite gravity fabric may be an artefact (Figure 2.26). The two selected profiles show a good correlation between the short-wavelength anomalies from the satellite-derived gravity grid with the ship gravity anomalies confirming that these anomalies are not artefacts in the satellite data.

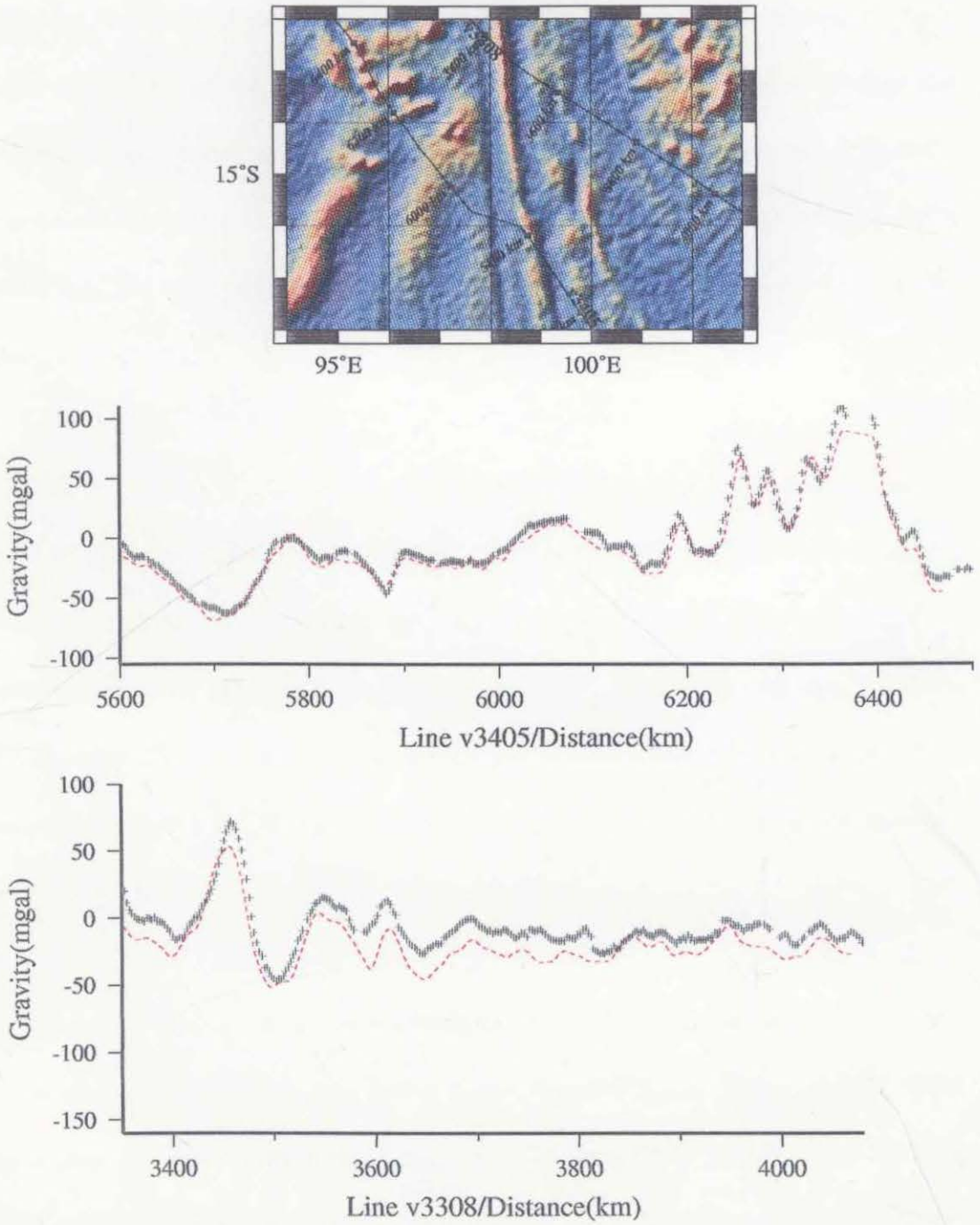

Fig.2.26 Comparison between the satellite gravity (red line) and ship track gravity (black stars). The small map shows the location of selected ship tracks.

2.6 Fracture zones

Images of the marine gravity field (*Sandwell and Smith*, 1997) from satellite altimetry provide improved interpretations of fracture zones as well as other tectonic features (extinct spreading ridges, COB, etc). The general northwest trend of the fracture zones interpreted from dense satellite gravity data differs from previously interpreted fracture zone (Figure 2.27). The new gravity anomaly data allowed to better map the fracture zones in the abyssal plains adjacent to the western Australian margin.

The location of fracture zones on gravity data recorded by satellite depends on the type of the ocean floor spreading regime. Large offset Pacific fracture zones (i.e. a fast spreading regime) exhibit a depth/age step (the old side is lower because of greater amount of subsidence during the geological time) (*Sandwell and Schubert*, 1992), whereas small to medium offset Atlantic and western Indian Ocean (slow spreading regime) are characterised by a central valley visible on geoid anomaly (*Van Andel*, 1971; *Fox and Gallo*, 1984).

Several major fracture zones were interpreted along the Argo, Gascoyne, Cuvier and Perth abyssal plains continuing further in the Wharton Basin. Some of these faults have large offsets as in the case of fault E (~ 300 km), CRTF – fault G - (~450 km), CTF – fault L (~230 km), WZTF (~800 km) and faults P and Q (~130 and ~180 km respectively) (Figs. 2.13, 2.17 and 2.21). In some cases the offset of the faults has been increased due to accreted fragments of the Indian Plate (330 km in the case of WZFZ, 150 km in the case of CRFZ and CTF and 70 km for fracture Q). Their trend

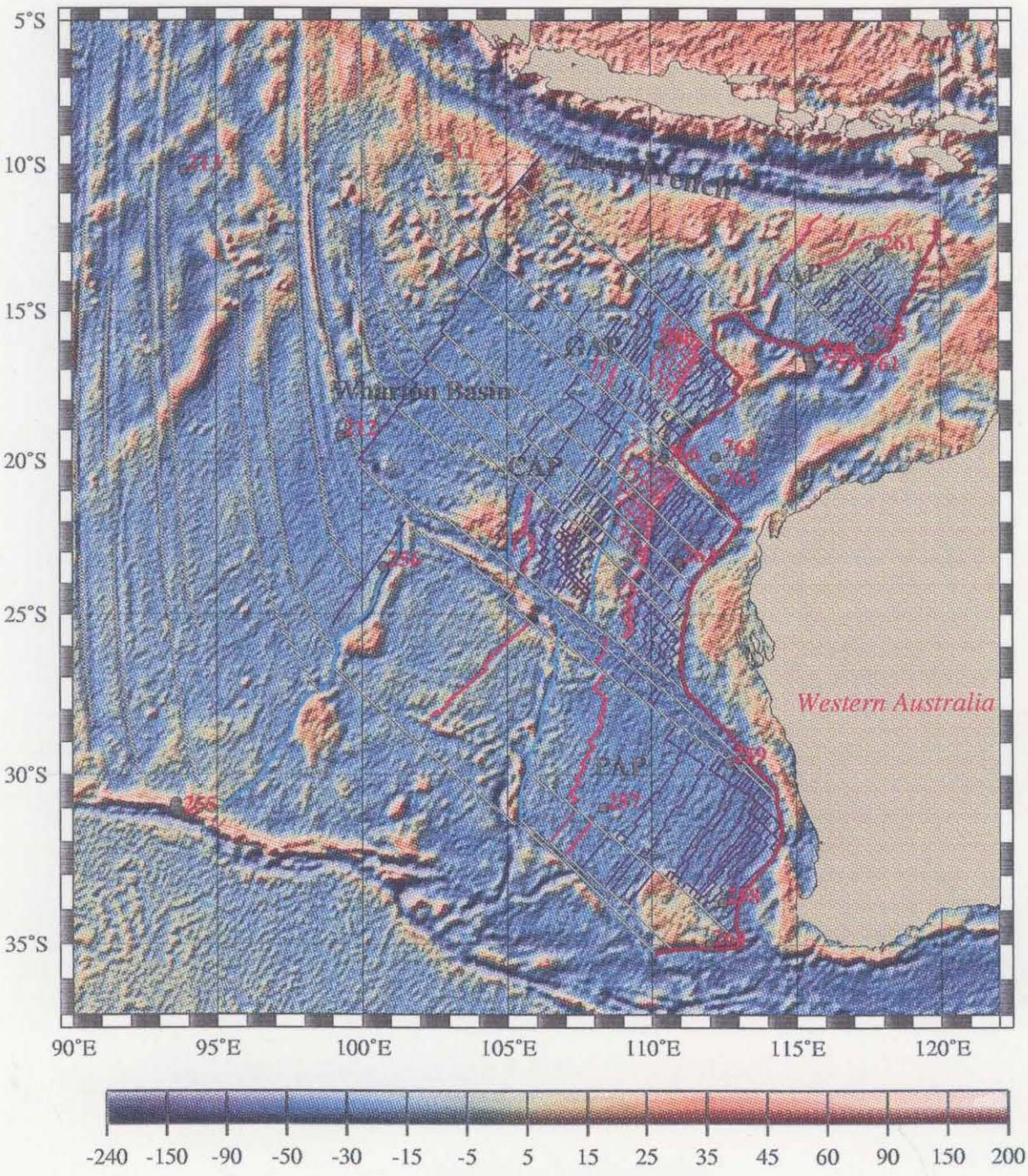

Fig. 2.27 Isochrons (blue for the Australian Plate and red for the accreted Indian Plate), COB (red), fracture zones (grey), extinct ridges (magenta), and pseudofaults (cuyan), superimposed on the satellite-derived gravity anomaly grid in the Wharton Basin and in the Argo (AAP), Gascoyne (GAP), Cuvier (CAP) and Perth (PAP) abyssal plains. Black dots represent DSDP and ODP sites.

of N45°W changes to N35°W after anomaly M5 (127.7 Ma). Fracture zones with small offset were also interpreted in all abyssal plains following offsets in magnetic anomalies and discontinuities in the gravity grid. Possibly these faults continue in the Wharton Basin.

2.7 Summary

Unknown and better defined existing seafloor features as well as trends observed in new satellite-derived gravity anomaly data (*Sandwell and Smith*, 1997) led to a re-evaluation of the seafloor spreading history along the western Australian margin. By combining gravity, magnetic, topography and seismic data it was possible to determine a northeast structural trend of the magnetic isochrons in the Argo Abyssal Plain. This trend is in agreement with the basement strike interpreted from seismic reflection data (*Gopala et al.*, 1994) and differs from the east-northeast trend of *Fullerton et al.* (1989) and *Sager et al.* (1992) based mainly on magnetic data. Also slightly different trends than described by *Fullerton et al.* (1989) and *Veevers et al.* (1985) were interpreted in the Gascoyne, Cuvier and Perth abyssal plains (N45°E from the former N30°E for anomalies older than M5 and N35°E from ~N33°E for anomalies younger than M5).

Several major fracture zones were recognized based on trends on the satellite-derived gravity anomaly data. Fracture D separates the Argo and Gascoyne abyssal plains (Fig.2.7), fracture E and F define the central Gascoyne basin (Figure 2.13).

Fractures G and K define the northern Cuvier Abyssal Plain, M, N and O fractures represent the Wallaby-Zenith Fracture Zone and separate the southern Cuvier and Perth abyssal plains (Figure 2.17). The fracture zones Q and R represent the southern margin of the Perth Abyssal Plain (Figure 2.21).

The satellite derived gravity anomaly grid along the western Australian margin displays many features whose previous structure and origin were only vaguely understood. Some of them were better explained in the light of the new interpretation (e.g. the Sonne, Sonja ridges in the Cuvier Abyssal Plain), whilst others still remain geological enigmas (e.g. the Batavia and Gulden Draak knolls). Undulating features identified on the satellite-derived gravity grid data, which do not follow the regional trend and also interpreted conjugate anomalies (red lines in Figure 2.27) led to the idea of accretion of pieces of Indian Plate to the Australian Plate by processes of ridge propagators. Nine such ridge propagator events (displaying extinct ridges and pseudofaults) were interpreted: one (or two) in the Argo Abyssal Plain, two in the Gascoyne and Perth abyssal plain, three in the Cuvier Abyssal Plain and one in the Wharton Basin. Fracture zones identified in the abyssal plains continue in the Wharton Basin changing their direction at about the 96 Ma isochron that was identified in the basin as following a low gravity trend.

COB follows a gravity low along the margin and is represented by a combination of rifted segments linked by transform faults. Some of the transform faults have large offsets as in the case of Cape Range Fracture Zone (G, H), Wallaby-Zenith Fracture Zone (M, N, O) and fracture Q.

The northeast-southwest trend of the satellite-derived gravity grain in the Wharton Basin was interpreted as a result of ridge propagator events. These events were probably triggered by the major change in the spreading direction, which took place after 96 Ma.

Chapter 3

Plate tectonic model

3.1 Introduction

Many authors (e.g. *McKenzie and Sclater*, 1971; *Sclater and Fisher*, 1974, *Johnson et al.*, 1976; *Duncan*, 1978; *Norton and Sclater*, 1979; *Powell et al.*, 1980; *Royer and Sandwell*, 1989; *Lee and Lawver*, 1995) have used the theory of plate tectonics to reconstruct the tectonic history of the eastern Indian Ocean and the past position of the continents surrounding this basin. This has resulted in a fairly well understood tectonic framework of the region. Recently declassified, dense satellite altimetry data (*Sandwell and Smith*, 1997) allow us to map the structure of the ocean floor in much more detail than previously possible and to better constrain fracture zone locations and, therefore, past plate motions. These data were utilized jointly with the magnetic anomaly data to investigate the Late Cretaceous plate kinematic framework of the eastern Indian Ocean. The Australian Plate has recorded complex deformational processes, which are expressed in major tectonic features. These include segments of the Indian Plate that were accreted to the Australian Plate as result of several ridge propagating events in the Gascoyne, Cuvier and Perth abyssal plains as well as anomalous ridges and troughs (e.g. Ninetyeast, Sonne, Sonja, Dirk Hartog ridges). The area of interest also includes such large submarine plateaus as the Wallaby, Zenith and Naturaliste plateaus (see Figures 2.14 and 2.18).

According to previous studies three main phases of seafloor spreading occurred among the major plates (India, Australia and Antarctica) in the eastern Indian Ocean (*Royer and Sandwell*, 1989). (1) From Late Jurassic to Early Cretaceous times, Greater India separated from Antarctica/Australia resulting in the Mesozoic basins along the western Australian margin (*Markl*, 1974, 1978; *Veevers et al.*, 1985;

Fullerton et al., 1989). (2) From Early Cretaceous to Middle Eocene times the northward motion of India opened the Wharton Basin (*Sclater and Fisher*, 1974; *Liu et al.*, 1983). (3) From Eocene to present time the Australian-Antarctic Basin (*Weissel and Hayes*, 1972) opened along the Southeast Indian Ridge. These phases of spreading were separated by two periods of basinwide plate reorganization (*Royer et al.*, 1992), the first in the Cretaceous Quiet Zone (Early/mid-Cretaceous) and the second during Middle Eocene time.

In the present study new and old magnetic anomaly data were combined with Seasat and Geosat satellite altimetry data to create a self-consistent data set for the eastern Indian Ocean. Finite rotations were estimated for 8 times from the time of opening of the Argo Abyssal Plain (~156 Ma) to 96 Ma isochron C34 (83.5 Ma). Although the absence of symmetric Mesozoic basins in the eastern Indian Ocean, subducted under the Eurasian Plate, represented a major problem, the reconstructions between India and Australia in a fixed reference frame by "restoring" the Indian oceanic crust based on using half-stage poles, created a self consistent plate kinematic model. This model includes India, Australia, Antarctica Africa and Madagascar. Indian Plate isochrons were restored from the Australian Plate isochrons by creating finite rotations from full stage rotations assuming symmetry of spreading.

If magnetic anomalies are preserved on both plates one can compute finite rotation poles from conjugate sets of magnetic anomalies from which to derive the stage poles. Due to the absence of magnetic anomalies on the Indian Plate conjugate to Australia it was necessary to calculate half stage rotations for the Australian M-sequence, full stage rotations assuming symmetry of spreading and then finite

rotations. Full stage rotations were calculated for times for which Indian Plate magnetic anomalies are preserved on the Australian Plate (M5-M11 and M2-M3).

3.2 Stage and finite rotations

3.2.1 Stage rotations

Stage rotations (instantaneous rotations or difference rotations) were required to calculate finite rotations, angular spreading rates, spreading directions and synthetic transform faults. A stage pole and a rotation angle describe the plate motion during an individual stage. The latitude and longitude of the stage poles that defined the motion between India and Australia between 156 and 96 Ma, were determined by a trial-and-error method superimposing two transform faults, one for the Indian Plate and the other for the Australian Plate. This method was used in the case of preserved magnetic anomalies from the Indian Plate (M5-M11 and M2-M3). For those reconstruction times for which no Indian Plate is preserved, stage rotations were determined whose flowlines parallel fracture zones on the Australian Plate. Two stage poles that describe the motion of the Indian Plate relative to the Australian Plate for the period of 156 – 96 Ma were determined (Table 3.1).

In the case of preserved crust from the Indian Plate the angle of rotation was determined by superimposing magnetic anomalies of the same age from both plates to determine full-stage rotation angle. When no crust from the Indian Plate was preserved (as in the case of magnetic anomalies older than M11 and younger than

M5) half-stage rotation angles were first determined by superimposing two adjacent magnetic anomalies and then multiplying by two to calculate full-stage rotation angle (assuming symmetry in spreading).

Table 3.1

Stage rotations calculated for the Indian Plate relative to the Australian Plate

Anomaly Interval	Latitude (+°N)	Longitude (+°E)	Angle (°) +=counterclockwise
C34 - 92 Ma	22.4	152.8	-12.30
92Ma-92 Ma	44.1	162.5	-5.89
96 Ma – M0	46.6	164.0	-5.54
M0 - M2	47.5	170.2	1.80
M2 - M3	47.5	170.2	0.60
M3 - M4	47.5	170.2	1.20
M4 - M5	47.5	170.2	0.60
M5 - M6	35.5	170.2	0.30
M6 - M7	35.5	170.2	0.30
M7 - M8	35.5	170.2	0.38
M8 - M9	35.5	170.2	0.49
M9 - M10	35.5	170.2	0.48
M10 - M10N	35.5	170.2	0.62
M10N - M11	35.5	170.2	0.81
M11 - M11A	35.5	170.2	1.02
M11A - M12	35.5	170.2	0.82
M12 - M12A	35.5	170.2	0.70
M12A - M13	35.5	170.2	0.50
M13 - M14	35.5	170.2	0.76
M14 - closure	35.5	170.2	0.60
M14 - M22A	35.5	170.2	2.79
M22A - M23	35.5	170.2	0.40
M23 - M24	35.5	170.2	1.12
M24 - M24A	35.5	170.2	0.78
M24A - M24B	35.5	170.2	0.48
M24B - M25	35.5	170.2	0.84
M25 - M25A	35.5	170.2	0.62
M25A - M26	35.5	170.2	0.80
M26 - closure	35.5	170.2	0.60

An extrapolated age for the COB of 156 Ma was derived and used to calculate the M26-closure stage pole for the central part of the Argo Abyssal Plain and an age of 136.2 Ma for M14-closure in the southern part of the Cuvier Abyssal Plain. In other areas the distance between the oldest magnetic anomaly interpreted and the COB was used to calculate the age of COB, assuming that no change in the spreading rate occurred. For calculating the rotation angle between M14 and M22A no change in spreading rate for this period was assumed.

3.2.2 Finite rotations

The basis for reconstructing plates is that one single equivalent rotation can restore them to their original position. For any position of any pair of plates relative to each other, one single finite reconstruction pole can be found that will restore the plates to their position at a time in the past. A direct geometrical reconstruction from the present day to a particular chron is that of a rotation in terms of latitude, longitude and angle (Table 3.2). However, there are other representations for rotations (e.g. quaternians, *Le Pichon*, 1973).

The method used in this study to compute finite rotation poles that describes the relative motion between the Australian Plate and Greater India, was to add stage rotations to the finite rotation for chron C34 from *Royer and Sandwell (*1989). These new finite rotations are different from those derived by *Veevers et al*'s (1991) and *Powell et al.* (1988) (Table 3.3). The values were used later in this chapter to

compare flowlines derived from the present interpretation with that of the earlier researchers, interpretation.

Table 3.2

Finite rotations calculated for the Indian Plate relative to the Australian Plate

Chron	Time (Ma)	Latitude (+°N)	Longitude (+°E)	Angle (°) +=counterclock-wise	Reference
closure	156.0	16.76	-170.46	72.62	
M26	155.0	16.47	-170.45	71.90	
M25A	154.5	16.17	-170.44	71.18	
M25	154.1	15.94	-170.43	70.62	
M24B	153.5	15.62	-170.41	69.87	
M24A	153.1	15.43	-170.40	69.44	
M24	152.1	15.12	-170.39	68.74	
M23	150.7	14.67	-170.37	67.74	
M22A	150.4	14.50	-170.35	67.39	
closure	136.2	13.23	-170.31	64.74	
M14	135.9	12.96	-170.30	64.23	
M13	135.3	12.62	-170.28	63.57	
M12A	135.0	12.39	-170.27	63.13	
M12	134.0	12.06	-170.26	62.52	
M11A	133.4	11.67	-170.24	61.80	
M11	132.1	11.17	-170.22	60.92	
M10N	130.9	10.77	-170.20	60.22	
M10	130.2	10.45	-170.19	59.69	
M9	129.5	10.20	-170.18	59.27	
M8	129.0	9.95	-170.16	58.86	
M7	128.4	9.75	-170.16	58.53	
M6	128.2	9.60	-170.15	58.29	
M5	127.7	9.47	-170.14	58.09	
M4	126.7	9.07	-170.21	57.65	
M3	124.7	8.24	-170.34	56.77	
M2	124.0	7.83	-170.40	56.34	
M0	120.4	6.52	-170.61	55.04	
	96.0	3.91	8.73	47.33	
C34	83.5	-0.4	176.90	42.16	Royer and Sandwell, 1989

Table 3.3

Finite rotations calculated for the Indian Plate relative to the Australian Plate (from *Veevers et al.*, 1991)

Chron	Time (Ma)	Latitude (+°N)	Longitude (+°E)	Angle (°) +=counterclockwise	Reference
C34	85.3	-0.59	-5.38	-42.20	Veevers et al., 1991
	96.0	-2.17	-5.80	-55.15	"
M0	118.0	-10.24	7.66	-59.90	"
M11	132.5	-14.49	15.3	-64.65	Powell et al., 1988
closure	160.0	-14.79	15.35	-64.65	"

3.3 Synthetic flowlines

The use of well identified fracture zones combined with magnetic anomaly data is crucial for constraining plate tectonic reconstructions. The interpretation of fracture zones in this study was based on offsets in magnetic anomalies and lineations on satellite-derived gravity anomaly data.

Transform faults are approximately oriented along small circles of plate motion. A straightforward way to verify the two positions of the stage poles derived for the M-sequence adjacent to the Australian margin (35.5°N/170.2°E for M5-M26 sequence and 47.5°N/170.2°E for M0-M4 sequence) is to compare small circles derived from these poles with the interpreted fracture zone directions. Figure 3.1 shows that the fracture zones parallel and correlate well with the computed small circles in the entire interpreted area.

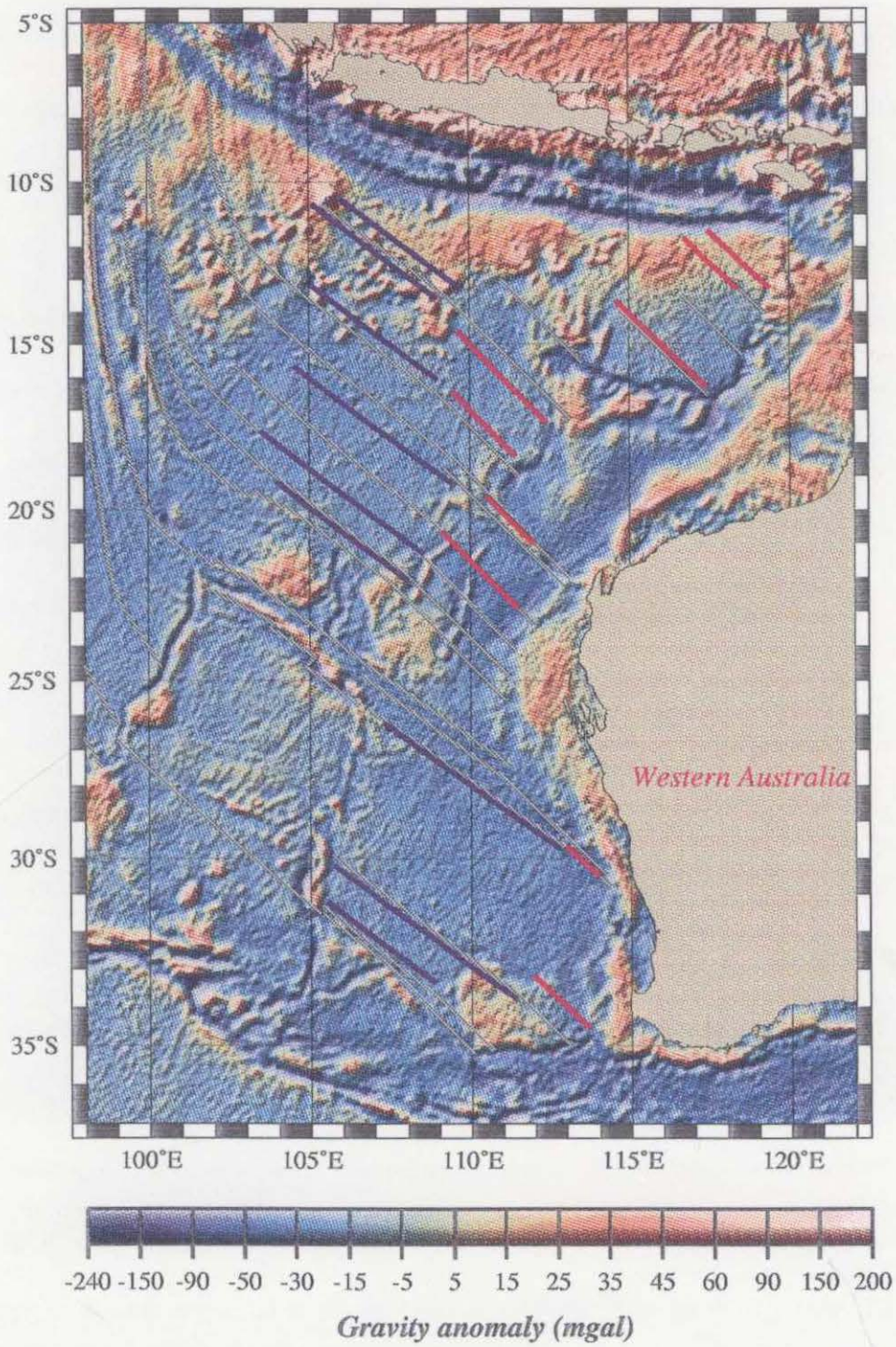

Fig. 3.1 Comparison between the fracture zone directions (grey lines) in the Argo, Gascoyne, Cuvier and Perth abyssal plains with small circles about two stage poles situated at 35.5°N/170.2°E and 47.5°N/170.2°E. These stage poles describe the motion of two pieces of Greater India (North and Middle Greater India) relative to the Australian plate for periods between 156 Ma - 126.7 Ma (red lines) and 126.7 Ma - 120.4 Ma (blue lines).

Synthetic fracture zones were computed from the new stage poles of motion between the Indian and Australian plates (Figure 3.2). By comparing the observed and synthetic transform trends, an estimate can be made (albeit indirectly) of the accuracy of calculated pole positions. In order to verify whether the motion between India and Australia reflects also the relative motion between India and Antarctica, synthetic fracture zones were computed for an area of the Eastern Antarctic margin considered to be conjugate to the eastern Indian and southern Madagascan margins (the Enderby Basin). Assuming that the seafloor spreading adjacent to the Australian margin after chron M0 (120.4 Ma) relates to the motion of Greater India-Australia/Antarctica, synthetic flowlines in the Enderby Basin should follow trends identified on the satellite derived gravity data in this basin (Figure 3.3).

Synthetic fracture zones were generated for spreading episodes corresponding to the M4-C34 sequence in the Gascoyne Abyssal Plain (Figure 3.2) and for the M0-C34 sequence in the Enderby Basin (Figure 3.3) and superimposed on the satellite derived gravity data. The present model (blue lines and stars) shows a relatively good correlation in both basins between the synthetic flowlines and fracture zones in the Gascoyne Abyssal Plain (Figure 3.2) and trends on the satellite derived gravity data in the Enderby Basin (Figure 3.3). Flowlines drawn at the Antarctic COB show that they match with the C34 interpretation considering that the opening between Antarctica and India occurred at about 120 Ma (Figure 3.3). In the Enderby Basin, the synthetic flowlines predict a history of Cretaceous opening since ~120 Ma (chron M0). In order to account for oceanic crust that formed at the same time east of the Enderby Basin (see reconstructions in this Chapter) a large offset (~500 km or more) pre chron C34 is required along the Kerguelen Fracture Zone.

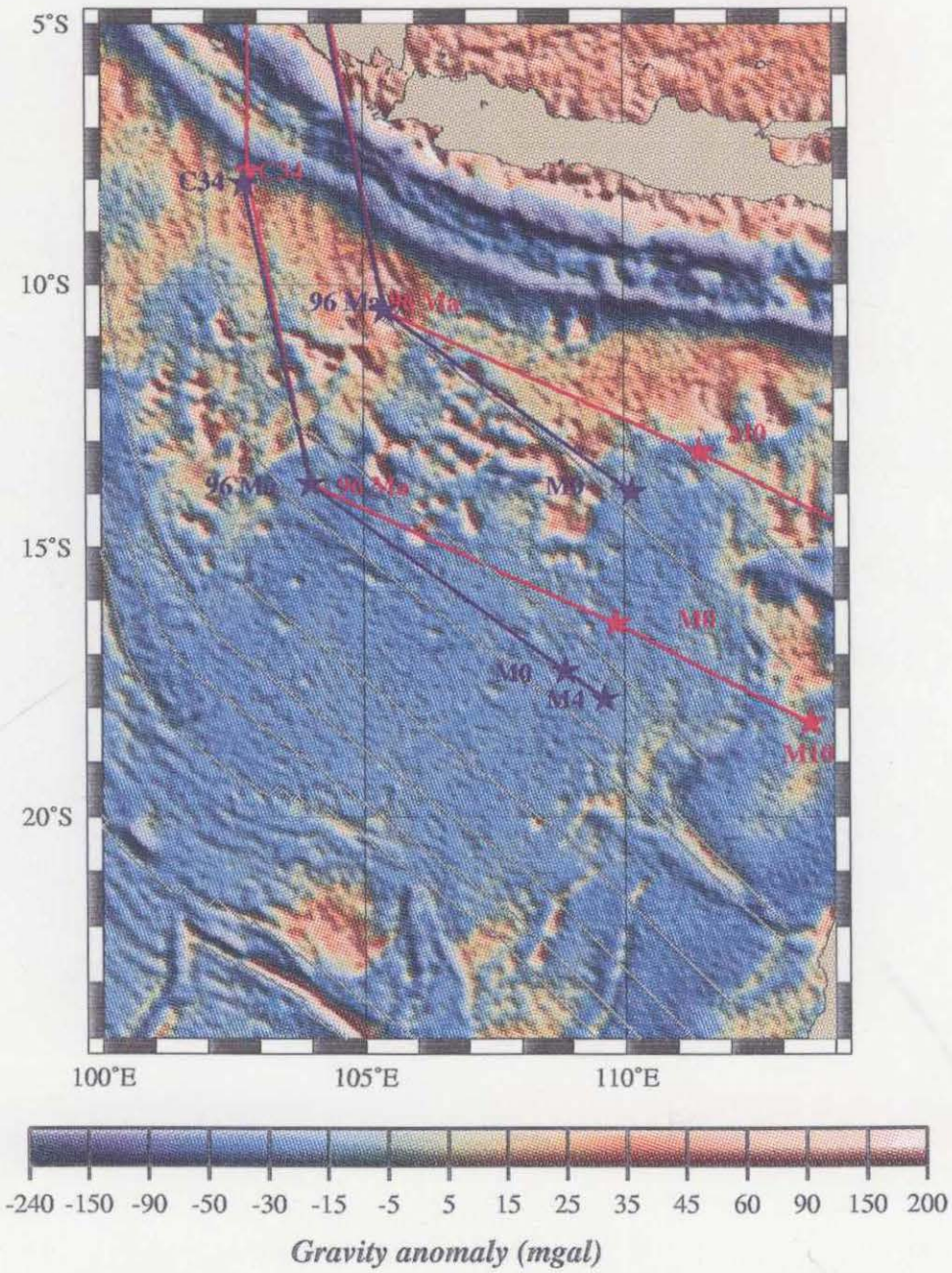

Fig. 3.2 Synthetic flowlines based on finite rotation angles computed in the present study - blue lines and stars - and from previous models (Powell et al., 1988; Veevers) et al., 1991) - red lines and stars - superimposed on the satellite-derived gravity anomaly grid (mgal) in the Gascoyne Abyssal Plain. Grey lines represent interpreted transform faults.

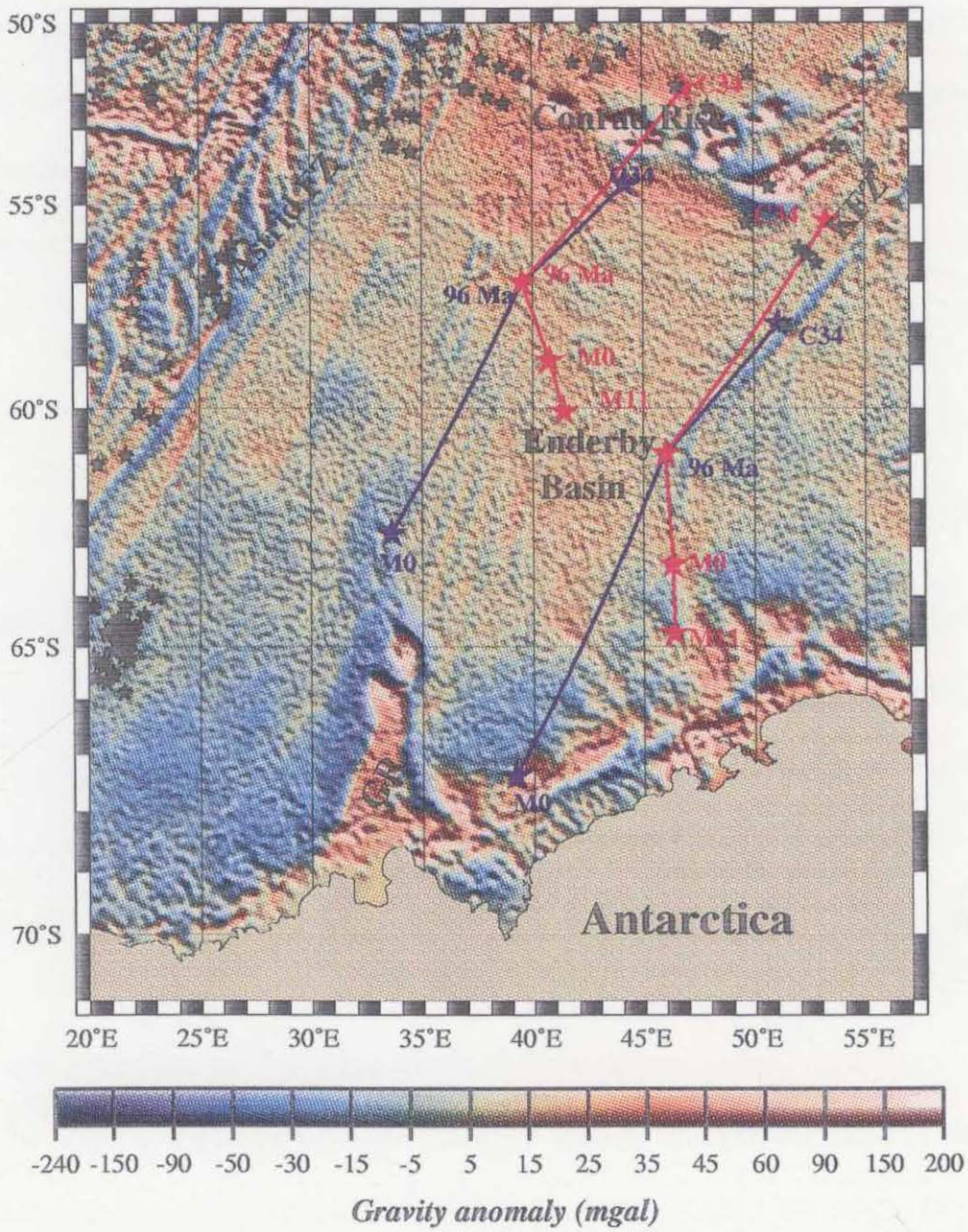

Fig. 3.3 Synthetic flowlines based on finite rotation poles computed in the present study - blue lines and stars - and from previous models (Powell et al., 1988; Veevers) et al., 1991) - red lines and stars - superimposed on the satellite-derived gravity anomaly grid (mgal) in the Enderby Basin. Black stars represent interpreted magnetic picks from the PLATE database (Coffin et al., 1992). Abbreviations are: GR-Gunnerus Ridge, KFZ-Kerguelen Fracture Zone.

Flowlines (red lines and stars) derived using previously interpreted finite rotation poles (*Powell et al.*, 1989; *Veevers et al.*, 1991) were also shown in Figures 3.2 and 3.3. There is an evident mismatch between the synthetic flowlines and the trends shown on the satellite derived gravity data in both basins. The present model shows that seafloor spreading in the Gascoyne, Cuvier and Perth abyssal plains after chron M0 is also related to the breakup of South Greater India and Antarctica (see reconstructions later in this Chapter).

3.4 Spreading rates

Variations in spreading rates and spreading directions were calculated for several points two of which are shown in Figure 3.4, one in the Argo Abyssal Plain situated on anomaly M22A in the central part of the basin and one for the Cuvier Abyssal Plain situated on anomaly M5. The directions and (half) rates of spreading were derived from the finite rotations (Table 3.2).

Seafloor spreading in the Argo Abyssal Plain began before chron M26 (at approximately 156 Ma) in a NE-SW direction with a high spreading rate of about 160 mm/yr. The spreading rate decreased to 80 mm/yr at 153.5 Ma (chron M24B) and to 60 mm/yr at 153.1 Ma (chron M24). The spreading direction remained relatively constant at northwest-southeast (Figure 3.4). In the Cuvier Abyssal Plain, following the same spreading direction, the high spreading rate of 140 mm/yr before chron M14 (at about 136.2 Ma) dropped to an average of 90 mm/yr between chron M12A (135 Ma) and M5 (127.7 Ma). It continued to decrease to 60 mm/yr between

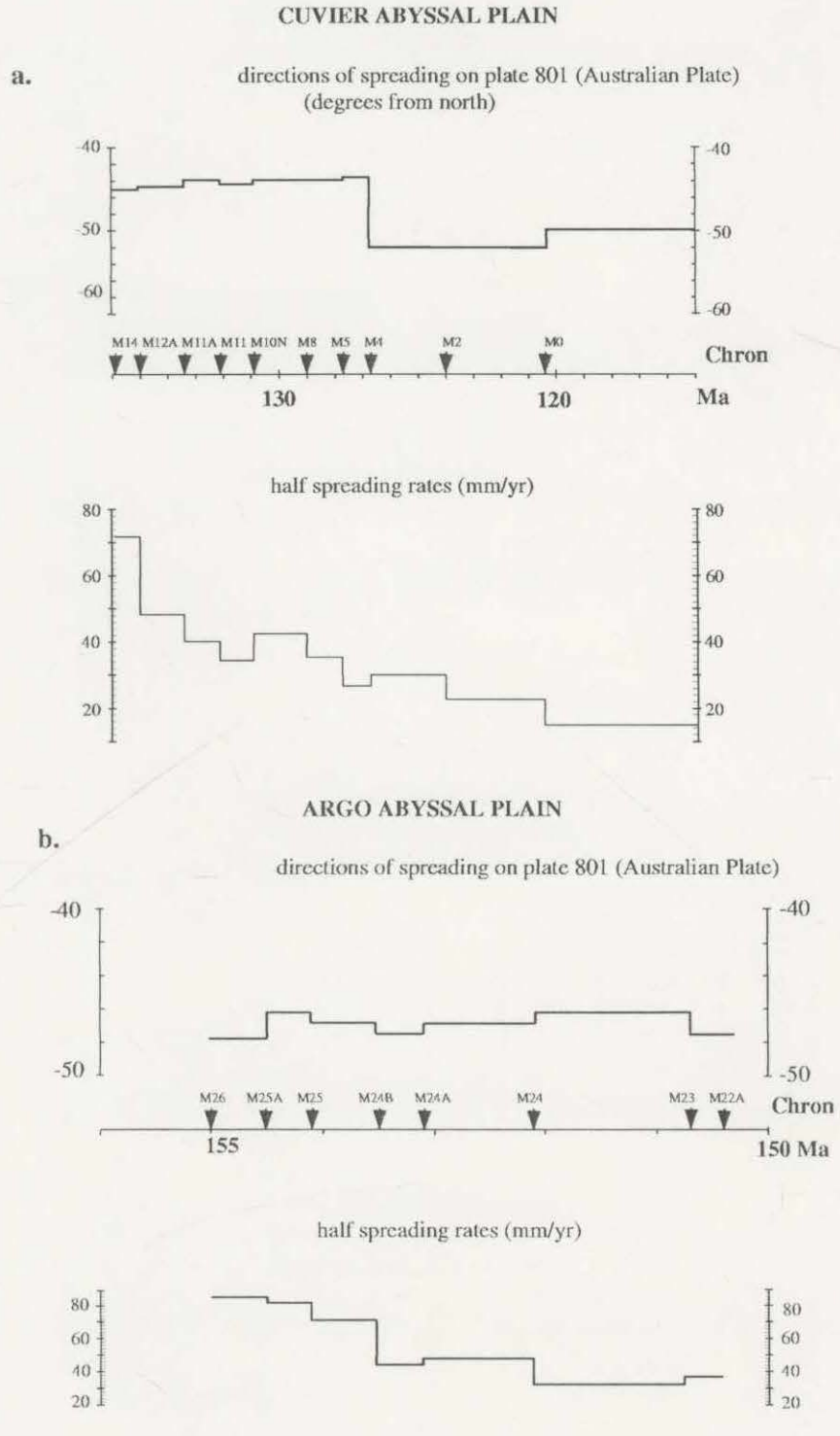

Fig. 3.4 Direction and half rate spreading in the Cuvier (a) and Argo (b) abyssal plains derived from finite rotations (Table 3.2) for points located on chron M4 (a) and on chron C22A (b).

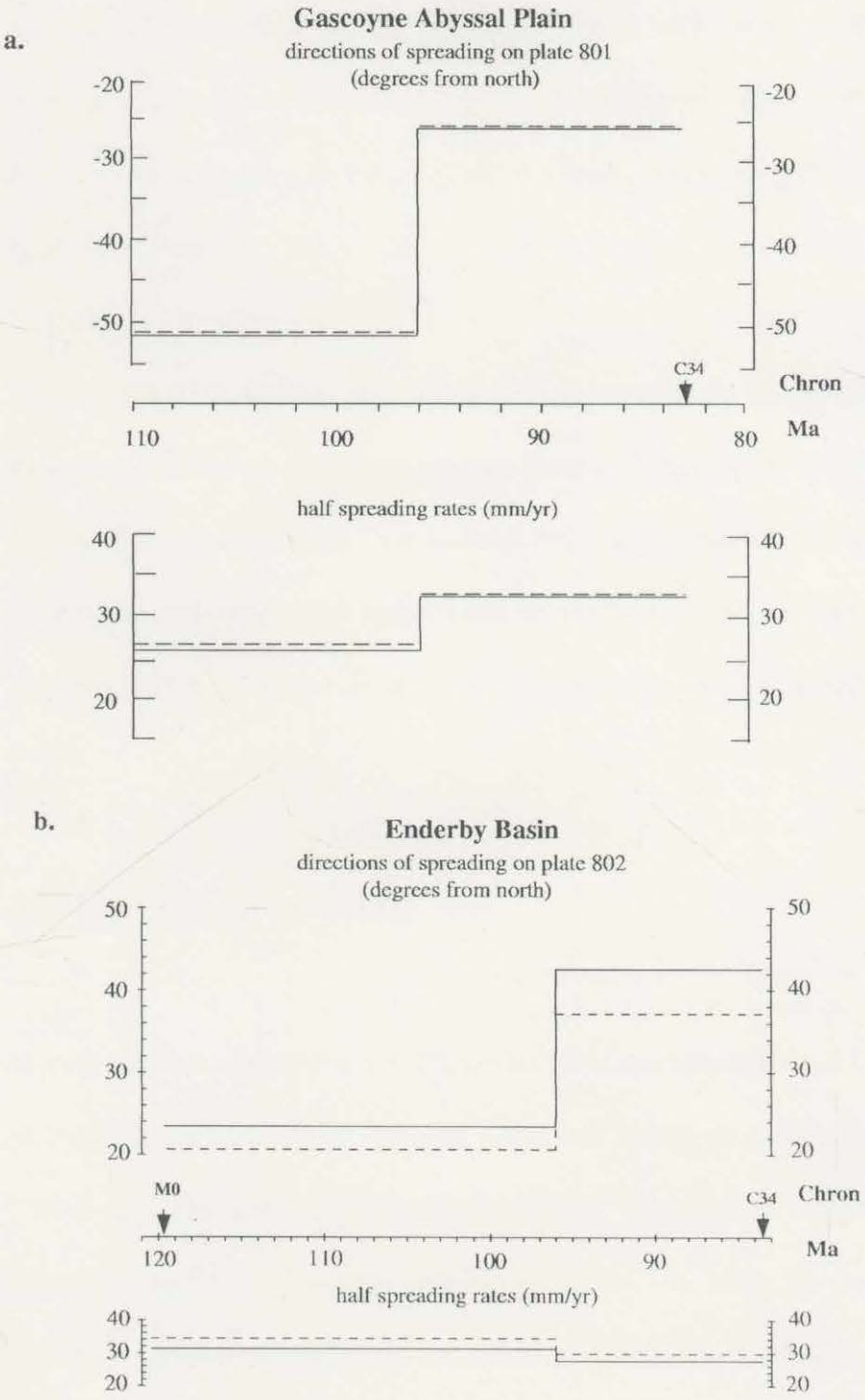

Fig. 3.5 Direction and half spreading rate evolution in the Gascoyne Abyssal Plain (a) and Enderby Basin (b) derived from finite rotations (Table 3.2) for two points located on 96 Ma isochrons.

chrons M5 and M0 (120.4 Ma) and to 30 mm/yr after chron M0. The spreading direction changed from about northwest-southeast (-45°) to about -52° at chron M5 corresponding also with a change in the spreading rate (from ~40 mm/yr to ~30 mm/yr). This change also corresponds to a major plate reorganization between the Indian and Australian plates.

Directions and spreading rates (for two points situated on the 96 Ma isochron) were also computed for the Gascoyne Abyssal Plain and Enderby Basin. As seen in Figure 3.5, there is a major change in spreading direction and rate at ~96 Ma in both basins. This represents the time when Greater India changed its spreading direction progressively from northwest to north (over ~5 m.y.) until it collided with Eurasia.

3.5 Reconstruction model

During the past twenty years, our knowledge of the Mesozoic and Cenozoic relative motion between the major tectonic plates has increased substantially even though "absolute" plate motions relative to a "fixed" mesosphere are still controversial. Identified magnetic anomalies, some as old as 156 Ma, along with tectonic lineations based on bathymetric and satellite altimetry data define relative plate motions for most of the major plates. One of the widely used methods of reconstructing plates relative to a fixed mesosphere utilizes linear chains of volcanoes that display age progression and are thought to be caused by focused spots of melting in the upper mantle. *Morgan* (1971, 1972) suggested that hotspots may be caused by upwelling

mantle plumes, which remain fixed relative to each other over geologically long periods of time ("fixed hotspot hypothesis"). Subsequently, numerous models were developed to determine motion of the lithosphere relative to fixed hotspots.

Large uncertainities might result in reconstruction of motion of any plate relative to the mantle for times before chron 34 (83.5 Ma). This is a result of using only two hotspots tracks that determine the choice of plate motions over the hotspots from early Cretaceous to present. These hotspot tracks are Tristan, Walvis Ridge/Rio Grande Rise (for Tristan da Cuhna hotspot) – 0-130 Ma and Corner Seamounts/New England Seamounts/younger White Mountains (for the Great Meteor hotspot) – 0-130 Ma (*Morgan*, 1983; *Müller et al.*, 1993). For times older than 130 Ma, for which no continuous hotspot tracks are available, the present model assumes that Africa was fixed relative to the mantle. Reconstructions are also constrained by new fracture zones and magnetic lineations interpreted in this study. All the reconstructions are presented in an absolute reference frame (plates moving relative to the mantle).

In the present reconstructions Greater India was considered to result from three pieces (herein referred to as North, Middle and South Greater India) that separated gradually by dextral strike slip motions from Gondwanaland and became fixed to each other (before 136 Ma – North and Middle Greater India – and at about 96 Ma – Middle and South Greater India). With the present data this model represents the only one consistent with all relative plate motions involved in the breakup of eastern Gondwanaland (Africa - Madagascar, Africa - Antarctica, Madagascar - India, India - Australia, Australia – Antarctica, India - Antarctica).

All the derived finite rotation poles were kept in a hierarchical "rotation file" (see Appendix 3). The architecture of a rotation file has a tree-like structure expressing relative rotations between pairs of plates. Figure 3.6 shows several "rotation trees" for periods when major events occurred. For example at 120.4 Ma seafloor spreading started between Antarctica and Australia (*Tikku and Cande*, 1977) and Middle Greater India (MGI) and Australia. At this time North Greater India (NGI) was fixed to MGI and Australia, South Greater India (SGI) and Madagascar were fixed to Africa that was kept fixed relative to the mantle (absolute framework). Also there was relative motion (along a dextral strike slip fault) between Madagascar and SGI due to a faster northward motion of Madagascar relative to SGI.

To complete the reconstructions, conjugate "Indian" isochrons, that were not accreted to the Australian Plate and were lost during the subduction of the Indian Plate under the Eurasian Plate, were restored and included in the reconstructions (see Table 3.4). Active mid-ocean ridges, COB, extinct ridges and pseudofaults are also shown in reconstructions (Figures 3.7a to 3.7g).

Figure 3.7a shows the initial outline of the east Gondwana province of Pangea by the fit of North Greater India (formerly Argo Land – e.g. *Veevers et al.*, 1988), Middle and South Greater India, Antarctica and Australia at the onset of plate divergence by spreading in the Argo Abyssal Plain and by continental extension between Australia and North Greater India. As shown before, fracture zones in the Argo Abyssal Plain follow small circles (Figure 3.1) about the same stage pole that describes the early opening of the Perth Abyssal Plain off southwest Australia after chron M10 (131.1 Ma). This similarity may indicate that the formation of the Argo Abyssal Plain was

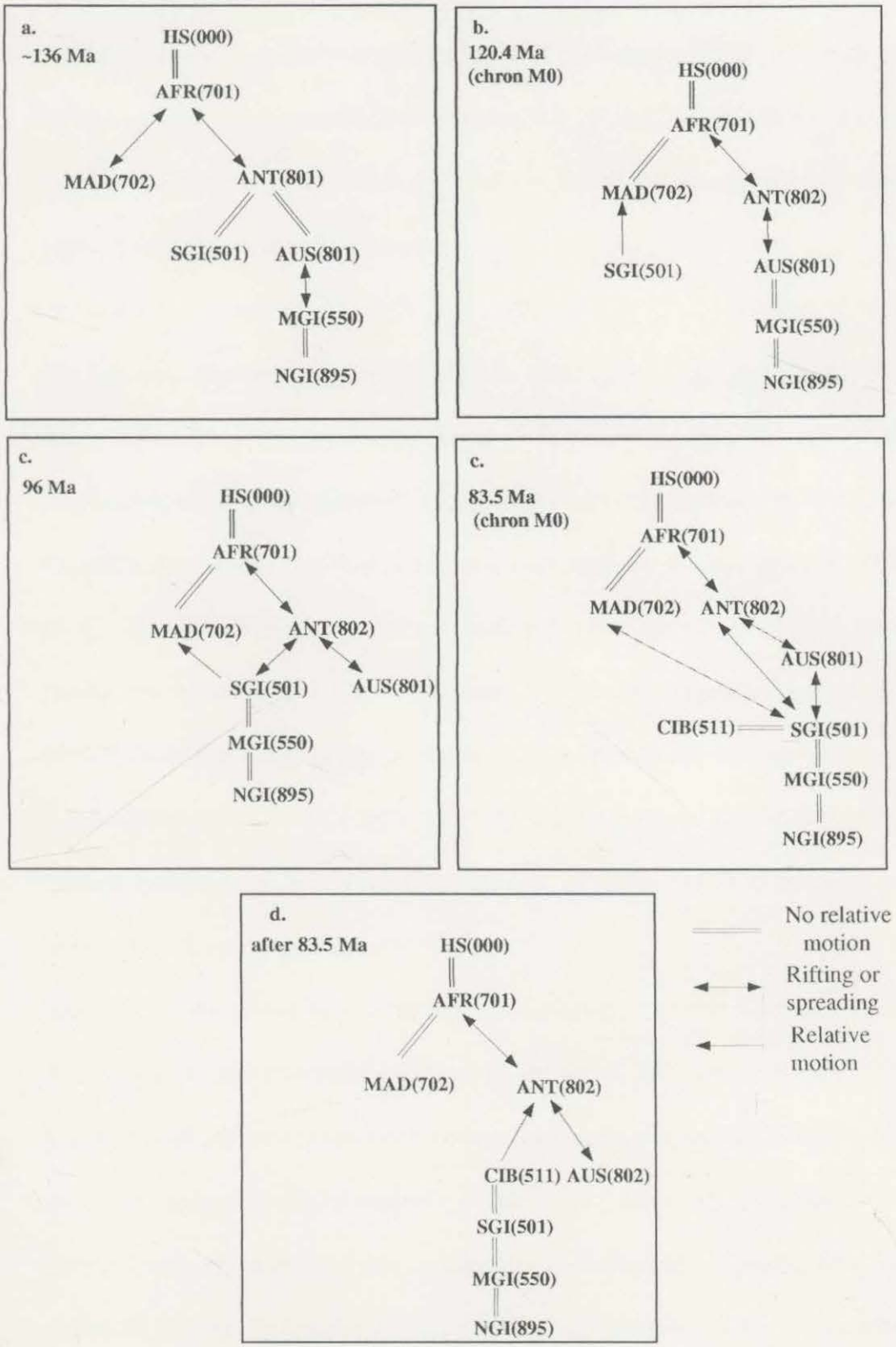

Fig. 3.6 Rotation trees for the major tectonic blocks in eastern Indian Ocean. Abbreviations are: HS-hotspot (reference frame), AFR-Africa, ANT-Antarctica, AUS-Australia, MAD-MAdagascar, NGI-, MGI-, SGI- North, Middle and South Greater India, CIB-Central Indian Ocean.. Numbers reffer to the plate identification in the rotation file.

not due to an unknown plate rifting off to the north (e.g *Veevers*, 1988;. *Fullerton et al.*, 1989), but rather due to a gradual breakup between Australia and North Greater India as a result of a southward propagating rift. If this idea is correct, the breakup in the Argo Abyssal Plain would represent the first phase of separation between one piece of Greater India and Australia.

The opening started in the late Jurassic at about **156 Ma** (Figures 3.7a and 3.8a). The margin's step-like appearance (Figure 2.7) was most likely due to several ridge propagation events. The direction of opening seems to be subparallel to the northern Exmouth Plateau and was interpreted as a transform margin that separated NGI from MGI. The age of **156 Ma** represents the extrapolated age for the COB in the central part of the Argo Abyssal Plain. However, because no magnetic interpretation was carried out in the northern part of the basin, the COB in this area may be older (see interpretation in Chapter 2.6.1.2). The COB shows the same age for the entire North Greater India for simplification of the model. In reality the COB becomes younger as the rift propagates to the south.

After the onset of seafloor spreading NGI started to move northwest relative to Australia at a high average spreading rate of about 160 mm/yr (Figure 3.4). The hypothesis of a hotspot associated with volcanism in the Joey Rise region (*Cook et al.*, 1978) along the entire northern sector of the Argo Abyssal Plain, and active during breakup, might be one explanation of the fast spreading rate between Australia and North Greater India. A stage pole in the Pacific Ocean located at 16.76°N and 170.46°W models the spreading pattern at that time.

At chron M25 (**154.1 Ma**) the main plate motion corresponded to the rapid NNE-ward drift of NGI away from eastern Gondwana which was located slightly west from the previous reconstruction (Figure 3.7b). At about 148 Ma (*Royer et al*, 1992) opening started between Africa and eastern Antarctica.

136.2 Ma (Figures 3.7c and 3.8b) marked the opening in the southern Cuvier and northern Gascoyne abyssal plains. Between M22A (the youngest magnetic anomaly interpreted in the Argo Abyssal Plain) and this time NGI became attached to MGI. The time when they formed one single piece is uncertain as no magnetic anomaly was interpreted between M22A and M14. By this time about 600 km of seafloor was formed between Africa and Antarctica (Figure 3.8b). Madagascar continued to be attached to India and there was no opening between SGI - Antarctica and Australia – Antarctica (Figure 3.6). The relative eastward movement of all plates between 156 Ma and 136.2 Ma was mainly a result of motion of Africa relative to the mantle, which is not well constrained for this period.

At **130.2 Ma** (Figure 3.7d) MGI continued to move some 800 km along a dextral transform fault past SGI, moving away from Australia. Initial extension between Antarctica and Australia also started around this time. Before this time seafloor spreading had begun in the Gascoyne (~133.5 Ma), north Cuvier (~135.8 Ma) and Perth abyssal plains (~130.9 Ma). A ridge propagator started at about 132 Ma and accreted a segment of MGI onto the Australian Plate in the southern Cuvier Abyssal Plain. The reconstructed COB for the Indian Plate shows more oceanic crust created than in the case of spreading onset at times documented by magnetic anomalies. An explanation for this discrepancy is that the onset of seafloor spreading in the

Gascoyne, Cuvier and Perth abyssal plains was similar to the onset in the southern Cuvier Abyssal Plain (~136.2 Ma) and the entire oceanic crust formed during this time was accreted onto the Indian Plate.

Figure 3.7e (**126.7 Ma**) shows that the seafloor spreading direction remained almost unchanged until chron M5 (127.7 Ma) when a 10° change occurred (see Table 3.1 and Figure 3.4). Between chron M10 and M4 two more ridge propagators accreted pieces of MGI onto the Australian Plate (one in the Gascoyne Abyssal Plain and one in the northern Cuvier Abyssal Plain). Australia, Antarctica, SGI and Madagascar were not yet separated and continued to move southeastward relative to the mantle.

At about chron M0 (**120.4 Ma**) spreading started between southern SGI – Antarctica and Australia - Antarctica at a very slow rate (*Tikku and Cande*, 1977) (Figures 3.7f and 3.8c). The opening between SGI and Antarctica is shown by synthetic flowlines in the Enderby Basin (Figure 3.3). Magnetic anomaly M0 has been interpreted on the conjugate Indian plate (*Munasinghe*, 1990). SGI started to move northwest relative to the mantle, faster than MGI and NGI. Two other short ridge propagators accreted small portions of the MGI onto the Australian Plate before chron M0 in the Gascoyne and Cuvier abyssal plains. At about 120.4 Ma a triple junction between SGI, Australia and Antarctica formed southeast of the Naturaliste Plateau.

96 Ma reconstruction (Figure 3.7g) marked the time when sub-plates of Greater India merged to form one plate. A major change in Greater India spreading direction relative to the Australian Plate occurred (see Figure 3.5 and Table 3.2). Greater India continued to move away from Australia and Antarctica and at about 96 Ma

started its journey to the north until collided with the Eurasian Plate at about 52 Ma (*Rowley*, 1996). Greater India and Antarctica moved relative to each other at a faster spreading rate than Antarctica relative to Australia which resulted in a southeastern motion of Australia and Antarctica relative to the mantle. Transform margins resulted for the western margin of Greater India and eastern margin of Madagascar as a consequence of faster seafloor spreading rate between Antarctica and Madagascar than between Antarctica and Greater India (Figure 3.8d). The overlap between MGI and SGI might be the result of internal plate deformation due to change in spreading direction.

83.5 Ma reconstruction (Figure 3.8e) shows Greater India, Australia and Madagascar continuing to move apart. Greater India moved to the north in an absolute reference frame and Australia was in its most southern position. This reconstruction is not extremely well constrained as no reliable C34 anomaly was interpreted in the present study in the Wharton Basin. One of the most recent finite rotations for India relative to Australia (*Royer and Sandwell*, 1989) was used for chron C34 in the Wharton Basin. As mentioned in the previous chapter, many of the previously interpreted picks (*Liu et al*, 1983; *Geller et al.*, 1983) in the Wharton Basin were located close to fracture zones and therefore possibly incorrect. However, the interpretation of chron C34 is beyond the purpose of this study.

Several other reconstructions were tested before reaching the conclusion that the best model that fits the interpretation of magnetic anomalies and fracture zones along the Australian margin, the trends in the Enderby Basin, together with reconstructions between Africa – Antarctica, Antarctica – Australia, Africa – Madagascar and India

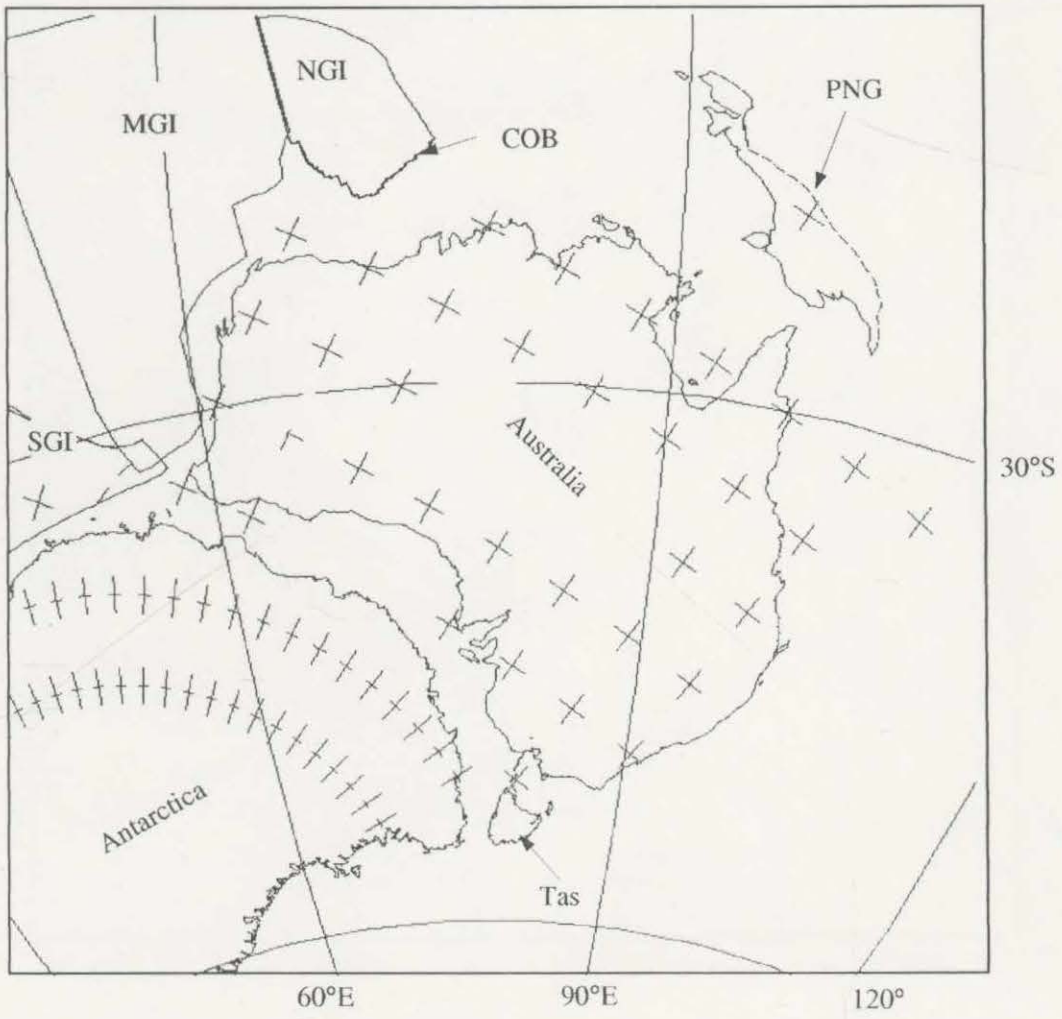

Fig. 3.7a Reconstruction at 156.0 Ma (in an absolute reference frame). The seafloor spreading started between the northern piece of Greater India (NGI) and Australia. Abbreviations are: MGI-Middle Greater India, SGI-South Greater India, PNG-Papua New Guinea, Tas-Tasmania, COB-Continent-Ocean Boundary.

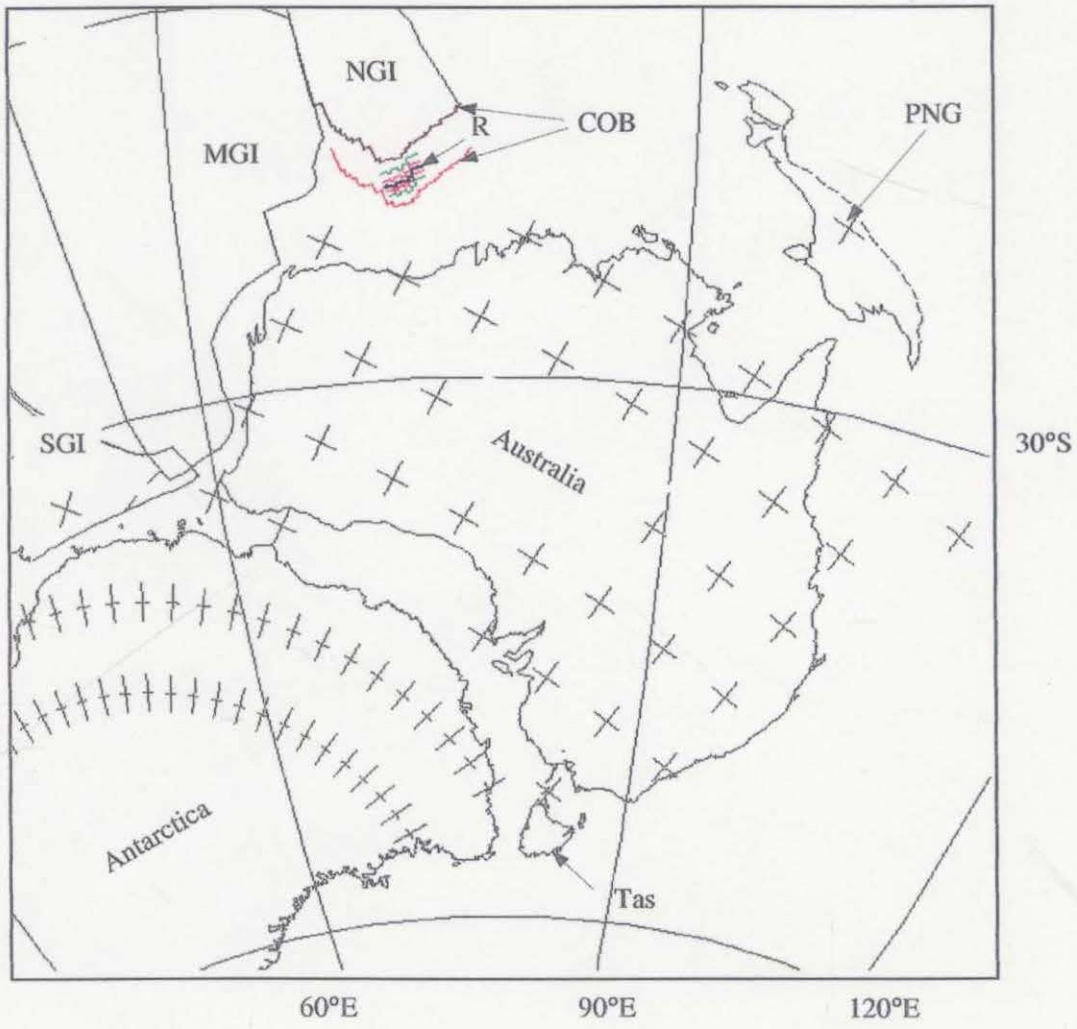

Fig.3.7b Reconstruction at 154.1 Ma (chron M25). Coloured, segmented lines represent isochrons: green-M26, red-M25A. Thick, dark-red line shows the active ridge (R). See Fig.3.7a for other abbreviations).

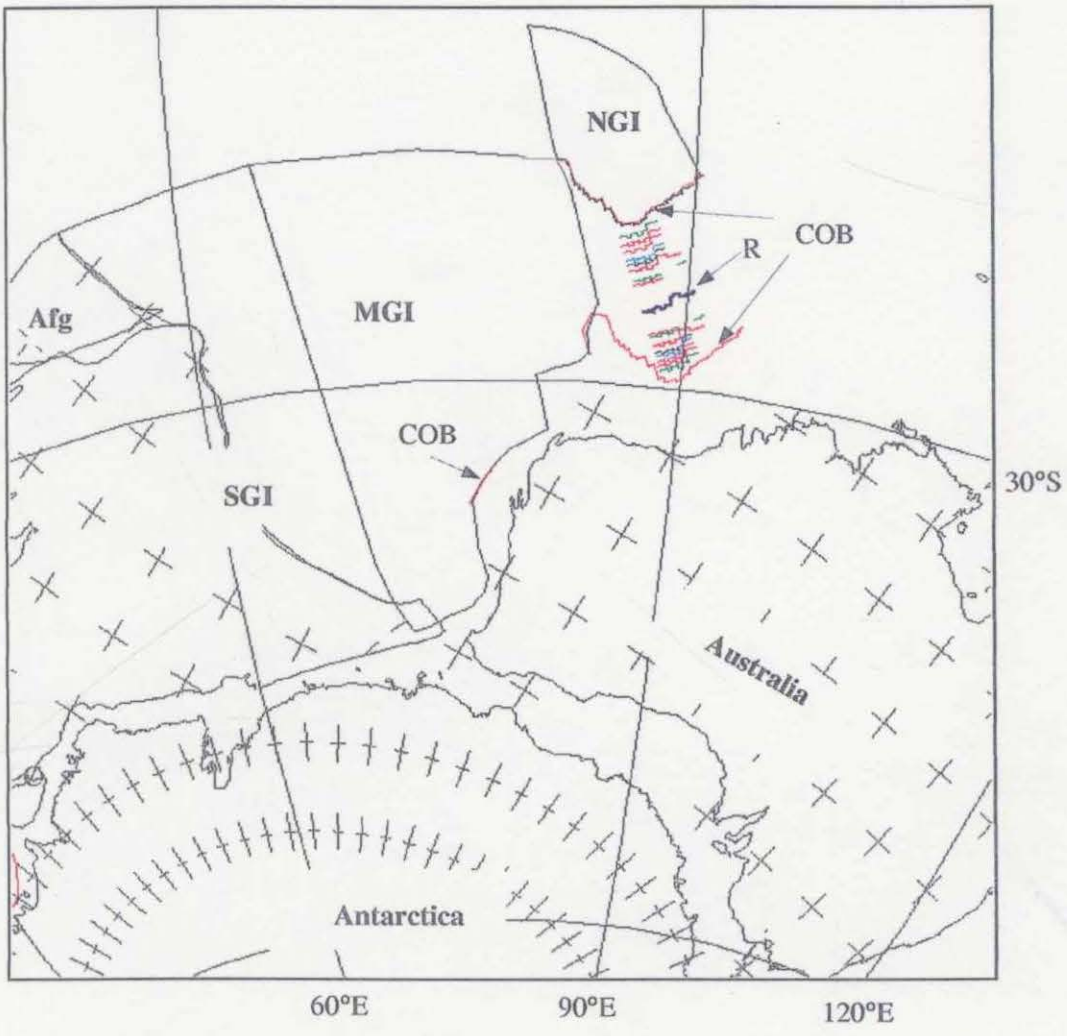

Fig. 3.7c Reconstruction at 136.2 Ma (opening in the southern Cuvier Abyssal Plain). Thin, coloured segmented lines represent isochrons: green-M23 and M26; red-M22A and M24, M25A; magenta-M25; blue-M24B; black-M24B. Abbreviations are: C-Ceylon (Sri Lanka), Afg-Afghanistan (see Fig. 3.7a for other abbreviations).

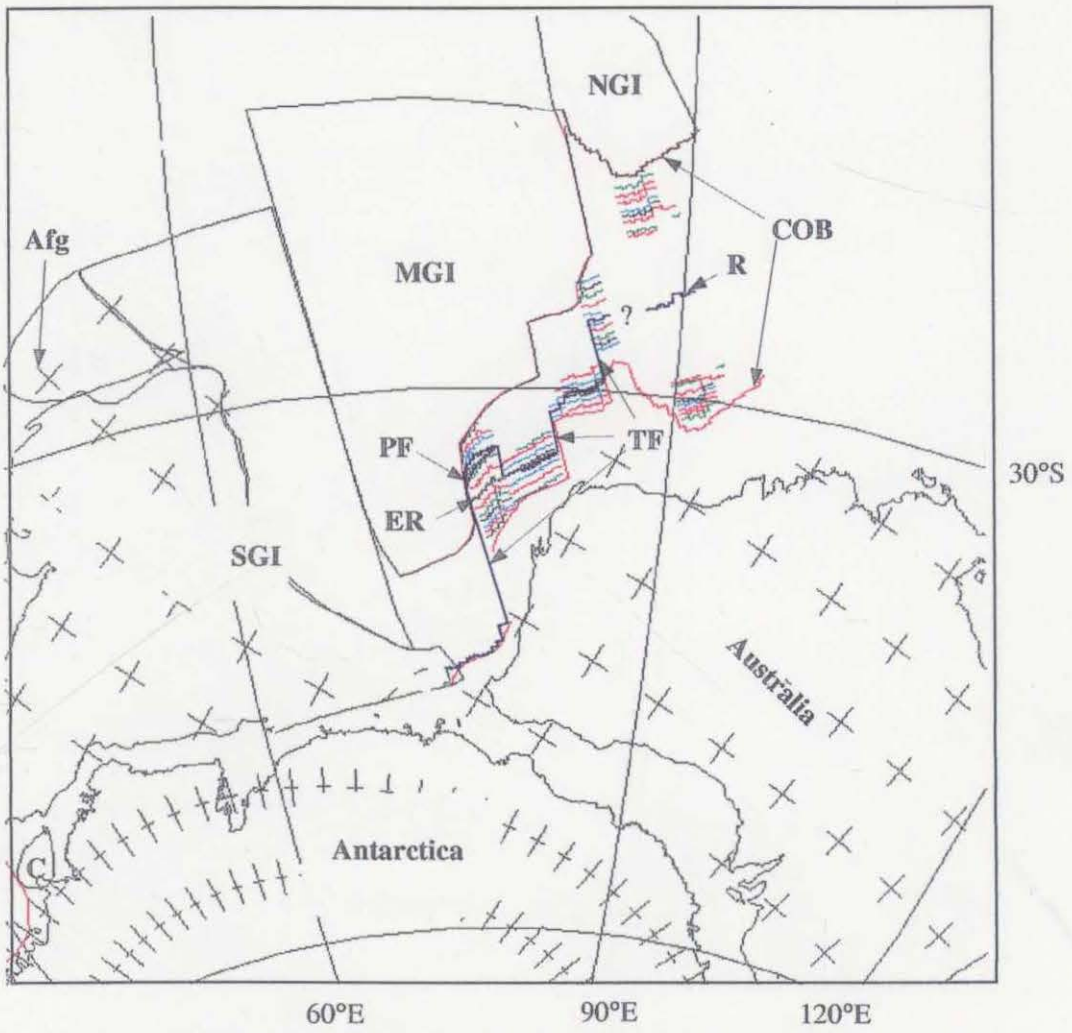

Fig.3.7d Reconstruction at 130.2 Ma (chron M10). Thin, coloured, segmented lines represent isochrons: green-M11, M23 and M26; red-M11, M22A, M24 and M25A; magenta-M13 and M25; blue-M10N, M12A and M24B; black-M10, M12 M14 and M24A. In grey are shown an extinct ridge (ER) and a pseudofault (PF); transform faults (TF) are shown in dark blue (see Fig. 3.7a and 3.7c for abbreviations).

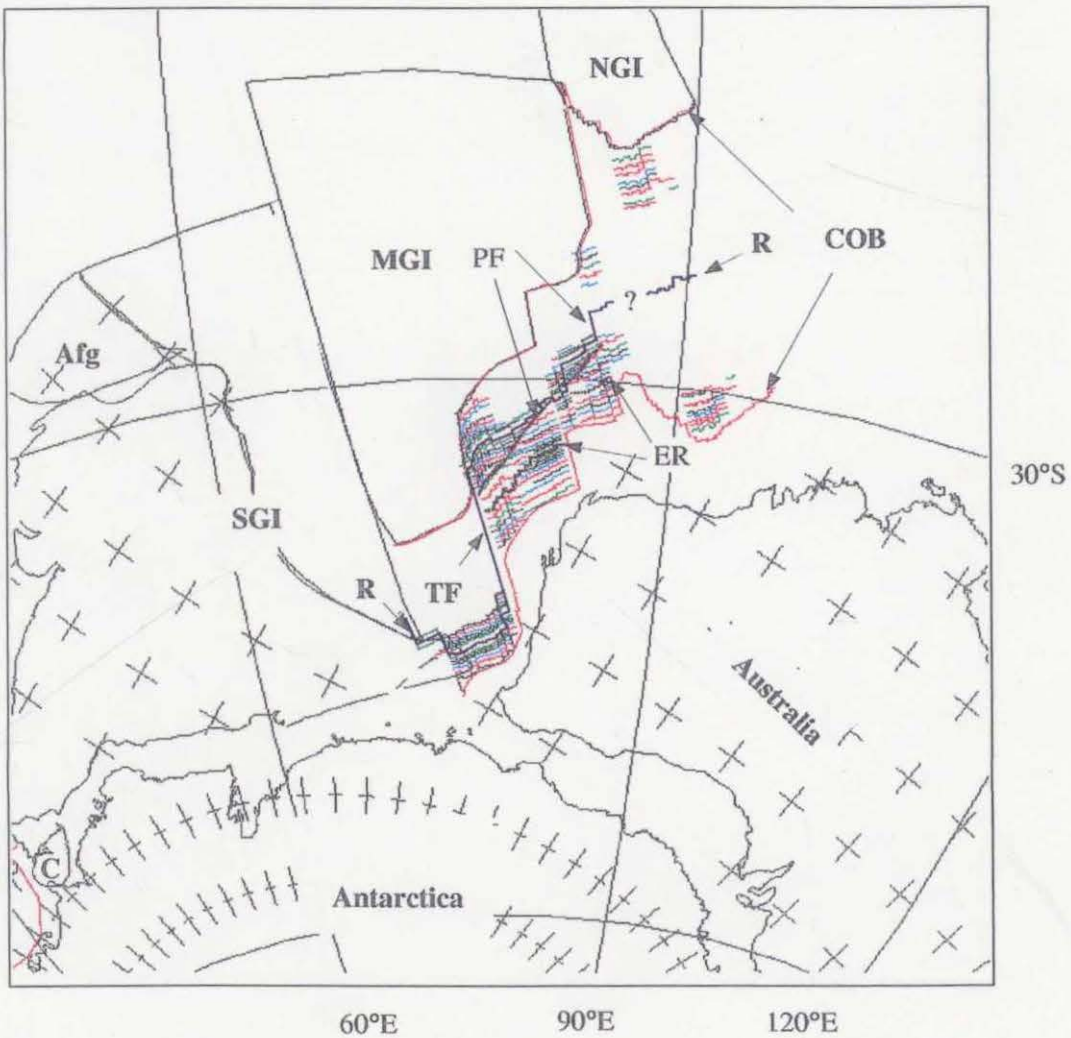

Fig.3.7e Reconstruction at 126.7 Ma (chron M4). Thin, coloured, segmented lines represent isochrons: green-M5, M11A, M23 and M26; red-M11, M22A, M24 and M25A; magenta-M9, M13, and M25; blue-M8, M10N M12A and M24B; black-M6, M7, M10, M12 M14 and M24A (see Fig. 3.7a, 3.7c and 3.7d for abbreviations).

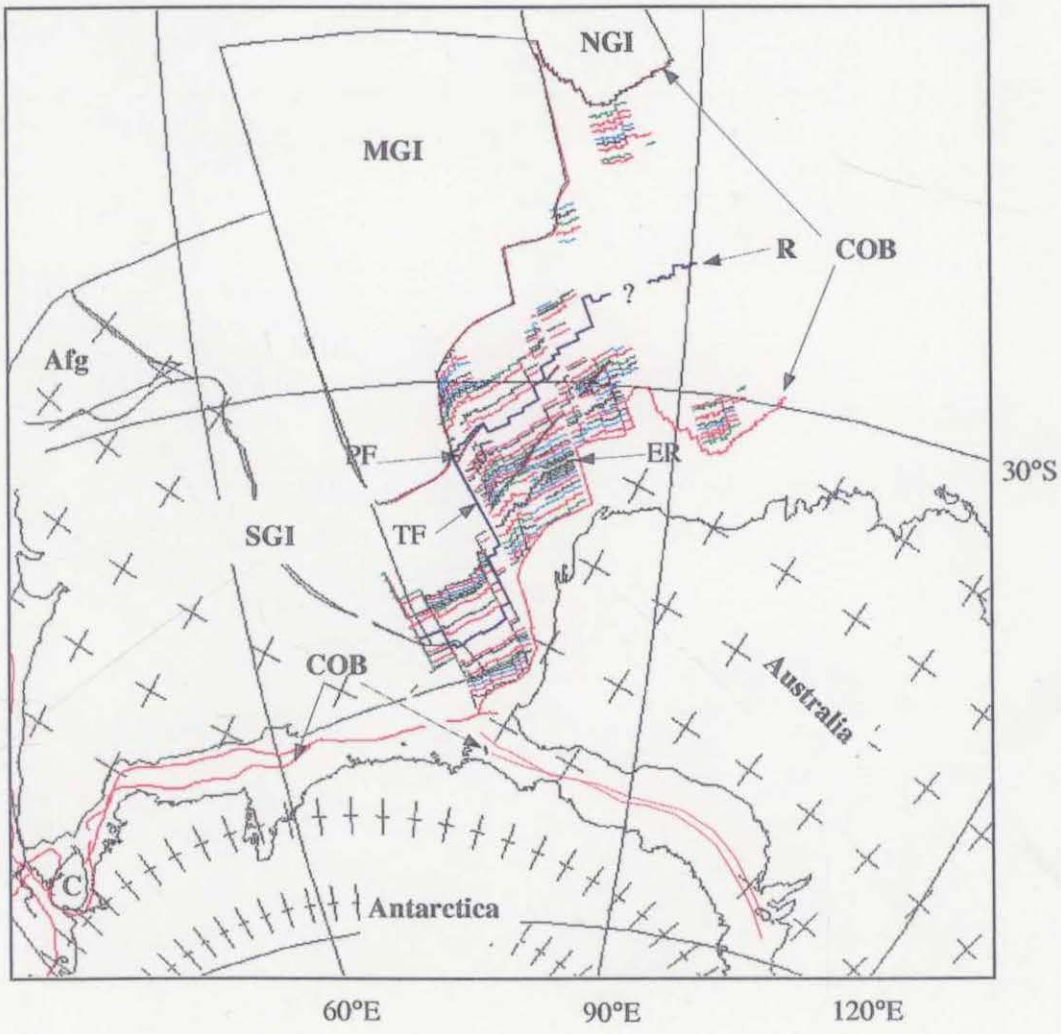

Fig.3.7f Reconstruction at 120.4 Ma (chron M0). Thin, coloured, segmented lines represent isochrons: green-M5, M11A, M23 and M26; red-M4, M11, M22A, M24 and M25A; magenta-M2, M9, M13 and M25; blue- M8, M10N, M12A and M24B;black-M3, M6, M7, M10, M12, M14 and M24A (see Fig.3.7a, 3.7c and 3.7d for abbreviations).

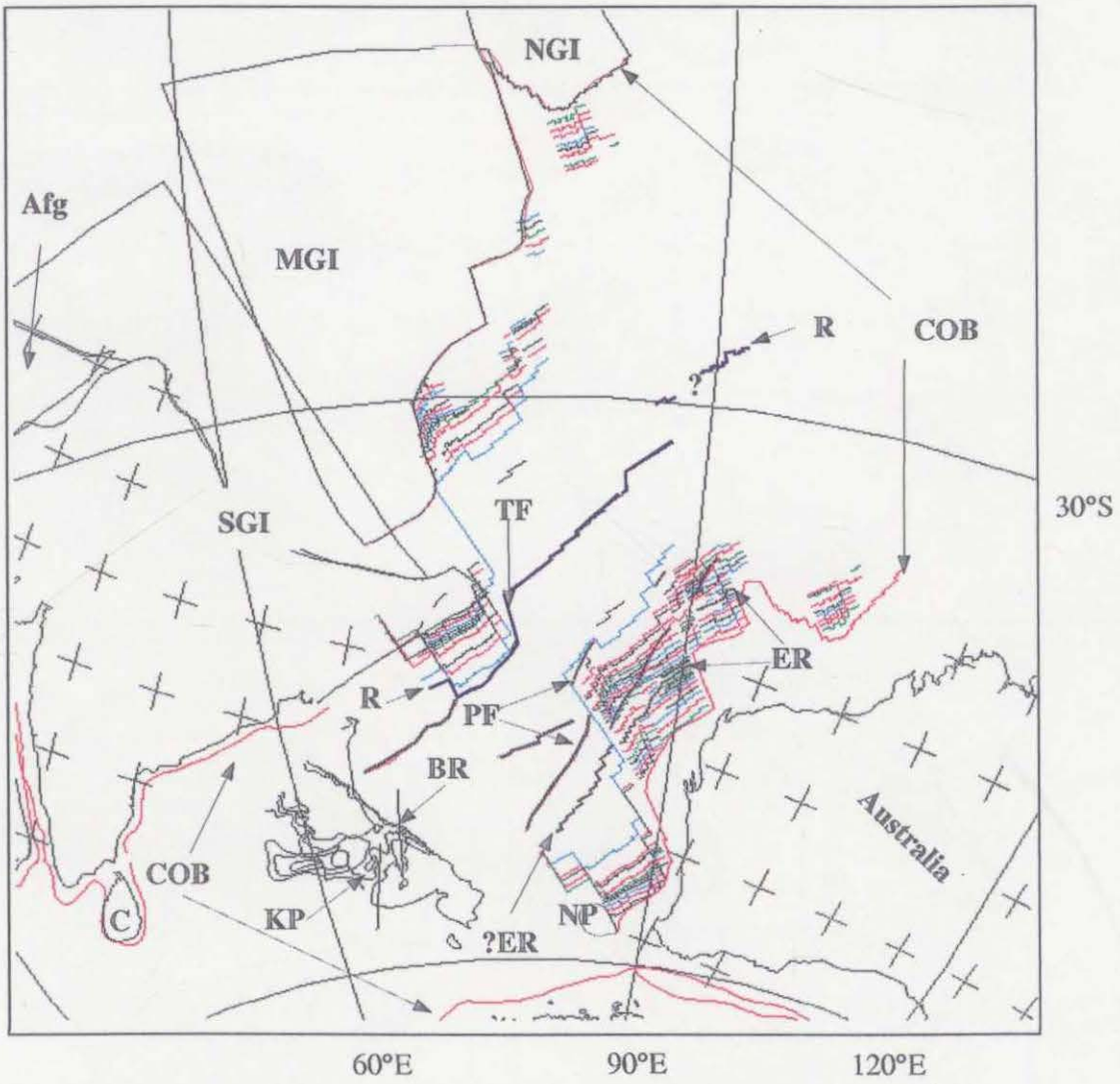

Fig.3.7g Reconstruction at 96 Ma. Thin, coloured, segmented lines represent isochrons:green-M5, M11A, M23 and M26; red-M4, M11, M22A, M24 and M25A; magenta-M2, M9, M13 and M25; blue- M0, M8, M10N, M12A and M24B; black-M1r, M3, M6, M7, M10, M12, M14 and M24A (see Fig.3.7a, 3.7c and 37d for abbreviations). Other abbreviations are: BR-Broken Ridge, KP-Kerguelen Plateau NP-Naturaliste Plateau.

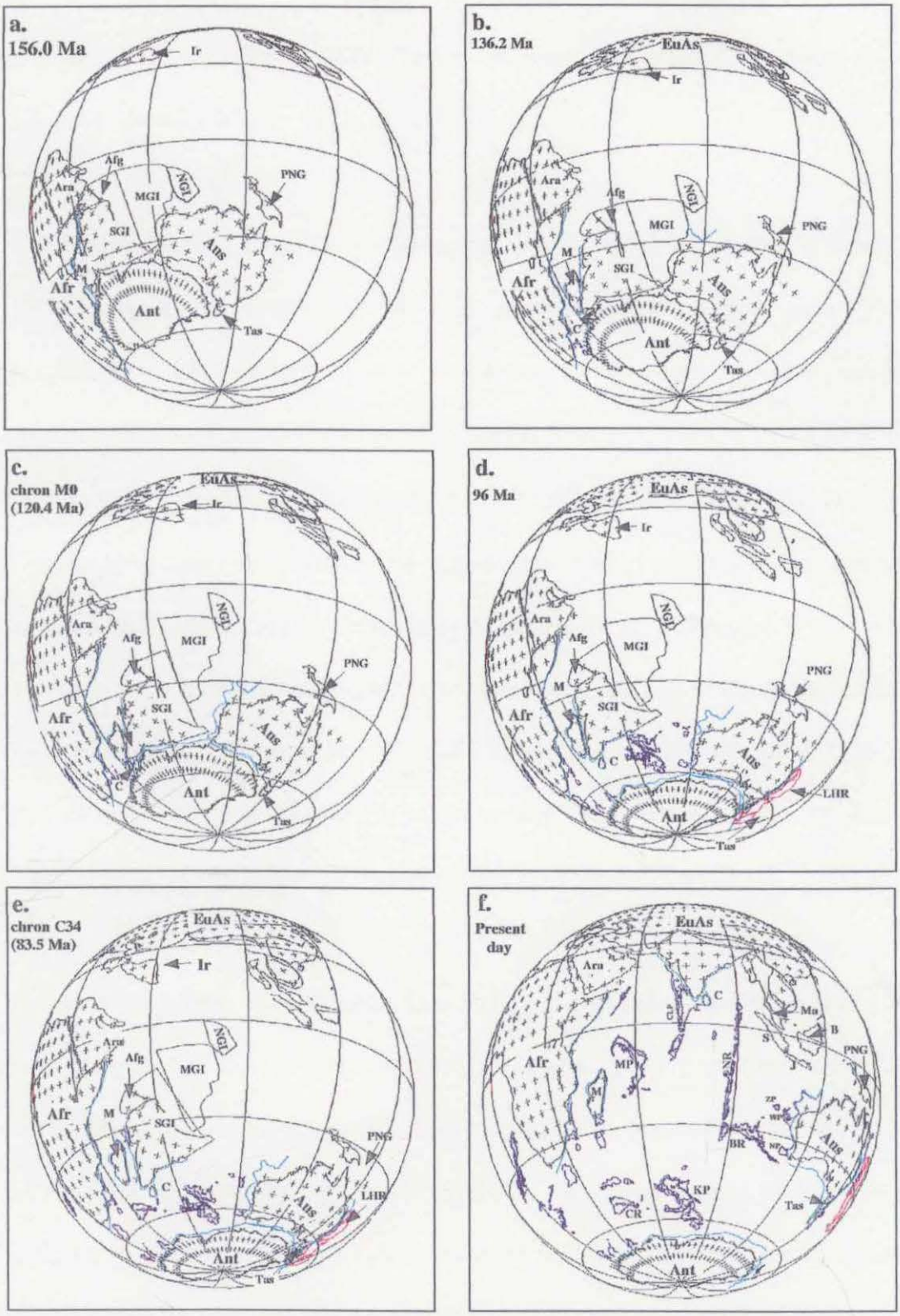

Fig. 3.8 Set of reconstructions for the opening of the eastern Indian Ocean in a scenario that assumes that Greater India was a three microplate system and seafloor spreading between Greater India and Antarctica started after 120.4 Ma (chron M0). COB is shown in cyan and submarine plateaus in dark blue and magenta. Abbreviation are: Aus-Australia, Ant-Antarctica, NGI-North Greater India, MGI-Middle Greater India, SGI-South Greater India, Afr-Africa, M-Madagascar, Afg-Afghanistan, Ara-Arabia, C-Ceylon, PNG-Papua New Guinea, B-Borneo, BR-Broken Ridge, CLP-Chagos-Laccadive Plateau, CR-Conrad Rise, J-Java, KP-Kerguelen Plateau, LHR-Lord Howe Rise, NR-Ninetyeast Ridge, MP-Mascarene Plateau, Ma-Malaysia, NP-Naturaliste Plateau, S-Sumatra, WP-Wallaby Plateau, ZP-Zenith Plateau, Ir-Iran.

– Madagascar is the above model. Two of these models are briefly discussed below (Figures 3.9 and 3.10).

The first model assumes a slower spreading rate between M0 and 96 Ma, with the Dirk Hartog Ridge the active 96 Ma ridge and Greater India a three plate system (Figure 3.9). This assumption is in disagreement with the crustal age of middle Albian determined at site 257 (located in the Perth Abyssal Plain at 30°59.16'S and 108°20.99'E – see Figure 2.21) (>102 Ma). In this scenario the breakup between Greater India and Antarctica started before chron M0 at about 130 Ma which is contradicted by flowlines in the Enderby basin (Figure 3.3). Between 120.4 – 83 5 Ma Greater India would have moved from a northern position to the south and then back to the north in an absolute reference frame. As a consequence about 1000 km of back and forth strike slip motion would have occurred between Greater India and Madagascar. The tip of Greater India overlaps Madagascar at chron M0.

Several authors have considered the Dirk Hartog Ridge as the active ridge at ~96 Ma (e.g., *Powell et al.* 1988). This would imply that about 400 km of crust west of Dirk Hartog Ridge represents only Indian crust accreted to the Australian Plate as a result of a major ridge jump which occurred at 96 Ma. This assumption is contradicted by the interpretation of an extinct ridge west of Dirk Hartog Ridge (Figures 2.25b and c). These results were based on combined study of gravity, topography and magnetic data.

The second model considers Greater India as a two plates system (Figure 3.10). The breakup between Greater India and Antarctica occurred at about 130 Ma as in the

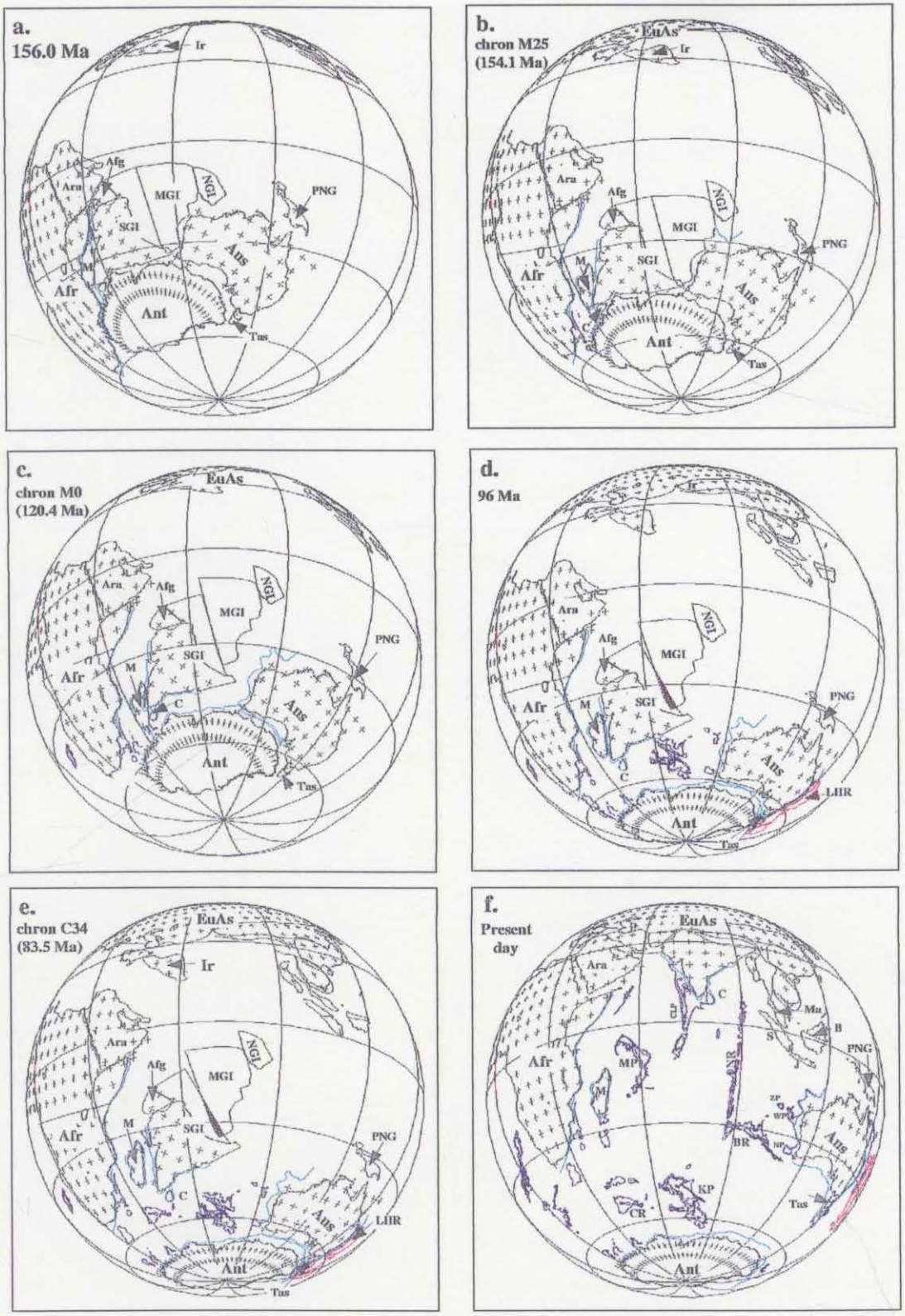

Fig. 3.9 Set of reconstructions for the opening of the eastern Indian Ocean in a scenario that assumes that Greater India was a three microplate system and seafloor spreading between Greater India and Antarctica started before 120.4 Ma (chron M0) at about 130 Ma (~chron M10). Legend and abbreviations as in Fig.3.8.

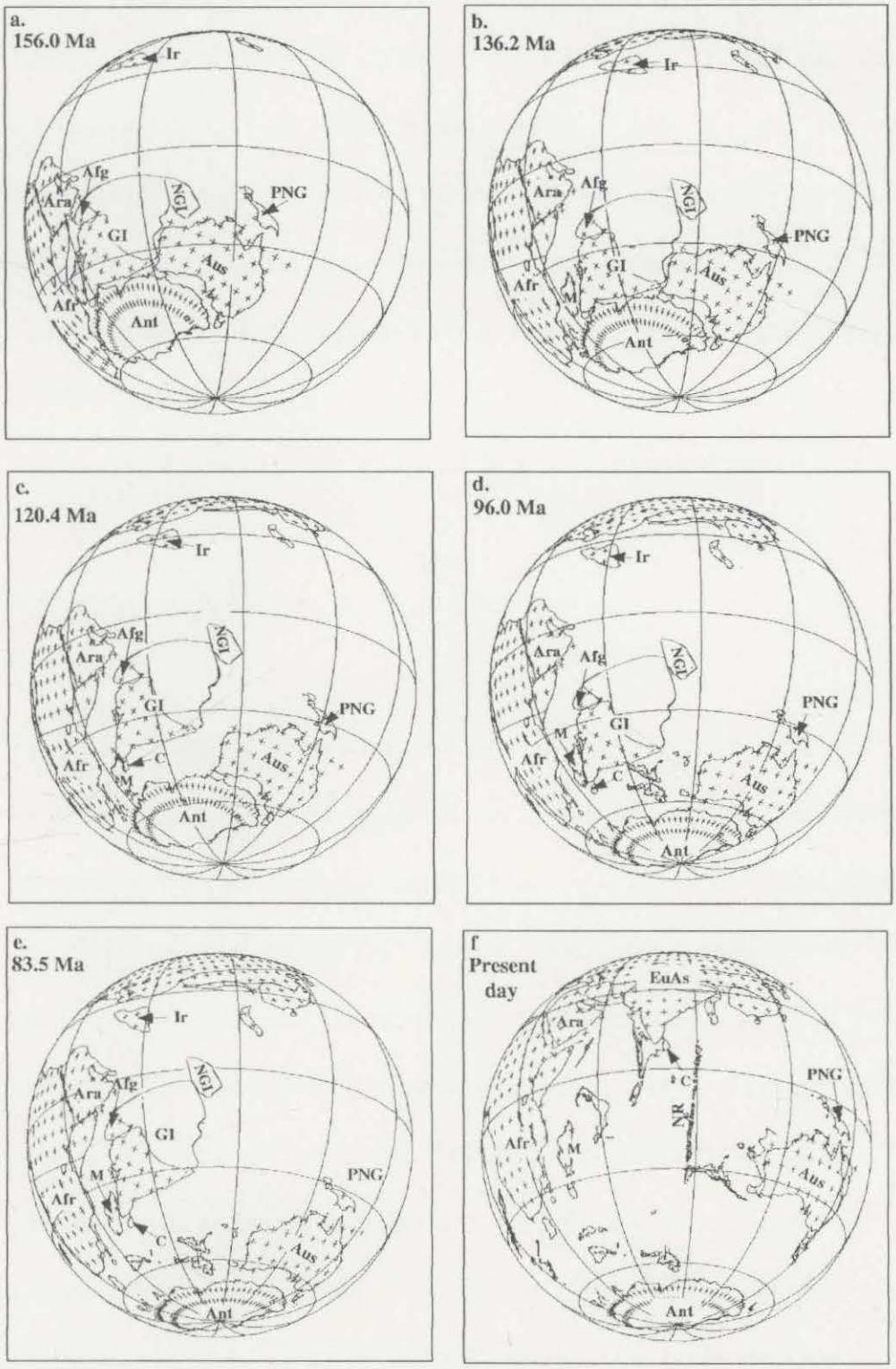

Fig. 3.10 Set of reconstructions of the opening of the eastern Indian Ocean in a scenario that assumes that Greater India was a two microplate system. Abbreviations are Aus-Australia, Ant-Antarctica, GI-Greater India, NGI-North Greater India Afr-Africa, M-Madagascar, Afg-Afghanistan, Ara-Arabia, EuAs-Eurasia, PNG-Papua New Guinea, Ir-Iran, C-Ceylon, NR-Ninetyeast Ridge. Grey shaded areas represent overlaps.

slow spreading model (Figure 3.9). As a result of this early opening the position of Greater India at chron M0 almost coincides with its position at chron C34. Greater India moved southeastward relative to the mantle until 96 Ma and then north-northwestward until 83.5 Ma (Figures 3.10b, c and d). As a consequence compression would have occurred between Greater India and Africa at about 83.5 Ma. Madagascar would have moved southward between 136.0 Ma and 120.4 Ma, then northward. The two plates overlap between chron M0 and 96 Ma (Figures 3.10c and d).

3.6 Summary

A new set of stage poles and rotations as well as finite rotation poles and rotations, between 96 – 156 Ma, were derived from magnetic anomaly and fracture zone interpretations in the northeast Indian Ocean. Also seafloor spreading rates were derived from stage poles and finite rotation poles. Apart from this information other constraints from outside the study area (see Figure 3.3), provided independent validity on the goodness of fit of predicted seafloor spreading patterns with mapped magnetic anomaly and bathymetric features in the eastern Indian Ocean. The stage rotations for spreading off the western margin of Australia account for:

(1) seafloor spreading in the Argo Abyssal Plain was the result of the gradual breakup between Australia and NGI, as indicated by the same stage pole that described the opening in this area and in the Gascoyne, Cuvier and Perth abyssal plains (Table 3.1); and

(2) the same stage rotations for 120 Ma (chron M0) and 83.5 Ma (chron C34) described the onset of spreading between Greater India and Australia and between the former and Antarctica.

The revised fit of Greater India, Australia Antarctica, Madagascar and Africa prior to any continental extension in east Gondwanaland extended Greater India to an area that included the Argo Land and implied that the size of Greater India was about 25% larger than previously thought. In this case the present size of the Indian continent may only represent about half its original size (e.g. Figure 3.8).

The tectonic evolution of the eastern Indian Ocean appears to be more complicated than described by previous workers. Greater India was the result of three pieces that separated by dextral lateral movement from Gondwanaland (see Figures. 3.6). At about 120.4 Ma (chron M0) a triple junction between the southern segment of Greater India, Australia and Antarctica formed southeast of the Naturaliste Plateau. 96 Ma marked the approximate time when Greater India became a single plate and also the major change in the direction of motion from northwest-southeast to north-south. Previous researchers speculated that the M-sequence interpreted along the Australian margin might be related to the breakup of Greater India and Antarctica (e.g. *Powell et al.*, 1988). An alternative reconstruction of an earlier spreading between India and Antarctica (Figures 3.9 and 3.10) was excluded by synthetic flowline interpretation in the Enderby Basin and Gascoyne Abyssal Plain (Figures 3.2 and 3.3).

Although details of the more recent history of the spreading between India, Australia and Antarctica are beyond the scope of this study, Figure 3.8 shows that 96 Ma represented an important moment in the tectonic history of Australia. It was the time when two changes in spreading direction occurred (Greater India relative to Australia and Antarctica relative to Australia -*Tikku and Cande*, 1997) and seafloor spreading started between Greater India and Madagascar and Australia and Lord Howe Rise (*Gaina et al.*, 1997). At this time Greater India started its journey to the north until it collided with the Eurasian Plate.

CHAPTER 4

The Carnarvon Terrace: Seismic interpretation and tectonic evolution

4.1 Introduction

During the last two decades, many authors have discussed the tectonic evolution of the western margin of Australia and although there is now a broad agreement on the timing of major events, some of them are still not well understood. Seismic data acquired during 1991 (Mobil) and 1993 (Geco-Prakla) provided a unique opportunity to reevaluate the tectonic evolution of one of the margin's least explored segments, the Carnarvon Terrace.

The seismic interpretation has focused on resolving the following aspects of the margin development: (1) the timing and evolution of the tectonic event which intiated the major Early Cretaceous uplift of the Bernier Platform and the southern Exmouth Sub-basin; (2) the geological interpretation of strong reflectors penetrating or paralleling sedimentary sequences and their time of emplacement; and (3) the sediment transport direction within the Carnarvon Terrace; and (4) one possible cause of the Late Miocene (and/or younger) event that affects most of the western Australian margin. Additional objectives were to establish the direction and the time of lateral movement of several sectors defined in the Exmouth Sub-basin and the Miocene reactivation in the Bernier Platform. The results of the seismic interpretation, combined with magnetic and satellite gravity data were used in Chapter 5 in order to investigate the cause of the pre- and post-breakup magmatism along the Cuvier Margin.

4.2 Regional geology and geomorphology

The Carnarvon Basin (divided into the Northern and the Southern Carnarvon basins) is an elongate basin extending for over 1,000 km along the western and northwestern coastline of Western Australia (Figure 4.1). The basin contains up to 15 km of sediments and covers a total area of 650,000 km^2, of which 535,000 km^2 represents the offshore area to the continental-oceanic crust boundary (*Hocking*, 1990).

The basin was initiated in the Early Palaeozoic with the deposition of over four kilometers of Ordovician and Silurian marine or marginal marine sandstones, carbonates and evaporites deposited in an intracratonic environment (Figure 4.2). Palaeocontinental reconstructions (e.g. *Veevers*, 1984) suggested that the basin was part of Greater India, situated in equatorial to low-tropical latitudes (*Embledon in Veevers*, 1984). Marine conditions in the mid-Devonian resulted in the deposition of about one km of sediments including reef development during the Frasnian. The basin was assumed to have been a relatively symmetrical, slightly northward-deepening gulf by the end of the Tournasian (*Hocking*, 1990).

Significant deformation took place in the mid-Carboniferous as a result of the collision between Gondwana and Laurasia, which formed the super-continent Pangea (*Chen et al.*, 1993; 1994). Later, in the Late Carboniferous and Permian, marine and marginal marine sedimentation was strongly influenced by widespread glacial conditions. Lack of clastic input allowed the deposition of a widespread carbonate sequence (the Chinty limestone). An early Late Permian rifting event terminated the Paleozoic sedimentation. A major reorientation of the basin associated with the

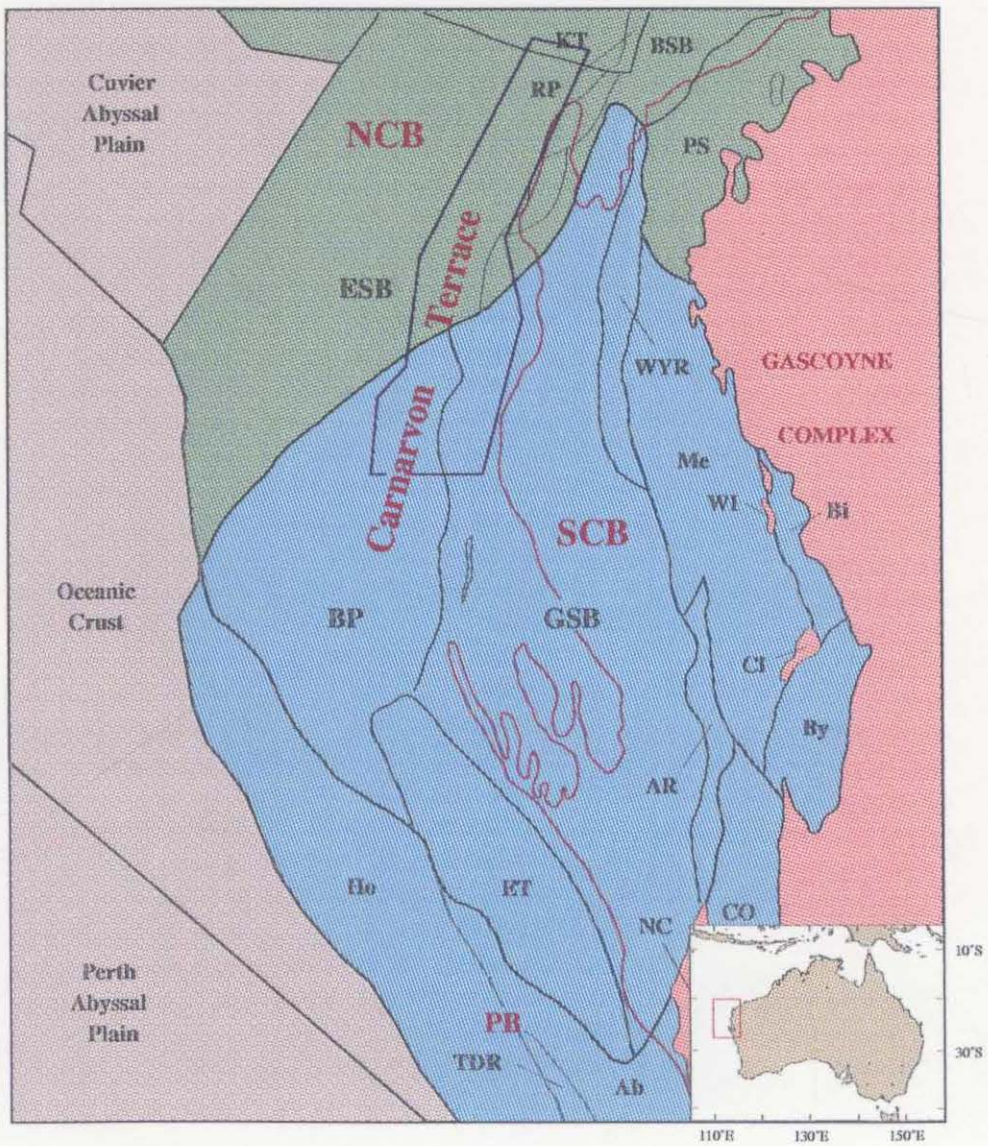

Fig. 4.1 The Carnarvon Terrace in the new basin classification of the western Australian margin. The blue polygon encompasses the area covered by seismic surveys used in this study. Abbreviations represent subdivisions of: (A) The Northern Carnarvon Basin -NCB (ESB-Exmouth Sub-basin, KT-Kangaroo Terrace, RP-Rankin Platform, BSB-Barrow Sub-basin PS-Peedamullah Shelf); (B) The Southern Carnarvon Basin - SCB (BP-Bernier Platform GSB-Gascoyne Sub-basin, WYR-Wandagee-Yanrey Ridge, Me- Merlinleigh Sub-basin, WI-Weedarra Inlier, Bi-Bidgemia Sub-basin, CI-Carrandibby Inlier, By-Byro Sub-basin, AR-Ajana Ridge, ET-Edel Terrace); (C) The Perth Basin - PB (CO-Coolcalalaya Sub-basin, Ho-Houtman Sub-basin, TDR-Turtle Dove Ridge, Ab-Abrolhos Sub-basin).

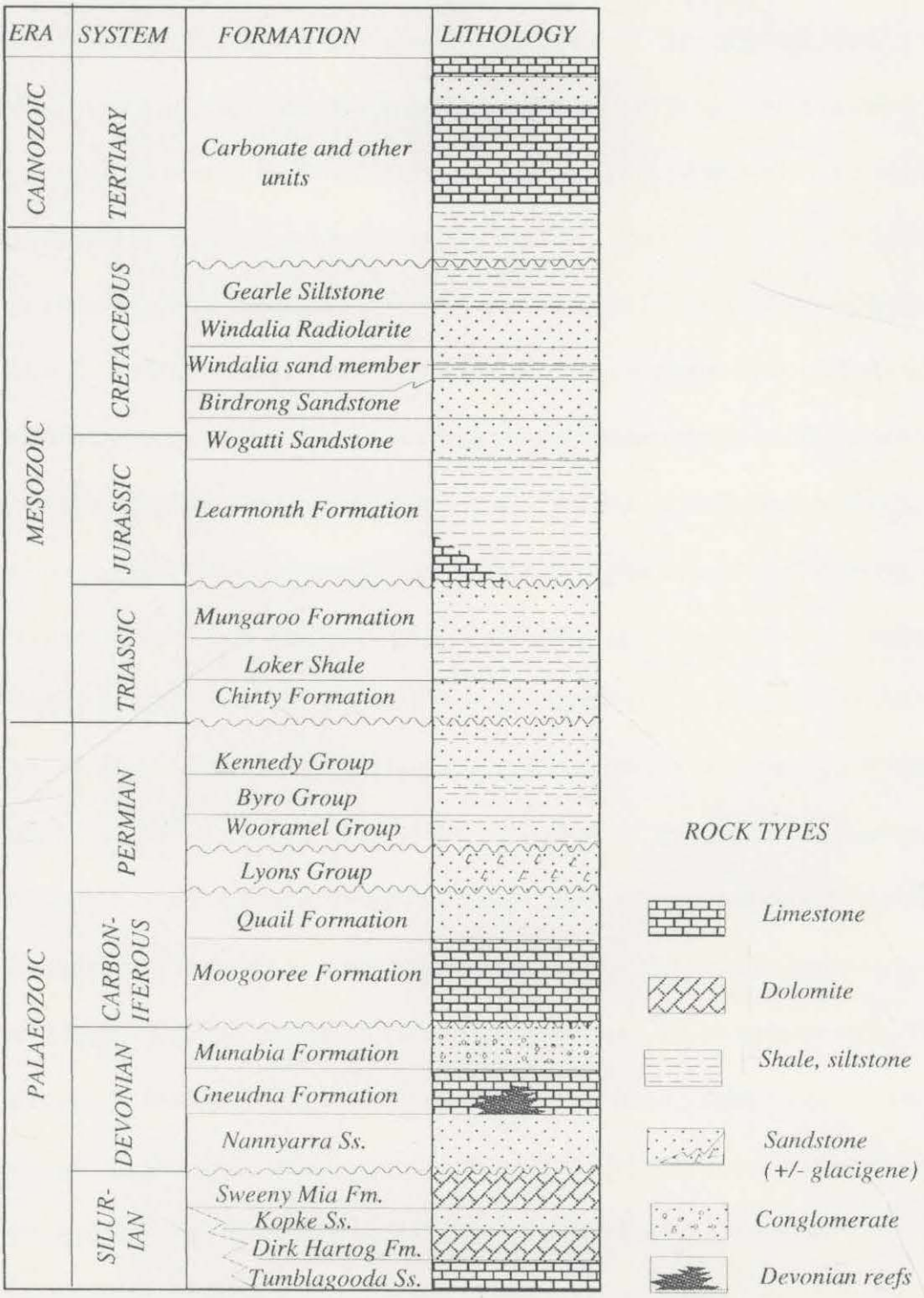

Fig. 4.2 Generalized stratigraphy in the Southern Carnarvon Basin; no linear vertical scale (modifies after Hocking et al., 1987).

beginning of the breakup of Pangea occurred during the Triassic (*Veevers*, 1989). This event was characterized by the development of northeasterly trending troughs aligned along the present-day coastline northeast of the Exmouth Gulf. The Westralian Superbasin was now fully open and incipient rifting related to that event caused some wrench faulting (*Peake and Bowes*, 1993). Sediments were initially deposited in a marine environment (the Locker shale), and were subsequently overlain by a thick, fluvio-deltaic coastal sequence (the Mungaroo Formation) in the Late Triassic (*Hocking*, 1990). At this time the onshore area of Palaeozoic sediments in the Southern Carnarvon Basin was uplifted; erosion of these sediments provided much of the terrigenous material to the Northern Carnarvon Basin. In either the early Late Triassic or earliest Jurassic times, rifting recommenced, and present-day structural elements, such as the Gascoyne Sub-basin and Wandagee-Yanrey Ridge (Figure 4.1), started to develop (*Hocking et al.*, 1987). The Jurassic syn-rift depositional phase was assumed to result from the separation of a continental block and the Australian Plate. This is represented by the Fitzroy movement (*Cockbain*, 1989) which is thought to involve the northward movement of 'Mount Victoria Land' away from Australia (*Veevers*, 1988). The Pilbara Craton remained in a higher location and acted as a sediment source. In Sinemurian time, rapid subsidence resulted in the accumulation of over 5 km of deltaic (the Learmonth Formation) to marine sediments (the lower Dingo Claystone) in the central deeper parts of the basin. Transform fault motion (e.g. Cape Range) initiated tear faults that eventually merged back into the initial transfer fault. These faults formed the terraces and troughs that are documented in the onshore Exmouth Sub-basin (*Malcolm et al.*, 1991).

The Late Jurassic breakup and onset of seafloor spreading along the Argo Abyssal Plain, followed by earliest Cretaceous breakup along the rest of the western Australian margin was a major event in Carnarvon Basin development. At this time, large volumes of sediments, transported along submarine fan systems developed in the North West Shelf, accumulated in association with both syn-rift events and/or repeated fluctuations in the eustatic sea-level. This phase of deposition concluded in earliest Cretaceous times with the formation of a transgressive/highstand deltaic complex in the Barrow Sub-basin. This complex was later abandoned when tectonism (associated with pull-apart basins along the western margin) disrupted the fluvial distributary system which supplied the delta (*Tait*, 1985). Some intrusions may have been emplaced in the southern part of the Exmouth Sub-basin during the Tithonian (e.g. Yardie East-1).

The final rift phase (Early Cretaceous), initiated as Greater India moved northwestward relative to Australia, concluded multiple rift activity along the western margin. As new oceanic crust formed, thermal doming caused "ridge push" to act toward the craton, renewing movement along pre-existing faults. In the Late Valanginian rifting was complete and erosion during a lowstand formed a fairly even surface to the basal Cretaceous unconformity. Following the Late Valanginian rifting little to no tectonic activity occurred. A major regional transgression resulted in the deposition of marine shales (the Muderong Shale) and sandstones in the eastern part of the basin. Basin subsidence and tilting to the west probably initiated at the close of the Valanginian (*Peake and Bowes*, 1993).

Prograding carbonates dominated the region throughout the Cenozoic (a generalized stratigraphy is shown in Figure 4.2). Compression and structural inversion took place in several areas of the Westralian Superbasin during the Miocene as the Australian Plate began to subduct under the Asian Plate to the north. This subduction is still active in the Timor Sea to the north (*Johnstone*, 1979; *Malcolm et al.*, 1991). The tectonic inversion also reversed motion along preexisting faults (the Rough Range Fault reversed in the eastern onshore area around Rough Range-1, location in Figure 4.3). The onshore anticlines in the Exmouth Sub-basin were also formed during this time.

4.2.1 The Carnarvon Terrace

The north and central Carnarvon Terrace (Figure 4.1) is a geographic term for the portion of the offshore Carnarvon Basin south of the Cape Range Transform Fault (CRTF). Geologically, the region lies within the Exmouth and the Bernier platforms (offshore Gascoyne sub-basin), and represents the boundary between the recently defined Northern and Southern Carnarvon basins (*Hocking et al.*, 1994). These two basins occur beneath the veneer of Early Cretaceous and younger sediments.

The geology of the Bernier Platform is similar to that of the western Gascoyne Sub-basin. The western Gascoyne Sub-basin is a northward-dipping, and structurally-high block of Palaeozoic sediments, deposited during the long tectonic rifting episode initiated in the Late Palaeozoic and later uplifted by the Late Jurassic - Early Cretaceous rifting episode (*Teichert, 1939; Yeates et al., 1987; Cockbain, 1989*). Its

northwestern boundary, a major down-to-the-west normal fault, has been interpreted as the offshore extension of the Rough Range Fault (*Symonds and Cameron, 1977; Malcolm et al., 1991*; *Middleton, 1992*). The platform is underlain by a Precambrian basement high cored north northeast - south southwest striking anticline paralleling the landward edge of the Carnarvon Terrace (*Symonds and Cameron, 1977*).

The Exmouth Sub-basin has undergone a more complex evolution. In the Early Jurassic (Sinemurian), a second major rifting phase commenced forming the Exmouth Sub-basin (*Malcolm et al., 1991*). A gentle half-graben formed, defining the eastern boundary of the Exmouth Sub-basin. The two major periods of continental breakup on the western Australian margin during the Mid-Jurassic and Neocomian (*Powell,* 1978) resulted in substantial unconformities (Callovian-Oxfordian and Beriassian-Valanginian), which have been identified in the onshore Exmouth Sub-basin (*Malcolm et al., 1991*). Magmatic intrusions emplaced within the sub-basin are considered to be associated with the continental breakup of the western Australian margin in the Early Cretaceous.

In the late Miocene a major compressional event affected several regions in the western margin of Australia and particularly the onshore Exmouth Sub-basin. This event was considered to be the result of the subduction of the Australian continent beneath the Asian plate in the vicinity of the present-day Timor Sea. The result was tilting, inversion, reactivation of preexisting faults and formation of new strike-slip faults (*Malcolm et al., 1991*).

4.3 Interpretation

The seismic interpretation is based on seismic data (multiple fold stack) supplied by Mobil Exploration and Producing Australia (MEPA). The data consists of 6,700 km of 2.4, 4, 6 or 8 second records covering a 23,750 km^2 area. The surveys were all acquired between 1972 and 1993. Due to the poor quality, sections of the pre-1985 seismic data were subsequently reprocessed by Halliburton Geophysical Services (HGS) for MEPA. The reprocessed data showed improvement in terms of attenuation of multiples, but in some areas the data quality beneath the basal Cretaceous unconformity was still extremely poor. The reprocessed lines (approximately 1700 km) are identified in the data listing (see Appendix 4). The entire seismic grid over the study area is shown in Figure 4.3.

4.3.1 Stratigraphy

The stratigraphy of the study area (Figure 4.2) is determined from only two offshore wells, Pendock-1 and Yardie East-1 that have direct ties to the seismic grid, but several onshore wells aid interpretation of the seismic data (*Malcolm et al.*, 1991; their figures 10 and 11).

Pendock-1 (Figures.4.4 and 4.5; *Geary and Garrett*, 1970), drilled in the Bernier Platform by Canadian Superior Oil Limited in 1969, targeted an anticline with a thick Mesozoic succession similar to that in the Exmouth Sub-basin.

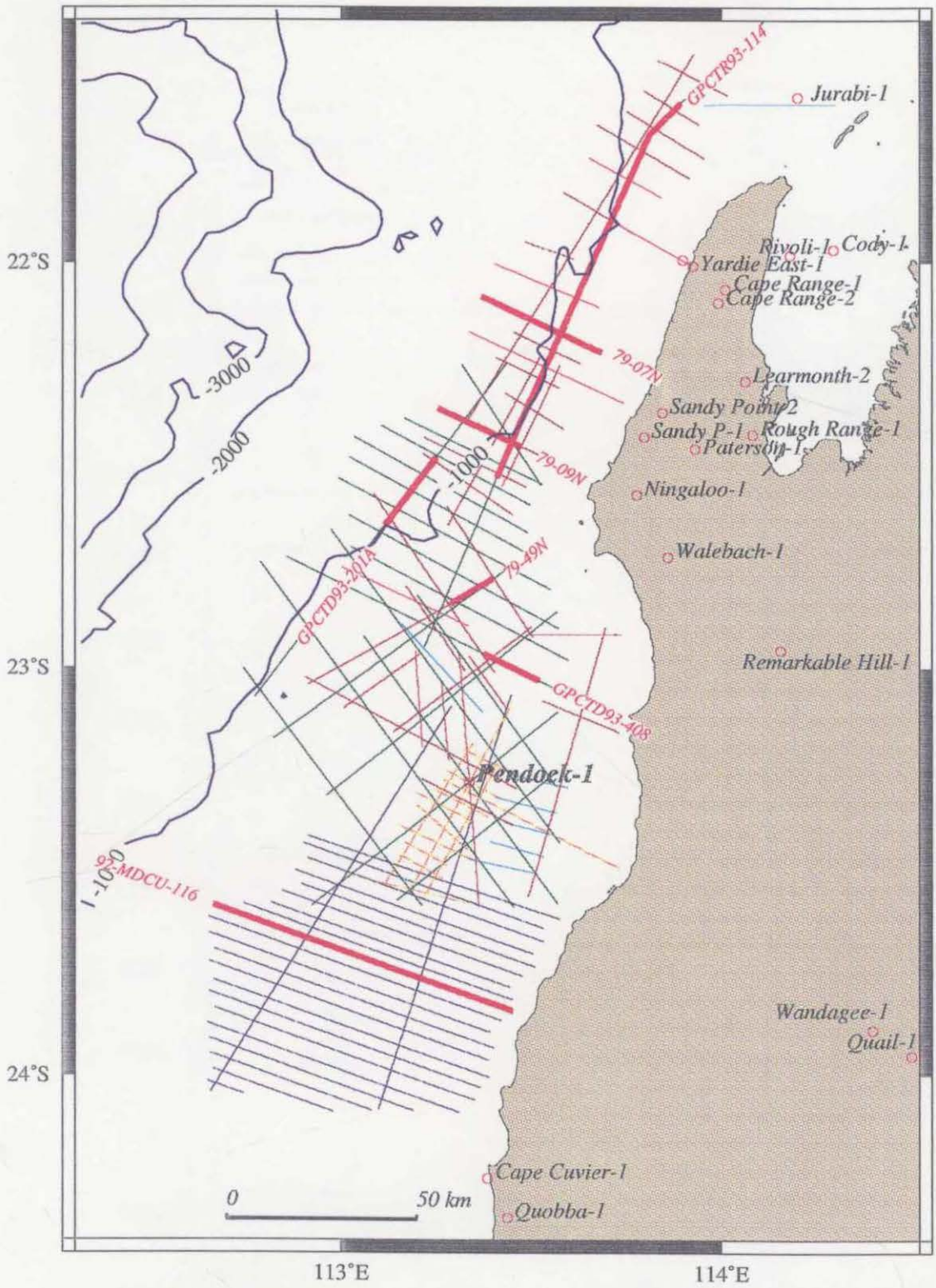

Fig. 4.3 Seismic database and well locations used in this study. Each seismic survey is shown with a different colour (1993-dark green, 1992-dark blue, 1982-orange, 1980-cyan, 1979-brown, 1972-magenta); thick red lines represent location of selected, interpreted seismic lines. Bathymetric contour displayed at 1000 m interval from ETOPO5.

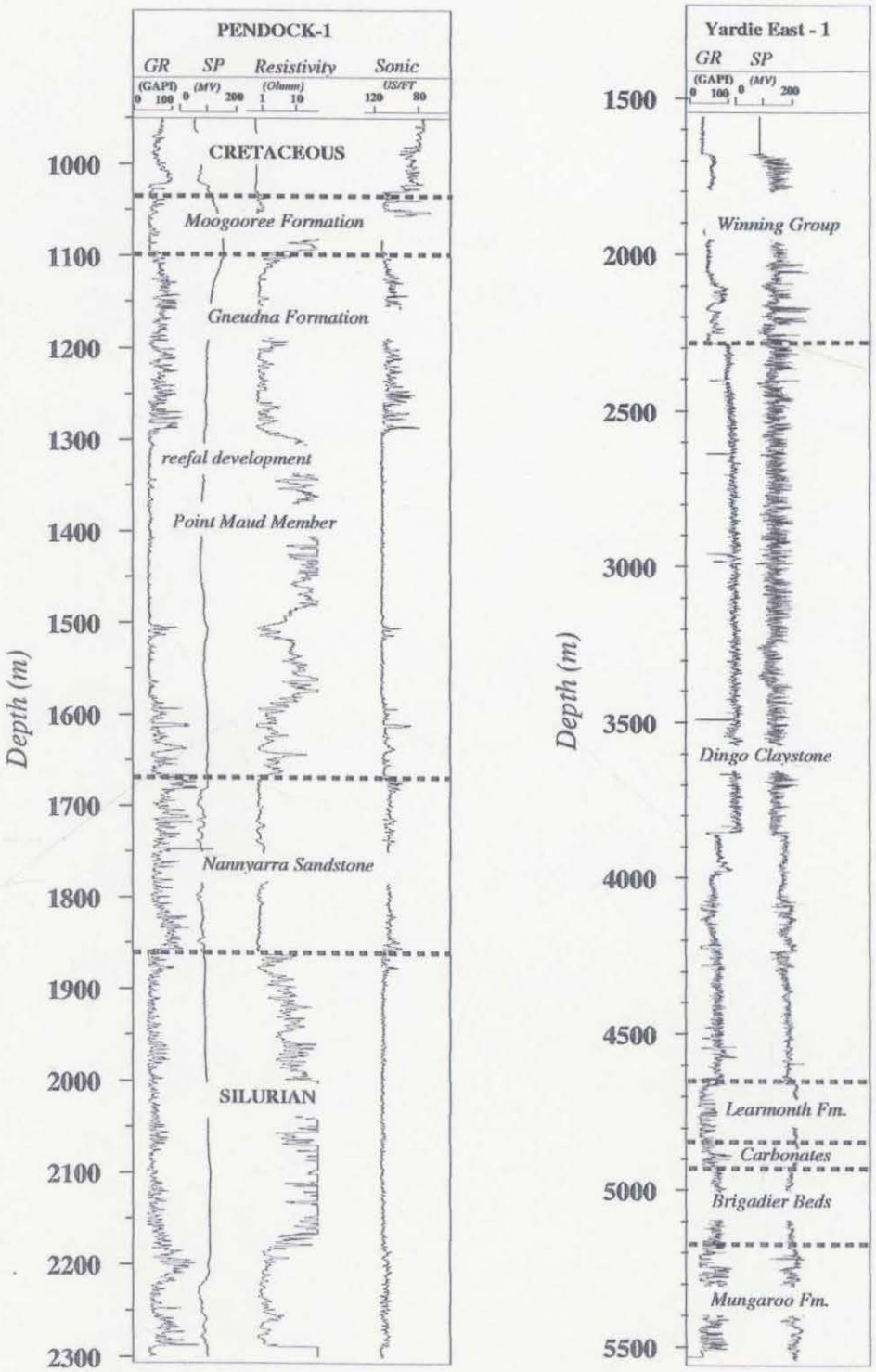

Fig. 4.4 Partial logs of Pendock-1 and Yardie East-1 with stratigraphic intervals indicated.

Fig. 4.5 Seismic tie to Pendock-1 – Line 79-31N (location in Fig. 4.3). Abbreviations are: EU – Eocene unconformity, TC – Top Cretaceous, BCU – basal Cretaceous unconformity. The vertical scale is in ms (TWT) and the horizontal scale is in meters (shown at the bottom of the figure). On the horizontal scale are also shown shot points and ties with other seismic lines.

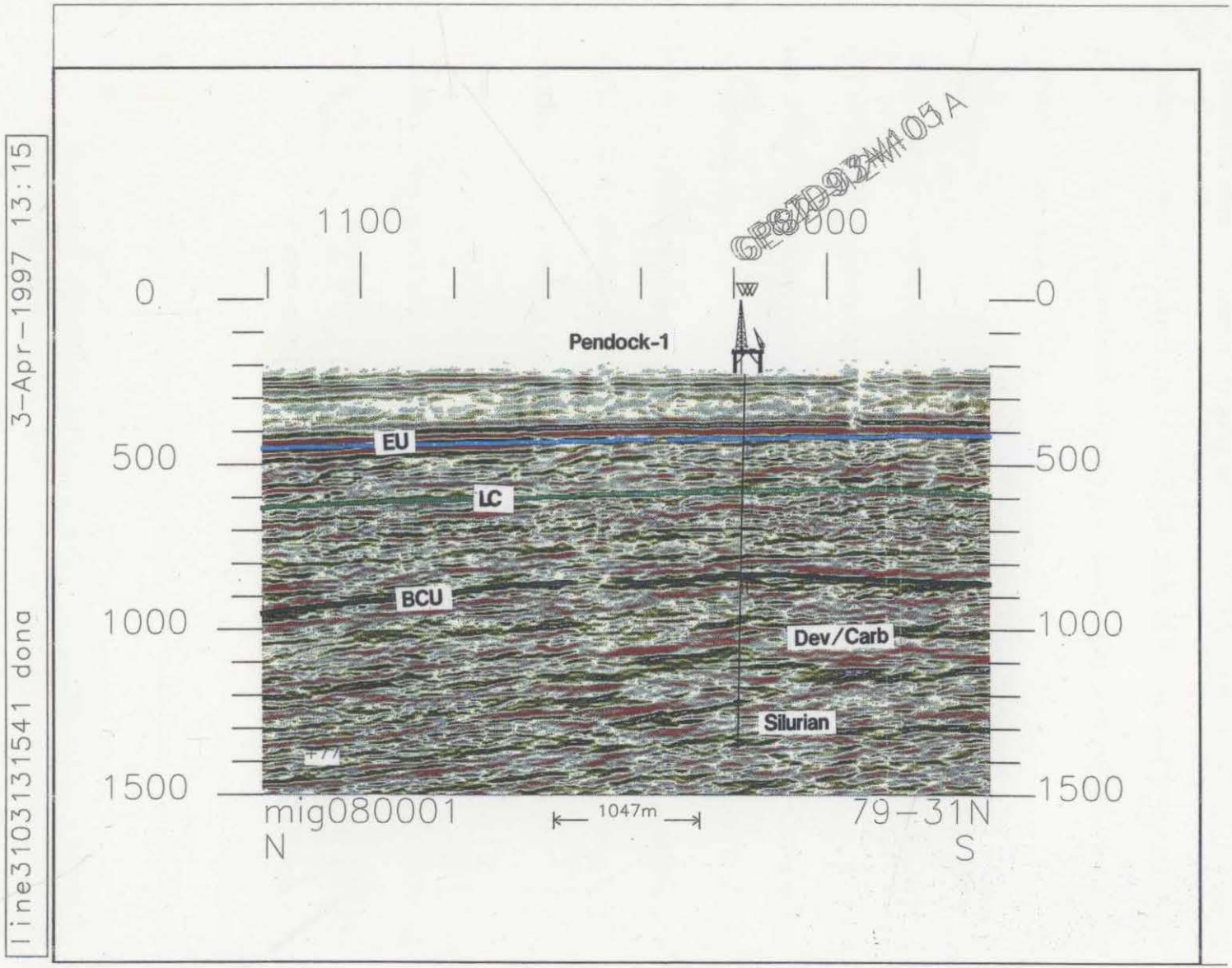
line310313154l dona 3-Apr-1997 13:15
1100
0
0
Pendock-1
EU
LC
BCU
Dev/Carb
Silurian
500
1000
1500
500
1000
1500
mig080001
N
1047m
79-31N
S

The well reached a total depth of 2,501 m and encountered 616 m of Cainozoic carbonates, sand and minor siltstone and 271 m of Cretaceous shale (including Muderong Shale equivalents) with some carbonate at the top and a thin sandstone unit (Birdrong Sandstone correlate) at the base which unconformably overlies a thick Paleozoic succession.

Underlying the Lower Cretaceous Birdrong Sandstone correlate (1029.6 m) is 77 m of Early Carboniferous dolomite (Moogooree Formation) overlying 564 m of Upper and Middle Devonian limestone, dolomite and mudstone (Gneudna Formation) including a reef unit (Point Maud Member). A 185 m thick Middle to Lower Devonian sandstone (Nannyarra Sandstone) overlies a 651 m thick succession of Upper Silurian dolomite with minor anhydrite and sandstone (Sweeney Mia, Kopke and Dirk Hartog formation correlates).

Pendock-1 has direct ties to several seismic lines interpreted in this study including lines 79-31N (Figure 4.5), 79-02N, GPCT93-101 and GPCT93-107. As the well encounters Cretaceous sediments unconformably overlying Lower Carboniferous sediments, it could only be used to correlate the top and base of the Cretaceous sediments over the study area and the top Silurian unit in the Bernier Platform (the top Silurian unconformity is not discussed here).

Yardie East-1 (Figures 4.4 and 4.6; *Kjellgren et al.*, 1982) was drilled in the Exmouth Sub-basin by Mesa Australia Limited in 1981. The well was directionally drilled from an onshore location to an offshore target, the potential reservoirs lying within the Lower Jurassic Learmonth Formation and Upper Triassic Mungaroo

Fig. 4.6 Seismic tie to Yardie East-1 - Line B72-05M (location in Fig. 4.3). Abbreviations are: EU - Eocene unconformity, TC - top Cretaceous, BCU - basal Cretaceous unconformity, TT - top Triassic (top Mungaroo Fm).

Formation. The well, with a total depth of 5,599 m, penetrated a sedimentary and igneous succession ranging in age from Recent to Late Triassic.

The stratigraphy encountered is composed of 1,191 m of Maastrichtian and Cainozoic carbonates overlying a 737 m section correlating the Gearle Siltstone, Windalia Formation, Muderong Shale and Birdrong Sandstone. Lying unconformably beneath the Birdrong Sandstone correlate is the 1,525 m thick Lower to Middle Jurassic Dingo Claystone, a claystone with minor carbonate and sandstone horizons. The 121 m thick unit underlying the Lower Jurassic Learmonth Formation consists predominantly of fine to medium-grained sandstone and overlies a Lower Jurassic 42 m thick unnamed carbonate sequence and fine-grained sediments correlated with the Triassic Brigadier Beds. The final succession encountered in the well is represented by interbedded sandstone, siltstone and claystone of the Upper Triassic Mungaroo Formation having a combined thickness of about 500 m.

Some 20 tholeiitic dolerite intrusions of unknown age with a maximum thickness of 3 m occur within the drill hole below 1,240 m in the lower part of the Dingo Claystone and older sediments. The intrusions display relatively short interval transit times on the sonic log, often in strong contrast to the surrounding sediments and thus, have the potential to form strong seismic reflections.

There is no synthetic seismic coverage of the shallow part of the section. Therefore, only the deeper portion of the well could be tied to the seismic line, 72-05M. The top of the Triassic Mungaroo Formation was identified by using interval velocities from the well and the known thickness of the sequence from onshore wells. The top

of the Triassic Mungaroo event was similarly identified by *Peake and Bowes* (1993) at the Juraby-1 well (offset approximately 2.5 km from line Ce80-05) in the northern part of the area (well location in Figure 4.3).

4.3.2 Seismic interpretation

The seismic interpretation has been carried out on a Sun workstation using Landmark Seiswork 2D software and on paper for non-reprocessed lines (e.g. 72-05). The horizons were gridded and contoured using the GMT software; the major fault planes are also displayed on maps.

The poor quality of data below the basal Cretaceous unconformity in the Bernier Platform detracted from a detailed seismic interpretation of the Palaeozoic units. However, sequences of subparallel reflectors were observed and were interpreted as a Devonian/Carboniferous section. Such an interpretation is consistent with the stratigraphy in onshore wells west of the study area (Cape Cuvier-1 and Quobba-1). Near to vertical faults separated the Devonian/Carboniferous section from a weak and reflection free sequence that has been interpreted as Precambrian horst blocks. The structural trend is north northwest - south southeast and the Precambrian sequence occurs immediately beneath the basal Cretaceous (breakup) unconformity and possibly corresponds to the early Permian to Late Jurassic (?) rifting episodes (Figure 4.7).

Fig. 4.7 Interpreted seismic line 92-MCDU-116 (location in Fig.4.3) showing main tectonic events affecting the Bernier Platform and near to vertical reactivated faults that separate the Devonian/Carboniferous sequence from older Precambrian horsts. Abbreviations are: EU – Eocene unconformity, LC- Late Cretaceous, BCU – Basal Cretaceous unconformity, Dev/Carb – Devonian/Carboniferous, PCamb – Precambrian. The vertical scale is in ms (TWT) and the horizontal scale is in meters (shown at the bottom of the figure). On the horizontal scale are also shown shot points and ties with other seismic lines.

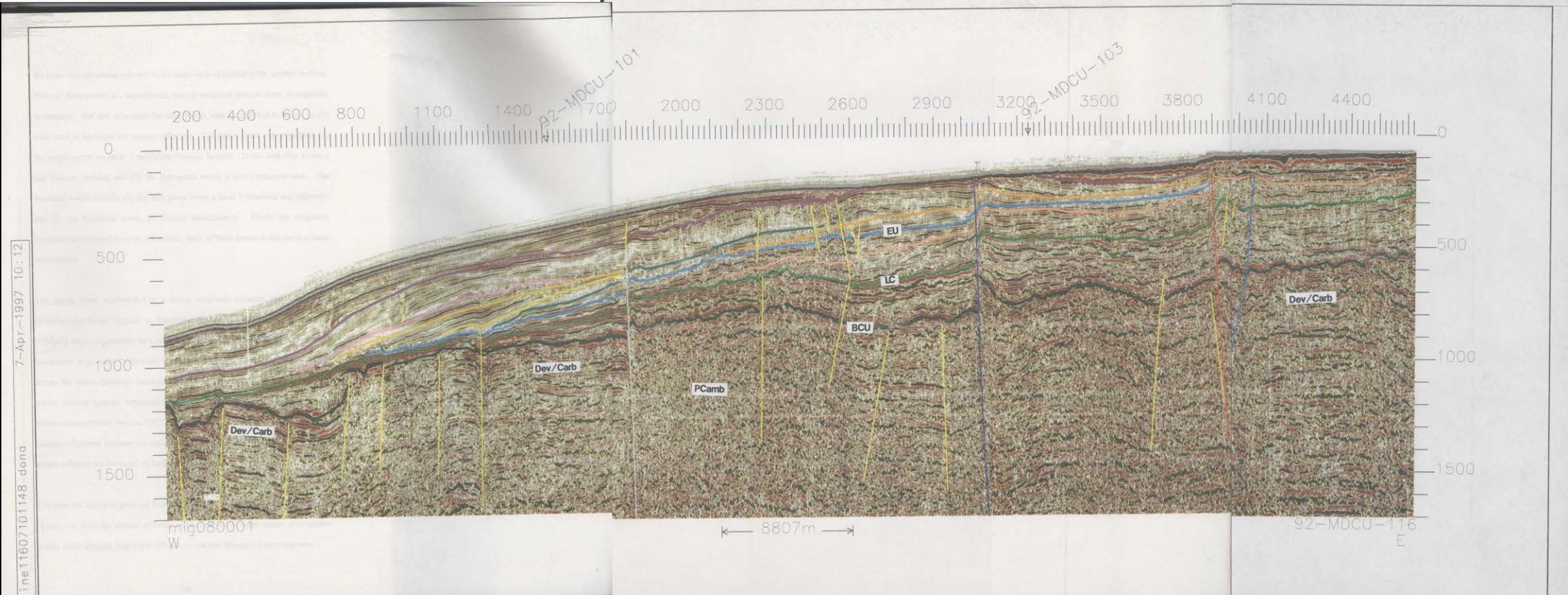

Six main tectonic events relevant to the study were identified in the seismic sections. Three of these events are depositional, two are erosional and one event is magmatic in character. For lack of a name for these events, they are referred to herein, by the color used to highlight the seismic reflectors. The depositional events include: (1) the purple event, an early Triassic/late Permian horizon; (2) the dark-blue event, a late Triassic horizon; and (3) the light-green event, a late Cretaceous unit. The erosional events include: (1) the dark-green event a basal Cretaceous unconformity; and (2) the light-blue event, an Eocene unconformity. Finally the magmatic intrusions are referred to as the red events. Each of these events is discussed in more detail below.

The purple event, represented by a strong amplitude reflector, was often easily identified due to the 'opaque' or featureless character of reflections typical of the overlying sequence, possibly the Locker Shale sequence (Figure 4.8). This event was interpreted as an early Triassic/late Permian (?) horizon which has been correlated across the entire Exmouth Sub-basin except in the south and southwest regions where inferred igneous intrusions above the horizon created difficulties in the seismic interpretation. On line GPCT93-114 (Figure 4.8) the chaotic character of the seismic reflections impedes the interpretation over about 26 km of the basin but the purple reflector can be traced on both sides of this area (see also Figure 4.12).

The complex structural geology, high level of volcanic intrusive activity, availability of only two wells for seismic reflector correlation and in some places, poor seismic quality made the dark-blue event difficult to interpret throughout the study area.

Fig. 4.8 Interpreted seismic line GPCT93-114 (location in Figure 4.3) showing main unconformities affecting the offshore of the Exmouth Sub-basin. Abbreviations are: EU- Eocene unconformity, LC – Late Cretaceous, BCU – Basal Cretaceous unconformity, LT – Late Triassic, ET – Early Triassic/Late Permian. The vertical scale is in ms (TWT) and the horizontal scale is in meters (shown at the bottom of the figure). On the horizontal scale are also shown shot points and ties with other seismic lines.

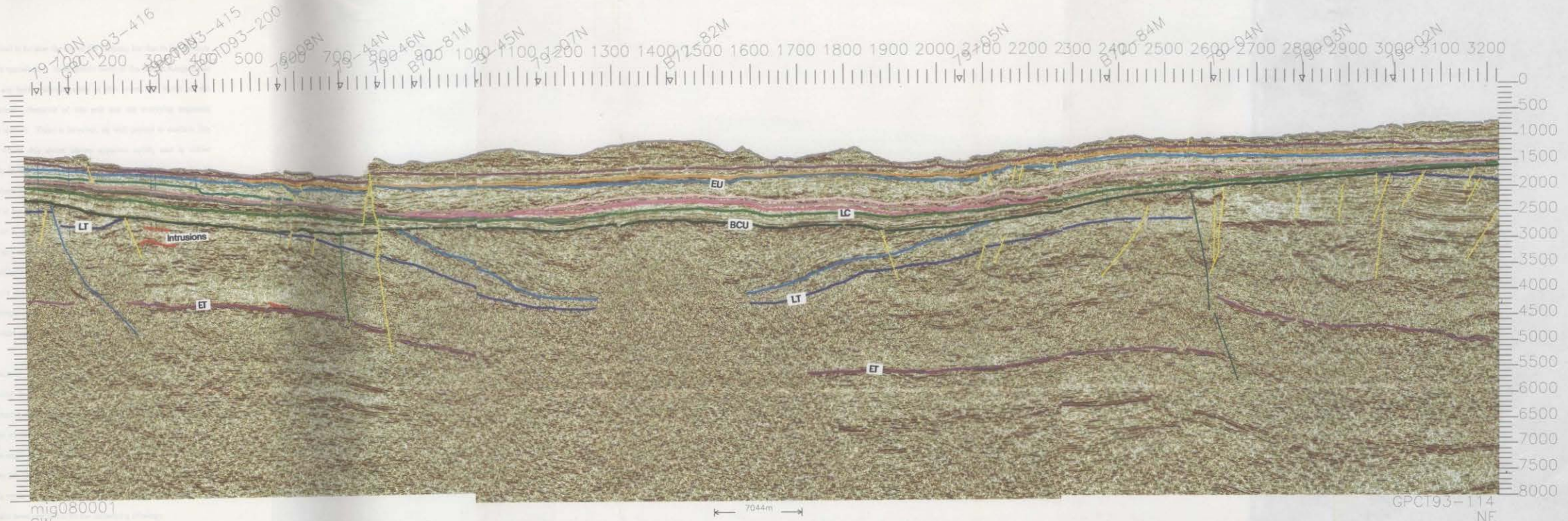
GPCTD93-416
GPCTD93-415
GPCTD93-200
79-100N
79-98N
79-44N
79-46N
B71-81M
79-45N
79-107N
B71-82M
79-105N
B71-84M
79-94N
79-103N
79-102N
EU
LC
BCU
LT
Intrusions
ET
LT
ET
7044m
mig080001
SW
GPCT93-114
NE
2-Apr-1997 06:17
linea1140206165g dona

The horizon was considered to be near the top of the Triassic, but due to the absence of well control this age is speculative. Immediately north of the Rough Range Fault (RRF), where the data are better, identification of this event was based on the contrast between the seismic character of this unit and the overlying sequence (possible Jurassic Dingo shales). There is however, no well control to confirm this interpretation. Areas where this event shows apparent uplift, and is either subcropped or completely eroded can be seen on the seismic section (Figure 4.9). In Figure 4.8, in the area where the purple event could not be interpreted, the overlying sequences are pulled up at the contact with the zone with chaotic seismic character giving the impression of a doming effect. Such a disturbance in the seismic character was attributed to a major magmatic intrusion discussed in more detail later in this chapter. The intrusions appear to penetrate and disturb both interpreted Jurassic reflectors but not the whole Jurassic sequence. Therefore, the intrusion possibly happened contemporaneously with the formation of the basin. Otherwise, all Jurassic sediments would wrap around the top of the intrusion.

The base of the Cretaceous section, the dark-green event, marks the breakup unconformity that resulted from the separation of Greater India and Australian plates. The angular contact between this unit and the underlying sequence allowed for an easy identification of this event throughout the study area (e.g. Figure 4.10). South of the RRF (a low-angle detachment fault) the sediments underlying the basal Cretaceous unconformity are Carboniferous and Devonian; north of the fault, in the Exmouth Sub-basin the event overlying Jurassic and/or Triassic sediments. The erosional pattern may have been controlled by the underlying lithology.

Fig. 4.9 Interpreted seismic line 79-49N (location in Figure 4.3) showing areas of complete erosion of the Jurassic sequence. Abbreviations as in Figure 4.8. The vertical scale is in ms (TWT) and the horizontal scale is in meters (shown at the bottom of the figure). On the horizontal scale are also shown shot points and ties with other seismic lines.

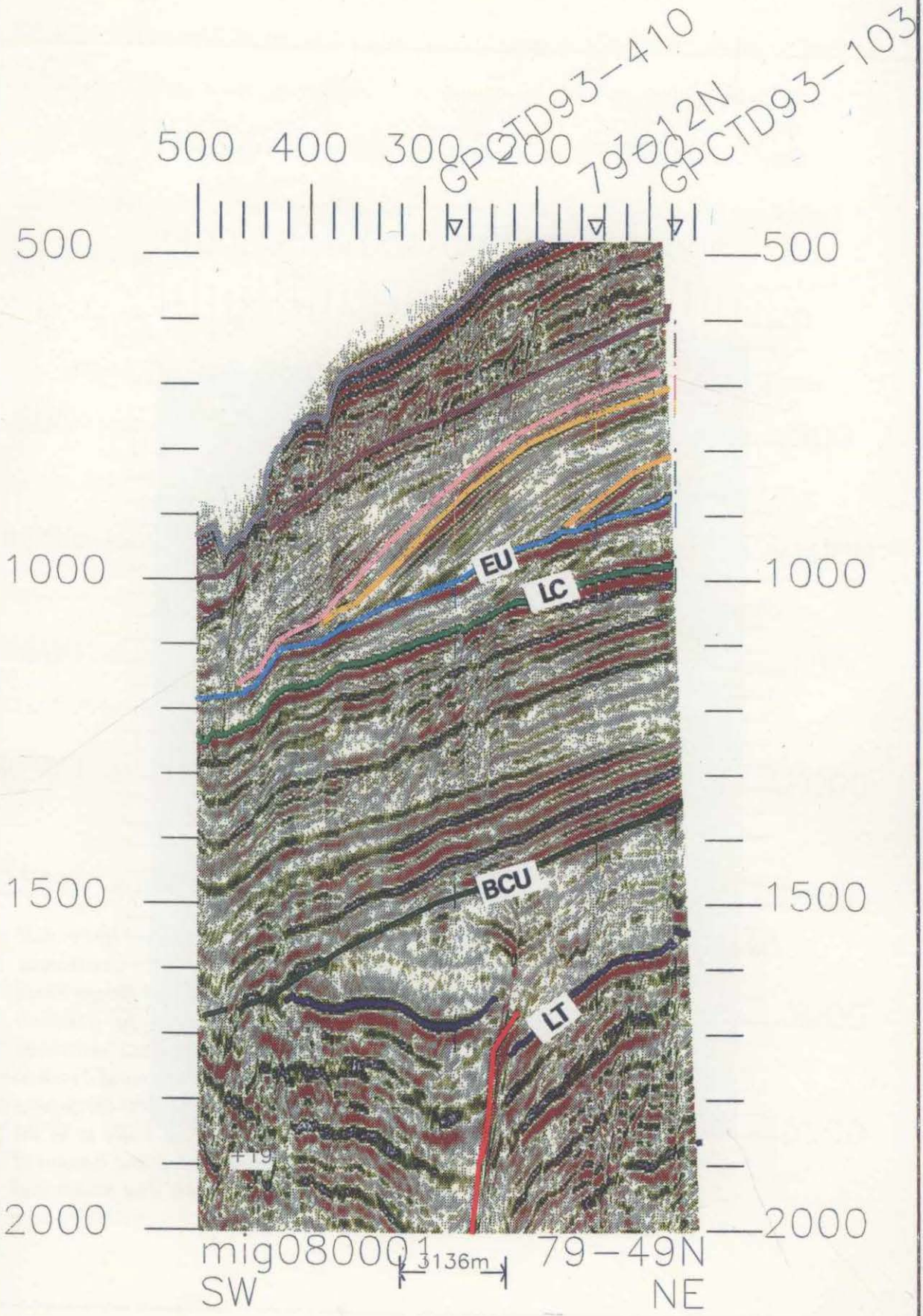

line490608274 3 dona 6-Feb-1997 08:27

Fig. 4.10 Interpreted seismic line GPCTD-408 (location in Figure 4.3) showing the angular contact between the basal Cretaceous unconformity, the underlying sequences and the Rough Range Fault (RRF), a low angle detachment fault that separates the Exmouth Sub-basin from the Bernier Platform. The basal Cretaceous unconformity is underlain west of the RRF by Jurassic and Triassic sediments and by Devonian/Cretaceous sediments east of the fault. . Other abbreviations as in Figure 4.8. The vertical scale is in ms (TWT) and the horizontal scale is in meters (shown at the bottom of the figure). On the horizontal scale are also shown shot points and ties with other seismic lines.

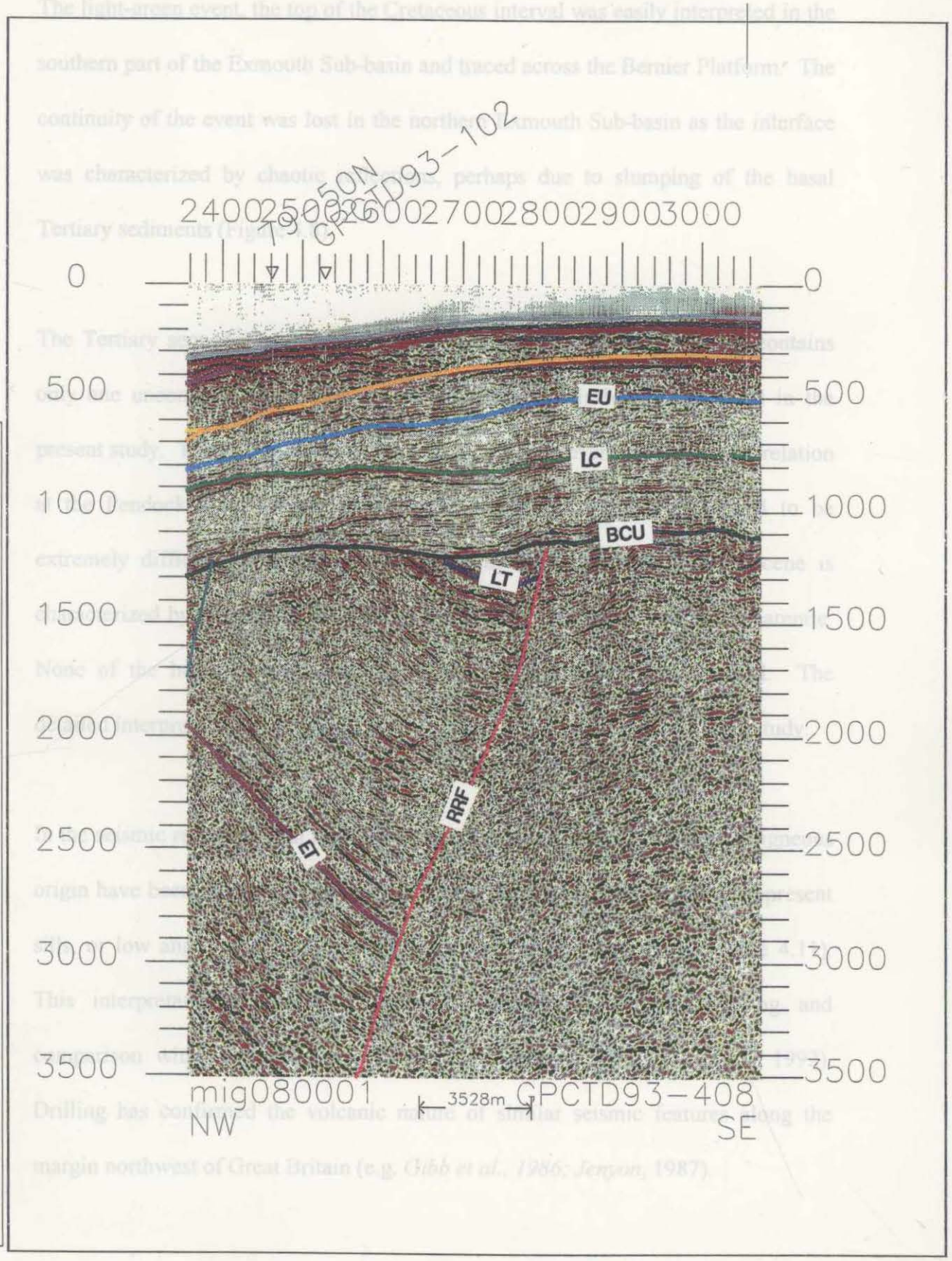
line408new03163112 dona 3-Feb-1997 16:31
2400 2500 2600 2700 2800 2900 3000
T9350N
GPCTD93-102
0
500
1000
1500
2000
2500
3000
3500
EU
LC
BCU
LT
RRF
ET
mig080001
NW
3528m
GPCTD93-408
SE

The light-green event, the top of the Cretaceous interval was easily interpreted in the southern part of the Exmouth Sub-basin and traced across the Bernier Platform. The continuity of the event was lost in the northern Exmouth Sub-basin as the interface was characterized by chaotic reflections, perhaps due to slumping of the basal Tertiary sediments (Figure 4.8).

The Tertiary sequence was separated into a series of sub-sequences, but contains only one unconformity, the Eocene unconformity that is briefly discussed in the present study. The Eocene unconformity (the light-blue event) despite its correlation at the Pendock-1 and Yardie East-1 wells (Figures 4.5 and 4.6) proved to be extremely difficult to identify especially south from the RRF. The Eocene is characterized by prograding shelf carbonate sediments of the Cardabia Calcarenite. None of the horizons interpreted in the Tertiary sequence were mapped. The detailed interpretation of the Tertiary sequence is beyond the purpose of this study.

In the seismic record several regional and local features that are of probable igneous origin have been identified (red events). These features are considered to represent sills, or low angle dikes within the Triassic and Jurassic sediments (Figure 4.11). This interpretation is based on seismic signature, stratigraphic setting and comparison with similar features in the Vøring Basin (*Skogseid et al.*, 1992). Drilling has confirmed the volcanic nature of similar seismic features along the margin northwest of Great Britain (e.g. *Gibb et al., 1986; Jenyon*, 1987).

Magmatism manifest itself by intrusions (sill and/or dykes) dominantly present in the southern part of the Exmouth Sub-basin. These intrusive features are common in

Fig. 4.11 Interpreted seismic line 79-09N (location in Figure 4.3) showing local features interpreted as sills or low angle dikes within the Triassic and Jurassic sediments. Abbreviations as in Figure 4.8. The vertical scale is in ms (TWT) and the horizontal scale is in meters (shown at the bottom of the figure). On the horizontal scale are also shown shot points and ties with other seismic lines.

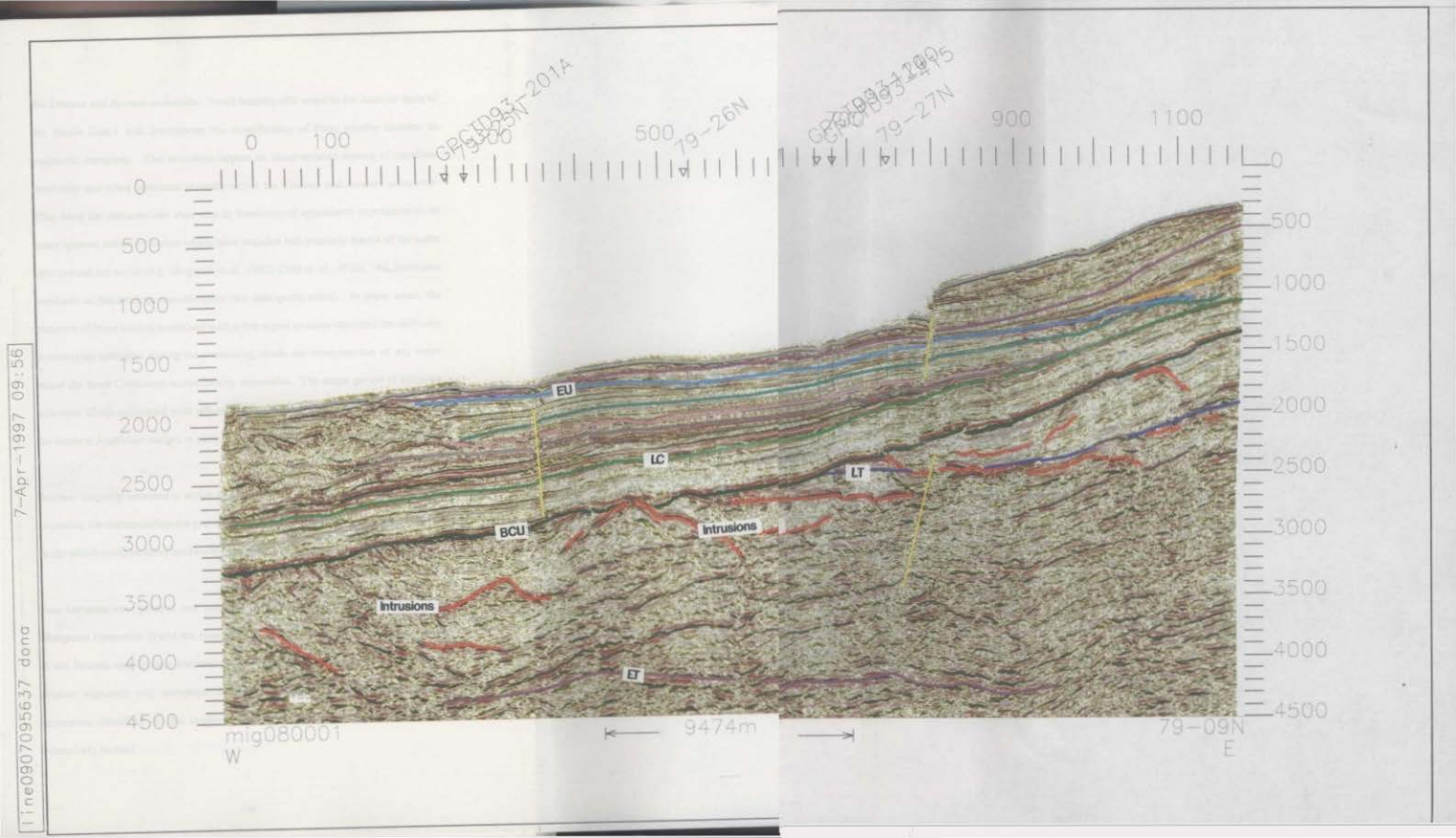

the Triassic and Jurassic sediments. Small basaltic sills noted in the Jurassic units of the Yardie East-1 well corroborate the identification of these seismic features as magmatic intrusions. The intrusions appear as sharp seismic signals of excellent continuity and often terminate abruptly within the Triassic and Jurassic sediments. They have the characteristic stair-step or bowl-shaped appearance representative of many igneous intrusive bodies which have intruded into similarly basins of the same ages around the world (e.g. *Skogseid et al., 1992; Gibb et al., 1986).* All intrusions terminate at the breakup unconformity (the dark-green event). In some areas, the presence of these bodies, combined with a low signal to noise ratio and the difficulty in removing multiples during the processing, made the interpretation of any event below the basal Cretaceous unconformity impossible. The major period of intrusion was most likely associated with rifting that occurred during continental breakup of the western Australian margin in early Cretaceous time.

Seismic mapping revealed a series of sedimentary and structural units that were important for understanding the pre- and post-breakup margin evolution. Only major faults which could be correlated on at least three seismic lines were displayed.

Four horizons were gridded and mapped: the Early (?) and Late Triassic (the Top Mungaroo Formation ?) and the base and top of the Cretaceous. The identification of the Jurassic and Triassic sections should be regarded as speculative, although the seismic signature was compared to and constrained by Jurassic and Triassic sequences identified in the onshore area of the Exmouth Sub-basin, an area extensively studied.

The Early Triassic event was hard to correlate on the entire Exmouth Sub-basin; therefore uninterpreted areas are present in Figure 4.12. Difficulties in the interpretation were due to a limited seismic database, extremely complicated tectonic structures, similar to that encountered onshore, the absence of wells to correlate the sequence over interpreted faults, and the igneous intrusions that obscured significant patterns of sequences. The horizon is dipping northward, thinned and eroded west and south as a result of half-grabens which formed along shallow-dipping detachment faults in the Early Jurassic. The Early Triassic – basal Cretaceous isopach map shows thinning to the south and west and thickening to the north (Figure 4.13).

The Late Triassic time structure map (Figure 4.14) is divided in three sectors as a result of subsequent uplift and erosion and lateral movement along fracture zones. To the north the horizon is flat and broken by normal faults with small offsets. The thick Jurassic Dingo section (approximately 2000 m at Jurabi-1) was eroded and thins to the west and is truncated by the steeply dipping basal Cretaceous unconformity. On one of the east-west dip lines across the mapped syncline (Figure 4.15), the depositional pattern of conformable Jurassic sediments indicates that the amount of uplift and erosion of the Jurassic Dingo Formation was more than 3000 m from its flanks. The timing of this major uplift was probably prior to breakup, i.e. the Late Jurassic - Early Cretaceous, and in agreement with the observations from the onshore wells which show an increase in erosion from east to west (up to 1500 m of sediments were eroded at Sandy Point-1 well relative to Paterson-1 well) during the same syn-rift event (the rift/breakup event).

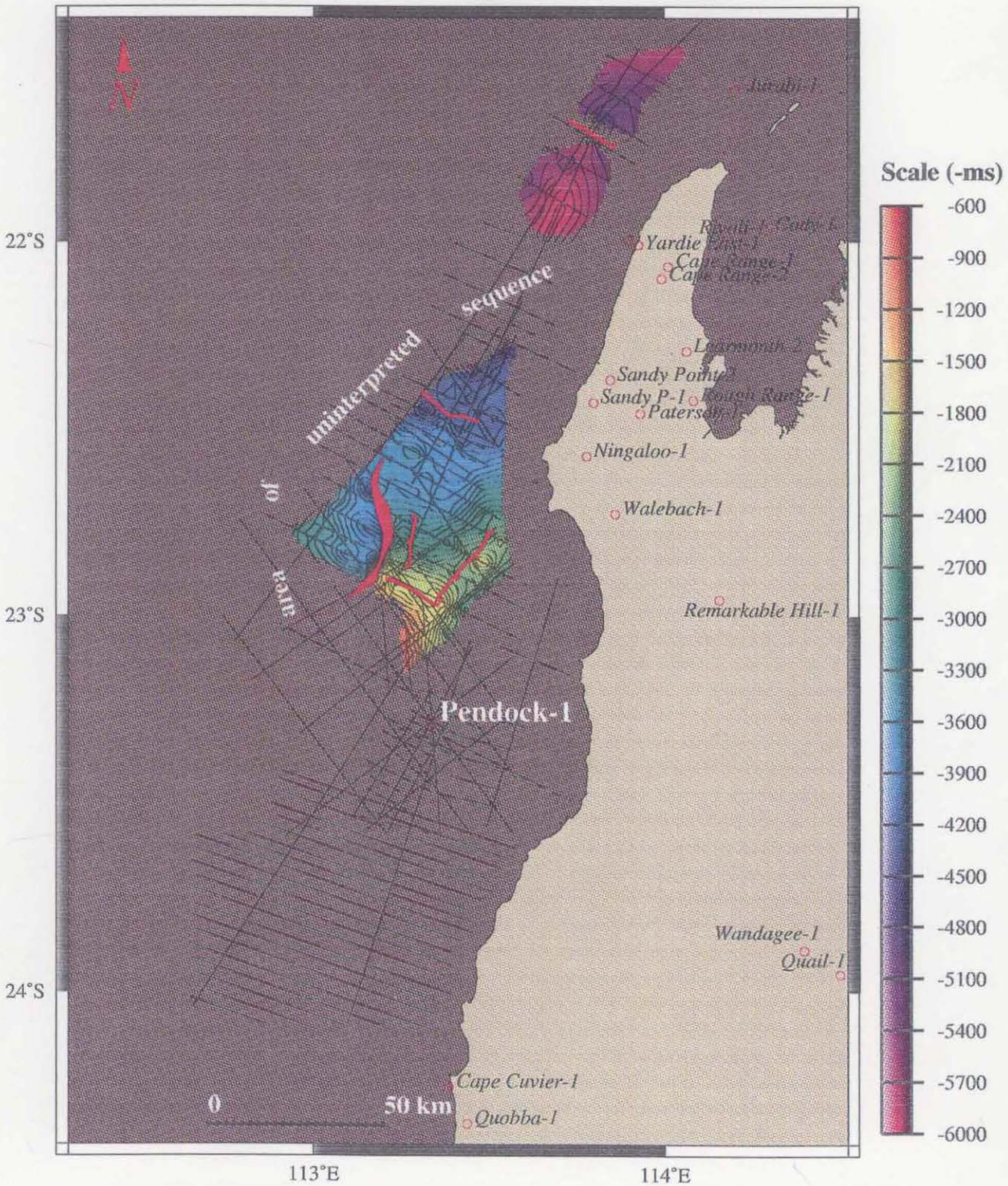

Fig. 4.12 Early Triassic/Late Permian TWT contour map (100 -ms interval) and major faults (red lines) derived from seismic interpretation.

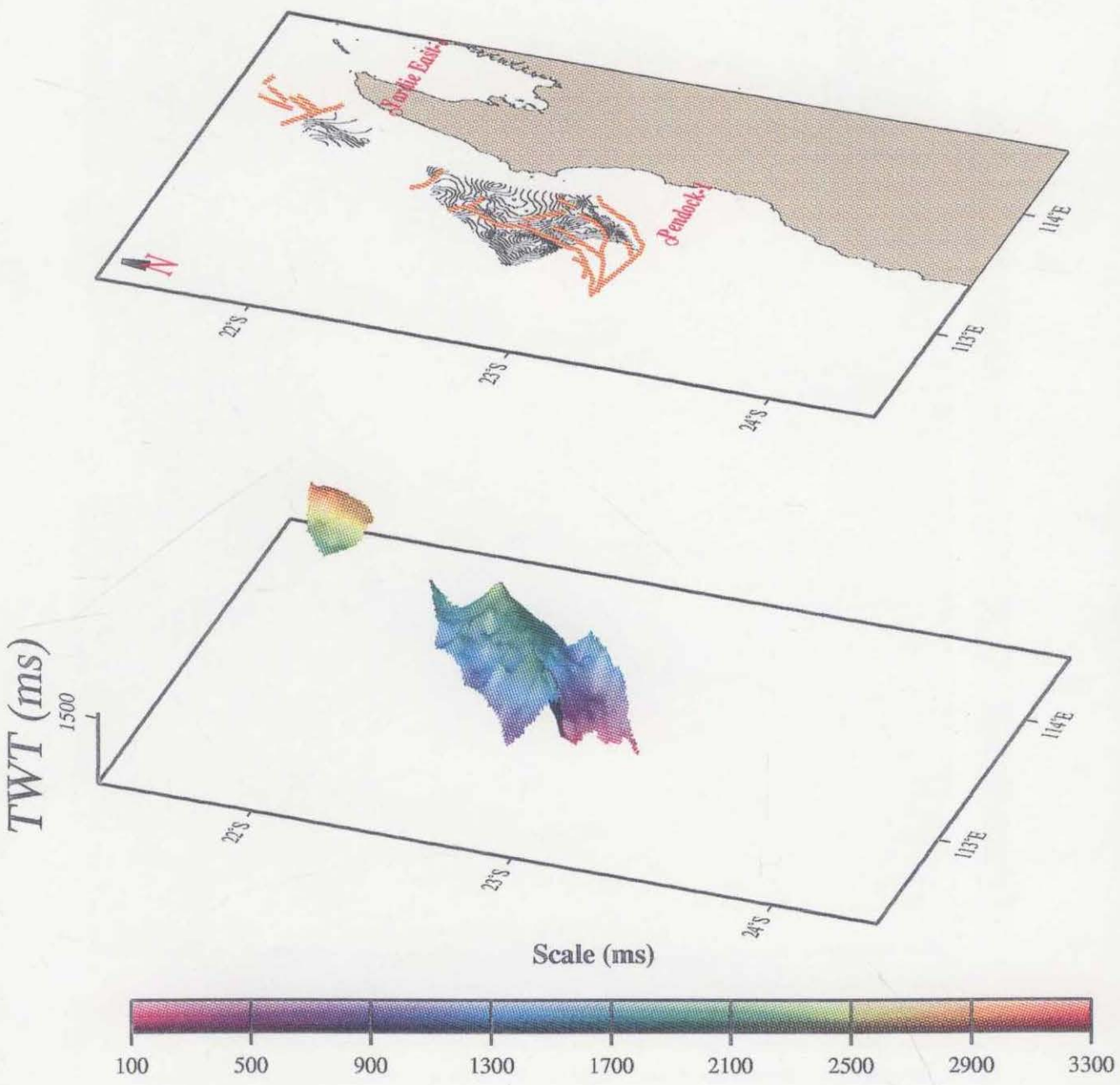

Fig. 4.13 Isopach Early Triassic - base Cretaceous TWT contour map (100 -ms interval) and perspective view.

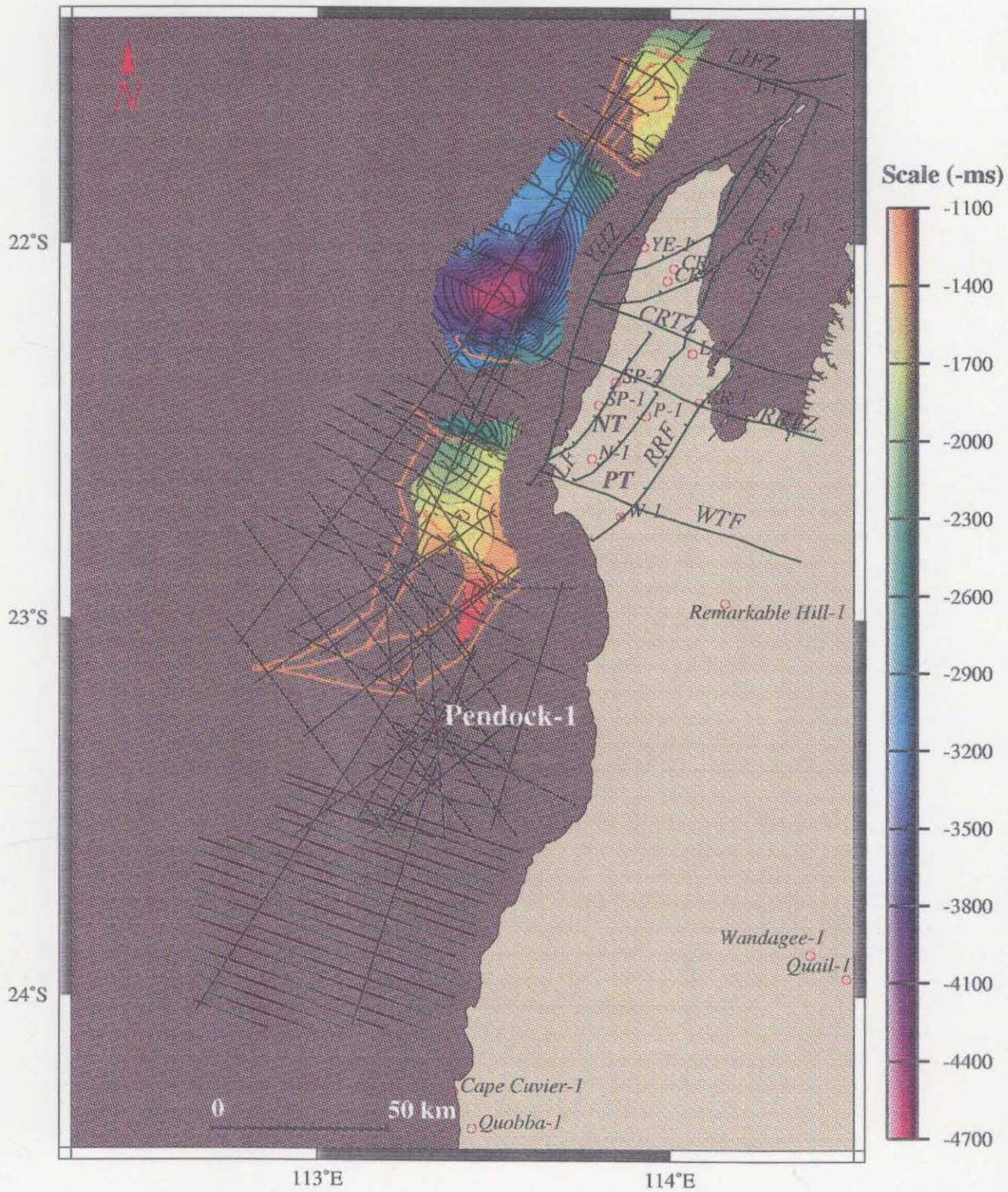

Fig. 4.14 Late Triassic (Top Mungaroo Formation ?) TWT contour map (100 -ms interval) and faults determined from seismic data (orange). Abbreviation key for onshore tectonic elements: LIFZ-Long Island Fracture Zone, CTRZ-Cape Range Transform Zone, RRTZ-Rough Range Transform Zone, WTF-Walebach Transform Fault, RRF-Rough Range Fault, YHZ-Yardie Hinge Zone, EF-Exmouth Fault, BF-Bundegi Terrace, PT-Paterson Trough, NT-Ningaloo Terrace, LF-Learmonth Fault (from Malcolm et al., 1991). Abbreviations for onshore well are: C-1 - Cody-1, R-1 - Rivoli-1, YE-1 - Yardie East-1, CR-1 and 2 -Cape Range 1 and 2, L-1 - Learmonth-1, SP-1 and 2 - Sandy Point-1 and 2, N-1 - Ningaloo-1,W-1 - Walebach-1.

Fig. 4.15 Interpreted seismic line 79-07N (location in Figure 4.3) showing the Jurassic section eroded, thinned to the west and truncated by the steeply dipping basal Cretaceous unconformity. Abbreviations as in Figure 4.8. The vertical scale is in ms (TWT) and the horizontal scale is in meters (shown at the bottom of the figure). On the horizontal scale are also shown shot points and ties with other seismic lines.

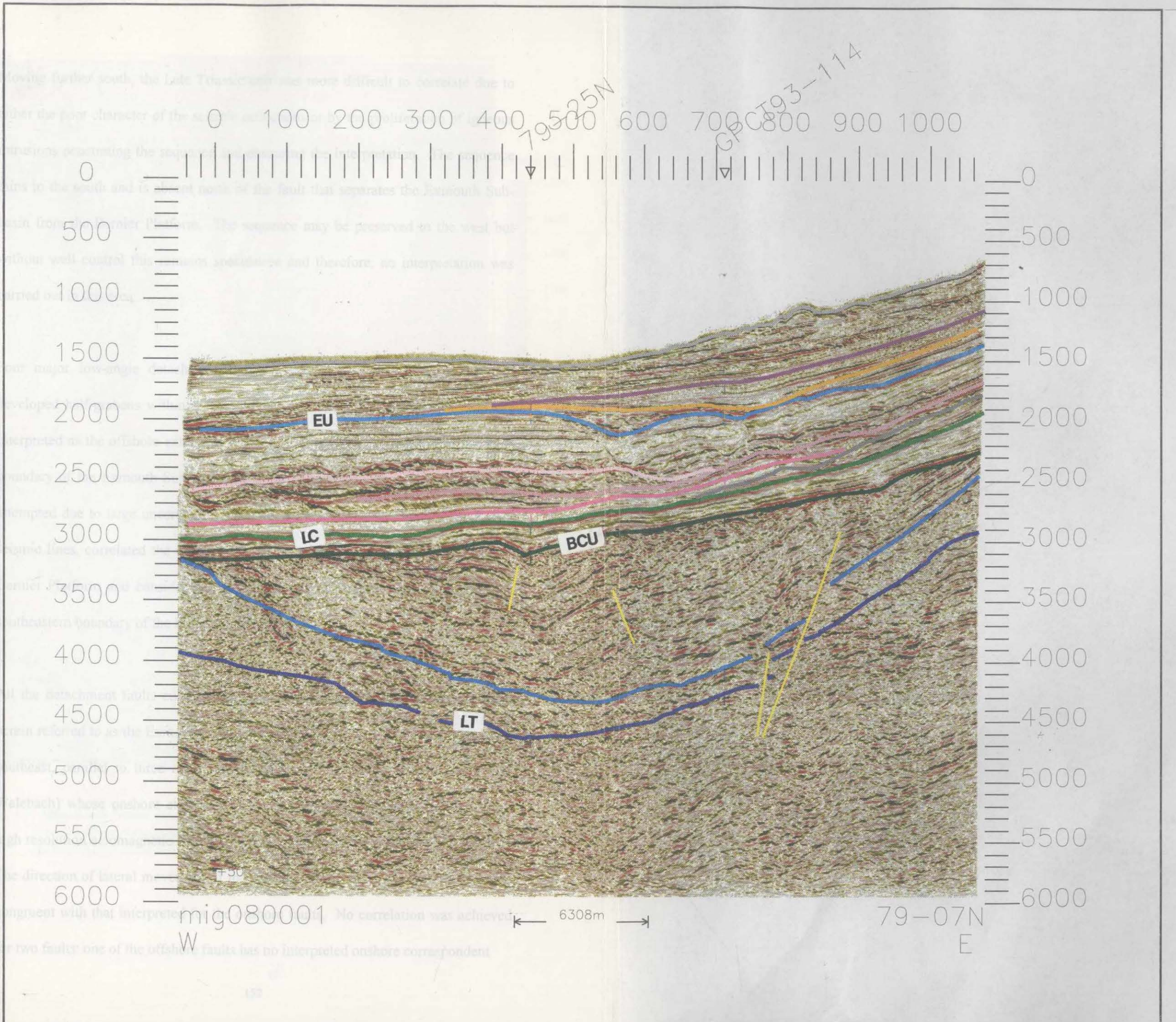
0 100 200 300 400 500 600 700 800 900 1000
79-25N
GPCT93-114
0
500
1000
1500
2000
2500
3000
3500
4000
4500
5000
5500
6000
EU
LC
BCU
LT
mig080001
W
6308m
79-07N
E
line07030943322.dona 3-Feb-1997 09:43

Moving further south, the Late Triassic unit was more difficult to correlate due to either the poor character of the seismic reflections or by the proliferation of igneous intrusions penetrating the sequence and obscuring the interpretation. The sequence thins to the south and is absent north of the fault that separates the Exmouth Sub-basin from the Bernier Platform. The sequence may be preserved to the west but without well control this remains speculative and therefore, no interpretation was carried out in this area.

Four major low-angle detachment faults (Figure 4.14 and 4.16) crosscut and developed half-grabens within the Late Triassic event. The easternmost one was interpreted as the offshore extension of the RRF (Figure 4.10), defining the eastern boundary of the Exmouth Sub-basin; no other correlation with onshore faults was attempted due to large uncertainties. *Baillie et al.* (1994), using only Geko-Prakla seismic lines, correlated the onshore RRF with one of the reactivated faults in the Bernier Platform and considered that the onshore Learmonth Fault represents the southeastern boundary of the Exmouth Sub-basin.

All the detachment faults curve gently westward and merge with a transfer fault, herein referred to as the Exmouth Transfer Fault (ETF). The ETF strikes northwest-southeast, parallel to three other transfer faults (Cape Range, Rough Range and Walebach) whose onshore extension have been mapped into the subsurface from high resolution aeromagnetic data and seismic interpretation (*Malcolm et al.*, 1991). The direction of lateral movement of the four transform faults identified offshore is congruent with that interpreted for the onshore faults. No correlation was achieved for two faults: one of the offshore faults has no interpreted onshore correspondent

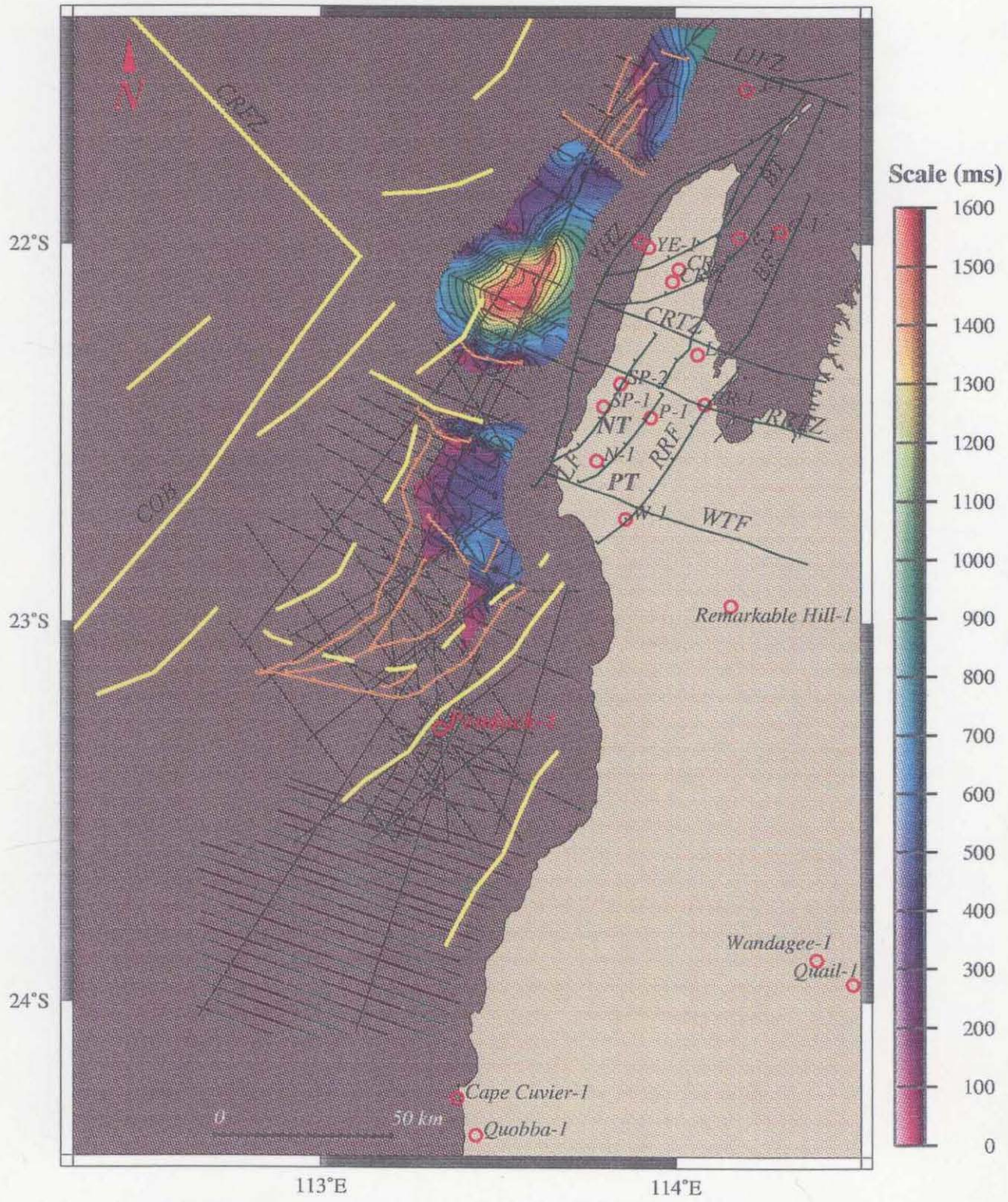

Fig. 4.16 Isopach Late Triassic (Mungaroo Fm.?) - base Cretaceous TWT (ms) contour map. Orange lines are faults interpreted from the seismic interpretation, yellow lines represent trends determined from satellite gravity grid. Abbreviations as in Fig. 4.14.

and the Cape Range Transform Zone (CRTZ), identified onshore, could not be recognized offshore possibly due to the presence of the major intrusion that has affected the Triassic and Jurassic sequences.

The base Cretaceous and top Cretaceous time structure maps (Figures 4.17 and 4.18 respectively) show a relatively similar regional monocline dipping steeply westward into the basin. The RRF seems to offset the base Cretaceous event, but not all interpreted lines show that offset (Figure 4.10). South of the RRF, which separates the Mesozoic Exmouth Sub-basin from the Bernier Platform, the map shows a regional dip to the northwest. Three major compressional structures (affecting both the base and top Cretaceous reflectors), in the Bernier Platform were caused by the approximately north/south trending Miocene reverse faults (blue lines on the map). Miocene compression features are absent north of the RRF where the shortening was probably taken over by the ETF.

The isopach map between the base and the top Cretaceous reflectors (Figure 4.19) shows thinning to the north and local variations in thickness especially in the southwestern part of the Bernier Platform, caused by the small depositional centers along possibly reactivated normal faults.

4.4 Synthesis and discussion

Four important issues are highlighted by the present study: the reason for and timing of the uplift of the Bernier Platform and the Exmouth Sub-basin; the time of

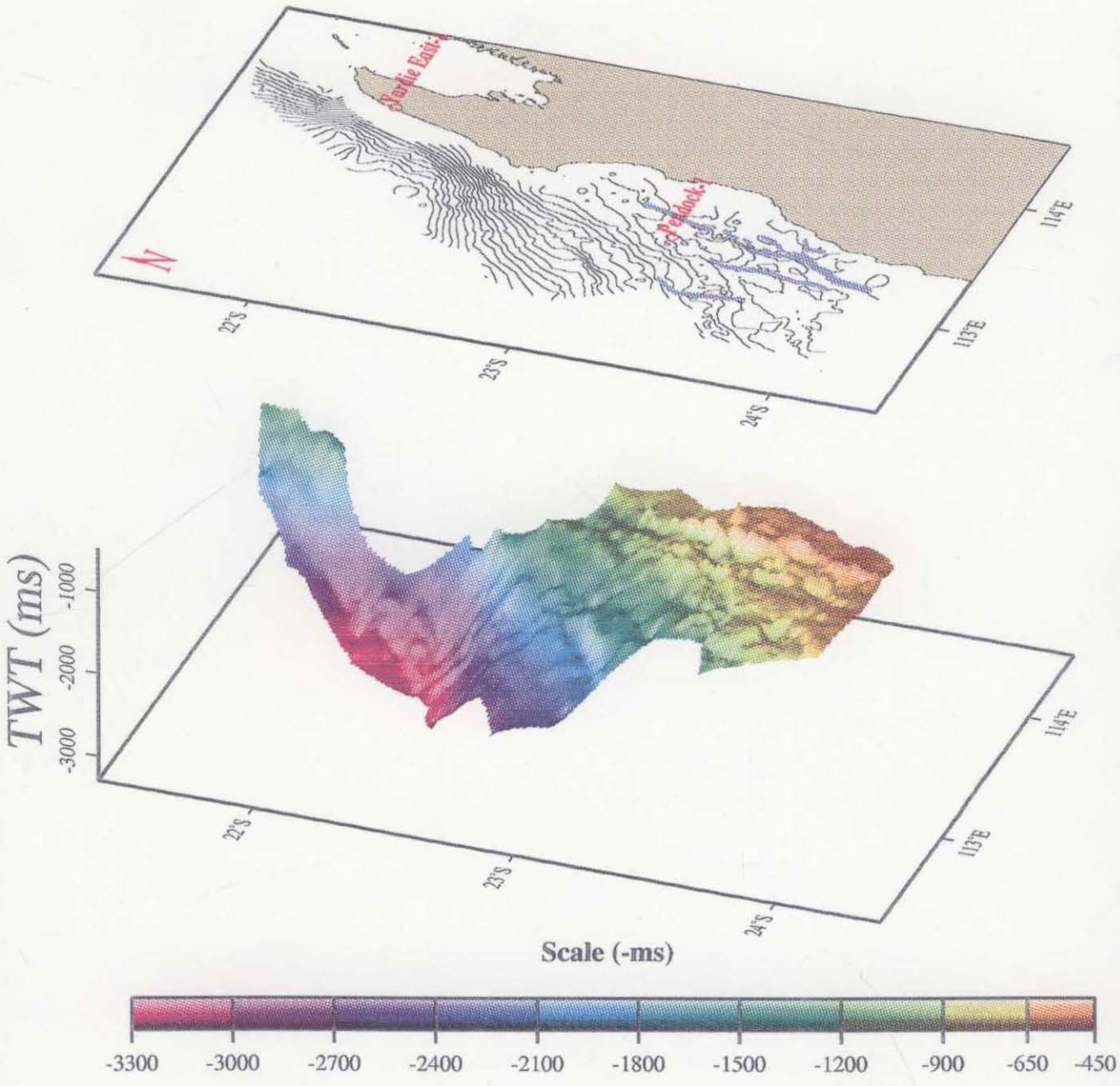

Fig. 4.17 Basal Cretaceous TWT contour map (100 -ms interval) and perspective view. Blue lines represent rectivated faults determined from seismic interpretation.

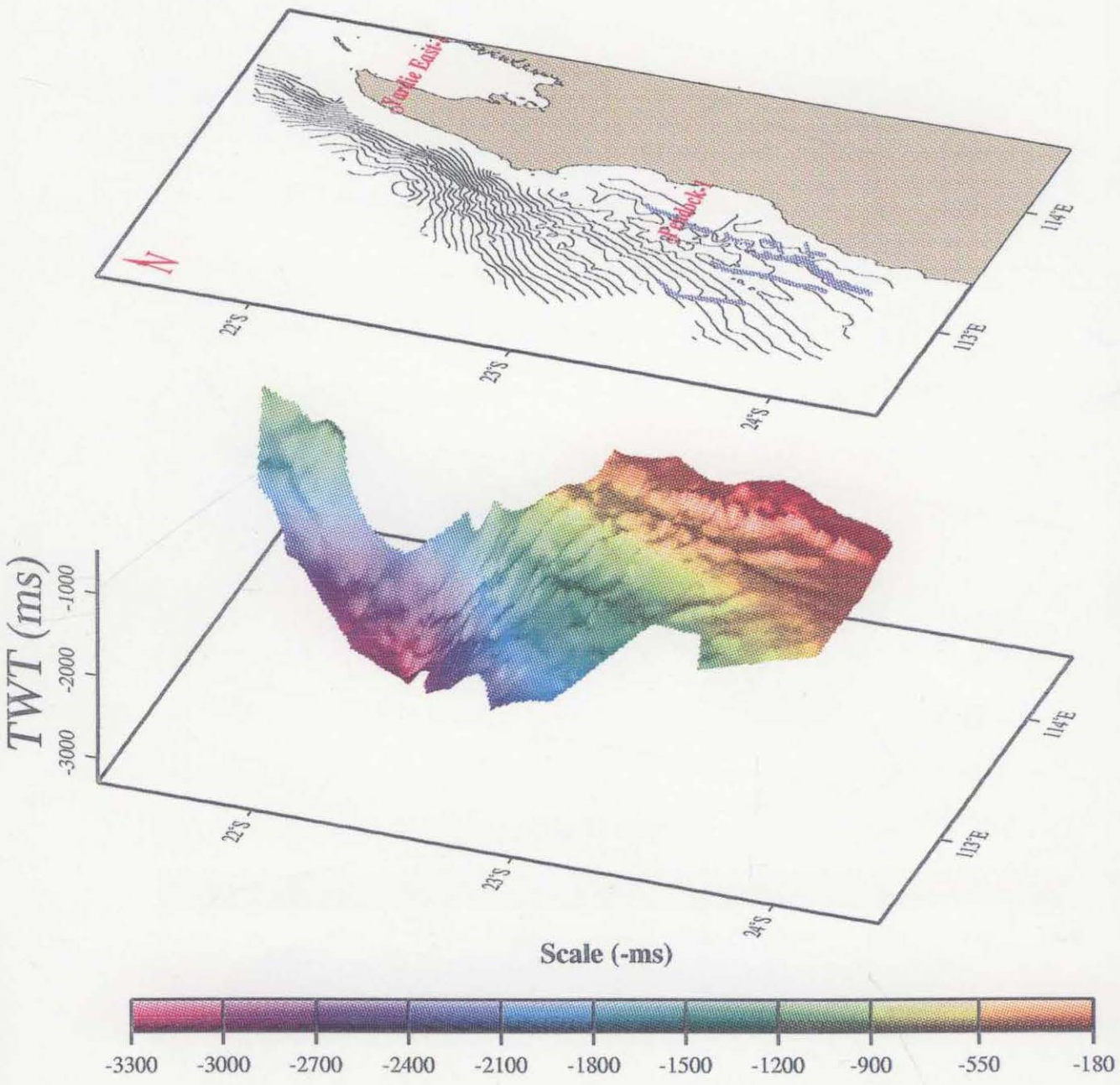

Fig. 4.18 Late Cretaceous TWT contour map (100 -ms interval) and perspective view. Blue lines represent reativated faults determined from seismic interpretation.

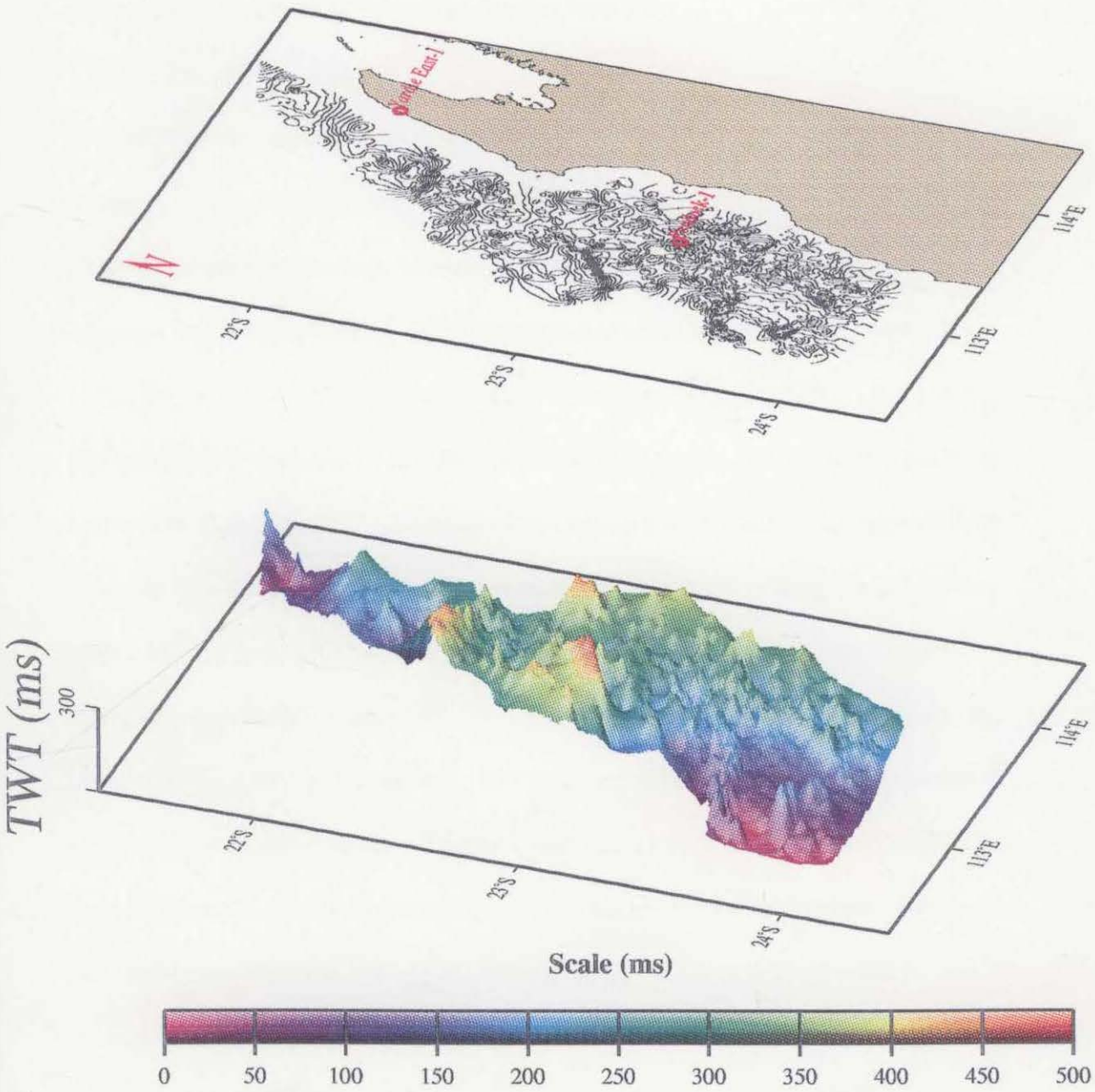

Fig. 4.19 Isopach basal - Late Cretaceous TWT (ms) contour map and perspective view.

emplacement of igneous intrusions; the sediment transport direction in this segment of the margin; and the possible cause of the Late Miocene (and/or younger) compressional event identified in the Bernier Platform.

Several tectonic episodes have contributed to the structural evolution of the Carnarvon Terrace. Of the three major episodes recognized by the present seismic interpretation, the Early/Late Jurassic rift events, the Early Cretaceous breakup and Miocene compressional event, only the breakup affected the entire study area.

Formation of the offshore Exmouth Sub-basin commenced in the Early Jurassic as movement along the RRF. Continued motion along the fault superimposed the Exmouth Sub-basin over the Palaeozoic northerly structural striking Gascoyne Sub-basin. Syn-rift sedimentation in the Exmouth Sub-basin progressed from the onset of rifting in the Early Jurassic to the completion of continental breakup in the Valanginian. During the Jurassic, the basin subsided quickly as a response to extensional stresses related to continental breakup north of the Exmouth Plateau. In the Late Jurassic - Early Cretaceous, before breakup, the entire Exmouth Sub-basin and the Bernier Platform had already undergone substantial uplift and erosion.

The timing of the uplift is subject to controversy. *Bradshaw et al.* (1988) interpreted the Bernier Platform as a block that was uplifted between the Southern Carnarvon and Perth basins during the Permian/Early Triassic to the Early Cretaceous, a theory partly confirmed by the absence of the Permian and Early Mesozoic sequence. Their palaeogeographic evolution implies that Triassic to Early Cretaceous sequences were never deposited and the Bernier Platform was originally part of the highland. The

presence of a small outcrop of Lower Jurassic rock preserved 250 km south of the study area (on Woodleigh Homestead 26°07'S 114°45'E) demonstrates that the lower Mesozoic sediments were initially deposited south of the RRF, and subsequently uplifted and eroded (*Peake and Bowes*, 1993).

The interpretation presented here supports the idea that although the Bernier Platform has been an elevated block since the Permian, major uplift and subsequent erosion took place in the Exmouth Sub-basin and the Bernier Platform before the breakup between Greater India and Australia occurred. It is proposed here that a thick sequence of Jurassic sediments was eroded in the Exmouth Sub-basin. The Jurassic section truncated by the steeply dipping basal Cretaceous unconformity provides evidence of this erosion (Figures 4.8 and 4.10). The geometry of the remaining Jurassic sediments with respect to the overlying basal Cretaceous unconformity leaves no doubt that the entire study area has been affected by uplift and subsequent erosion. Since the upper Triassic isopach map (Fig. 4.16) shows that the Jurassic sequence was completely stripped off in the southern part of the basin, the erosion must have also affected the Bernier Platform.

Two models have been hypothesized to explain the uplift: the rift flank uplift model (*Weissel and Karner*, 1989; *Karner and Driscoll*, 1993) and the mantle plume model (*White and McKenzie*, 1989). The rift flank uplift model accounts for the permanent uplift of rift flanks as a result of flexural isostatic rebound in response to mechanical unloading of the lithosphere during extension. The second model allows for igneous activity (e.g. underplating) caused by a deep-seated (~650 km) and a small thermal anomaly (100°-200°C above the normal mantle temperature) in the asthenosphere

underlying the rift. Both models rely on the buoyancy of the crust to produce uplift although it is obtained by different mechanisms. The crust becomes buoyant and uplift occurs in the underplating model as the thickness of the crust increases at the expense of the mantle, while thinning both the crust and mantle lithosphere during extension creates buoyancy for the tectonic unloading model (Figure 4.20). Where direct refraction measurements of crustal thickness are not available, gravity anomalies may provide a way to distinguish between these two mechanisms. Thus in general, free-air and Bouguer gravity anomalies tend to be large in amplitude and positive for the flexural rebound case and are expected to be low in amplitude and negative for the underplating case (e.g. *Karner and Driscoll*, 1993).

The Bernier Platform exhibits a broad positive gravity anomaly (Figures 4.21 and 4.22), with a wavelength distinctly different from narrow rift flank anomalies such as those of Broken Ridge or the Rankin Platform. Its appearance suggests a buried load rather than a narrow rift flank uplift. The absence of deep seismic data except for one line on the northern edge of the platform makes it difficult to model this gravity anomaly; however there are two observations that shed some light on its origin:

1. The Exmouth Sub-basin was uplifted at the same time as the Bernier Platform, but does not show any evidence for an uplifted rift shoulder.

2. Gravity anomalies over underplated volcanic margins are not necessarily negative. A good example is the Vøring Plateau (*Hollinger and Klemperer*, 1990).

A simple qualitative gravity model (Figure 4.22) over the Bernier Platform, assuming underplating as the cause of uplift shows the modeled gravity is in good agreement

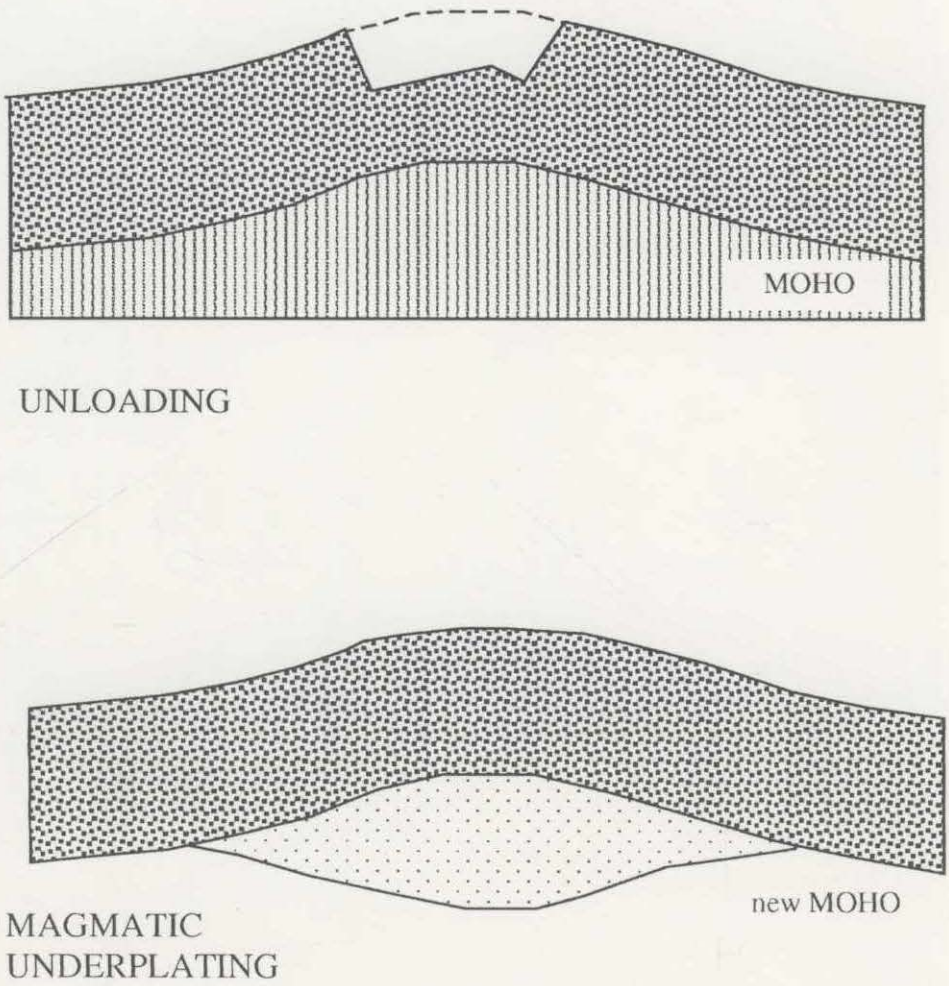

Fig. 4.20 Simple models illustrating the deflection generated by unloading (a) (e.g crustal extension and erosion) and by magmatic underplating (b) of the crust. The diference between these rift flank generation mechanisms is the relationship between the surface and Moho topographies (from Karner and Driscoll, 1993).

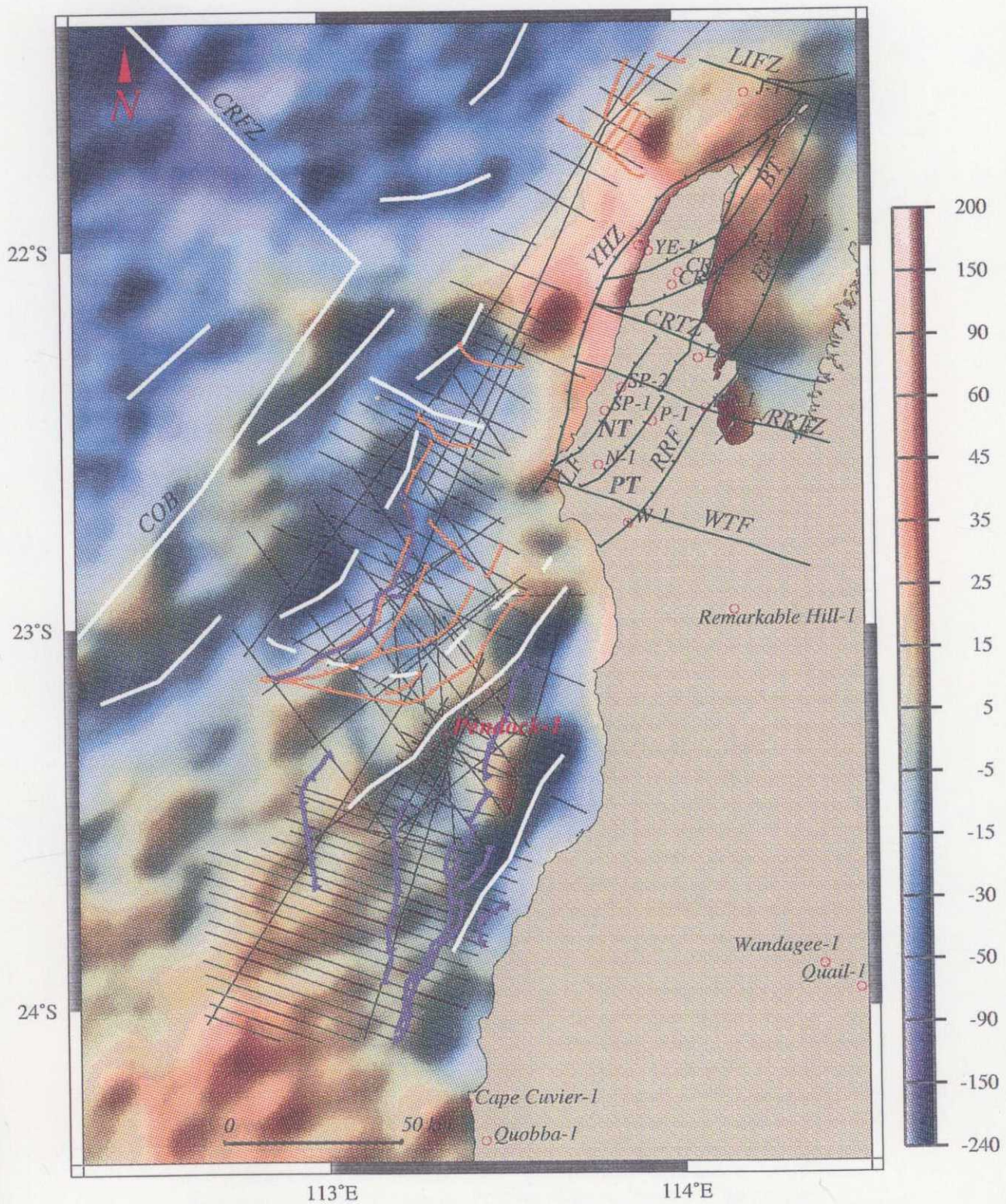

Fig. 4.21 Satellite gravity map (mgal), showing the continent-ocean boundary (COB), Cape Range Fracture Zone (CRFZ), and major tectonic elements determined using gravity (white) and seismic data (orange and blue) . Abbreviations key as in Fig. 4.14.

a.

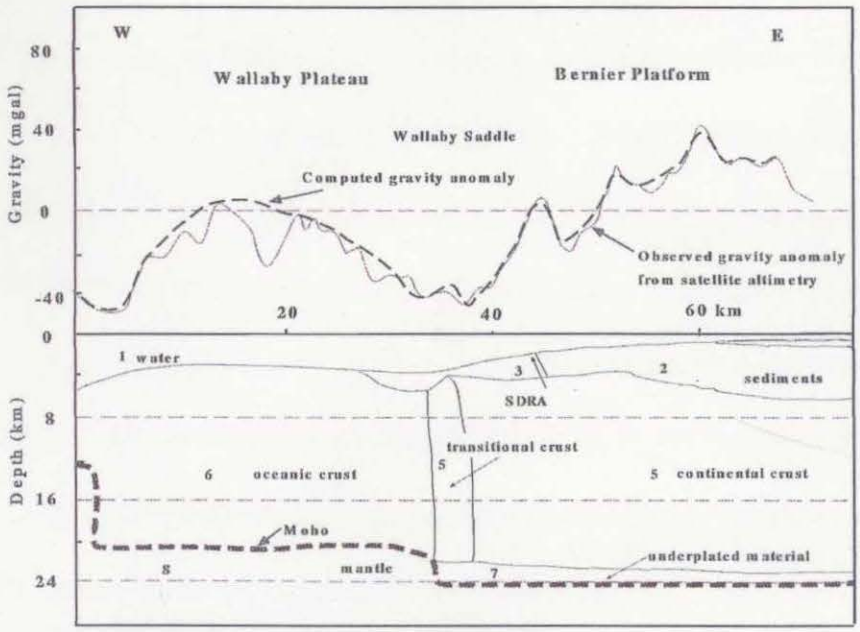

Densitiy values used for individual bodies
1 - 1.075 g/cmc; 2 - 2.45 g/cmc; 3- 2.65 g/cmc;
4 - 2.7 g/cmc; 5 - 2.75 g/cmc; 6 - 2.8 g/cmc;
7 - 3.0 g/cmc; 8 - 3.2 g/cmc.

b.

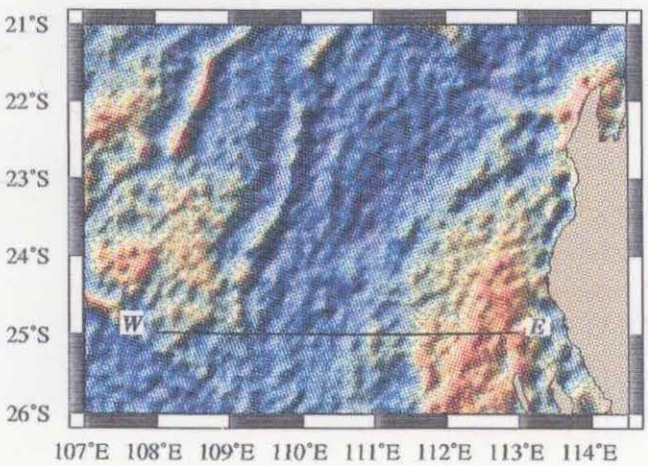

Fig. 4.22 - Tentative gravity model over the Bernier Platform and the Wallaby Plateau. Crustal columns are in Airy isostasyc equilibrium and constrained by topography, reflection seismic data and a model of lithospheric densities from a similar volcanic margin (Vöring Margin, Norway). The crustal thickness of the Wallaby Plateau was calculated using the method of Sandwell and Schubert (1989). SDRA- Seaward dipping Reflector Area.
b.- Satellite derived gravity map showing the profile location.

with the observed gravity. The densities used were taken from a model tested in the Vøring Basin; an interpreted deep seismic line in the northern Bernier Platform was used for locating the Moho (*Hopper et al.*, 1992). This model suggests that it is possible that the Bernier Platform was uplifted by underplating caused by an elevated temperature prior to continental breakup. Still, the presence of underplated material in the Bernier Platform will remain an open question until refraction studies are carried out. Underplating of the Bernier Platform by the mechanism described by the mantle plume model would explain, not only the uplift of the Bernier Platform and the Exmouth Sub-basin, but also the presence of the pre-breakup sills, dikes and igneous bodies and later, the post-breakup emplacement of large igneous plateaus (the Wallaby and Zenith plateaus). This subject is discussed in more detail in Chapter 5.

Magnetic anomalies of the Exmouth Sub-basin were studied in order to account for volcanic intrusions. Although the interpreted igneous intrusions are widespread, especially in the southern part of the basin, the sparseness of the magnetic data impede a clear evaluation. The only major anomaly directly identified is expressed by a dipole located on the northern part of the Exmouth Sub-basin above the area of chaotic seismic character, which was interpreted as an intrusive body. A 2D magnetic model (Figure 4.23) of the intrusive structure was created using a remanent inclination of -67°, a 150 Ma paleomagnetic pole of latitude 45°S, longitude 179°E (*Irvin and Irvin*, 1982), an intrusive body of 0.1 SI, an intensity of 10 A/m and 0.01 as the susceptibility for the surrounding sediments. The excellent correlation between the observed and calculated magnetic anomalies (Figure 4.23) as well as the seismic interpretation which shows no disturbance on the post-breakup sedimentary

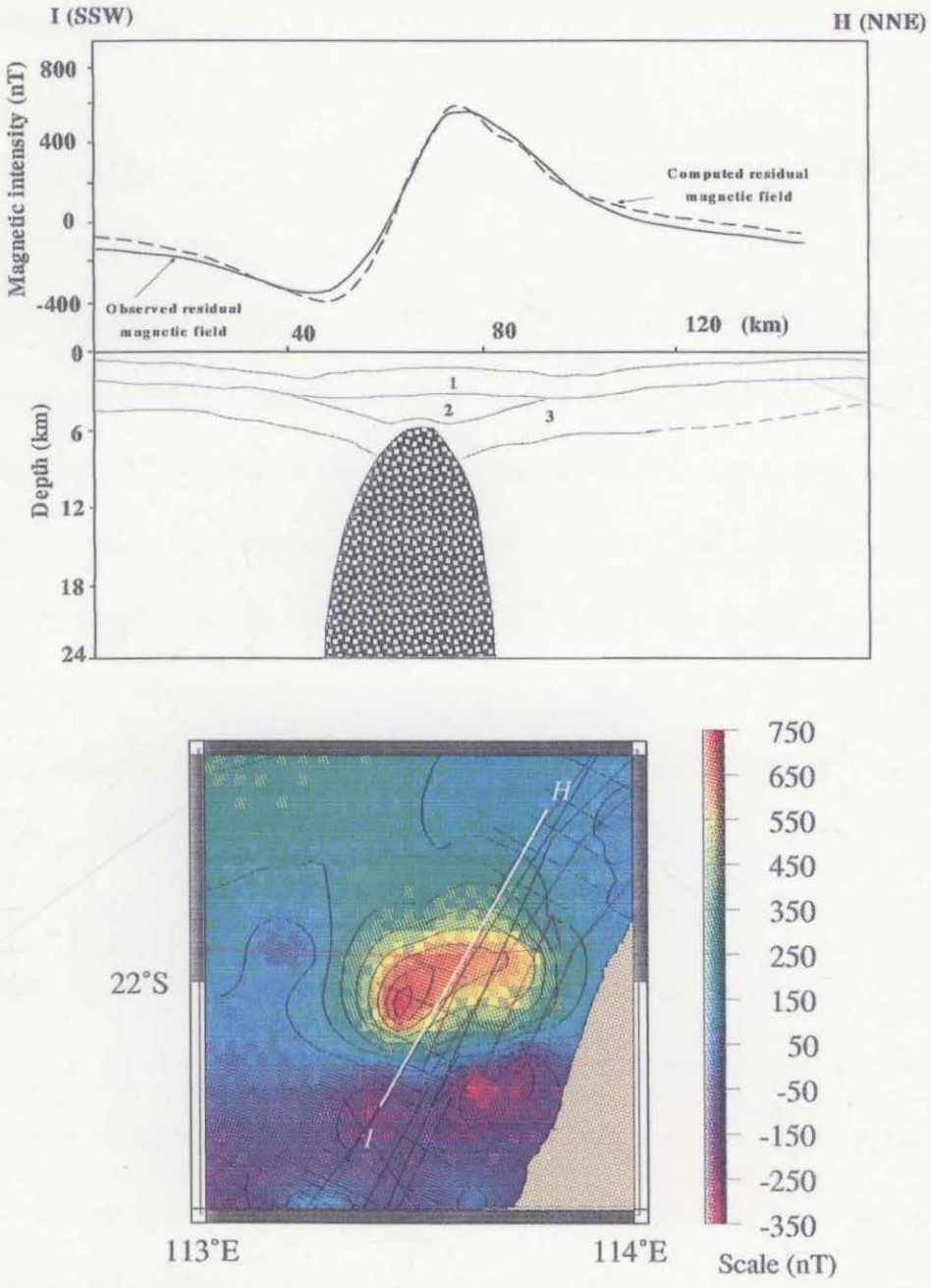

Fig. 4.23 a.- 2D magnetic model of an intrusive body. The depth at which the intrusive body was placed is constrained by reflection seismic data. Other layers represent major sedimentary sequences (1-Tertiary and Cretaceous; 2-Jurassic; 3-Triassic). Values used in the model: susceptibility for the surrounding sediments, 0.01 SI; susceptibility for the intrusive body, 0.1 SI and 10 A/m respectively; remanent inclination of -67°, remanent declination 0.5°, present inclination -55°, present declination 5°; total magnetic intensity, 55,000 nT. b.- Magnetic grid location of the profile (white line).

sequence (Figure 4.8) support the presence of an igneous body emplaced shortly before breakup time.

According to the present interpretation (Chapter 3) the breakup of this segment of the Australian margin took place at about 133-136 Ma (early Valanginian), the same time as a major unconformity is observed event on seismic lines. This interpretation combined with the fact that the uplift and erosion of the Bernier Platform and the Exmouth Sub-basin took place before the breakup, as in a mantle plume scenario, and not after, also leads to the conclusion that the Barrow Group (deposited north of the study area in the southern Exmouth Plateau, the Kangaroo Trough and the southern Barrow and Dampier basins), or at least the upper part of this formation was predominantly supplied by sediments eroded from the Bernier Platform and the Exmouth Sub-basin.

Palynological studies of Barrow Delta sediments performed by petroleum exploration companies (e.g. *Helby et al.*, 1987) indicate that the Barrow Delta developed between mid-Berriasian to mid-Valanginian. The presence of two depocenters (*Ross and Vail*, 1995), one to the west (the older lower delta) and one to the east (the younger upper delta) is caused by a shift in sediment transport direction in the Late Beriassian (137 Ma) at the time of breakup. *Ross and Vail* (1995) considered that prior to the time of this switch the Barrow Delta headwaters eroded a large domal uplift of the Indian craton and carried the sediments northward. A "Barrow River" located in the newly formed rift valley was the sediment supply for the upper delta. Considering all observations, it appears that a rift valley river is not required in order to explain the depocentre shift. Following the shift, the only source

of sediments was from the south, from the Bernier Platform, the Exmouth Sub-basin and possibly to a lesser extent, from the Pilbara Block.

An east-northeast - west southwest oriented compressional phase in the Late Miocene inverted and most likely reactivated older faults resulting in the formation of several small anticlines in the Bernier Platform (Figure 4.7). The compressional phase appears to be still active today as deformation continues within some of the newly formed anticlines. In-situ stress measurements from onshore wells show a present day direction of compression similar to that of the Late Miocene.

Various models have been published on the origin of the stress field in continental Australia and the adjacent margins (e.g. *Cloetingh and Wortel*, 1986; *Etheridge et al.*, 1991; *Hillis*, 1991; *Hillis and Williams*, 1992, 1993; *Coblentz et al.*, 1995). The Australian intraplate stress field is not uniform as in the case of the North and South American plates. The regional stress field measured for the Australian continent show variations from an east-west direction in southwestern and southeastern Australia, to a northwest –southeast orientation along the Westralian Superbasin, to a north-south direction in northern Australia. These different orientations cannot be described in terms of a single tectonic process. Furthermore, in order to understand the variations in stress direction in the western Australian continent, it is important to decipher the tectonic evolution/deformation in the Indian Ocean.

Intraplate stress models for a single Indo-Australian plate, (*Cloetingh and Wortel*, 1986; *Cloetingh et al., 1992; Coblentz et al.*, 1995), have attempted to explain the diversity in compressional stress directions. Two hypotheses have been proposed.

The diverse compression stress directions are: (1) a consequence of the geographical position of the Australian continent relative to the surrounding trench segments and the variations of the forces acting on the downgoing slab (*Cloetingh and Wortel*, 1986); or (2) a combination of torques due to topographic forces (mainly ridge push) and resistance along the collisional boundary of the Himalayas, Papua New Guinea and New Zealand. Many articles have been published analyzing dynamic aspects of the deformation, especially horizontal contraction in the equatorial Indian Ocean . The most recent model (*Gordon and Royer*, in prep.) shows the composite India-Australian plate not as two plates, as suggested by *Stein and Gordon* (1984), and *Wiens et al.* (1985), but as three plates: the Indian, the Capricorn (which includes Ninetyeast Ridge) and the Australian plates. The plates are separated by two diffuse plate boundaries: a zone of stretching along the Southeast Indian Ridge and a zone of shortening near Ninetyeast Ridge. The direction of maximum horizontal shortening is roughly consistent with the predicted northwest-southeast direction of convergence between the new Capricorn Plate and the Australian Plate. The three-plate model also accounts for north-south oriented compression at the Java-Sumatra trench. These directions match the compressional directions observed in wells in northern and western Australia and those for the Bernier Platform. The three-plate model explains not only the variations in stress direction in the western part of the Australian continent, but it also resolves some of the inconsistencies in plate reconstructions in the Indian Ocean that could not be clarified by simpler model of one or two plates.

4.5 Summary

The under-explored Carnarvon Terrace represents one of the remaining frontier areas on the northwest Australian margin. The area has Tertiary/Cretaceous and Palaeozoic sedimentary successions, as well as a substantial section of intermediately aged sediments in some parts. The age of these sedimentary sequences can only be resolved with further exploration drilling.

The structural grain of the region was probably pre-determined by structures presents within the Proterozoic basement of the Bernier Platform. However, no obvious north-south features representing older Palaeozoic or Proterozoic structures are observed in the Exmouth Sub-basin. Most of the faulting in the northern Carnarvon Terrace, as noted in previous studies (*Malcolm et al.*, 1991; *Baillie et al.*, 1994), appears to be genetically related and is probably caused by the Mesozoic Gondwanaland breakup since all faults show a broadly similar orientation and style. Uplift and erosion has frequently been encountered on the Bernier Platform since the Early Triassic (*Hocking*, 1988, *Bradshaw et al.*, 1988). This study describes another major uplift and phase of erosion affecting both the Bernier Platform and the Exmouth Sub-basin shortly before the last breakup event between Greater India and Australia. The uplift and subsequent erosion of the Bernier Platform is considered to be the result of a mantle plume located underneath the Bernier Platform prior to breakup. Such a mantle plume would have allowed for the penetration of the sills and dikes encountered in the Triassic and Jurassic sequences of the Exmouth Sub-basin. Alternative models for the cause of this syn-rift magmatism are discussed in the next chapter.

The upper section of the Barrow Delta formation deposited in the "upper delta" was mainly supplied by sediments eroded from the Exmouth Sub-basin and Bernier Platform during the Early Cretaceous syn-rift uplift. The shift in depocenters may have been a result of the loss of the Indian Plate sediment source since the onset of seafloor spreading at about 137 Ma had removed this source from the area.

The timing of formation of the major bounding faults in the Exmouth Sub-basin cannot be determined and is equivocal elsewhere. In a study of the Leatherbach oil discovery (north of the present study), *Bauer et al.* (1994) suggested a multiphase history of faulting and sediment accumulation in which major bounding faults were active during the Late Triassic and Early Jurassic times. Also, *Malcolm et al.* (1991) proposed that the Learmonth Fault formed during the Berriasian-Valanginian syn-rift event.

Late Miocene reactivation, a continent-wide event, is well developed in the Bernier Platform and elsewhere in the Carnarvon Basin. The development of small parallel anticlines south of the Rough Range Fault and Exmouth Transfer Fault is considered to be the result of northeast-southwest oriented compression between the Capricorn and Australian plates.

Chapter 5

The Cuvier Margin - a volcanic segment of the western Australian margin

5.1 Introduction

Continental breakup is frequently associated with massive, transient volcanism forming volcanic rifted margins. These volcanic margins were described based on seismic data by the presence of seaward dipping reflector sequences (SDRS) near the continent-ocean transition, core samples and dredges. The magmatism may have significant influence on the regional, and possibly global, environment, and plays an important role in generation of continental crust by magmatic underplating and emplacement of extrusives and intrusives (e.g. *Coffin and Endholm*, 1992).

The formation of volcanic margins can be caused by hotspot activity related to mantle plumes. Examples are the northeast Atlantic volcanic margins which formed near the Iceland hotspot and the south Atlantic volcanic margins, which were formed in the presence of the Tristan da Cuhna hotspot (*White and McKenzie*, 1989). However, other volcanic margins may be unrelated to mantle plumes e.g. the US East Coast margin (*Holbrook and Kelemen*, 1993).

Vast areas of the western Australian margin were affected by magmatic activity before and after breakup (*Symonds et al.*, 1996) (Figure 1.3). The volcanics are expressed as seaward dipping reflectors on the Cuvier margin and as intrusives in the Exmouth Sub-basin. Further, the large Wallaby and Zenith plateaus are possible volcanic constructions accompanying the western Australian margin and formed during seafloor spreading on young oceanic crust. Mantle plume (*White and McKenzie*, 1989; *Mihut and Müller*, submitted to JGR) and non-mantle plume

(*Hopper et al.*, 1992, *Holbrock and Kelemen*, 1993; *Colwell et al.*, 1994; *Planke and Symonds*, 1995) scenarios were proposed to explain this volcanism.

Many aspects of the tectonic evolution of the Cuvier margin have not been studied due to a lack of high quality data. However in the past few years new and old reprocessed seismic data have become available which were used along with bathymetry, magnetic and satellite derived gravity data (*Sandwell and Smith*, 1995) to investigate the structure of the Cuvier Margin. In Chapter 4 the seismic interpretation shows that uplift of the Bernier Platform and the Exmouth Sub-basin predates breakup. It is also shown that the appearance of the gravity anomaly over the Bernier Platform suggests a buried load rather than a narrow rift flank uplift as in the case of the Broken Ridge and the Rankin Platform (Figure 4.22a).

In this chapter, a mantle plume hypothesis is tested for this volcanic margin by combining the results from all preceding chapters. The presence of a hotspot situated under the Bernier Platform before the breakup between the Australian and Indian plates would explain: (1) the uplift at the Bernier Platform and the Exmouth Sub-basin predating breakup and (2) the rift magmatism and the dimensions, crustal thicknesses and volumes of the Wallaby and Zenith plateaus. About 5 m.y. earlier, breakup (~136.2 Ma) along the southern Cuvier Margin and three rift propagation events (Figure 5.1) transferred portions of the Indian Plate onto the Australian Plate and increased the offsets of three major fracture zones.

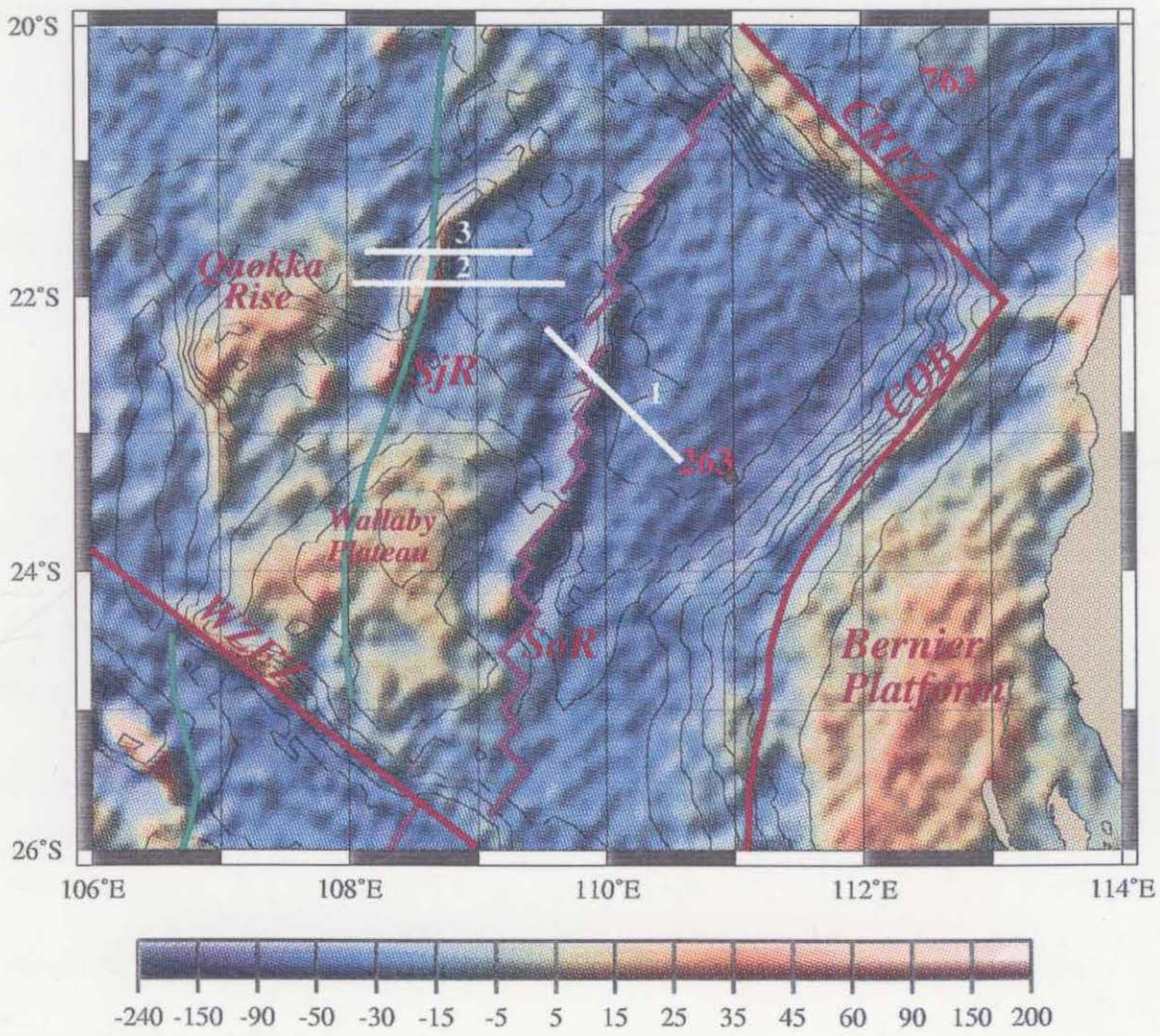

Fig. 5.1 Satellite-derived gravity map in the Cuvier Margin showing major tectonic features. Abbreviations are: SoR and SjR - Sonne and Sonja ridges, CRFZ and WZFZ- Cape Range and Wallaby-Zenith fracture zones, COB-continent ocean boundary. In magenta and green are extinct ridges and pseudofaults respectively. Black dots represent DSDP and ODP sites.

5.2 Volume and thicknesses of the volcanic plateaus

In order to evaluate the magnitude of the mantle thermal anomaly which may have caused the Wallaby and Zenith plateaus, the volume and thickness of the volcanic igneous material of the plateaus was calculated using *Schubert and Sandwell's* (*1989*) method, based on bathymetry, oceanic crustal densities and the assumption of Airy isostasy. This model is based on the premise that both plateaus are underlain by oceanic crust (Table 5.1). Gravity anomalies were also used in order to constrain the area of anomalous oceanic crust for both plateaus. Crust of uniform density is divided into three layers, which float on the higher density mantle. Layer 1 lies between sea level and the normal seafloor depth (base depth) z_b, layer 2 corresponds to the thickness of normal oceanic crust and layer 3 is the compensating root for layer 2. The total crustal volume V_T of a plateau is the sum of these three volumes (see Table 5.1): V_1 is equal to the area of the plateau times the average height of the plateau above the normal seafloor depth; V_2 is equal to the area of the plateau times the normal crustal thickness h_2; $V_3 = V_1 \frac{(\rho_c - \rho_w)}{(\rho_m - \rho_c)}$ where ρ_w (1025 kg/m^3) is the seawater density, ρ_c (2800 kg/m^3) is the crustal density and ρ_m (3200 kg/m^3) is the mantle density. The maximum crustal thickness h_M is represented by the sum of the individual layer thicknesses:

$$h_M = z_b[1 + \frac{(\rho_c - \rho_w)}{(\rho_m - \rho_c)}] + h_2.$$

In order to calculate the base depth z_b the histogram of depths method proposed by *Schubert and Sandwell* (1989) was used. The peak in the histogram (1/4° x 1/4°

areas) was chosen as the base depth. The thicknesses of the two plateaus at their centers were calculated to be 17.4 km (for the Wallaby Plateau) and 18.2 km (for the Zenith Plateau). In comparison, seismic studies of spreading centers influenced by the Iceland mantle plume show a crustal section with a mean of 10.3 ± 1.7 km, while the oceanic crustal thickness generated directly above a plume averages 20 ± 1 km (*White and McKenzie, 1992*). These results indicate that the Wallaby and Zenith plateaus would have most likely formed above a plume. However, the thicknesses of the plateaus decrease towards their margins to about 15-16 km.

Table 5.1

Crustal volumes and thicknesses of plateaus

Plateau	a. km^2x10^6	h_1 km	z_b km	h_2 km	h_3 km	age Ma	V_T km^3x10^6	h_M km
Wallaby	0.11	2.00	-5.00	6.50	8.87	130-133	1.13	17.47
Zenith	0.03	2.15	-5.50	6.50	9.48	120-118?	0.48	18.13

5.3 Admittance analysis

The Sonne and Sonja ridges were interpreted in Chapter 2 as a sequence of failed ridges and a pseudofault respectively, represented by narrow topographic ridges, accompanied by gravity highs. If these features are constructional volcanic ridges, then analysis of their admittance should provide some clues as to whether they were formed soon after the ridge propagation event, or on much older oceanic crust. Therefore gravity anomalies were computed from the topography, using Airy isostasy and A best fit equivalent thickness (EET) of the plate, for one profile across

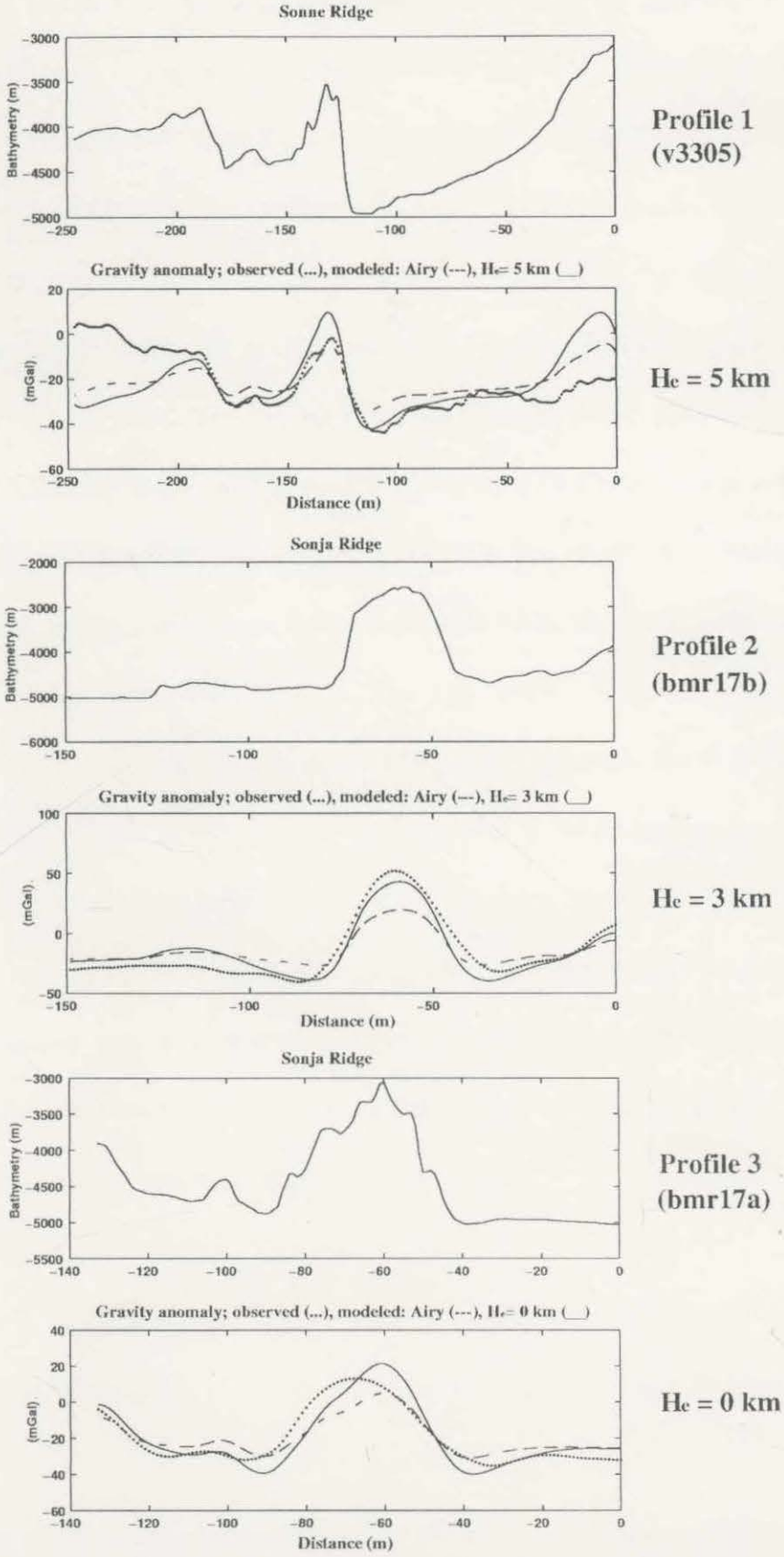

Fig. 5.2 Isostatic compensation from admittance models. Bathymetry, observed gravity anomalies and modeled gravity anomalies across the Sonne and Sonja ridges. The best fit elastic plate thickness (H_e) range from 0-5 km and indicate that both ridges were constructed on young ocean floor. Porfiles located on Fig. 5.1 (left=east).

the Sonne Ridge and two profiles across the Sonja Ridge (Figure 5.2, profile location in Figure 5.1) using the method by *Liu et al.* (1982). Fitting flexural moats with the modeled gravity anomaly is more indicative of the best fit EET than fitting the peak topography, as the shortest wavelengths in the topography are not always resolved in the gravity anomaly, due to upward continuation. Therefore the best fit EET's, ranging from 0 (Airy compensation) to 5 km, are based on the criterion of fitting the flexural moats. The low EETs indicate that the ridges were constructed on ocean floor at most as old as 10 m.y. using the relationship between age and EET of oceanic lithosphere from *Bodine et al.* (1981), and imply that constructional volcanism took place along both the extinct Sonne Ridge and the pseudofault (Sonja Ridge) soon after they were formed. The only datable tholeitic basalt from the Wallaby Plateau (*von Stackelberg et al.*, 1980) is a weathered sample dredged from its southern margin which yielded a K/Ar age of mid-Cretaceous (~90 Ma). However, since the sample was altered, the K/Ar age is likely a minimum owing to loss of argon during weathering, it is more likely to consider that the Wallaby and Zenith plateaus were formed contemporaneously with the Sonne and Sonja ridges which were constructed on young ocean floor. The constructional volcanism took place along both features soon after they were formed.

5.4 Hotspot model

Rifting in the presence of a mantle plume (*White and McKenzie*, 1989) may account for the igneous activity caused by a deep-seated (~650 km) and small thermal anomaly (100-200°C above the normal mantle temperature) in the asthenosphere

underlying the rift. Partially molten asthenosphere wells up passively owing to decompression and fills the space generated by the stretched and thinned lithosphere. Dynamic seafloor uplift of 1000-2000 m (*White and McKenzie,* 1989) at the plume center is a typical effect of a hotspot.

A published model was used for the motion of the major plates in the Atlantic and Indian oceans (*Müller et al.*, 1993) to constrain the absolute motion of the Australian Plate. Between 130 and 125 Ma the hotspot model is based on the tracks of the Tristan da Cunha hotspot (present location: 37°S, 12°W), the Great Meteor Tablemount (present location: 30°N, 28.5°W) as well as relative plate motions, used for tying the Australian Plate to the South American, North American and African plates (*Müller et al.*, 1993). In order to estimate the absolute motion of the Australian Plate from 136 to 130 Ma, Africa was assumed to be fixed relative to the mantle for this time period (i.e. before the onset of seafloor spreading in the South Atlantic). Keeping Africa fixed to the mantle is a reasonable assumption since there is no evidence for fast absolute motion of Africa from paleomagnetic or other data for this time. The result is a slow southeastward motion of the Australian plate for this time.

The Early Cretaceous uplift and erosion of the Bernier Platform and Exmouth Sub-basin (described in chapter 4) and the thicknesses and volumes of the oceanic plateaus could be accounted for by the presence of a mantle plume from the time of rifting. Using the new finite rotations that describe the motion of MGI relative to Australia a plume model was tested by placing a hotspot at 25.7°S and 111.2°E, at the margin of the Bernier Platform (underneath the ridge) at about 136 Ma, and

computed its track from that time to 96 Ma. The dimension of this plume would have been small (~400 km in diameter) as indicated by seismic and gravity data which constrain the regional uplift. In this scenario a hotspot located close to the ridge (Figures 5.3 and 5.4) at about 136 Ma would have contributed to an earlier breakup between greater India and Australia close to the Bernier Platform, creating the southern compartment of the Cuvier Abyssal Plain.

Figures 5.4 show a sequence of reconstructions in which a hypothetical hotspot is held fixed in the mantle. In the first reconstruction (Figure 5.4a, 130.9 Ma), the hotspot is located underneath the ridge. The spreading ridge is moving to the southeast, leaving the hotspot northwest of the ridge. Subsequently, two ridge propagation events toward the model hotspot would effectively "pin" the ridge at the hotspot location and transfer oceanic crust from the Indian Plate to the Australian Plate. The propagators start at the WZFZ and initially propagate toward the hotspot. The first ridge propagation event starts at ~133 Ma (approximately chron M11) and propagates north to the Cape Range Fracture Zone, where it comes to a halt at chron M4 (127.6 Ma) (Figure 5.4b). Its western edge is interpreted as a pseudofault which separates the old Indian crust of the plateau from the younger Australian crust of the Quokka Rise. In this model the Wallaby Plateau is the result of excess volcanism caused by a mantle plume between about 130 and 133 Ma as indicated by the magnetic lineations and the absolute plate motion model. More than half of the plateau would have been created on the Indian Plate and then transferred to the Australian Plate. This observation is independent of whether or not a hotspot would have been present, as it is based on magnetic lineations alone. Farther north, the edges of the captured Indian fragment are defined by the Sonne and Sonja ridges

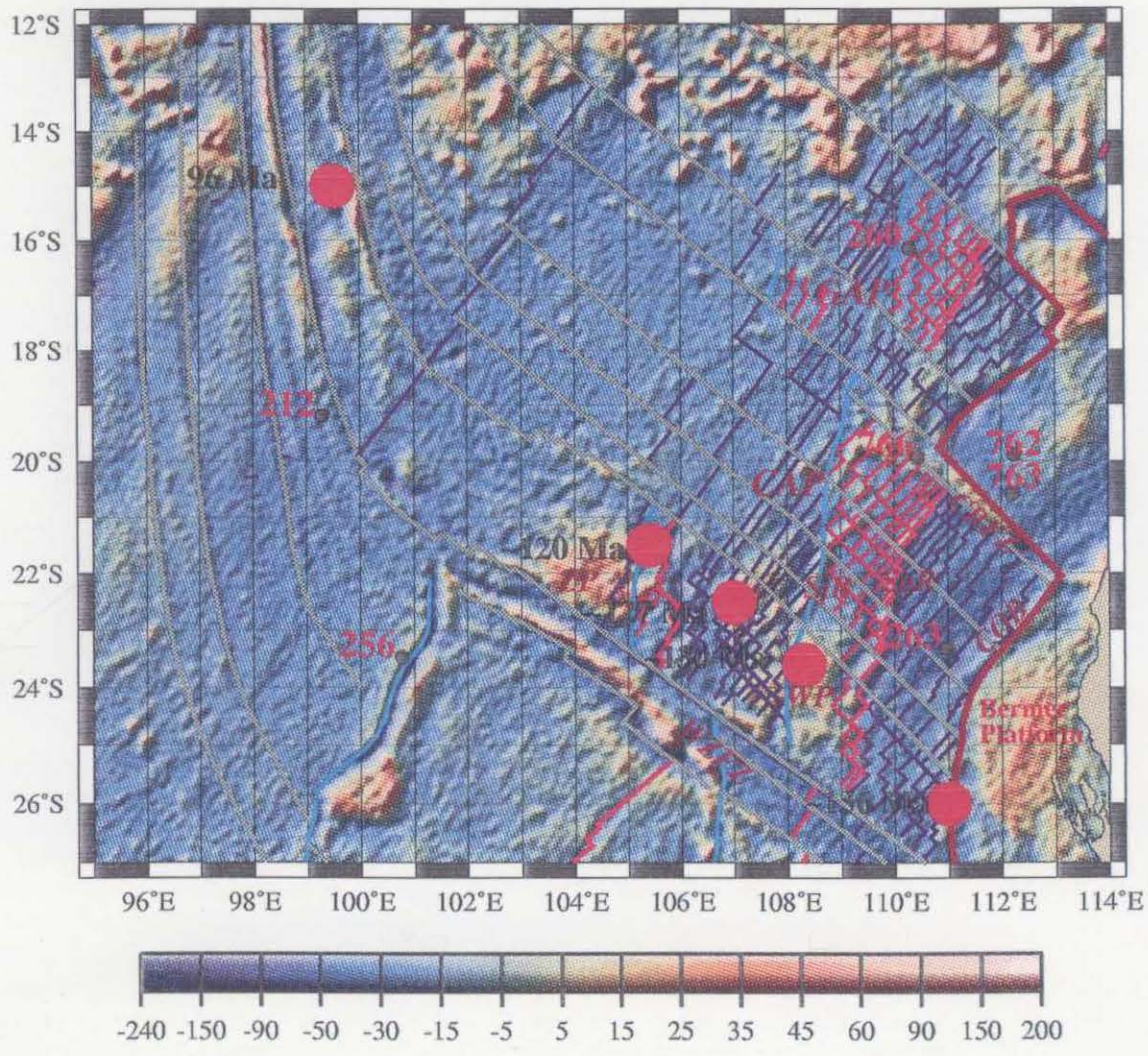

Fig. 5.3 Satellite-derived gravity map in the Cuvier Margin showing major tectonic features. Abbreviations are: SoR and SjR - Sonne and Sonja ridges, CRFZ and WZFZ- Cape Range and Wallaby-Zenith fracture zones, COB-continent ocean boundary. Red dots represent hotspot location between 136-96 Ma. Legend as in Figure 2.27.

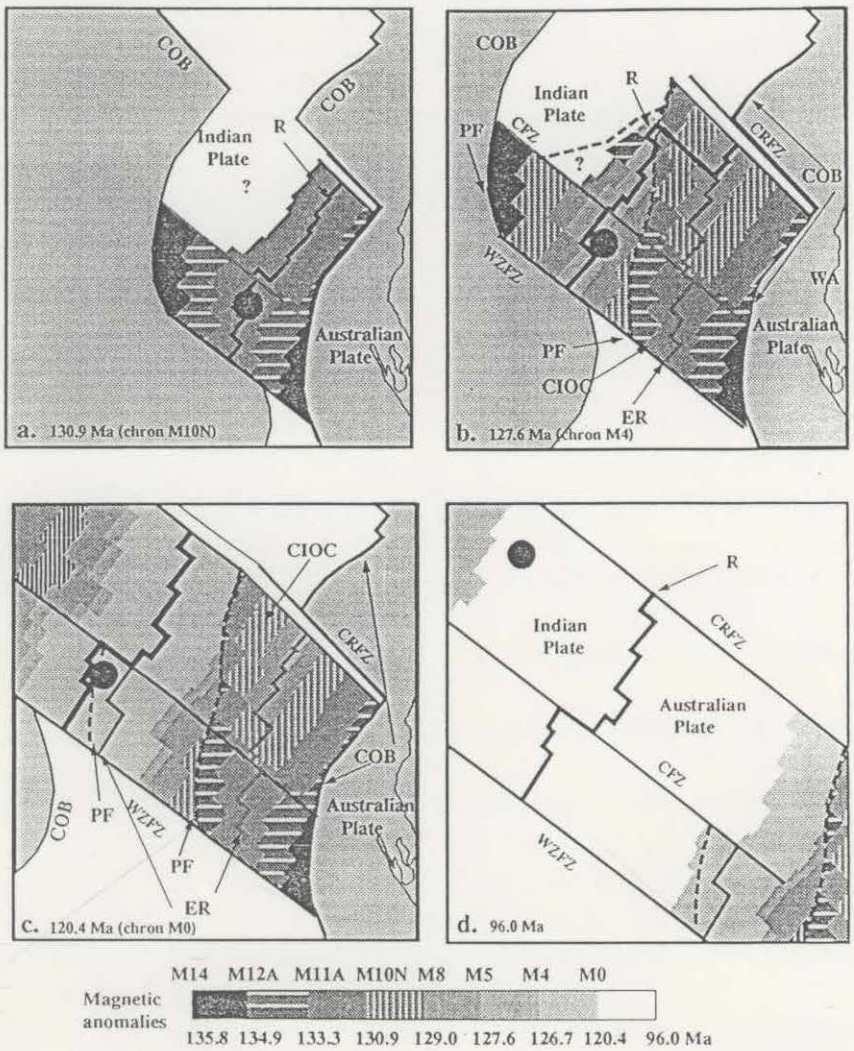

Figure 5.4. Schematic evolution of the Cuvier Margin between 136 Ma and 96 Ma. Shown are the positions of the continental margins and isochrons through time. The large solid circle serves as a fixed reference point in the mantle, illustrating the absolute motion of the plates and the active ridge. In a mantle plume scenario, the circle also represents the location of the center of a hotspot. COB, boundary between continental and oceanic crust, WZFZ, Wallaby Zenith Fracture Zone, CFZ, Cuvier Fracture Zone, CRFZ, Cape Range Fracture Zone, PF, pseudofault, ER, extinct ridge, R, spreading ridge, CIOC, captured Indian oceanic crust, WA, West Australia. (a) Seafloor spreading starts at chron M14 (135.8 Ma) in the southern Cuvier Abyssal Plain. It is unknown whether spreading commenced at the same time in the northern Cuvier Abyssal Plain. If it did, then all seafloor created between chrons M14 and M12 (134.0 Ma) would have been left on the Indian Plate, as M12 is the oldest magnetic anomaly in this area. Alternatively, lithospheric thinning may have continued until chron M12 in the northern Cuvier area. The spreading ridge moved to the southeast relative to the mantle, leaving the hotspot northwest of the ridge. Shortly after chron M11, the first rift propagation event was initiated. (b) At chron M4 (127.6 Ma) the first ridge propagation event terminated, and a segment of the Indian Plate outlined by a sequence of extinct ridges (ER) and a pseudofault (PF) was accreted to the Australian Plate. (c) At ~chron M0 (120.4 Ma) the second ridge propagation event is completed, accreting a portion of the Zenith Plateau formed on the Indian Plate to the Australian Plate. (d) After chron M0, the southeastward motion of the ridge is accelerated, leaving the mantle reference point northwest of the ridge. In a mantle plume scenario the propagators would be initiated by two successive ridge propagation events toward a hotspot, whereas in a nonmantle plume scenario they would be caused by changes in spreading direction at the large-offset Wallaby-Zenith Fracture Zone.

(extinct ridges and pseudofault, respectively). In this scenario they may have become the sites of excess volcanism due to their proximity to the plume soon after they were formed and were thus transformed into volcanic ridges. The two ridges would have been the sites of young crust at the time of their formation (confirmed by the admittance analysis), underlain by thick asthenospheric channels representing preferred sites of migration for magma fed by the plume. *Sleep* (1997) suggested that plume material preferentially ponds and migrates along regions where the lithosphere is thinned locally. The Sonne and Sonja ridges may represent examples of lateral flow of plume material along an extinct ridge and pseudofault caused by ridge propagation, as they would have provided upside-down drainage channels for buoyant plume material. A second ridge propagation event (Figure 5.4c) started shortly before chron M2 (124.1 Ma) and ended at about chron M0 (120.4 Ma). It transferred another fragment of the Indian Plate onto the Australian Plate. West of this accreted Indian fragment, the Zenith Plateau (124-128 Ma) developed mostly on the Australian Plate. A reconstruction for 96 Ma shows that this hotspot model has been left on the Indian Plate, about 700 km northwest of the spreading ridge, due to accelerated southeastward motion of the Australian plate relative to the mantle (Figure 5.4d). Once a critical distance between the hotspot and the ridge was exceeded, no further ridge propagation events would have been initiated. This would explain why there is no evidence for volcanism west of the Zenith Plateau, as the hotspot would have been located under the Indian Plate after chron M0 and produced a track on ocean crust, which is now subducted.

The two ridge propagation events resulted in an increase of the offsets of the Cuvier and Wallaby-Zenith fracture zones by 320 km and the Cape Range Fracture Zone by

180 km, due to the accreted fragments from the Indian Plate. The total offsets of the fracture zones after the propagation events were ~830 km for the Wallaby-Zenith Fracture Zone, ~480 km for the Cuvier Transform Fault, and ~300 km for the Cape Range Fracture Zone. The resulting large offset of the Wallaby-Zenith Fracture Zone explains its complicated tectonic structure visible on the gravity anomaly grid (Figure 5.3), as the fracture zone would have shown severe responses to both transtensional and transpressional changes in spreading direction.

White and McKenzie (1989) suggested that the Wallaby and Zenith plateaus are related to the Kerguelen hotspot, whereas *Colwell et al.* (1994) suggested that a hotspot became active after breakup of greater India and Australia. It is highly unlikely that the two plateaus are products of the Kerguelen hotspot, since the continental margin between the Bernier Platform and the Naturaliste Plateau is largely nonvolcanic (*Marshall et al.*, 1989). *Colwell et al.*'s (1994) model of nonplume-related rift volcanism and a hotspot postdating breakup cannot account for the localized uplift of the Bernier Platform before breakup, and also it is more likely that all observed volcanism is due to one cause only.

The main problems with the mantle plume model are as follows: (1) there is no documented evidence of substantial onshore rift-volcanism, (2) breakup magmatism is not restricted to the Cuvier Abyssal Plain, but also occurs farther north around the Exmouth Plateau bordering the Gascoyne Abyssal Plain (*Planke and Symonds*, 1995), even though it is not as voluminous as the Wallaby-Zenith plateau province, (3) there is no present-day hotspot that tracks back to the Bernier Platform at breakup time (the presently active hotspot at St. Paul island in the central Indian Ocean is a possible

candidate, but it would have been located about 500 km south of the Bernier Platform at breakup time), and (4) the Wallaby and Zenith plateaus are conspicuously aligned with the Wallaby-Zenith large-offset fracture zone, suggesting that there may be a causal relationship.

5.5 Non plume model

Non plume models require shallow thermal anomalies and/or rapid upwelling of mantle through the melting zone in the absence of a deep-seated thermal anomaly. The accumulation of thick igneous material in nonplume models may be generated by dynamic mantle upwelling during rifting if the upwelling rate of the asthenosphere exceeds the rate of lithospheric extension (*Holbrook and Kelemen,* 1993*; Holbrook et al.*, 1994). Alternatively, excess volcanism may be generated by passive mantle upwelling, if small-scale convection in the mantle is generated during the initiation of seafloor spreading caused by the difference in thermal gradient between the thick, unstretched, and cold continental lithosphere and hot asthenosphere in a continental rift (*Mutter et al.*, 1988) or by the focusing of strain along a boundary between thick and thin lithosphere (*King and Anderson,* 1995). Such thermal anomalies are dissipated rapidly by seafloor spreading.

In terms of a non mantle-plume scenario, an alternative model is that the cause of the breakup volcanics and flood basalts was small-scale convection due to the juxtaposition of thick and thin lithosphere along a transform margin, similar to the magmatism observed at the southern Exmouth Plateau transform margin (*Lorenzo et*

al., 1991). Figure 5.4 illustrates how the southern margin of the Wallaby and Zenith plateaus was gradually transformed from a continental strike-slip margin to an oceanic transform between breakup and about chron M0, when the easternmost tip of the Indian continent had passed by the Zenith Plateau. Following *King and Anderson's* (1995) model, the difference in heat flow between the Indian craton and the ocean floor to the north may have maintained small-scale convection vigorous enough to produce a large igneous province. Once the mid-ocean ridge had migrated past the edge of the Indian continental crust, excess melting would have ceased. It should be noted that the passage of the active ridge past the Indian continental crust was delayed due to the ridge propagation events described earlier, thereby maintaining a steep heat flow gradient until about chron M0 (120.4 Ma). However, the influence of ridge-continental margin interaction for causing small-scale convection was not explored by *King and Anderson* (1995). Whether or not *King and Anderson's* (1995) mechanism would provide a sufficient amount of melt to create oceanic plateaus 17-18 km thick at their centers is not known. If it does, then it would provide an attractive alternative explanation for most of present observations including why no excess magmatism is observed west of the Zenith Plateau. Also, *King and Anderson's* (1995) model does not require any lithospheric extension, thereby explaining the occurrence of a large igneous province (LIP) along a strike-slip margin, whereas both *White and McKenzie's* (1989) and *Holbrook and Kelemen's* (1993) models require lithospheric extension. As in the plume scenario, in the non plume model the magmatic Sonne and Sonja ridges would have been formed by excess melting on young oceanic crust by melt ponding in and migration along an extinct ridge and pseudofault. The Early Cretaceous uplift of the Bernier Platform/Exmouth Sub-basin would have been caused by the onset of small-scale

convection and flexural rift-flank uplift. However, since part of the uplift of the Exmouth Sub-basin was transient, the rift-flank uplift mechanism alone would not be sufficient. The observation that no sills or dikes are present above the breakup unconformity in the Exmouth Sub-basin could be the result of a rapid reduction in temperature gradients along the Cuvier passive rifted margin after breakup, halting small-scale convection.

In the non mantle plume scenario, the observed rift propagators may have been triggered by changes in the crustal stress regime at the large-offset Wallaby-Zenith Fracture Zone (WZFZ) caused by changes in spreading direction. The first rift propagation event (approximately chron M11) in the Cuvier Abyssal Plain started shortly after the onset of spreading and came to a halt at chron M4 (~126.7 Ma), close to a time at which fracture zones in the Perth, Cuvier, and Gascoyne abyssal plains indicate a change in spreading direction (M5, 127.7 Ma). The second propagation event, which started at about anomaly M3 (124.7 Ma) and ended at chron M0 (120.4 Ma), cannot be related to any mapped changes in spreading direction. However, since the offset of the WZFZ was extremely large, even small changes in spreading direction might have triggered ridge propagation events.

Problems and questions concerning the non mantle plume model include: Why is there no large igneous province in the northern Perth Abyssal Plain south of the Wallaby-Zenith Fracture Zone, where a ridge–strike-slip margin intersection existed for about 15 m.y.? If heatflow and temperature gradients were large enough to drive small-scale convection at the northern ridge-transform intersection, why weren't they at the southern one? Can any small-scale convection process produce ocean crust

about 3 times its normal thickness? If small-scale convection caused both the breakup magmatism in the Cuvier Abyssal Plain as well as rifted-margin magmatism farther north (Gascoyne Abyssal Plain margin, Exmouth Plateau, see *Planke and Symonds* (1995)), why is the Perth Abyssal Plain margin south of the Bernier Platform non-volcanic?

Chapter 6

Conclusions

The main goals of the present study were: (1) to reinterpret magnetic lineations along the northwestern and western Australian margin jointly with the new satellite-derived gravity data; (2) to investigate the Late Cretaceous plate kinematic framework of the eastern Indian Ocean; (3) to re-evaluate the tectonic evolution of the Carnarvon Terrace, and (4) to examine the cause of the associated syn-rift and post-rift magmatism along the Cuvier Margin and the adjacent abyssal plain. A revised tectonic model was developed for the evolution of the continental margin, ocean floor and oceanic plateaus in this area, which accounts for many enigmatic observations which were not synthesized before.

An analysis of the tectonic evolution of the Carnarvon Terrace revealed a major phase of uplift and erosion which affected both the Bernier Platform and the Exmouth Sub-basin, different from results of previous studies (e.g. *Hocking*, 1988; *Bradshaw et al.*, 1988). This event took place shortly before breakup between Middle Greater India and Australia. Uplift and subsequent erosion of the Bernier Platform were considered the result from a mantle plume located underneath the Bernier Platform prior to breakup. Such a mantle plume would have allowed penetration of sills and dikes encountered in the Triassic and Jurassic sequences of the Exmouth Sub-basin. The Bernier Platform exhibits a broad positive gravity anomaly with a wavelength distinctly different from narrow rift flank anomalies e.g. as described by *Karner and Driscoll* (1993). Its appearance suggests a buried load, rather than a narrow rift flank uplift, as in the case of Broken Ridge and the Rankin Platform, supporting a mantle plume model. The gravity model suggests that the Bernier Platform was uplifted by underplating caused by an elevated temperature prior to continental breakup. Underplating would explain, not only the uplift of the

Bernier Platform and the Exmouth Sub-basin, but also the presence of pre-break-up sills, dikes and igneous bodies and the post-breakup emplacement of large igneous plateaus (the Wallaby and Zenith plateaus).

A controversial issue discussed in this study was the source of sediments for the Barrow Delta following the shift in sediment transport direction, from west to east, at the time of breakup (~137 Ma). The sediments eroded from the Bernier Platform and the Exmouth Sub-basin were considered to be the only potential source of sediments for the eastern, younger depocenter of the Barrow Delta after breakup (*Ross and Vail*, 1994). A rift valley river, as postulated by this study was not required in order to explain the depocenter shift. The shift in depocenters may have been a result of the loss of the Indian Plate sediment source since the onset of seafloor spreading at about 136.2 Ma had removed this source from the area.

A consistent model for the evolution of the eastern Indian Ocean since the Late Cretaceous was developed using fracture zone trends from the satellite-derived gravity anomaly grid along with reinterpreted magnetic anomalies in the abyssal plains adjacent to the nortwestern and western Australian margin. The main results are as follows:

By combining gravity, magnetic, topography and seismic data is was possible to determine a northeast structural trend of the magnetic isochrons in the Argo Abyssal Plain. This trend is in agreement with the strike of the basement structures interpreted from seismic reflection data (*Gopala et al.*, 1992) and differs from the

east-northeast trend of *Fullerton et al.* (1989) and *Sager et al.* (1992) based mainly on magnetic data.

The present model for Australian-Indian and Indian-Antarctic plate motions is significantly different from *Veevers et al.*'s (1991) model for the M-sequence. The fracture zones from previous interpretations (e.g. *Fullerton et al.*, 1989; *Veevers et al.*, 1985b) were based only on magnetic anomalies and are less well constrained than a model based on combined magnetic and satellite altimetry data. Synthetic flowlines derived from these stage poles do not follow trends observed on the satellite-derived gravity map on either abyssal plains adjacent to the Australian margin or the Enderby Basin (adjacent to the Antarctic margin). Although the magnetic anomaly data used in this study and previous ones were similar (except for five magnetic profiles collected by AGSO on the Wallaby Plateau in 1994), the constraints on fracture zones trends from both offsets in magnetic anomalies and satellite derived gravity anomaly data result in stage and finite rotation poles for the motion of the Indian Plate relative to the Australian Plate which are substantially different from previous models.

The revised fit of Greater India, Australia, Antarctica and Madagascar prior to any continental extension in east Gondwanaland shows that the original size of Greater India might have been underestimated by about 25%. In this case the present size of India may only represent about half of its original size. In this model Greater India was composed of three tectonic units (North – NGI -, Middle –MGI - and South Greater India – SGI -) that separated successively from Gondwana by dextral strike-slip and subsequently became fixed to each other at about 136 Ma (NGI fixed to MGI) and 96 Ma (MGI fixed to SGI).

Separation of NGI and Gondwana occurred at about 156 Ma as a result of a southward propagating rift, at about 136.2 Ma seafloor spreading started in the north Gascoyne and south Cuvier abyssal plains by further rift propagation. At chron M5 (127.7 Ma) a 10° change in spreading direction occurred along the entire Australian margin and is reflected in changes in fracture zones trends in the Gascoyne, Cuvier and Perth abyssal plains. The model presented here implies that a triple junction was formed at about 120.4 Ma (chron M0) southeast of the Naturaliste Plateau as a result of the onset of seafloor spreading between SGI, Australia and Antarctica. *Veevers et al.*'s (1991) model inferred a triple junction at about the same location, while *Powell et al.*'s (1988) triple junction is situated southwestward. NGI and MGI, fixed to each other, became fixed to SGI at 96 Ma, marking also a major change in the spreading direction of the Indian Plate relative to the Australian Plate (~ 25°). The Indian Plate continued to move away from the Australian and Antarctic plates and started its journey to the north until it collided with the Eurasian Plate at about 52 Ma (*Rowley*, 1996).

Previous models (e.g. *Fullerton et al.*, 1989) accounted for two ridge jumps (one in the Gascoyne and one in the Cuvier abyssal plains). The present interpretation includes at least seven accretions of pieces of conjugate seafloor to the Australian Plate by ridge propagators. These are expressed as undulating linear features on the satellite-derived gravity grid. The cause of these ridge propagators is not yet clear, although on the Cuvier Abyssal Plain the propagators were most likely triggered by the presence of a mantle plume situated beneath the ridge that was slowly moving away from the plume.

A tentative identification of a 96 Ma isochron is based on fracture zone interpretations, age control (from DSDP sites) and bathymetry data and is consistent with the age estimated by *Powell et al.* (1988). West of the Perth Abyssal Plain the interpretation presented here implies that the 96 Ma has a more westerly location than interpreted by *Powell et al.* (1988). This isochron is interpreted to be the result of a northward propagating ridge, which resulted in the accretion of a large section of the Indian Plate to the Australian Plate. The location of the isochron is also consistent with the age control at DSDP site 256 (*Davies et al.*, 1974).

Late Miocene reactivation, a continent-wide event, was shown to be widespread both on Bernier Platform and in other parts of the Carnarvon Basin. The directions of compression observed in the Bernier Platform match the northwest-southeast direction of convergence between the Capricorn and Australian plates described by the new three-plate model of India-Australia Plate of *Gordon and Royer* (in prep).

While the essentials of the eastern Indian Ocean spreading history are now well documented, there are several localities where magnetic data coverage is insufficient. These include the eastern Wharton Basin, the southern Argo Abyssal Plain, the eastern Gascoyne Abyssal Plain and the area between the Wallaby and Zenith plateaus. A revised interpretation of all available magnetic data combined with the new satellite-derived gravity anomaly data would also be required in order to better constrain the tectonic history of the eastern Indian Ocean after chron M0.

A plume and a nonplume model were tested to account for the extensive rift-related and postrift magmatism occurring in the area of the Exmouth Sub-basin, Wallaby and

Zenith plateaus and the Quokka Rise. The hotspot model accounts for uplift of the Bernier Platform and south Exmouth Sub-basin in the Early Cretaceous, pre-breakup magmatism in the Exmouth Sub-basin, seaward dipping reflectors west of the Bernier Platform (*Planke and Symonds*, 1995), the formation of the Sonne and Sonja ridges on young oceanic crust, the formation of the Wallaby and Zenith plateaus with thicknesses (17-18 km) similar to other LIPs formed by mantle plumes (*White and McKenzie*, 1989), the triggering of ridge propagators by ridge-plume interaction and the lack of magmatism west of the Zenith Plateau. The main problems with this model are that there is no documented evidence for substantial onshore rift volcanism, that breakup magmatism also occurs farther north around the Exmouth Plateau bordering the Gascoyne Abyssal Plain (*Planke and Symonds*, 1995), and that there is no present-day hotspot that tracks back to the Bernier Platform at breakup time. Also, the Wallaby and Zenith Plateaus are conspicuously aligned with the large-offset Wallaby-Zenith Fracture Zone, suggesting that there may be a causal relationship.

An alternative nonmantle-plume scenario is based on a small-scale convection model (*King and Anderson's*, 1995) due to focusing of strain along the boundary between thick and thin lithosphere. Most observations could be explained by this model if it could be shown that a sufficient amount of melt can be generated by this mechanism in the absence of a large (100-200∞C) thermal mantle anomaly to create LIPs such as the Wallaby and Zenith plateaus. An effect not explored by *King and Anderson* (1995) is the role of a spreading ridge migrating past a continental transform margin in initiating small scale convection. If this process was responsible for creating the Wallaby and Zenith plateaus, then the question needs to be investigated under which

conditions small-scale convection of sufficient magnitude is initiated depending on the mantle temperature, its fertility and water content as well as the deep structure of the rifted plates.

It is evident that our understanding of the tectonic evolution of the eastern Indian Ocean during the Late Cretaceous has improved. The western Australian margin is a unique area with well characterized volcanic features related to both volcanic rifted margin- and oceanic plateau-type LIPs. This margin reveals a more moderate level of magmatism than previously drilled LIPs and many of the primary features and attributes may remain intact and accessible. Wide zones of rift were left uncovered by volcanics due to the moderate level of breakup volcanism, which provide unique seismic image quality of the rift structures. Understanding rift magmatism and uplift will require not only more sophisticated numerical models, but foremost better knowledge of the boundary conditions for these models based on observations. With only dredged, weathered tholeitic basalt samples available from the Wallaby Plateau (*von Stackelberg et al.*, 1980), it is clear that drilling will be necessary to better understand the petrology, structure, subsidence, uplift and thermal history of this LIP and the associated passive margin. Therefore the western Australian margin provides an ideal setting in which to study tectono-magmatic rift and breakup processes in volcanic provinces.

References

Baillie, P.W. and Jacobson, E., 1995, Structural evolution of the Carnarvon Terrace, western Australia, *APEA, J.*, 35 321-332.

Baillie, P.W., Powell, C.McA., Li, Z.X., Ryall, A.M., 1994, Tectonic framework of Western Australia's Neoproterozoic to Recent sedimentary basins, in *The Sedimentary Basins of West Australia*, edited by Purcell, P.G., and Purcell, R.R. 45-62.

Barber, P.M., 1988, The Exmouth Plateau deep water frontier: a case history, PESA, in *The NW Shelf of Australia.* NW Shelf Symposium, Perth, 173-188.

Bauer, J.A., Hooper, E.C.D. and Crowley, J., 1994, The Leatherback discovery, Carnarvon Basin, in *The sedimentary basins of Western Australia,* edited by Purcell, P.G. and Purcell, R.R., Proceed. of PESA Symp. Perth, 574-582.

Besse, J. and Courtillot, V., 1991, Revised and synthetic apparent polar wander paths of the African, Eurasian, North American and Indian Plates, and true polar wander since 200 Ma, *J. of Geophys. Res.*, 96, 4029-4050.

Bodine, J.H., Steckler, M.S. and Watts, A.B., 1981, Observations of flexure and the rheology of the oceanic lithosphere, *J. of Geophys. Res.*, 86, 3695-3707.

Borissova I., 1995, Seafloor morphology and tectonics of the Christmas Island area, Indian Ocean, *AGSO Project* 121.32 (unpublished report).

Bott, M.H.P., 1967, Solution of the linear inverse problem in magnetic interpretation with application to oceanic magnetic anomalies, *Geophys. J. R. Astr. Soc.*, 13, 313-323.

Bradshaw, M.T., Yeates, A.N., Beynon, R.M., Brakel, A.T., Langford, R.P., Totterdell, J.M., and Yeung, M., 1988, Paleogeographic evolution of the North West Shelf region. PESA, in *The NW Shelf of Australia.* NW Shelf Symp., Perth, 29-53.

Brozena, J.M. and White, R.S., 1990, Ridge jumps and propagations in the South Atlantic Ocean, *Lett. to Nature,* 348, 149-152.

Cande, S.C., Kent, D.V., 1995, Revised calibration of the geomagnetic polarity timescale for the Late Cretaceous and Cenozoic, 1995, *J. of Geophys. Res.*, 100, 6093-6095.

Chen, Z., Li, Z.X., Powell C.McA and Balme, B.E., 1993, Paleomagnetism of the Brewer Conglomerate in central Australia, and fast movement of Gondwanaland during the Late Devonian, *Geophys. J. Internat.*, 115, 564-574.

Chen, Z., Li, Z.X., Powell C.McA and Balme, B.E., 1994, An Early Carboniferous paleomagnetic pole for Gondwanaland: new results from the Mount Eclipse Sandstone in the Ngalia Basin, central Australia, *J. of Geophys. Res.*, 99, 2909-2924.

Cloetingh, S., Stein, C., Reemst, P, Gradstein, F.M., Williamson, P., Exon, N. and von Rad, U., 1992, Continental margin stratigraphy, deformation and intraplate stresses for the Indo-Australian region, in *Proceed. of the ODP, Sci. Res.*123, edited by Gradstein, F.M. et al., 671-713.

Cloetingh, S. and Wortel, R., 1986, Stress in the Indo-Australian plate, *Tectonophys.*, 132, 49-67.

Coblentz, D.D., Sandiford, M., Richardson, R.M., Zhou, Shaohua and Hillis, R., 1995, The origin of the intraplate stress field in continental Australia, *Earth and Planet. Sci. Lett.*, 133, 299-309.

Cockbain, A.E., The North West Shelf. 1989, *The APEA Journal*, 29(1), 529-545.

Coffin, M.F. and Eldholm, O., 1992, Volcanism and continental breakup: a compilation of large igneous provinces, in *Magmatism and the causes of continental breakup*, edited by Storey, B.C., Alabaster, T., and Pankhurst, R.J., 21-34, Geological Society of London Spec. Publ., 68.

Colwell, J.B., Symonds, P.A., and Crawford, A.J., 1994 The nature of the Wallaby (Cuvier) Plateau and other igneous provinces of the west Australian margin. *AGSO J, of Austr. Geol. and Geophys.*, 15/1, 137-156.

Condon, M.A., 1954, Progress report on the stratigraphy and structure of the Carnarvon Basin, western Australia, *Australia BMR, Rep.* 15.

Condon, M.A., 1965, The geology of the Carnarvon Basin, western Australia, Part-1: Pre-Permian stratigraphy, *Australia BMR, Bull.* 77.

Condon, M.A., 1967, The geology of the Carnarvon Basin, western Australia, Part-2: Permian stratigraphy, *Australia BMR, Bull.* 77.

Condon, M.A., 1968, The geology of the Carnarvon Basin, western Australia, Part-3: Post-Permian stratigraphy; structure; economic geology, *Australia BMR, Bull.* 77.

Cook, P.J., Veevers, J.J., Hiertzler, J.R. and Cameron, P.J., 1978, The sediments of the Argo Abyssal Plain and adjacent areas, northeast Indian Ocean, *BMR, J. of Austr. Geol. and Geophys.*, 3, 113-124.

Crawford, A.J. and von Rad, U., 1994, Petrology, geochemistry and implications of basalt dredges from Rowley Terrace-Scott Plateau and Exmouth Plateau margins. Northwestern Australia, *J. of Austr. Geol. and Geophys.*, 15 (1), 11-42.

Curray, J.R., Emmel, F.J., Moore, D.G. and Russel, W.R., Structure, tectonics, and geological history of the northwestern Indian Ocean, 1982, in *The Ocean Basins and Margins*, vol. 6, *The Indian Ocean,* edited by Nairn, A.E. and Stheli, F.G., 399-450, Plenum, New York.

Davies, H.L., Sun S-s, Frey, F.A., Gautier, I., McCulloch, M.T., Price, R.C., Bassias, Y., Klootwijk, C.T., and Leclaire, L., 1989, Basalt basement from the Kerguelen Plateau and the trail of a Dupal plume, *Contributions to mineralogy and Petrology*, 103, 457-469.

Davies, T.A, Luyendyk, B.P., Rodolfo, K.S., Kempe, D.R.C., MvKelvey, R.D., Leidy, R.D., Horvath, G.J., Hyndman, R.D., Thierstein, H.R., Herb, R.C., Boltovskoy, E. and Doyle, P, 1974, *Init. Repts.of DSDP* 26, US Gov. Print. Office, Washington, D.C.

Du Toit, A.L., 1937, Our wandering continents, edited by Oliver and Boyd, Edinburgh.

Duncan, R.A., 1987, Geochronology of basalts from the Ninetyeast Ridge and continental dispersion in the East Indian Ocean, *J. Volcanol. Geotherm. Res.*, 4, 283-305.

Embleton, J.J., 1984, Continental palaeomagnetism, in Phanerozoic earth history of Australia, edited by Veevers, J.J., Clarendon Press, Oxford, 11-17.

Exon, N.F., (*Assoc. Ed*) 1994, Thematic isssue: The geology of the outer North West Shelf, Australia, *AGSO J. of Austr. Geol. and Geoph., Sp. Issue*, 15 (1), 1-190.

Exon, N.F., and Buffler, R.T., 1992, Mesozoic seismic stratigraphy and tectonic evolution of the western Exmouth Plateau. In von Rad, U., Haq, B.U., et al., in *Proceeding of the ODP, Sci. Res. of Leg 122*, edited by Haq, B.U., von Rad, U et al., pp. 61-81 ODP, College Station, Texas.

Falvey, D.A., 1972, Seafloor spreading in the Wharton Basin (Northeast Indian Ocean) and the breakup of eastern Gondwanaland, *APEA J.*, 12, 86-88.

Falvey, D.A. and Mutter, J.C., 1981, Regional plate tectonics and the evolution of Australia's passive margins, *J. of Austr. Geol. and Geophys.*, 6, 1-29.

Fox, P.J. and Gallo, D.G., 1984, A tectonic model for the ridge-transform-ridge plate boundaries: implications for the structure of the oceanic lithosphere, *Tectonophys.*, 104, 205-242.

Frey, F.A., McNaughton, N.J., Nelson, D.R., deLaeter, J.R. and Duncan, R.A., 1996, Petrogenesis of the Bunbury Basalt, Western Australia: interaction between the Kerguelen plume and Gondwana lithosphere?, *Earth Planet. Sci. Lett.*, 144, 163-183.

Fullerton, L.G., Sager, W.W. and Handschumacher, D.W., 1989, Late Jurassic-Early Cretaceous evolution of the eastern Indian Ocean adjacent to northwest Australia, *J. of Geophys. Res.*, 94, 2937-2953.

Gaina, C., Müller, R.D., Royer, J.-Y., Stock, J., Hardebeck, J. and Symonds, P., The tectonic history of the Tasman Sea: A puzzle with thirteen pieces, *submitted to J. Geophys. Res.*

Geary, J.K. and Garrett, R.D., 1970, Well completion report Pendock ID No.1, Western Australia. Canadian Superior Oil (Aust.) Pty. Ltd. (GSWA accession no. S493 A2) unpublished.

Geller, C.A., Weissel, J.K. and Anderson, R.N., 1983, Heat transfer and intraplate deformation in the central Indian Ocean, *J. Geophys. Res.*, 88, 1018-1032.

Gentilli, J. and Fairbridge, R.W., 1951, The physiographical regions of Australia, *The Geographical Press. Colombia Univ. NY.*

Gibb, F.G.F., Kanaris-Sotiriou, R. and Neves, R., 1986, A new Tertiary sill complex of mid-ocean ridge basalt type NNE of the Shetland Isles: a preliminary report, *Trans. R.. Soc. Edinburgh: Earth Sci.*, 77, 223-230.

Gopala Rao, D., Krishna, K.S., Pillipenko, A.I., Subrahmanyan, V., Dracheva, V.I., and Exon, N.F., 1994, Tectonic and sedimentary history of the Argo Abyssal Plain, eastern Indian Ocean, *AGSO, J. of Austr. Geol. And Geophys.*, 15/1, 165-176.

Gordon, R.G. and Royer, J.-Y., Nonclosure of the Somalia-Australia-Antarctica plate motion circuit since Chron 5; hypothesised existence of distinct Australian and Capricorn plates separated by a diffuse plate boundary, *in prep.*

Gradstein, F.M., Agterberg, F.P., Ogg, J.G., Hardenbol, J., Veen, van P., Thierry, J. and Huang, Z., 1994, A Mesozoic time scale, *J. of Geophys. Res.*, 100, 24051-24074.

Gradstein, F.M., Ludden, J.N., Adamson, A.C., Baumgartner, P.O., Beausillon, R., Bolmer, T., Bown, P.R., Brereton, R., Buffler, R.T., Castillo, D., Compton, J., Dumoulin, J.A., Griffiths, C.M., Haig, D., Ishiwatari, A., Kaminski, M.A., Kodama, K., Kopaska-Merkel, D.C., Arcoux, J.P., McMinn, A., Moran, M.J., Mutterlose, J., Ogg, J.G., O'Neill, B., Plank, T, Riggins, M., Schott, M., Simmons, G., Thurow, J., 1992, *Proceed. of the ODP, vol.123, Sci. Res.*, Argo Abyssal Plain/Exmouth Plateau, Prep. by ODP Texas A&M Univ.

Harland, W.B., Cox, A.V., Llewellyn, P.G., Pickton, C.A.G., Smith, A.G. and Walters, R., 1982, A geologic timescale, *Cambridge Earth Sci. Series*, Cambridge Univ. Press.

Heirtzler, J.R., Cameron, P., Cook, P.J., Powell, T. McA., Roeser, H.A., Sukardi, S. and Veevers, J.J., 1978, The Argo Abyssal Plain, *Earth Planet. Sci. Lett.*, 41, 21-31.

Helby, R., Morgan, R. and Partridge, A.D., 1987, A palynological zonation of the Australian Mesozoic, in *Studies in Australian Mesozoic palynology,* edited by Jell, P.A., *Assoc. of Australasian Paleontologists, Memoir* 4, 1-85.

Hey, R.N. and Wilson, D.S., 1982, Propagating rift explanation for the tectonic evolution of the northeast Pacific – the pseudomovie, *Earth Planet. Sci. Lett.*, 58, 167-188.

Hillis, R.R., 1991, Australia-Banda Arc collision and in situ stress in the Vulcan Sub-basin (Timor Sea) as revealed by borehole breakout data, *Explor. Geophys.*, 22, 189-194.

Hillis, R.R. and Williams, A.F., 1992, Borehole breakouts and stress analysis in the Timor Sea, *Geol. Soc. London Spec. Pub.* 66, 157-168.

Hillis, R.R. and Williams, A.F., 1993, the stress field of the North West Shelf and wellbore stability, *APEA J.*, 33, 373-385.

Hocking, R. M., 1988, Regional geology of the Northern Carnarvon, in *The NW Shelf*, Proceed. of PESA Symp., Perth, edited by Purcell, P.G., and Purcell, R.R., 97-114.

Hocking, R.M, 1990, Carnarvon Basin, *GSWA Memoir* 3, *457-495.*

Hocking, R.M., Moors, H.T. and Graaf, W.J.E., 1987, Geology of the Carnarvon Basin, Western Australia, *Geol. Survey of WA, Bull.* 133.

Hocking, R.M., Mory, A.J., Williams, I.R., 1994, An Atlas of Neoproterozoic and Phanerozoic basins of Western Australia, in *The sedimentary Basins of West Australia*, edited by Purcell, P.G., and Purcell, R.R., 21-43.

Holbrook, W.S. and Kelemen, P.B., 1993, Large igneous province on the US Atlantic margin and implications for magmatism during continental breakup. *Nature*, 364, 433-436.

Holbrook, W.S., Reiter, E.C., Purdy, G.M., Sawyer, D., Stoffa, P.L., Austin, J.A., Oh, J. and Makris, J., 1994, Deep structure of the US Atlantic continental margin, offshore South Carolina, from coincident ocean bottom and multichannel seismic data. *J. of Geophys. Res.*, 99, 9155-9178.

Hollinger, K. and Klemperer, S.L., 1990, Gravity and deep seismic reflection profiles across the North Sea rifts, in *Tectonic evolution of the North Sea rifts*, edited by Blundell, D.J., and Gibbs, A.D., Oxford *Science Publ., International Lithosph. Progr.*, 181, 82-100.

Hopper, J.R., Mutter, J.C., Larson, R.L., Mutter, C.Z. and Northwest Australia Study Group, 1992, Magmatism and rift margin evolution: evidence from Northwest Australia, *Geology*, 20, 853-857.

Horstman, E.L. and Purcell, P.G., 1988, The offshore Canning Basin – a review, in *The NW Shelf, Proceed. of PESA Symp., Perth*, edited by Purcell, P.G., and Purcell, R.R., 253-277.

Irving, E., and Irving, G.A, 1982, Apparent polar wander paths Carboniferous through Cenozoic and the assembly of Gondwana. *Geophys. Surveys*, 5, 141-188.

Jenyon, M.K., 1987, Characteristics of some igneous extrusive and hypabyssal features in seismic data, *Geology*, 15, 237-240.

Johnson, B.D., Powell, C.McA., Veevers, J.J., 1976, Spreading history of the eastern Indian Ocean and Greater India's northward flight from Antarctica and Australia, *Geol. Soc. of Am. Bull.*, 87, 1560-1566.

Johnson, B.D., Powell, C.McA. and Veevers, J.J., 1980, Early spreading history of the Indian Ocean between India and Australia, *Earth Planet. Sci. Lett.*, 47, 131-143.

Johnstone, M.H., 1979, A case history of Rough Range, *APEA J.*, 19 (1), 1-6.

Karner, G.D. and Driscoll, N.W., 1993, Rift flank topography and extensional basin architecture: formation of Broken Ridge, southeast Indian Ocean, *An. Acad. Bras. Ci.*, 65 (Supl. 2), 263-294.

Kent, R.W., 1991, Lithospheric uplift in eastern Gondwana: evidence for a long-lived mantle plume system?, *Geology*, 19, 19-23.

King, S.D. and Anderson, D.L., 1995, An alternative mechanism of flood basalt formation, *Earth Planet. Sci. Lett.*, 136, 269-279.

Kjellgren, G.M., Hollams, R.R.F., Marks, T.H., and White, H.W., 1982, Yardie East No. 1 Well Completion report, Mesa Australia Ltd. Perth W.A. (GSWA accesion number S1968 A1) unpublished.

Kleinrock, M.C. and Hey, R.N., 1989, Migrating transform zone and lithospheric transfer at the Galapagos 95.5°W propagator, *J. of Geophys. Res.*, 94, 13859-13878.

Krishna, K.S., Gopala Rao, D., Ramana, M.V., Subrahmanyam, V. and Sarma, K.V.L.N.S., 1995, Tectonic model for the evolution of the oceanic crust in the northeastern Indian Ocean from the Late Cretaceous to the early Tertiary, *J. of Geophys. Res.*, 100, 21011-20024.

Larson R.L., 1975, Late Jurassic seafloor spreading in the Eastern Indian Ocean, *Geology*, 69-71.

Larson, R.L., 1977, Early Cretaceous breakup of Gondwanaland off western Australia, *Geology*, 5, 57-60.

Larson, R.L., Mutter, J.C., Diebold, J.B., Carpenter, G.B., and Symonds, P., 1979, Cuvier Basin: A product of ocean crust formation by early Cretaceous rifting off western Australia, *Earth Planet. Sci. Lett.*, 45, 105-114.

Laughton, A.S., Matthews, D.H. and Fisher, R.L., 1970, The structure of the Indian Ocean, edited by Maxwell, A.E., in *The Sea*, 4, 543-586.

Lawver, L.A., Royer, J.-Y., Sandwell, D.T. and Scotese, C.R., 1991, Evolution of the Antarctic continental margins, in *Geological evolution of Antarctica*, edited by Thomson, M.R.S., Crame, J.A. and Thomson, J., Cambridge University Press, New York, 533-539.

Lawver, L.A., Gahagan, L.M. and Coffin, M.F., 1992, The development of paleoseaways around Antarctica, in, The Antarctic Paleoenvironment: a perspective on global change, *Antarctic Res. Series*, 56, 7-30.

Lee, T.-Y. and Lawver, L.A., 1995, Cenozoic plate reconstruction of Southeast Asia, *Tectonophys.*, 251, 85-138.

Le Pichon, X., Francheteau, J. and Bonnin, J., 1972, Plate tectonics, Elsevier Amsterdam.

Liu, C.S., Curray, J.R. and McDonald, J.M., 1983, New constraints on the tectonic evolution of the Eastern Indian Ocean, *Earth Planet. Sci. Lett.*, 65, 331-342.

Lorenzo, J.M., Mutter, J.C. and Larson, R.L., and the Northwest Australia Study Group, 1991, Development of the continent-ocean transform boundary of the southern Exmouth Plateau, *Geology*, 19, 843-846.

Luyendyk, B.P., Forsyth, D. and Phillips, J.D., 1972, Experimental approach to the paleocirculation of the oceanic surface waters, *Geol. Soc. Am. Bull.*, 83, 2649-2664.

Luyendyk B.P. and Davies, T.A., 1974, Results of DSDP Leg 26 and the geologic history of the southern Indian Ocean, in Davies et al., *Init. Repts. of DSDP 26,* US Gov. Print. Office, Washington, DC, 909-944.

Mahoney, J.J., Jones, W.B., Frey, F.A., Salters, V.J.M., Pyle, D.G. and Davies, H.L., 1995, Geochemical characteristics of lavas from Broken Ridge, the Naturaliste Plateau and southernmost Kerguelen Plateau: Cretaceous plateau volcanism in the southeast Indian Ocean, *Chem. Geol.*, 120, 315-345.

Maitland, A.G., and Montgomery, A., 1924, The geology and mineral industry of Western Australia, *WA Geol. Survey, Bull.50.*

Malcolm I.R., Vail, P.R., 1994, Sequence stratigraphy of the Lower Neocomian Barrow Delta, Exmouth Plateau, Northwestern Australia, in *The Sedimentary Basins of Western Australia,* edited by Purcell, P.G. and Purcell, R.R., 435-447.

Malcolm, R.J., Pott, M.C. and Delfos, E., 1991, A new tectono-stratigraphic synthesis of the North West Cape area, *APEA J.*, 32, 94-102.

Markl, R.G., 1974, Evidence for the breakup of eastern Gondwanaland by the Early Cretaceous, *Nature,* 251, 196-200.

Markl, R.G., 1978, Evidence for the early Cretaceous breakup of Gondwanaland off southwestern Australia, *Marine Geol.* 26, 41-48.

Marks, K.M., 1996, Short wavelength resolution of the Scripps/NOAA marine gravity field from satellite altimetry, *EOS Trans.AGU,* 77, S79.

Marshall, G.F., Lee, C.S., Ramsay, D.C., O'Brien, G.W. and Moor A.M.G., 1989, *B.M.R. Continental Folio nr.3*, North Perth Basin.

Marshall, J. and Lee, C.S., 1988, North Perth Basin workshop, *B. of Res. Sci., Rec,* 35, Canberra (unpublished).

McKenzie, D.P. and Sclater, J.G, 1971, The evolution of the Indian Ocean since the Late Cretaceous, *Geophys. J. R. Astron. Soc.*, 25, 437-528.

Middleton, M.F., 1992, The Carnarvon Terrace: A bright future in petroleum exploration, *Oil and Gas Australia,* 19-23.

Mihut, D. and Müller, R.D., Volcanic margin formation and Mesozoic rift propagators triggered by a hotspot off west Australia, *submitted to J. Geophys. Res.*

Morgan, W.J., 1971, Convective plumes in the lower mantle, *Nature,* 230, 42-43.

Morgan, W.J., 1972, Plate motion and deep mantle convection, *AAPG Bull.* 56, 203-213.

Morgan, W.J., 1983, Hotspot tracks and the early rifting in the Atlantic, *Tectonophys.*, 94, 123-139.

Müller, R.D., Royer, J.Y. and Lawver, L.A., 1993, Revised plate motion relative to the hotspots from combined Atlantic and Indian Ocean hotspot tracks, *Geology* 21, 275-278.

Munasinghe, T., 1990, Some aspects of the tectonic evolution of the Sri Lanka continental margin, *Ph.D. Thesis,* Univ. of California, San Diego, 50-76.

Mutter, J.C., Buck, W.R. and Zehnder, C.M., 1988, Convective partial melting. 1. A model for the formation of thick basaltic sequences during the initiation of spreading, *J. of Geophys. Res.*, 93, 1031-1048.

---- National Geophysical Data Center, 1988, ETOPO-5 bathymetry-topography data. Data Announc. 88-MGG-02, Natl. Oceanic and Atmos. Admin., U.S. Dep. Commer., Boulder, Colo.

Norton, I.O. and Sclater, J.G., 1979, A model for the evolution of the Indian Ocean and the breakup of Gondwanaland, *J. of Geophys. Res.*, 84, 6803-6830.

O'Brien, G.W., Etheridge, M.A., Willcox, J.B., Morse, M., Symonds, P., Norman, C. and Needham, D.J., 1993, The structural architecture of the Timor Sea, northwestern Australia: implications for basin development and hydrocarbon exploration, *APEA, J.*, 33, 258-278.

Peake, R.J. and Bowes, F.G., 1993, Mesozoic potential of the Exmouth Sub-basin, western Australia, Calgary, G.I.S. (unpublished report).

Planke, S. and Symonds, 1995, Volcanic evolution of the Western Australian rifted continental margin, *Eur. Geophys. Soc.*, paper presented at XXth Gen. Assembly, Hamburg.

Playford, P.E., Cockbain, A.E. and Low, G.H., 1976, The geology of the Perth Basin, *WA Geol. Survey, Bull. 124.*

Pierce, J., Weissel, J., Taylor, E., Dehn, J., Driscoll, N., Farrell, J., Fourtanier, E., Frey, F., Gamson, P.D., Gee, J.S., Gibson, I.L., Janecek, T., Klootwijk, C., Lawrence, J.R., Littke, R., Newman, J.S., Nomura, R., Owen, R.M., Pospichal, J.J., Rea, D.K., Resiwati, P., Saunders, A.D., Smit, J., Smith, G.M., Tamaki, K., Weis, D., Wilkinson, C., 1991, *Proceed. of the ODP, Sci. Res.*, 121, Broken Ridge and Ninetyeast Ridge, Prep. by ODP Texas A&M Univ.

Powell, C. McA., Johnson, B.D. and Veevers, J.J., 1980, A revised fit of east and west Gondwanaland, *Tectonophys.*,63, 13-29.

Powell, C.McA., Roots, S.R. and Veevers, J.J., 1988, Pre-breakup continental extension in East Gondwanaland and the early opening of the eastern Indian Ocean, *Tectonophys.*,155, 261-283.

Powell, T.S., 1978, The sea-floor spreading history of the eastern Indian Ocean (MS thesis), Univ. of California at Santa Barbara.

Powell, T.S. and Luyendyk, B.P., 1982, The seafloor spreading history of the eastern Indian Ocean, *Mar. Geophys. Res.*, 5, 225-247.

Quaife, P. and Lee, C.S., 1994, The structural architecture and stratigraphy of the offshore northern Perth Basin, WA, in *The sedimentary basins of WA*, PESA, Perth, edited by Purcell, P.G. and Purcell, R.R., 811-823.

Ramsay, D.C., and Exon, N.F., 1994, Structure and tectonic history of the northern Exmouth Plateau and the Rowley Terrace, northwest Australia, *AGSO J. of Austral. Geol. and Geoph., Sp. Issue,*15 (1), 55-70.

Ross, M.I. and Vail, P.R., 1994, Sequence stratigraphy of the Lower Neocomian Barrow Delta, Exmouth Plateau, northwest Australia, in *The sedimentary basins of Western Australia,* edited by Purcell, P.G. and Purcell R.R., 435-447.

Royer, J.-Y., Coffin, M.F., 1992, Jurassic to Eocene plate reconstructions in the Kerguelen Plateau Region, in *Proceed. ODP, Sci. Res 120,* edited by Wise, S.W., Schlich, Jr. R., et al., 917-928, ODP, College Station, TX.

Royer, J.-Y., Patriat, P., Bergh, H., and Scotese, C.R., 1988, Evolution of the Southwest Indian Ridge from the Late Cretaceous (anomaly 34) to the Middle Eocene (anomaly 20), *Tectonophys.*, 155, 235-260.

Royer, J-Y. and Sandwell, D.T., 1989, Evolution of the eastern Indian Ocean since the Late Cretaceous: constraints from geosat altimetry, *J. of Geophys. Res.*, 94 13755-13782.

Royer, J.-Y., Sclater, J.G., Sandwell, D.T., Cande, S.C., Schlich, R., Munschy, M., Dyment, J., Fisher, R.L., Müller, R.D., Coffin, M.F., Patriat, P., Bergh, H.W., 1992, Appendix 1 – Indian Ocean plate reconstructions since the Late Jurassic, in Duncan, R.A., Rea, D.K., Kidd, R.B., von rad, U. and Weissel, J.K., *The Indian Ocean: A Synthesis of results from the ODP, Geoph. Monograph,* 70, AGU Washington, D.C.

Rowley, D.B., 1996, Age of initiation of collision between India and Asia: a review of stratigraphic data, *Earth and Planet. Sci. Lett.*, 145, 1-113.

Sager, W.W., Fullerton, L.G., Buffler, R.T., and Handschumacher, D.W., 1992, Argo Abyssal Plain magnetic lineations revisited: implications for the onset of seafloor spreading and tectonic evolution of the eastern Indian Ocean, in *Proc. ODP. Sci. Res.*, 123: College Station, TX ODP, edited by Gradstein, F.M., Ludden, J.N., et al., 659-669.

Sandwell, D.T. and Schubert, G., 1982, Lithospheric flexure at fracture zones, *J. Geophys. Res.*, 87, 4657-4667.

Sandwell, D.T. and Smith, W.H.F., 1997, Marine gravity anomaly from Geosat and ERS-1 satellite altimetry, *J. of Geophys. Res.* 102, 10039-10054.

Schouten, H., 1971, A fundamental analysis of magnetic anomalies over mid-ocean ridges, *Mar. Geophys. Res.*, 1, 111-144.

Schouten, H., and McCamy, K., 1972, Filtering marine magnetic anomalies, *J. of Geophys. Res.*, 77, 7089-7099.

Schouten, H. and Cande, S.C., 1976, Paleomagnetic poles from marine magnetic anomalies, *Geophys. J. R. Astr. Soc.*, 44, 567-575.

Schubert, G., and Sandwell, D., 1989, Crustal volumes of the continents and of oceanic and continental submarine plateaus, *Earth Planet. Sci. Lett.*, 92, 234-246.

Sclater, J.G., von der Borch, C., Veevers, J.J., Hekinian, R., Thompson, R.W., Pimm, A.C., McGowran, B., Gartner, Jr.S., and Johnson, D.A., 1972, Regional synthesis of the deep sea drilling results from Leg 22 in the eastern Indian Ocean, *Init. Rep. of the DSDP*, vol.XXII, 815-831.

Sclater, J.G. and Fisher, R.L., 1974, Evolution of the East Central Indian Ocean, with emphasis on the tectonic setting of the Ninetyeast Ridge, *Geol. Soc. Am. Bull.*, 85, 683-702.

Scotese, C.R., Gahagan, L.M. and Larson, R.L., 1988, Plate tectonic reconstructions of the Cretaceous and Cenozoic ocean basins, *Tectonophys.*, 155, 27-48.

Skogseid, J., Pedersen, T., Eldholm, O. and Larsen B.T., 1992, Tectonism and magmatism during NE Atlantic continental break-up: the Vøring Margin, in *Magmatism and the Causes of Continental Break-up*, edited by Storey, B.C., Alabaster, T., and Pankhurst, R.J., 305-320, *Geol. Soc. Sp. Publ.*, 68.

Sleep, N.H., 1997, Lateral flow and ponding of starting plume material, *J. of Geophys. Res.*, 102, 10001-10012.

Smith, A.G. and Hallam, A., 1970, The fit of the southern continents, *Nature*, 225, 139-144.

Smith, W.H.F. and Sandwell, D.T, 1994, Bathymetric prediction from dense satellite altimetry and sparse shipboard bathymetry, *J. of Geophys. Res.*, 99, 21803-21-824.

Smith, W.H.F. and Sandwell, D.T, 1997, Global sea floor topography from satellite altimetry and ship depth soundings, *Science*, 277, 1956-1962.

Stagg, M.J. and Colwell, J.B., 1994, The structural foundation of the Northern Carnarvon Basin, in *The Sedimentary basins of WA*, edited by Purcell, P.G. and Purcell R.R, 349-364.

Stein, S. and Gordon, R.G., 1984, Statistical tests of additional plate boundaries from plate motion inversions, *Earth Planet. Sci. Lett.*, 69, 401-412.

Storey, M., Kent, R.W., Saunders, A.D., Salters, V.J.M., Hergt, J., Whitechurch, H., Sevigny, H.J., Thirlwall, M.F., Leat, P., Chose, N.C., Gifford, M., 1992, Lower

Cretaceous volcanic rocks on continental margins and their relationships to the Kerguelen Plateau, *Proceed of the ODP, Sci. Res.*, 120, 33-53.

Symonds, P.A. and Cameron, P.J., 1977, The structure and stratigraphy of the Carnarvon Terrace and Wallaby Plateau, *APEA J.*, 30-41.

Symonds, P.A., Planke, S., Colwell, J.B. and Crawford, A.J., 1996, Volcanic evolution of the western Australian continental margin, *Australian Geol. Convention,* Canberra, Feb. 19-23, 1996.

Tait, A.M., 1985, A depositional model for the Dupuy Member and the Barrow Group in the Barrow Sub-basin, Western Australia, *APEA J.*, 25(1), 282-290.

Teichert, C., 1939, The Mesozoic transgression in Western Australia, *Austr. J. of Sci.*, 2, 84-86.

Tikku, A. and Cande, S.C., New plate tectonic reconstructions of Australia and Antarctica from the Late Jurassic to the Early Tertiary, Abstract, Chapman Conference, 1997.

Thomas, B.M. and Smith, D.N., 1976, Carnarvon Basin, in Economic geology of Australia and Papua New Guinea, 3, Petroleum., edited by Leslie, R.B., Evans, H.J. and Knight, C.L., *Australasian Institute of Mining and Metallurgy, Monograph 7,* 126-155.

Van Andel, Tj.H., 1971, Fracture zones, comments on Earth Sciences, *Geophysics,* 1, 159-166.

Veevers, J.J., (editor), 1984, Phanerozoic earth history of Australia, Clarendon Press, Oxford, 418 p.

Veevers, J.J., 1988, Morphotectonics of Australia's north-western margin – a review, in *The NW Shelf of Australia*, edited by Purcell, P.G. and Purcell, R.R., 19-27.

Veevers, J.J., 1989, Middle/Late Triassic (230±Ma) singularity in the stratigraphic and magmatic history of Pangean heat anomaly, *Geology,* 17, 732-734.

Veevers, J.J., Cotterill, D., 1978, Western margin of Australia: Evolution of a rifted arch system, *Geol. Soc. of Am. Bull.*, 89, 337-355.

Veevers, J.J. and Johnstone, M.H., 1974, Comparative stratigraphy and structure of the Western Australian margin and the adjacent deep ocean floor in *Init. Rep. of the DSDP 27*, edited by in Veevers, J.J., Heirtzler, J.R., et al., 571-585.

Veevers, J.J. and Li, Z.X., Review of seafloor spreading around Australia, 1991, II. Marine magnetic anomaly modeling, *Austral. J. of Earth Sci.*, 38, 391-408.

Veevers, J.J., Powell, C.M. and Roots, S.R., 1991, Review of seafloor spreading around Australia. I. Synthesis of the patterns of spreading, *Austral. J. of Earth Sci.*, 38, 373-389.

Veevers, J.J., Tayton, J.W., Johnson, B.D., and Hansen, L., 1985, Magnetic expression of the continent-ocean boundary between the western margin of Australia and the eastern Indian Ocean, *J .Geophys.*, 56, 106-120.

von der Borch, C., Sclater, J.C., Veevers, J.J., Hekinian, R., Thompson, R.W., Pimm, A., McGowran, B., Gartner, S. and Johnson, D.A., 1974, *Init. Repts. of DSDP* 22, US Gov. Print. Office, Washington, D.C.

von Rad, U., and Exon, N.F., 1983, Mesozoic-Cenozoic sediments and volcanics from Exmouth, Scott and Wallaby Plateaus off northwest Australia, *AAPG Geol. Memoir*, 34, 253-281.

von Rad, U., Exon, N.F., Boyd, R. and Haq, B.U., 1992, Mesozoic paleoenvironment of the rifted margin off NW Australia (ODP Legs 122/123). Synthesis of results from scientific drilling in the Indian Ocean. *AGU Geophys. Monograph*, 70, 157-184.

von Rad, U., Haq, B.U., O'Connell S., Bent, A., Blome, C.D., Borella, P.E., Boyd, R., Bralower, T.J., Brenner, W.W., De Carlo, E.H., Dumond, T., Exon, N., Galbrun, B., Golovchenko, X., Görür, N., Ito, M., Lorenzo, J.M., Meyers, P.A., Moxon, I., O'Brien, D.K., Oda, M., Sarti, M., Siesser, G., Snowdon, L.R., Tang, C., Wilkens, R.H., Williamson, P., Wonders, A.A.H., 1991, *Proceed. of the ODP, Sci. Res.*, 122, Exmouth Plateau, Prep. By ODP Texas A&M Univ.

von Stackelberg, U., Exon, N.F., von Rad, U., Quilty, P., Shafik, S., Beiersdorf, H., Seibertz, E., Veevers, J.J., 1980, Geology of the Exmouth and Wallaby plateaus off northwest Australia: sampling of seismic sequences, *J. of Austr. Geol. and Geophys.*, 5, 113-140.

Weissel, J.K. and Hayes, D.E., 1972, Magnetic anomalies in the southeast Indian Ocean, in *Antarctic Oceanology II, The Australian-New Zealand Sector, Antarct. Res. Ser.*, vol.19, edited by Hayes, D.E., 165-196, AGU, Washington, D.C.

Weissel, J.K. and Karner, G.D., 1989, Flexural uplift of rift flanks due to mechanical unloading of the lithosphere during extension, *J. of Geoph. Res.*, 94, 13919-13950.

White R.S. and McKenzie, D., 1989, Magmatism at rift zones: the generation of volcanic continental margins and flood basalts. *J. of Geophys. Res.*, 94, 7685-7729.

White, R.S., McKenzie, D. and O'Nions, R.K., 1992, Oceanic crustal thickness from seismic measurements and rare earth element inversion. *J. of Geophys. Res.*, 97, 19683-19715.

White, R.S., McKenzie, D., 1995, Mantle plumes and flood basalts, *J. of Geophys. Res.*, 100, 17543-17586.

Wiens, D.A., DeMets, D.C., Gordon, R.G., Stein, S., Argus, D., Engeln, J.F., Lundgren, P., Quible, D., Stein, C., Weinstein, S. and Woods, D.F. 1985, A diffuse plate boundary model for Indian Ocean tectonics, *Geophys. Res. Lett.*, 12, 429-432.

Wilcox, J.B., 1981, Petroleum prospectivity of Australian marginal plateaus, in *Energy resources of the pacific region*, edited by Halbouty, M.T., *AAPG Studies in Geol.* 12, 245-272.

Willis, I., 1988, Results of exploration, Browse Basin, NW Shelf, western Australia, in *The NW Shelf, Australia,* Proceedings of PESA Symposium, Perth, edited by Purcell, P.G. and Purcell, R.R., 259-272.

Wilson, D.S., Hey, R.N. and Nishimura, C., 1984, Propagation as a mechanism of reorientation of the Juan de Fuca Ridge, *J. of Geophys. Res.*, 89, 9215-9225.

Wiseman, J.F., 1979, Neocomian eustratic changes – biostratigraphic evidence from the Carnarvon Basin, *APEA J.*, 19 (1), 66-63.

Woodhead, J.D. and McCulloch, M.T., 1989, Ancient seafloor signals in Pitcairn Island lavas and evidence for large amplitude, small length-scale mantle heterogeneities, *Earth Planet. Sci. Lett.*, 94, 257-273.

Yeates, A.N., Bradshaw, M.T., Dickins, J.M., Brakel, A.T., Exon, N.F., Langford, R.P., Mulholland, S.M., Totterdell, J.M. and Yeung, M., 1987, The Westralian Superbasin, an Australian link with Tethys, in *Shallow Tethys 2: Int. Symp.on Shallow Tethys 2*, edited by McKenzie K.G., Wagga Wagga, Proc., 199-213.

Appendix 1

Geophysical cruise data for study area

Institution	Ship/Aircraft	Cruise/Year	Code	Data	Navigation
NORDA	Op. SEASCAN	81I01MAG/81	io010	M	inertial
	RP-3D Orion	81I02MAG/81	io012/13	M	inertial
		81I04MAG/81	io014	M	inertial
		81I05MAG/81	io015	M	inertial
			io016/17	M	inertial
			io050-io059	M	inertial
	U.S.N.S.	BA71FMAG/71	bb12c	M	satellite
	Bartlett	BA71GMAG/71	bb112d	M	satellite
		BA71KMAG/71	bb12e/f	M	satellite
		WI343811/78	wi811	MG	satellite
		WI343815/71	wi815/821	MG	satellite
			wi901	MG	satellite
Australian	H.M.A.S.	Moresby/68	cn006	M	celestial
Navy	Moresby	Moresby/70	cn007	M	celestial
Woods Hole	R/V Atlantis II	A2015104/65		MB	satellite
Oceanographic		A2093L14/76	a9311-a9314	MGB	satellite
Institution	R/V Chain	CH100L07/71		MGB	satellite
Scripps	R/V Argo	MONS02AR/60	msn02/03	M	celestial
Institution		MONS03AR/60	msn4a/4b	M	celestial
		LUSI6CAR/62	lus6c	MB	celestial
		LUSI6DAR/62-63	lus6d	MB	celestial
		DOD005AR/64	dodo5/9	MB	celestial
	R/V Horizon	LUSI03HO/62	lus7d/6e	MB	celestial
	R/V Melville	INMD06MV/78	inm05/06	MB	celestial
	R/V Eltanin	ELT/72	ee54a/55a	MB	satellite
		ELT/68	ee135	MB	satellite
		ELT/70	ee144.145	MB	satellite
		ELT/71	ee147-50	MB	satellite
		ELT/72	ee53/54	MB	satellite
		/74-75	erd04-06	MB	satellite
		/77-78	ind10-14MB	satellite	
		/80-81	ram05/06/12	MB	satellite
		/68	cir04/05	M	celestial
Lamont-Doherty	R/V Vema	V1606/60	v1607	MGB	celestial
Geological		V1811/62	v1811/12	MGB	celestial
		V1909/63	v1909	MGB	celestial
		V2009/64	v2009	MGB	celestial
		V3302/75	v3302	MGB	celestial
		V3516/80	v3516	MGB	celestial
Observatory		V2410/67	v2410	MGB	celestial
		V2819/67	v2819	MGB	celestial

		V2819/67	v2819	MGB	celestial
		V3308/67	v33003-08	MGB	celestial
		V3405/67	v3405	MGB	celestial
	R/V Conrad	C0909/67	c0909	MB	celestial
		C1105/7/67	c1105-07	MBG	celestial
		C1402/4/71	c1402-04	MBG	celestial
		C0802/3/64	c0802/3	MB	celestial
		C0907/8/65	c0907/8	MB	celestial
Oceanographic Res. Institute of Japan	R/V Umitaka Maru	UM66-D66	um66c/d	MB	celestial
		UM69/69	um690	MB	celestial
Australian Marine Science BMR	H.M.A.S Cook	COOK/1984	cook8_2	M	celestial
			cook9_0/1	M	celestial
		BMR17/1962	bmr17	MBG	celestial
		BMR18/1963	bmr18	MBG	celestial
		BMR19/1972	bmr19	MGB	celestial
		BMR36/1980	bmr36	MGB	celestial
AGSO	R/V Seismic	AGSO/1994	agso135	MGB	celestial

Appendix 2

Combined time scale of Cande and Kent (1995) and Gradstein et al., (1994)

Normal Polarity Interval (Ma)		Normal Polarity Interval (Ma)		Normal Polarity Interval (Ma)		Normal Polarity Interval (Ma)	
0	0.78	20.996	21.32	62.499	63.634	148.116	149.491
0.99	1.07	21.768	21.859	63.976	64.745	149.535	149.579
1.77	1.95	22.151	22.248	65.578	67.61	149.623	149.693
2.581	3.04	22.459	22.493	67.735	68.737	150.428	150.542
3.11	3.22	22.588	22.75	71.071	71.338	150.7	151.098
3.33	3.58	22.804	23.069	71.587	73.004	151.399	151.432
4.18	4.29	23.353	23.535	73.291	73.374	152.19	152.465
4.48	4.62	23.677	23.8	73.619	79.075	152.863	152.895
4.8	4.89	23.999	24.118	83.5	100.187	153.11	153.25
4.98	5.23	24.73	24.781	102.761	105.335	153.541	153.928
5.894	6.137	24.835	25.183	107.91	115.333	154.1	154.305
6.269	6.567	25.496	25.648	115.483	120.398	154.489	154.612
6.935	7.091	25.823	25.951	121	123.673	154.67	154.752
7.135	7.17	25.992	26.554	124.051	124.721	154.811	154.922
7.341	7.375	27.027	27.972	126.723	127.699	155.3	155.085
7.432	7.562	28.283	28.512	128.176	128.313	155.144	155.202
7.65	8.072	28.578	28.745	128.425	128.58	155.26	155.319
8.225	8.257	29.401	29.662	128.966	129.276	155.36	155.506
8.699	9.025	29.765	30.098	129.58	129.774	155.681	155.827
9.23	9.308	30.479	30.939	130.221	130.556	155.991	156.137
9.58	9.642	33.058	33.545	130.874	131.201	156.283	156.423
9.74	9.88	34.655	34.94	131.252	131.57	156.47	156.633
9.92	10.949	35.343	35.526	131.588	131.88	156.657	156.762
11.052	11.099	35.685	36.341	132.069	132.679	156.838	157.165
11.476	11.531	36.618	37.473	133.025	133.06	157.363	157.393
11.935	12.078	37.604	37.848	133.355	133.627	157.444	157.55
12.184	12.401	37.92	38.113	133.641	133.911	157.656	157.918
12.775	12.819	38.426	39.552	133.988	134.216	158.041	158.076
12.991	13.139	39.631	40.13	134.777	134.846	158.117	158.281
13.302	13.51	41.257	41.521	134.999	135.248	158.415	158.608
13.703	14.076	42.536	43.789	135.338	135.525	158.713	158.765
14.178	14.612	46.264	47.906	135.843	136.044	158.836	158.871
14.8	14.888	49.037	49.714	136.675	137.222	158.958	159.174
15.034	15.155	50.778	50.946	137.877	139.631	159.25	159.373
16.014	16.293	51.047	51.743	140.335	140.79	159.48	159.525
16.327	16.488	52.364	52.663	142.44	143.021	159.577	159.753
16.556	16.726	52.757	52.801	143.476	143.616	159.788	159.893
17.277	17.615	52.903	53.347	143.73	144.691	160.027	160.226
18.281	18.781	55.904	56.391	145.094	145.366	160.296	160.331
19.048	20.131	57.554	57.911	145.418	145.996	160.47	160.454
20.518	20.725	60.92	61.276	146.75	147.704	160.518	160.664

Appendix 3

Rotation file used in the reconstruction

(ID1- moving plate; ID2-fixed plate; Ma-age; Lat-latitude; Lon-longitude; Ang-rotation angle)

Plate ID - 201- South America; 501-India (Southern Greater India); 502-Sri Lanka; 503-Arabia; 504-Turkey; 505-Iran; 506-Afganistan (Fara); 507-Afganistan (Sistan); 508-Sinai; 511-Central Indian Ocean; 550-Middle Greater India; 601-North China Platform; 602-South China Platform; 607-Boutma; 612-North South China Sea; 615-Papua New Guinea; 616-North Tibet; 673-North Sumatra; 701-Africa; 702-Madagascar; 704-Seychelles-Saya de Maya; 705- Saya de Maya; 709-Somalia; 712-Lake Victoria Block; 713-North Mozambique; 801-Australia; 802-Antarctica; 804-Marie Bird Land; 814-Bellinghaus; 831-North Kerguelen Plateau; 833-North Lord Howe Rise; 850-Middle Lord Howe Rise; 871-872-propagator central Gascoyne AP; 873-propag.ator south Gascoyne AP; 874-875-propagator north Cuvier AP; 876-propagaror south Cuvier AP; 877-propagator west Cuvier AP; 880-propagator west Perth AP; 895-North Greater India; 901-Pacific.

```
ID1  Ma    Lat   Lon    Ang  ID2  Comments
201   0.0  90.0    0.0   0.0  701 !SAM-AFR South America-Africa
201   2.7  62.20 -39.40  0.83 701 !SAM-AFR AN 2a NUVEL-1
201   9.7  63.31 -37.58  3.18 701 !SAM-AFR AN 5 Mueller et al., 1993
201  19.0  59.08 -35.82  7.07 701 !SAM-AFR AN 6 Mueller et al., 1993
201  25.8  56.73 -34.79 10.02 701 !SAM-AFR AN 8 Mueller et al., 1993
201  33.1  55.37 -33.70 13.43 701 !SAM-AFR AN 13 Mueller et al., 1993
201  38.4  56.92 -32.67 15.85 701 !SAM-AFR AN 18 Mueller et al., 1993
201  42.5  56.79 -31.65 17.52 701 !SAM-NWA AN 20 Mueller et al., 1993
201  46.2  56.81 -31.71 19.13 701 !SAM-AFR AN 21 Mueller et al., 1993
201  49.0  57.85 -31.67 20.08 701 !SAM-NWA AN 22 Mueller et al., 1993
201  52.4  58.27 -31.26 21.41 701 !SAM-AFR AN 24 Mueller et al., 1993
201  55.9  61.08 -32.31 22.25 701 !SAM-AFR AN 25 Mueller et al., 1993
201  65.6  63.25 -33.18 24.75 701 !SAM-AFR AN 30 Mueller et al., 1993
201  71.1  63.42 -33.26 26.57 701 !SAM-AFR AN 32 Mueller et al., 1993
201  73.6  63.43 -33.76 28.10 701 !SAM-AFR AN 33 Mueller et al., 1993
201  79.1  62.73 -33.71 30.99 701 !SAM-AFR AN 33r Mueller et al., 1993
201  83.5  61.64 -33.74 33.52 701 !SAM-AFR AN 34 Mueller et al., 1993
201 120.4  51.6  -35.0  52.92 701 !SAM-AFR Nuernberg & Mueller 1991
201 126.7  50.4  -33.5  54.42 701 !SAM-AFR Nuernberg & Mueller 1991
201 131.7  50.0  -32.5  55.08 701 !SAM-AFR Nuernberg & Mueller 1991
201 600.0  50.0  -32.5  55.08 701 !SAM-AFR Nuernberg & Mueller 1991
501   0.0   0.0    0.0   0.0  702 !IND-CIB Indian Central Basin AN 5 JYR 7/4/89
501   0.0   0.0    0.0   0.0  511 !IND-CIB AN 5 JYR 7/4/89
501   9.9  -8.7   76.9   2.75 511 !IND-CIB AN 5 JYR 7/4/89
501  20.2  -5.2   74.3   5.93 511 !IND-CIB Royer & Chang 1991
501  83.5   2.9 -171.9   1.46 511 !IND-CIB switchover -DM -5/6/97
501  83.5  -0.4  176.9  42.16 801 !C34 JYR 89 89 DM model
501  96.0   2.5 -178.2  49.89 801 ! 3 june swithcover
501  96.0  20.43  23.74 -57.62 702 ! new IND-MAD DM
501 120.4  17.2   33.9  -65.34 702 !IND-MAD
501 130.0  17.2   33.9  -65.34 702 !IND-MAD  switchover
501 130.0  -4.4   16.7  -92.77 802 !IND-ANT Lawver & Scotese 1987
501 245.0  -4.4   16.7  -92.77 802 !IND-ANT Lawver & Scotese 1987
502   0.0   0.0    0.0   0.0  501 !SLK-IND Sri Lanka-India
502 130.4   0.0    0.0   0.0  501 !SLK-ANT Lawver & Scotese 1987
502 130.4  12.2 -151.2 103.96 802 !SLK-ANT Lawver & Scotese 1987
502 600.0  12.2 -151.2 103.96 802 !SLK-ANT
503   0.0   0.0    0.0   0.0  701 !ARB-NEA Arabia-Nubia (Africa)
503   9.9  26.1   23.1  -3.86 701 !ARB-AFR JYR 1988
```

503 20.2 26.0 30.5 -8.04 701 !ARB-AFR AN 6 ARAB(=IND)/AFR JYR 1988
503 20.6 30.9 17.5 -6.32 701 !ARB-AFR FIT JYR 1988
503 121.6 30.9 17.5 -6.32 701 !ARB-NEA FIT JYR 1988
503 600.0 30.9 17.5 -6.32 701 !ARB-NEA FIT JYR 1988
504 0.0 0.0 0.0 0.0 301 !TRK-EUR Turkey-Europe
504 47.9 -14.37 -148.6 24.29 301 !TRK-EUR CRS 05/22/87 OPEN BLACK SEA
504 130.6 -14.37 -148.6 24.29 301 !TRK-EUR CRS 05/22/87 OPEN BLACK SEA
504 195.0 24.42 39.6 -21.31 301 !TRK-EUR CRS 05/22/87 CIMMERIAN COLLISION
504 195.0 45.4 -18.2 52.52 503 !TRK-ARB cross-over
504 255.0 2.02 36.90 -24.60 503 !TRK-ARB
504 600.0 2.02 36.90 -24.60 503 !TRK-ARB BP MODEL, CRS 1984
505 0.0 0.0 0.0 0.0 504 !IRN-TRK Iran-Turkey
505 28.5 19.12 38.95 16.8 504 !IRN-TRK LG 08/89 fix IRN-AFF overlap
505 140.9 22.19 46.67 14.28 504 !IRN-TRK CRS 05/22/87 ADJUSTMENT
505 195.0 33.70 44.25 20.23 504 !IRN-TRK CRS 05/22/87 CIMMERIAN COLLISION
505 216.0 32.00 43.1 37.83 504 !IRN-TRK CRS 05/22/87
505 232.0 40.48 46.21 27.04 504 !IRN-TRK CRS 01/18/87
505 255.0 17.72 44.24 11.19 504 !IRN-TRK CRS 01/18/87
505 600.0 17.72 44.24 11.19 504 !IRAN FIXED TO TURKEY
506 0.0 0.0 0.0 0.0 501 !AFF-IND Afghanistan(Fara)-India
506 600.0 0.0 0.0 0.0 501 !AFF-IND
507 0.0 0.0 0.0 0.0 701 !AFS-AFR Afghanistan(Sistan)-Africa
507 600.0 0.0 0.0 0.0 701 !AFS-AFR
508 0.0 0.0 0.0 0.0 701 !SIN-AFR Sinai-Africa
508 10.9 0.0 0.0 0.0 701 !SIN-AFR AN 5 CRS 11/04/86
508 24.1 36.79 31.31 -2.62 701 !SIN-AFR CRS 11/04/86
508 31.0 36.79 31.31 -3.62 701 !SIN-AFR FIT CRS 11/04/86
508 600.0 36.79 31.31 -3.62 701 !SIN-AFR FIT CRS 05/08/86
550 0.0 52.88 118.41 -10.43 501 !IND-CIB India-Central Indian Basin
550 96.0 52.88 118.41 -10.43 501 !96 DM&DM-97 switchover
550 96.0 3.91 8.73 -47.33 801 !96 DM&DM-97 for high spreading rate
550 120.4 6.52 -170.61 55.04 801 !M0 DM&DM-97
550 124.0 7.83 -170.40 56.34 801 !M2 DM&DM-97
550 124.7 8.24 -170.34 56.77 801 !M3 DM&DM-97
550 126.7 9.07 -170.21 57.65 801 !M4 DM&DM-97
550 127.7 9.47 -170.14 58.09 801 !M5 DM&DM-97
550 128.2 9.60 -170.15 58.29 801 !M6 DM&DM-97
550 128.4 9.75 -170.16 58.53 801 !M7 DM&DM-97
550 129.0 9.95 -170.16 58.86 801 !M8 DM&DM-97
550 129.5 10.20 -170.18 59.27 801 !M9 DM&DM-97
550 130.2 10.45 -170.19 59.69 801 !M10 DM&DM-97
550 130.9 10.77 -170.20 60.22 801 !M10N DM&DM-97
550 132.1 11.17 -170.22 60.92 801 !M11 DM&DM-97
550 133.4 11.67 -170.24 61.80 801 !M11A DM&DM-97
550 134.0 12.06 -170.26 62.52 801 !M12 DM&DM-97
550 135.0 12.39 -170.27 63.13 801 !M12A DM&DM-97
550 135.3 12.62 -170.28 63.57 801 !M13 DM&DM-97
550 135.9 12.96 -170.30 64.23 801 !M14 DM&DM-97
550 136.2 13.23 -170.31 64.76 801 !closure DM&DM-97
550 245.0 13.23 -170.31 64.76 801 !IND-AUS IND fixed to AUS
601 0.0 0.0 0.0 0.0 301 !NCH-EUR North China Platform-Europe
601 260.0 0.0 0.0 0.0 301 !NCH-EUR fixed Ji & Coney 1985
601 260.0 35.5 99.4 -64.92 000 !NCH-Paleomag APW crossover CRS 01/11/87
601 306.0 -41.31 -101.0 60.62 000 !NCH-Paleomag APW CRS 01/15/87 ALONG APW
601 324.0 -44.56 -100.37 87.82 000 !NCH-Paleomag APW CRS 01/15/87 ALONG APW
601 342.0 -47.27 -98.58 98.32 000 !NCH-Paleomag APW CRS 01/15/87 SORT OF ALONG

```
601 363.0 -45.19 -118.13  71.06 000 !NCH-Paleomag APW CRS 01/15/87 ALONG APW
601 404.0 -43.31 -129.78  69.28 000 !NCH-Paleomag APW CRS 01/14/87 ALONG APW
601 458.0 -45.51 -145.50  71.49 000 !NCH-Paleomag APW CRS 01/14/87 APW (M.ORD PO
601 497.0 -50.87 -162.08  88.21 000 !NCH-Paleomag APW CRS 01/14/87 ALONG APW
601 532.0 -48.74 -163.0   81.71 000 !NCH-Paleomag APW CRS 01/18/87 ALONG APW
601 555.0  35.68  25.41 -68.65 000 !NCH-Paleomag APW CRS 01/14/87 APW (N. POLE)
601 600.0  30.94  16.46 -70.70 000 !NCH-Paleomag APW CRS 01/18/87 NEAR APW APW
602   0.0   0.0    0.0   0.0 601 !SCH-NCH South China Platform-N.China Platfo
602 210.0   0.0    0.0   0.0 601 !SCH-NCH fixed Ji & Coney 1985
602 235.0  45.95  35.48 -18.31 601 !SCH-NCH TYL 07/89, Liou & Maruyama 1986
602 245.0  44.38  64.33 -39.65 601 !SCH-NCH TYL 07/89, Liou & Maruyama 1986
602 245.0  46.2   69.1   15.20 000 !SCH-global framework cross-over
602 255.0   7.94 146.07  48.28 000 !SCH-Paleomag APW CRS/MIR 01/11/87 APW
602 277.0   0.0  162.0   36.0  000 !SCH-Paleomag APW S. CHINA APW
602 306.0  -1.73 140.70  60.90 000 !SCH-Paleomag APW CRS 01/15/87 ALONG APW
602 324.0 -12.50 126.57  69.85 000 !SCH-Paleomag APW CRS 01/15/87 APW U. CARB P
602 342.0 -34.56 134.17  57.64 000 !SCH-Paleomag APW CRS 01/18/87 NEAR LATE PZ
602 350.0  31.2  -41.1  -58.61 000 !SCH-Paleomag APW interpolated tmp
602 350.0   5.7  141.7   47.11 801 !SCH-AUS cross-over tmp
602 600.0   5.7  141.7   47.11 801 !SCH-AUS cross-over tmp
607   0.0   0.0    0.0   0.0 603 !BMP-SBM Burma Plate-Sino/Burma/Malaya
607  11.0  17.51 137.86   5.01 603 !BMP-SBM Spreading, FROM CURRAY ET AL., 1979
607  14.9   1.82  26.76  -6.01 603 !BMP-SBM TYL 1991 Rifting in Mergui Basin
607  78.9   1.82  26.76  -6.01 603 !BMP-SBM TYL 1991
607 600.0   1.82  26.76  -6.01 603 !BMP-SBM TYL 1991
612   0.0   0.0    0.0   0.0 602 !NCS-NCH North South China Sea-South China
612 600.0   0.0    0.0   0.0 602 !NCS-NCH
614   0.0   0.0    0.0   0.0 647 !KLM-MLP Kalimantan-Malay Peninsula
614  23.8   0.0    0.0   0.0 647 !KLM-MLP
614  42.8   0.0    0.0   0.0 647 !KLM-MLP TYL 1991
614 600.0   0.0    0.0   0.0 647 !KLM-MLP from McCabe, pers. comm.
615   0.0   0.0    0.0   0.0 801 !PNG-AUS Papua New Guinea-Australia
615 600.0   0.0    0.0   0.0 801 !PNG-AUS
616   0.0   0.0    0.0   0.0 601 !NTB-NCH North Tibet-North China Platform
616 230.0   0.0    0.0   0.0 601 !NTB-NCH fixed from Smith 1988
616 600.0   0.0    0.0   0.0 601 !NTB-NCH
673   0.0   0.0    0.0   0.0 647 !NSM-MLP North Sumatra-Malay Peninsula
673  78.9   0.0    0.0   0.0 647 !NSM-MLP
673 600.0   0.0    0.0   0.0 647 !NSM-MLP
701   0.0  90.0    0.0   0.00 001 !AFR-AHS Africa-African Hotspots
701   9.8  60.0  -30.0   -1.80 001 !interpolated from Duncan & Richards 1991
701  19.7  51.5  -44.4   -4.25 001 !interpolated from Duncan & Richards 1991
701  28.5  43.0  -45.0   -6.60 001 !interpolated from Duncan & Richards 1991
701  37.1  38.6  -41.8   -9.00 001 !AFR-AHS RDM 6/91
701  42.8  37.1  -40.8  -10.21 001 !AFR-AHS RDM 8/90
701  47.6  33.0  -40.8  -12.02 001 !AFR-AHS RDM 8/90
701  52.2  30.7  -40.9  -13.16 001 !AFR-AHS RDM 8/90
701  57.3  29.9  -42.0  -14.18 001 !AFR-AHS RDM 8/90
701  63.5  29.3  -42.9  -15.21 001 !AFR-AHS RDM 8/90
701  69.4  25.3  -40.2  -16.68 001 !AFR-AHS RDM 8/90
701  74.3  21.3  -39.4  -18.25 001 !AFR-AHS RDM 3/91
701  78.9  17.9  -38.8  -19.90 001 !AFR-AHS RDM 3/91
701  84.6  19.2  -41.4  -21.94 001 !AFR-AHS RDM 04/92
701  89.9  19.4  -41.9  -23.31 001 !AFR-AHS RDM 04/92
701  95.2  19.6  -42.4  -24.68 001 !AFR-AHS RDM 04/92
701 100.5  18.9  -41.4  -25.35 001 !AFR-AHS RDM 04/92
```

701 111.1 17.7 -39.5 -26.71 001 !AFR-AHS RDM 3/91
701 121.6 18.9 -39.7 -27.47 001 !AFR-AHS RDM 3/91
701 130.4 16.7 -37.5 -28.52 001 !AFR-AHS RDM 3/91
701 136.0 16.7 -37.5 -28.52 001 !AFR-AHS RDM 3/91
701 180.0 47.9 -81.4 -44.69 001 !AFR-AHS RDM 12/90 Kerguelen under ANT, Bouv
701 180.0 47.9 -81.4 -44.69 000 !AFR-000 RDM cross-over
701 240.0 0.0 144.0 37.0 000 !AFR-Global APW path Ziegler et al. 1983
701 255.0 0.0 152.0 50.0 000 !AFR-Global APW path Ziegler et al. 1983
701 277.0 0.0 147.40 59.40 000 !AFR-Global APW path 01/10/86
701 306.0 0.0 142.60 66.10 000 !AFR-Global APW path
701 342.0 -16.0 106.0 50.0 000 !AFR-Global APW path
701 363.0 -14.90 125.70 56.90 000 !AFR-Global APW path
701 404.0 -2.70 108.50 78.30 000 !AFR-Global APW path BP MODEL, CRS 1984
701 425.0 -1.0 106.30 88.0 000 !AFR-Global APW path GONDWANA APW
701 497.0 -7.0 87.0 131.0 000 !AFR-Global APW path
701 532.0 -2.0 89.0 144.0 000 !AFR-Global APW path
701 600.0 43.20 110.0 111.20 000 !AFR-Global APW path
702 0.0 0.0 0.0 0.0 701 !MAD-AFR Madagascar-Africa
702 120.0 90.00 0.00 0.00 701 !MAD-AFR
702 121.0 5.4 -76.2 0.90 701 !MAD-AFR M0 JYR 11/87
702 124.7 5.4 -76.2 1.96 701 !MAD-AFR M2 JYR 11/87
702 127.7 5.4 -76.2 3.19 701 !MAD-AFR M4 JYR 11/87 7/5/89
702 130.2 5.4 -76.2 4.20 701 !MAD-AFR M9 JYR 11/87
999 133.4 0.0 -83.84 6.56 701 !MAD-AFR AN M11
702 140.3 5.4 -76.2 8.32 701 !MAD-AFR M16 JYR 11/87
999 140.3 2.21 -90.85 11.18 701 !MAD-AFR AN M16
702 148.1 4.0 -71.4 11.32 701 !MAD-AFR M21 JYR 11/87
702 155.0 -3.41 -81.70 19.73 701 !MAD-AFR FIT Lawver & Scotese 1987
702 245.0 -3.41 -81.70 19.73 701 !MAD-AFR FIT Lawver & Scotese 1987
'704 0.0 0.0 0.0 0.0 705 !SEY-MAS Seychelles-Saya de Maya/Mascarene
704 78.9 0.0 0.0 0.0 705 !SEY-MAS
704 78.9 28.9 -35.5 28.95 501 !SEY-IND cross-over, fit
704 600.0 28.9 -35.5 28.95 501 !SEY-IND
705 0.0 90.0 0.0 0.0 702 !MAS-MAD Saya de Maya/Mascarene-Madagascar
705 60.9 90.0 0.0 0.0 702 !MAS-MAD AN 27 no more seafloor spreading
705 62.5 -15.1 49.9 -10.48 702 !MAS-MAD AN 28 Patriat Unpub. Man.
705 67.7 5.9 30.0 -12.74 702 !MAS-MAD AN 31 Patriat Unpub. Man.
705 72.8 4.3 32.8 -20.01 702 !MAS-MAD AN 32 Patriat Unpub. Man.
705 83.5 -4.5 46.0 -45.16 702 !MAS-MAD AN 34 JYR 1989
705 96.3 -2.9 44.8 -50.00 702 !MAS-MAD 96Ma fit 7/6/89
705 245.0 -2.9 44.8 -50.00 702 !MAS-MAD 96Ma fit 7/6/89
709 0.0 0.0 0.0 0.0 503 !SOM-ARA Somalia Plate-Arabia
709 9.9 25.9 24.4 4.16 503 !SOM-ARA AN 5 JYR 2/7/89
709 24.1 24.58 16.99 6.19 503 !SOM-ARA FIT B CRS 11/06/86
709 31.0 22.54 27.07 9.46 503 !SOM-ARA FIT CRS/KW 01/25/87
709 600.0 22.54 27.07 9.46 503 !SOM-ARA FIT CRS/KW 01/25/87
712 0.0 0.0 0.0 0.0 701 !LVB-AFR Lake Victoria Block-Africa
712 600.0 0.0 0.0 0.0 701 !LVB-AFR
713 0.0 0.0 0.0 0.0 701 !NMZ-AFR North Mozambique-Africa
713 600.0 0.0 0.0 0.0 701 !NMZ-AFR
714 0.0 0.0 0.0 0.0 701 !NWA-AFR Northwest Africa-Africa
714 83.5 0.0 0.0 0.0 701 !NWA-AFR
714 120.4 16.5 6.7 -1.15 701 !NWA-AFR Nuernberg & Mueller 1991
714 120.4 50.8 -34.2 -53.69 201 !NWA-AFR Nuernberg & Mueller 1991
714 600.0 50.8 -34.2 -53.69 201 !NWA-AFR Nuernberg & Mueller 1991
801 0.0 90.00 0.00 0.00 802 !Australia-Antarctica

801 9.7 13.10 36.10 -6.55 802
801 20.1 15.40 32.70 -11.97 802
801 33.6 13.45 33.92 -20.52 802
801 40.1 14.32 31.75 -23.77 802
801 46.2 14.25 32.52 -24.48 802 !AUS-ANT AN 20 Ani
801 61.2 7.86 35.81 -25.54 802 !AUS-ANT AN 27 Ani
801 95.0 5.50 36.58 -28.14 802 !AUS-ANT 95 Ma Ani
801 120.0 -1.24 37.70 -30.20 802 !AUS-ANT Fit Ani
801 245.0 -1.24 37.70 -30.20 802 !AUS-ANT Fit Ani
802 0.0 0.0 0.0 0.0 701 !ANT-AFR
802 6.7 16.58 -23.15 1.18 701 !ANT-AFR LAL 10-29-91
802 9.9 8.2 -49.4 1.53 701 !ANT-AFR AN 5 Royer & Chang 1991
802 20.2 10.7 -47.9 2.78 701 !ANT-AFR AN 6 Royer & Chang 1991
802 33.2 12.0 -48.4 5.46 701 !ANT-AFR AN 13 Royer & Chang 1991
802 40.1 17.1 -46.6 7.22 701 !ANT-AFR A18 JYR 06/90 triple junction closu
802 43.8 10.8 -42.7 7.79 701 !ANT-AFR A20 JYR 06/90 triple junction closu
802 47.9 10.3 -42.9 8.77 701 !ANT-AFR A21 Royer et al. 1988
802 53.3 8.0 -40.0 9.99 701 !ANT-AFR A24 JYR 06/90 triple junction closu
802 57.9 3.1 -38.4 10.60 701 !ANT-AFR A26 JYR 06/90 triple junction closu
802 62.5 2.2 -38.6 11.32 701 !ANT-AFR A28 JYR 06/90 triple junction closu
802 64.7 1.9 -41.0 11.76 701 !ANT-AFR A29 JYR 06/90 triple junction closu
802 67.7 1.1 -41.6 11.84 701 !ANT-AFR AN 31old Royer et al. 1988
802 73.0 -1.8 -41.4 13.47 701 !ANT-AFR AN 32 Royer et al. 1988
802 79.1 -4.70 -39.70 16.04 701 !ANT-AFR AN 33 Royer et al. 1988
802 83.5 -2.6 -38.1 17.91 701 !ANT-AFR AN 34 JYR 06/90 triple junction clo
999 121.0 -4.2 -29.1 42.80 701 !ANT-AFR AN M0 JYR 1987
802 121.0 -4.2 -29.1 43.34 701 !ANT-AFR AN M0 angle fixed DM
999 124.7 -4.6 -29.1 44.17 701 !ANT-AFR M2 JYR 1987
802 124.7 -4.6 -29.1 44.45 701 !ANT-AFR M2 JYR 1987
802 127.7 -4.2 -29.6 45.23 701 !ANT-AFR M4 JYR 1987
802 130.2 -4.9 -28.5 46.65 701 !ANT-AFR M9 JYR 1987
802 140.3 -7.0 -26.9 50.39 701 !ANT-AFR M16 angle fixed DM
999 140.3 -7.0 -26.9 50.70 701 !ANT-AFR M16 JYR 1987
802 148.1 -4.7 -29.0 52.84 701 !ANT-AFR M21 JYR 1987
802 155.0 -7.78 -31.42 58.0 701 !ANT-AFR FIT Lawver & Scotese 1987
802 180.0 0.5 147.6 -65.87 701 !ANT-AFR FIT 1000km strike-slip Powell model
802 245.0 0.5 147.6 -65.87 701 !ANT-AFR FIT
804 0.0 0.0 0.0 0.0 802 !MBL-ANT Marie Byrd Land-East Antarctica
804 0.0 0.0 0.0 0.0 802 !MBL-ANT Marie Byrd Land-East Antarctica
804 100.5 0.0 0.0 0.0 802 !MBL-ANT Fixed MBL to E.ANT. with Ross Embay
804 156.6 72.6 -10.7 12.97 802 !MBL-ANT
804 156.6 -45.51 -78.96 39.13 291 !MBL-SAM LAL & ION cross-over
804 600.0 -45.51 -78.96 39.13 291 !MBL-SAM LAL ION 8/20/91
814 0.0 0.0 0.0 0.0 901 !BEL-PAC Bellinghaus-Pacific
814 0.0 0.0 0.0 0.0 901 !PAC-MBL Pacific-Marie Byrd Land
814 4.2 66.92 -77.75 -3.22 901 !PAC-MBL An 3y Stock, unpubl.
814 5.1 67.73 -78.91 -4.61 901 !PAC-MBL An 3o Stock, unpubl.
814 7.9 69.49 -75.92 -6.95 901 !PAC-MBL An 4 Stock, unpubl.
814 8.9 67.76 -79.85 -7.76 901 !PAC-MBL An 4a Stock, unpubl.
814 19.0 73.96 -69.54 -16.27 901 !PAC-MBL An 6y Stock, unpubl.
814 22.7 74.84 -65.95 -19.17 901 !PAC-MBL An 6b Stock, unpubl.
814 24.1 74.72 -67.28 -19.55 901 !PAC-MBL An 6c Stock, unpubl.
814 25.8 74.73 -67.22 -20.79 901 !PAC-MBL An 8y Stock, unpubl.
814 28.0 74.69 -66.78 -22.71 901 !PAC-MBL An 9o Stock, unpubl.
814 29.4 74.66 -65.70 -24.33 901 !PAC-MBL An 11y Stock, unpubl.
814 30.9 74.34 -66.31 -25.19 901 !PAC-MBL An 12o Stock, unpubl.

814 33.1 74.44 -64.12 -27.07 901 !PAC-MBL An 13y Stock, unpubl.
814 33.5 74.62 -61.14 -27.98 901 !PAC-MBL An 13o Stock, unpubl.
814 34.7 75.02 -57.81 -28.85 901 !PAC-MBL An 15y Stock, unpubl.
814 40.1 72.78 -64.61 -29.89 901 !BEL-PAC AN 18 CLM 9.27.87 SAME AS 901-804
814 47.9 72.09 -63.44 -33.93 901 !BEL-PAC AN21 CLM 10/04/87
814 56.4 71.81 -60.67 -39.39 901 !BEL-PAC AN 25 Mayes et al. 1990
814 63.6 70.77 -58.37 -45.52 901 !BEL-PAC AN 28 Mayes et al. 1990
814 68.7 70.31 -56.34 -50.92 901 !BEL-PAC AN 31 Mayes et al. 1990
814 73.3 69.92 -54.75 -56.33 901 !BEL-PAC AN 32 CLM 10.7.87
814 600.0 69.92 -54.75 -56.33 901 !BEL-PAC AN 32 CLM 10.7.87
831 0.0 90.0 0.0 0.0 802 !NKG-ANT Northern Kerguelen-East Antarctica
831 40.4 90.0 0.0 0.0 802 !NKG-ANT AN 24 N.KER/ANT
831 40.4 17.1 30.6 23.68 801 !NKG-AUS JYR 3/24/88
831 152.7 17.1 30.6 23.68 801 !NKG-AUS JYR 3/24/88
831 245.0 17.1 30.6 23.68 801 !NKG-AUS JYR 3/24/88
833 0.0 0.0 0.0 0.00 850 !N-LHR/AUS North Lord Howe Rise
833 64.0 0.0 0.0 0.00 850 !N-LHR/AUS Stop motion
833 84.0 8.10 -35.62 -2.72 850 !
833 84.0 3.51 -43.60 12.27 801 !
833 90.0 3.51 -43.60 12.27 801 !
833 600.0 3.51 -43.60 12.27 801 !
850 0.0 0.0 0.0 0.00 801 ! m_lhr
850 52.2 0.0 0.0 0.0 801 !LHR-AUS
850 53.3 -12.02 130.02 -0.66 801 !LHR-AUS AN24 CG 08/07/1996
850 55.8 -16.63 134.79 -2.23 801 !LHR-AUS AN25 CG 08/07/1996
850 57.9 -15.83 135.67 -3.58 801 !LHR-AUS AN26 CG 08/07/1996
850 61.2 -0.40 128.91 -4.02 801 !LHR-AUS AN27 CG 08/07/1996
850 62.5 -3.49 131.75 -5.01 801 !LHR-AUS AN28 CG 08/07/1996
850 64.0 0.57 129.37 -5.38 801 !LHR-AUS AN29y CG 08/07/1996
850 65.6 -4.62 131.84 -6.81 801 !LHR-AUS AN30 CG 08/07/1996
850 67.7 -9.24 134.31 -8.84 801 !LHR-AUS AN31 CG unchanged
850 71.1 -14.88 139.03 -13.09 801 !LHR-AUS AN32 CG 26/06/1996 unchanged
850 73.6 -7.43 136.32 -12.14 801 !LHR-AUS AN33 CG unchanged
850 84.0 4.50 -42.26 14.96 801 !
850 86.0 4.06 -42.35 15.51 801 !
850 90.0 3.27 -42.59 16.61 801 !C-LHR/AUS
850 600.0 3.27 -42.59 16.61 801 !C-LHR/AUS
871 128.2 9.60 -170.15 58.29 801 ! swichover M5
871 128.4 9.75 -170.16 58.53 801 ! er gas1 M6
871 129.0 9.95 -170.16 58.86 801 ! er gas1 M8
871 129.5 10.20 -170.18 59.27 801 ! er gas1 M9
871 130.2 10.45 -170.19 59.69 801 ! er gas1 M10
871 130.9 10.77 -170.20 60.22 801 ! er gas1 M10N
871 132.1 11.17 -170.22 60.92 801 ! er gas1 M11
871 200.0 11.17 -170.22 60.92 801 ! er gas1 M11
872 0.0 9.75 -170.16 58.53 801 ! er gas2
872 128.4 9.75 -170.16 58.53 801 ! M7 swichover
872 129.0 9.95 -170.16 58.86 801 ! er gas2 M8
872 129.5 10.20 -170.18 59.27 801 ! er gas2 M9
872 130.2 10.45 -170.19 59.69 801 ! er gas2 M10
872 130.9 10.77 -170.20 60.22 801 ! er gas2 M10N
872 132.1 11.17 -170.22 60.92 801 ! er gas2 M11
872 600.0 11.17 -170.22 60.92 801 ! er gas2 -
874 0.0 9.50 -170.10 57.91 801 !
874 127.3 9.50 -170.10 57.91 801 ! swich_over before M4
874 127.7 9.47 -170.14 58.09 801 ! er cuv1 M5

874 128.2 9.60 -170.15 58.29 801 ! er cuv1 M6
874 128.4 9.75 -170.16 58.53 801 ! er cuv1 M7
874 129.0 9.95 -170.16 58.86 801 ! er cuv1 M8
874 129.5 10.20 -170.18 59.27 801 ! er cuv1 M9
874 130.2 10.45 -170.19 59.69 801 ! er cuv1 M10
874 130.9 10.77 -170.20 60.22 801 ! er cuv1 M10N
874 132.1 11.17 -170.22 60.92 801 ! er cuv1 M11
874 600.0 11.17 -170.22 60.92 801 ! er cuv1 -
875 0.0 9.75 -170.16 58.53 801 ! er cuv2
875 128.4 9.75 -170.16 58.53 801 ! swichover M7
875 129.0 9.95 -170.16 58.86 801 ! er cuv2 M8
875 129.5 10.20 -170.18 59.27 801 ! er cuv2 M9
875 130.2 10.45 -170.19 59.69 801 ! er cuv2 M10
875 130.9 10.77 -170.20 60.22 801 ! er cuv2 M10N
875 132.1 11.17 -170.22 60.92 801 ! er cuv2 M11
875 600.0 11.17 -170.22 60.92 801 ! er cuv2 -
876 0.0 10.77 -170.20 60.22 801 ! er cuv3
876 130.9 10.77 -170.20 60.22 801 ! swichover M10N
876 132.1 11.17 -170.22 60.92 801 ! er cuv3 M11
876 133.4 11.67 -170.24 61.80 801 ! er cuv3 M11A
876 600.0 11.67 -170.24 61.80 801 ! er cuv3 -
877 0.0 7.80 -170.40 55.89 801 ! er cuv4
877 123.0 7.80 -170.40 55.89 801 ! swichover M2_M1
877 124.0 7.83 -170.40 56.34 801 ! er cuv4 M2
877 124.7 8.24 -170.34 56.77 801 ! er cuv4 M3
877 600.0 8.24 -170.34 56.77 801 ! er cuv4 -
880 0.0 6.50 -170.60 53.94 801 ! er perth1
999 118.0 6.50 -170.60 53.94 801 ! swit-chover
880 120.4 6.52 -170.61 55.04 801 ! er perth1 M0
880 600.0 6.52 -170.61 55.04 801 ! er perth1 -
873 0.0 8.01 -170.41 56.59 801 ! er gas3
873 123.0 7.80 -170.40 55.89 801 !
873 124.0 7.83 -170.40 56.34 801 !er gas3 M2
873 124.7 8.24 -170.34 56.77 801 !er gas3 M3
873 600.0 8.24 -170.34 56.77 801 !er gas3 -
895 0.0 52.88 118.41 -10.43 501 !IND-CIB India-Central Indian Basin
895 96.0 52.88 118.41 -10.43 501 !96 DM&DM-97 switchover
999 96.0 59.8 113.3 -8.28 501 !96 DM&DM-97 switchover keep 999
999 96.0 1.14 -2.59 -45.75 801 !96 DM&DM-97 for high spreading rate/rotate
895 96.0 3.91 8.73 -47.33 801 !96 DM&DM-97 for high spreading rate
895 120.4 6.52 -170.61 55.04 801 !M0 DM&DM-97
895 124.0 7.83 -170.40 56.34 801 !M2 DM&DM-97
895 124.7 8.24 -170.34 56.77 801 !M3 DM&DM-97
895 126.7 9.07 -170.21 57.65 801 !M4 DM&DM-97
895 127.7 9.47 -170.14 58.09 801 !M5 DM&DM-97
895 128.2 9.60 -170.15 58.29 801 !M6 DM&DM-97
895 128.4 9.75 -170.16 58.53 801 !M7 DM&DM-97
895 129.0 9.95 -170.16 58.86 801 !M8 DM&DM-97
895 129.5 10.20 -170.18 59.27 801 !M9 DM&DM-97
895 130.2 10.45 -170.19 59.69 801 !M10 DM&DM-97
895 130.9 10.77 -170.20 60.22 801 !M10N DM&DM-97
895 132.1 11.17 -170.22 60.92 801 !M11 DM&DM-97
895 133.4 11.67 -170.24 61.80 801 !M11A DM&DM-97
895 134.0 12.06 -170.26 62.52 801 !M12 DM&DM-97
895 135.0 12.39 -170.27 63.13 801 !M12A DM&DM-97
895 135.3 12.62 -170.28 63.57 801 !M13 DM&DM-97

895 135.9 12.96 -170.30 64.23 801 !M14 DM&DM-97
895 136.2 13.23 -170.31 64.76 801 !closure DM&DM-97
895 150.4 14.50 -170.35 67.39 801 !M22A DM&RDM-96
895 150.7 14.67 -170.37 67.74 801 !M23 DM&RDM-96
895 152.1 15.12 -170.39 68.74 801 !M24 DM&RDM-96
895 153.1 15.43 -170.40 69.44 801 !M24A DM&RDM-96
895 153.5 15.62 -170.41 69.87 801 !M24B DM&RDM-96
895 154.1 15.94 -170.43 70.62 801 !M25 DM&RDM-96
895 154.5 16.17 -170.44 71.18 801 !M25A DM&RDM-96
895 155.0 16.47 -170.45 71.90 801 !M26 DM&RDM-96
999 156.0 16.76 -170.46 72.62 801 !fake for closure
895 156.0 16.76 -170.46 73.22 801 !fake using 1.46 stpol recalculated
895 200.0 16.76 -170.46 73.22 801 !IND-AUS IND fixed to

Appendix 4

Table of seismic lines used in this study

LINE NUMBER (SURVEY)	S.P.	KMS	DATE
(ALPHA)	*(6 s TWT)*		
B72-78	1D- 269	35.83	1972
B72-81	96D- 189	12.53	1972
B72-82	1D- 233	31.03	1972
B72-84	46D- 169	16.53	1972
(NINGALOO 1)	*(48 TRACE/48 FOLD; 5.9 s TWT)*		
79-01N	1- 630	20.96	1979
79-02N	1- 525	17.46	1979
79-03N	1- 751	25.00	1979
79-04N	1- 877	29.20	1979
79-05N	1- 691	23.00	1979
79-06N	1- 426	14.17	1979
79-07N	1- 1082	36.03	1979
79-08N	1- 556	18.50	1979
79-09N	1- 1185	39.46	1979
79-10N	1- 915	30.46	1979
79-11N	1- 872	29.03	1979
79-12N	1- 1278	42.56	1979
79-14N	1- 1753	58.36	1979
79-15N	1- 845	28.13	1979
79-16N	1- 681	22.66	1979
79-17N	1- 1929	64.26	1979
79-20N	1- 822	27.36	1979
79-25N	1- 3564	118.75	1979
79-26N	1- 1590	52.96	1979
79-27N	1- 1096	36.50	1979
79-28N	1- 744	24.76	1979
79-31N	1- 1867	62.19	1979
79-32N	1597- 3789	73.06	1979
(NINGALOO 2)	*(96 TRACES/48 FOLDS)*		
79-44N	119- 568	14.97	1979
79-45N	1- 601	20.00	1979
79-46N	1- 571	19.00	1979
79-49N	101- 882	62.69	1979
79-50N	1- 1408	46.90	1979

79-51N	1- 514	17.10	1979
79-52N	1- 637	21.20	1979
79-53N	1- 784	26.10	1979
79-54N	1- 751	25.00	1979

(TANTABIDDI) *(6 s TWT)*

CE80-05M	1- 1255	31.35	1980
CE80-23M	1- 1294	32.33	1980
CE80-30M	1- 651	16.25	1980
CE80-31M	1- 691	17.25	1980
CE80-32M	31- 565	13.35	1980
CE80-33M	1- 608	15.18	1980
CE80-34M	26- 731	17.63	1980

(*reprocessed by HGS in 1992*)

(CAPRICORN) *(2.5 s TWT)*

CE82-01MA	1- 539	16.14	1982
CE82-06	1- 631	18.90	1982
CE82-08	1- 440	13.17	1982
CE82-09	1- 440	13.17	1982
CE82-11	1- 1517	45.48	1982
CE82-12	1- 1981	59.40	1982
CE82-13	1- 1399	41.94	1982

(*reprocessed by Mobil in 1991*)

TOTAL KMS REPROCESSED **1663.93**

CE82-02M	1- 539	15.82	1982
CE82-03	1- 1264	37.17	1982
CE82-04	1- 539	15.82	1982
CE82-05	1- 547	16.08	1982
CE82-07	1- 761	22.38	1982
CE82-10	1- 990	29.08	1982

(CUVIER) *(240 CHANNELS/80 FOLD; 4 s TWT)*

92-MDCU-100	101- 3885	70.95	1992
92-MDCU-101	101- 6658	122.94	1992
92-MDCU-102	15- 3748	68.38	1992
92-MDCU-103	101- 6312	118.35	1992
92-MDCU-104	101- 3675	68.90	1992
92-MDCU-106	101- 3695	67.38	1992
92-MDCU-108	101- 3630	66.17	1992
92-MDCU-110	101- 3748	68.38	1992
92-MDCU-112	108- 3728	68.00	1992

92-MDCU-114	101- 4166	76.22	1992
92-MDCU-116	101- 4631	84.94	1992
92-MDCU-118	101- 4530	83.04	1992
92-MDCU-120	101- 4347	79.61	1992
92-MDCU-122	101- 4324	79.18	1992
92-MDCU-124	101- 4336	79.22	1992
92-MDCU-126	101- 4255	77.89	1992
92-MDCU-128	101- 4184	76.56	1992
92-MDCU-130	101- 4035	73.58	1992
92-MDCU-132	15- 3837	71.66	1992
92-MDCU-134	101- 3186	57.84	1992
92-MDCU-136	101- 2531	45.56	1992
92-MDCU-138	101- 1917	34.05	1992
92-MDCU-140	101- 1319	22.83	1992
(GEKO-PRAKLA)	*(8 s TWT)*		
GPCTD93-100	8- 2226	60.99	1993
GPCTD93-101a	101- 1398	38.41	1993
GPCTD93-101b	11399-13387	54.67	1993
GPCTD93-102	1- 3194	94.79	1993
GPCTD93-103	3- 3450	94.79	1993
GPCTD93-200	1- 2642	72.62	1993
GPCTD93-201a	1- 2292	63.00	1993
GPCTD93-201b	12293-14553	62.15	1993
GPCTD93-402	4- 3213	88.25	1993
GPCTD93-404a	4- 2075	56.95	1993
GPCTD93-404b	12076-14632	70.29	1993
GPCTD93-405	1- 3589	98.67	1993
GPCTD93-406	2- 4202	115.50	1993
GPCTD93-407	23- 2588	70.54	1993
GPCTD93-408	1- 3330	91.55	1993
GPCTD93-409	1- 2648	72.79	1993
GPCTD93-410	20- 2591	70.70	1993
GPCTD93-411	6- 2602	71.39	1993
GPCTD93-412	1- 2271	62.42	1993
GPCTD93-413	2- 2138	58.74	1993
GPCTD93-414	1- 1828	50.24	1993
GPCTD93-415	1- 1568	43.09	1993
GPCTD93-416a	4- 606	16.56	1993
GPCTD93-416b	10607-11680	29.51	1993
GPCT93-114	1- 5193	194.70	1993
TOTAL KM		**6873.83**	